REDOX REGULATION OF PROTEIN KINASE B/AKT FUNCTION BY AN ALLOSTERIC DISULPHIDE BOND

Reichelle Yeo

Faculty of Medicine

The University of Sydney

A thesis submitted in fulfilment of the requirements for the degree of Doctor of Philosophy

2019

THE UNIVERSITY OF SYDNEY

Table of Contents

Statement of Originality

This is to certify that to the best of my knowledge, the content of this thesis is my own work. This thesis has not been submitted for any degree or other purposes.

I certify that the intellectual content of this thesis is the product of my own work and that all the assistance received in preparing this thesis and sources have been acknowledged.

Reichelle Yeo

February 2019

Acknowledgements

I would first and foremost like to thank my incredible supervisor, Philip Hogg. Thank you for all your support throughout my candidature, I would never have achieved as much as I have without your guidance or developed into the budding scientist I am today. I am incredibly fortunate to have learnt as much as I have from you and am so grateful that you decided to take a chance on me. I have enjoyed every moment of being your student and it has been an absolute honour to be mentored by you.

To my brilliant co-supervisor, Joyce Chiu, who has taken the time to help me develop every single one of my lab skills – thank you for teaching me everything I know, the informative chats about research and helping me build up confidence as a scientist. Your constant support and assistance has been incredibly invaluable and I cannot wait to see the progression of your career.

A sincere utmost thank you to those who have generously given their time and expertise to help me construct this thesis. Aster Pijning (Centenary Institute), thank you for your help in the bioinformatics component of the project and for the coffee chats (best travel buddy!). Stefan Oehlers (Centenary Institute) and Elinor Hortle (Centenary Institute) for your key involvement in the zebrafish component of the project. Zhiduan Su (University of Sydney) and James Burchfield (University of Sydney) for your expertise in the membrane binding component of the project. John Rasko (Centenary Institute) and John Pimanda (University of New South Wales) for providing lentiviral plasmids essential to the project. Advanced Cytometry Facility (Centenary Institute) for your assistance in FACS and the Biological Testing Facility (Garvan Institute) for your assistance at the zebrafish aquarium.

To members of the Hogg group who has helped me during my PhD candidature. Heng Woon, thank you for your help with cloning (there were so many!). Diego Butera, Kristina Cook and Emma Ramsay, thank you for teaching me how to use the (once) intimidating lab equipment and long chats about disulphide bonds. Pierre Dilda, thank you for your guidance and patience during my Honours year.

To all the wonderful researchers at the Charles Perkins Centre, Centenary Institute and Lowy Cancer Research Centre who have helped me develop into the scientist I am today. To the Cool People Club – Athena Phoa, Abigail Vallejo, Timothy Couttas, Stefanie Portelli, Laura Hunter, Jonathan Teo, Dylan Harney, Ramzi Abbassi, Cassandra Malecki, Isobel Tenison-Collins and Michael Ellis, thank you all for eating lunch with me in the dark enclave and for being the greatest bunch of people to work with. Regina Ryan, Michelle van Geldermalsen, Ashwin Unnikrishnan, Collin Tran, Mona Lei, Holly McEwen and Blake Zhang, thank you all for being so helpful and encouraging in the entirety of my candidature and most importantly…telling me that I make amazing coffee. I am so extremely fortunate to have you all as friends.

To my friends outside the lab (Cheltenham pink elephants and UNSW crew!), thank you all for your support. Peggy Wong, thank you for the encouragement, brunch dates, hiking adventures, photo shoots, and being the best friend anyone could ask for (21 years and counting!). Catherine Tonthat, thank you for being so supportive whenever I have doubts about anything, in and out of the lab (cheese and wine night soon?). Michelle Panandam, thank you for the constant encouragement and being my most reliable concert buddy. Alison Chan and Yvonne Chan (Hamilton, the musical or the island?), Vennisa Santoro, Thomas Peters, Jessie Thomas and Lloyd Rogers (Cradle Mountain!), Luke Exton (I think it's 'Young'?), Albert Baky, Laurence Luu, Nathan Millar, Megan Siew, Stephanie Feher, Colin Taylor and Lachlan Bostock, thank

you all so much for the ongoing reassurance and genuine interest in my journey as a PhD student. I am incredibly lucky to have you all.

To my extended family around the world, thank you for all the encouragement and well wishes throughout my candidature. Tim and Jason, thank you for your constant support and for being incredible brothers. I know you will both succeed in whatever you do in life and I cannot wait to see what the future brings. And finally, the biggest thank you to the most selfless and generous people I know, Mum and Dad. I cannot thank you enough for all the love and support you have provided throughout my PhD candidature and my life. I wholeheartedly appreciate all that you do and I hope I make you proud. I owe you both the world. I love you.

Abstract

Most proteins in nature are chemically modified after they are made to control how, when and where they function. One type of chemical modification is the cleavage of disulphide bonds that link pairs of cysteine residues in the polypeptide chain. These cleavable bonds are known as allosteric disulphides. From an analysis of labile disulphide bonds in all protein structures from the Protein Data Bank (PDB), my colleagues and I identified a potential allosteric disulphide in the serine/threonine protein kinase B/Akt; linking cysteine residues 60 and 77 in the N-terminus pleckstrin homology (PH) domain. Akt plays a central role in glucose metabolism, cell survival and angiogenesis and is often hyper-activated in cancer cells. Akt is activated at the plasma membrane via binding to phosphatidylinositol-3,4,5-trisphosphate (PIP_3) through its PH domain. Dissociation of Akt from the plasma membrane leads to PH domain-mediated autoinhibition of the kinase by a mechanism that is currently unknown. I hypothesised that the PH domain Cys^{60}–Cys^{77} disulphide is an allosteric bond that regulates autoinhibition and inactivation of the kinase. To elucidate the role of the Cys^{60}–Cys^{77} disulphide bond in Akt function, wild-type and reduced (Cys^{60} and/or Cys^{77} substituted with Ser) PH domain or full-length Akt mutants were analysed for PIP_3 plasma membrane binding, Akt phosphorylation and Akt downstream substrate activation, transformation of fibroblasts, and angiogenesis, survival and development of zebrafish. Ablation of the Cys^{60}–Cys^{77} disulphide bond did not appreciably affect binding of recombinant PH domain to PIP_3, but markedly impaired insulin-stimulated binding of full-length Akt to the plasma membrane of adipocytes. Ablation of the Cys^{60}–Cys^{77} disulphide bond had mixed effects on insulin-stimulated phosphorylation of Akt in fibroblasts. The Cys60Ser mutant was phosphorylated to the same extent as the wild-type, while the Cys77Ser mutant was poorly phosphorylated. Wild-type but not disulphide mutant Akt induced transformation of fibroblasts, indicating an oncogenic role for oxidised but not reduced Akt. Expression of disulphide mutant Akt in zebrafish increased the induction of angiogenesis and

development of embryos but did not affect zebrafish survival. My findings imply that the Cys^{60}–Cys^{77} disulphide bond in the PH domain of Akt is an allosteric disulphide involved in autoinhibition and functioning of the kinase.

List of Figures

List of Tables

List of Abbreviations

Abbreviation	Extension
^{12}C-IPA	carbon-12 isotope linked 2-iodo-*N*-phenylacetamide
^{13}C-IPA	carbon-13 isotope linked 2-iodo-*N*-phenylacetamide
4EBP	4E-binding protein
A or Ala	alanine
Akt	protein kinase B
ANOVA	analysis of variance
ANT	adenine nucleotide translocase
ATCC	American type culture collection
ATP	adenosine 5'-triphosphate
BCA	bicinchoninic acid
BSA	bovine serum albumin
C or Cys	cysteine
cDNA	complementary deoxyribonucleic acid
COSMIC	catalogue of somatic mutations in cancer
CRISPR	clustered regularly interspaced short palindromic repeats
DMEM	Dulbecco's Modified Eagle's medium
DMSO	dimethyl sulfoxide
DNA	deoxyribonucleic acid
dNTP	deoxyribose nucleoside triphosphate
DSE	dihedral strain energy
DTT	1,4-dithiothreitol
E or Glu	glutamic acid
E. coli	*Escherichia coli*
ECL	enhanced chemi-luminescence
EDTA	ethylenediaminetetraacetic acid
EGF	epidermal growth factor
EGFP	enhanced green fluorescent protein
eIF4E	eukaryotic translation initiation factor 4E
Elavl	ELAV like neuron-specific RNA binding protein
ELISA	enzyme-linked immunosorbent assay
Ex/Em	excitation/emission
FGF	fibroblast growth factor
fli1a	fli-1 proto-oncogene, ETS transcription factor a
FoxO	forkhead box O
G	gram(s)
GLUT	glucose transporter
GPCR	G-protein-coupled receptor
GSAO	4-(*N*-(*S*-glutathionylacetyl)amino)phenylarsonous acid
GSK	glycogen synthase kinase
h	hour(s)

HA	hemagglutinin
Her	hairy-related
HF	high fidelity
HIF	hypoxia-inducible factor
hpf	hour(s) post-fertilisation
HRP	horseradish peroxidase
IB	immunoblotting
IGF	insulin-like growth factor
IgG	immunoglobulin G
IP	immunoprecipitation
IP_4	inositol 1,3,4,5-tetrakisphosphate
IPTG	isopropyl β-D-1-thiogalactopyranoside
IRES	internal ribosomal entry site
ISV	intersegmental vessel
K or Lys	lysine
KD	kinase domain
L	litre(s)
LB	Luria-Bertani
Lck	lymphocyte-specific protein tyrosine kinase
LC-MS	liquid chromatography-mass spectrometry
LDL	low density lipoprotein
LDS	lithium dodecyl sulfate pH 8.4
LeGO-iG2	lentiviral gene ontology vector, eGFP
m	milli-
M	mole(s) per litre
MAPK	mitogen-activated protein kinase
MICA	major histocompatibility complex class I chain-related A
min	minute(s)
MOPS	3-(*N*-morpholino)propanesulfonic acid
mRNA	messenger ribonucleic acid
MRP	multidrug resistance protein
mTORC	mammalian target of rapamycin complex
Myr	myristoylation
n	nano-
Ngn	neurogenin
NSCLC	non-small cell lung cancer
p	pico-
p2a	polyadenylation
p3E	3’-entry clone
p5E	5’-entry clone
PAGE	polyacrylamide gel electrophoresis
PBS	phosphate-buffered saline
PCR	polymerase chain reaction
PDB	Protein Data Bank

PDGF	platelet-derived growth factor
PDI	protein disulphide isomerase
PDK	phosphoinositide-dependent kinase
PENAO	4-(*N*-(*S*-penicillaminylacetyl)amino)phenylarsonous acid
PH domain	pleckstrin homology domain
PHLPP	PH domain and leucine rich repeat protein phosphatase
PI3K	phosphoinositide 3-kinase
PIP_2	phosphatidylinositol-3,4-bisphosphate
PIP_3	phosphatidylinositol-3,4,5-trisphosphate
pME	middle-entry clone
PMSF	phenylmethylsulfonyl fluoride
PP2A	protein phosphatase 2
PTEN	phosphatase and tensin homolog deleted on chromosome 10
PTM	post-translational modification
PTU	phenylthiourea
PVDF	polyvinylidene fluoride
RD	regulatory domain
RFP	red fluorescent protein
RIPA	radio immunoprecipitation assay
RNA	ribonucleic acid
ROS	reactive oxygen species
RT	retention time
RT-qPCR	reverse transcriptase quantitative polymerase chain reaction
RTK	receptor tyrosine kinase
s	second(s)
S or Ser	serine
s.d.	standard deviation
SDS	sodium dodecyl sulfate
SLIM	site-directed ligase independent mutagenesis
SREBP1	sterol regulatory element-binding protein 1
SUMO	small ubiquitin-related modifier
T or Thr	threonine
Tbp	TATA-box binding protein
TBST	25 mM Tris, 150 mM NaCl, pH 7.4 and 0.1% TWEEN® 20
td	tandem
TE	10 mM Tris-HCl, pH 8.0, 1 mM EDTA
tg	transgenic
TIRF	total internal reflection fluorescence
Trx	thioredoxin
TrxR	thioredoxin reductase
TSC	tumour suppressor complex
ubb	ubiquitin
V	volt(s)
VEGF	vascular endothelial growth factor

VL	variable loop
WT	wild-type
α	alpha
β	beta
γ	gamma
μ	micro-
ζ	zeta
χ	dihedral or chi
Å	Ångström

List of Publications

1. Aster E. Pijning, Joyce Chiu, Reichelle X. Yeo, Jason W. H. Wong & Philip J. Hogg (2018). Identification of allosteric disulphides from labile bonds in X-ray structures. *R Soc Open Sci*, 5:171058.
2. Martin Howell, Reichelle Yeo, Allison Tong, Jonathan Craig, Kirsten Howard & Germaine Wong (2017). The consistency and reporting of quality of life outcomes in trials of immunosuppressive agents in kidney transplantation: systematic review and meta-analysis. *Nephrol Dial Transplant;* 1-9.
3. Stéphanie Decollogne, Swapna Joshi, Sylvia A. Chung, Peter P. Luk, Reichelle X. Yeo, Sheri Nixdorf, André Fedier, Viola Heinzelmann-Schwarz, Philip J. Hogg, Pierre J. Dilda (2015). Alterations in the mitochondrial responses to PENAO as a mechanism of resistance in ovarian cancer cells. *Gynecol Oncol*; 138(2):363-71.

Oral & Poster Presentations

1. Reichelle X. Yeo, Joyce Chiu & Philip J. Hogg. Investigation of a potential allosteric disulphide in Akt1. FASEB Functional Disulfide Bonds in Health & Disease at Leesburg, VA, USA. June 17th-21st 2018.
2. Aster E. Pijning, Joyce Chiu, Reichelle X. Yeo, Jason W. H. Wong & Philip J Hogg. Identification of allosteric disulphides from labile bonds in X-ray structures. FASEB Functional Disulfide Bonds in Health & Disease at Leesburg, VA, USA. June 17th-21st 2018.
3. Reichelle X. Yeo, Joyce Chiu & Philip J. Hogg. Regulation of tumour cell glucose phosphorylation by an allosteric disulphide bond. 2016 Postgraduate Cancer Research Symposium at University of Sydney, NSW, Australia. December 2nd 2016.
4. Reichelle X. Yeo, Joyce Chiu & Philip J. Hogg. Regulation of tumour cell glucose phosphorylation by an allosteric disulphide bond. FASEB: Functional Disulfide Bonds in Health & Disease at Steamboat Springs, CO, USA. August 14-17th 2016.
5. Reichelle X. Yeo, Joyce Chiu & Philip J. Hogg. Regulation of cancer cell glucose phosphorylation by an allosteric disulphide bond. Bosch Institute Annual Scientific Meeting 2016: Ideas and Technology – Engines of Medical Science at University of Sydney, NSW, Australia.
6. Reichelle X. Yeo, Joyce Chiu & Philip J. Hogg. Characterisation of glucose phosphorylation in glioblastoma. 24th ASMR (Australian Society of Medical Research) NSW Annual Scientific Meeting at Powerhouse Museum, NSW, Australia. June 6th 2016.
7. Reichelle X. Yeo, Joyce Chiu & Philip J. Hogg. Characterisation of cancer phosphorylation of glucose. Sydney Catalyst 2016 Post Graduate & Early Career Researcher Symposium at Chris O'Brien Lifehouse, NSW, Australia. April 27th 2016.

1. Introduction

1.1 Tumour Metabolism

For the last few decades, there has been a focus on identifying hallmarks of cancer; such as cell proliferative signalling, resistance to cell death, and tissue invasion and metastases (Hanahan & Weinberg, 2000). Multiple attempts have been made on developing therapeutic approaches to target genetic abnormalities in cancer cells (Holland, 2000), however, these abnormal cells ultimately evade signalling pathways that these therapies target. An increasing amount of research has suggested that deregulation of cellular energetics is involved in the pathogenesis of cancer (Hanahan & Weinberg, 2011; Neary & Pastorino, 2013; Ramsay et al., 2011; Warburg et al., 1927; Weinberg & Chandel, 2015; Wolf et al., 2011; Zhao et al., 2013). Cancer cells excessively consume nutrients in their environment to meet increased demands of cell growth. An increased uptake of glucose and high glycolysis rate are channelled toward the biosynthesis of deoxyribonucleic acid (DNA), lipids and proteins to support new cancer cell division (Ward & Thompson, 2012).

Cancer cells express an aberrant metabolic phenotype known as the 'Warburg effect'. In aerobic conditions, quiescent cells generate 36 adenosine 5'-triphosphate (ATP) molecules per glucose molecule from both glycolysis and mitochondrial oxidative phosphorylation. In proliferating tumour cells, however, energy production shifts from oxidative phosphorylation to glycolysis – generating two ATP molecules per glucose even in the presence of oxygen. This phenomenon was named 'aerobic glycolysis' by Otto Warburg and is characterised by increased lactic acid production (Warburg, 1956a, 1956b). Surrounding cancer cells utilise this lactic acid as an energy source to promote cell growth (Hanahan & Weinberg, 2011), and thus autonomously maintain their aberrant metabolic phenotype. Glycolysis is much less efficient than oxidative phosphorylation in yielding ATP, however, cancer cells adapt by increasing

their glucose uptake; thus increasing the rate of glycolysis (Ganapathy-Kanniappan & Geschwind, 2013). Increased aerobic glycolysis and glucose uptake has previously been shown to be directly activated by the human oncogene, Akt (Elstrom et al., 2004). Akt-induced tumour metabolism dominates cancer cell proliferation and survival, suggesting constitutively active Akt is sufficient in inducing the shift to aerobic glycolysis, and rendering cancer cells dependent on aerobic glycolysis for survival (Elstrom et al., 2004). Therapeutics can, in principle, be developed to selectively target cancer cell metabolism without being toxic to normal cells.

1.1.1 Cell signalling in tumour metabolism

Except for white blood cells and skin cells, normal cells from tissues usually forgo cell proliferation unless signalling cascades are initiated by extracellular stimuli, i.e. glucose, chemokines, hormones or growth factors (Baxter, 2014; Tan et al., 2012; Wang et al., 2000). The PI3K/Akt/mTOR signalling pathway is an extensively studied pathway that is tightly controlled by tumour suppressor phosphatase and tensin homolog deleted on chromosome 10 (PTEN). PTEN dephosphorylates phosphatidylinositol-3,4,5-trisphosphate (PIP_3) to phosphatidylinositol-3,4-bisphosphate (PIP_2), and acts as a negative regulator of phosphoinositide 3-kinase (PI3K) (Carracedo & Pandolfi, 2008; Chalhoub & Baker, 2009). Mutations or loss of PTEN expression is also frequently observed in cancer (Leslie & Downes, 2004). Dysregulation of the PI3K/Akt/mTOR signalling pathway is critically involved in disease progression – especially in cancers with poor prognoses (Bellacosa et al., 2005; Testa & Bellacosa, 2001). Cancer cells acquire mutations that constitutively activate the PI3K/Akt/mTOR pathway (DeBerardinis et al., 2008). Protein kinase Akt is the central node of this pathway, and has a pleiotropic effect on a number of cellular processes; playing a crucial

role in tumourigenesis when hyper-activated (Testa & Bellacosa, 2001; Testa & Tsichlis, 2005).

1.1.2 PI3K/Akt/mTOR cell signalling pathway

Akt is a highly conserved human serine/threonine-specific protein kinase critically involved in the tight regulation of the PI3K/Akt/mTOR signalling pathway (**Figure 1.1**). Extracellular ligands mediate physiological effects via receptor tyrosine kinases (RTK) or G-protein-coupled receptors (GPCR) to activate PI3K, and subsequently phosphorylate PIP_2 to PIP_3. Akt is localised in the nucleus and cytosol until activation by PIP_3 at the plasma membrane. Three direct downstream substrates of Akt are Forkhead box protein O1 (FoxO1), glycogen synthase kinase 3α/β (GSK3α/β) and the TSC1/TSC2 (hamartin-tuberin) complex; responsible for cell growth and proliferation (Fujita et al., 2002; Song et al., 2005), cell survival and death (Datta et al., 1997; Yamaguchi & Wang, 2001; Zhou et al., 2000), angiogenesis (Harada et al., 2009; Pore et al., 2006) and glucose and glycogen metabolism (Diehl et al., 1998; Kohn et al., 1996; Pap & Cooper, 1998).

- Cell survival and proliferation

The FoxO family of transcription factors is sensitive to insulin or insulin-like growth factor (IGF) signalling (Webb et al., 2016). Insulin-activated Akt directly phosphorylates FoxO1 at conserved residues; Thr^{24} at the N-terminus, Ser^{256} on the nuclear localisation sequence and Ser^{319} near the nuclear export sequence (Zhang et al., 2002). Phosphorylation of FoxO1 generates motifs recognised by 14-3-3 proteins that assist in the exporting of FoxO1 out of the nucleus into the cytosol (Tzivion et al., 2011). Inhibition of FoxO1 represses transcriptional activity; thus inhibiting apoptosis, autophagy, cell cycle arrest and catabolism (Manning & Toker, 2017; Webb & Brunet, 2014; Zhang et al., 2011).

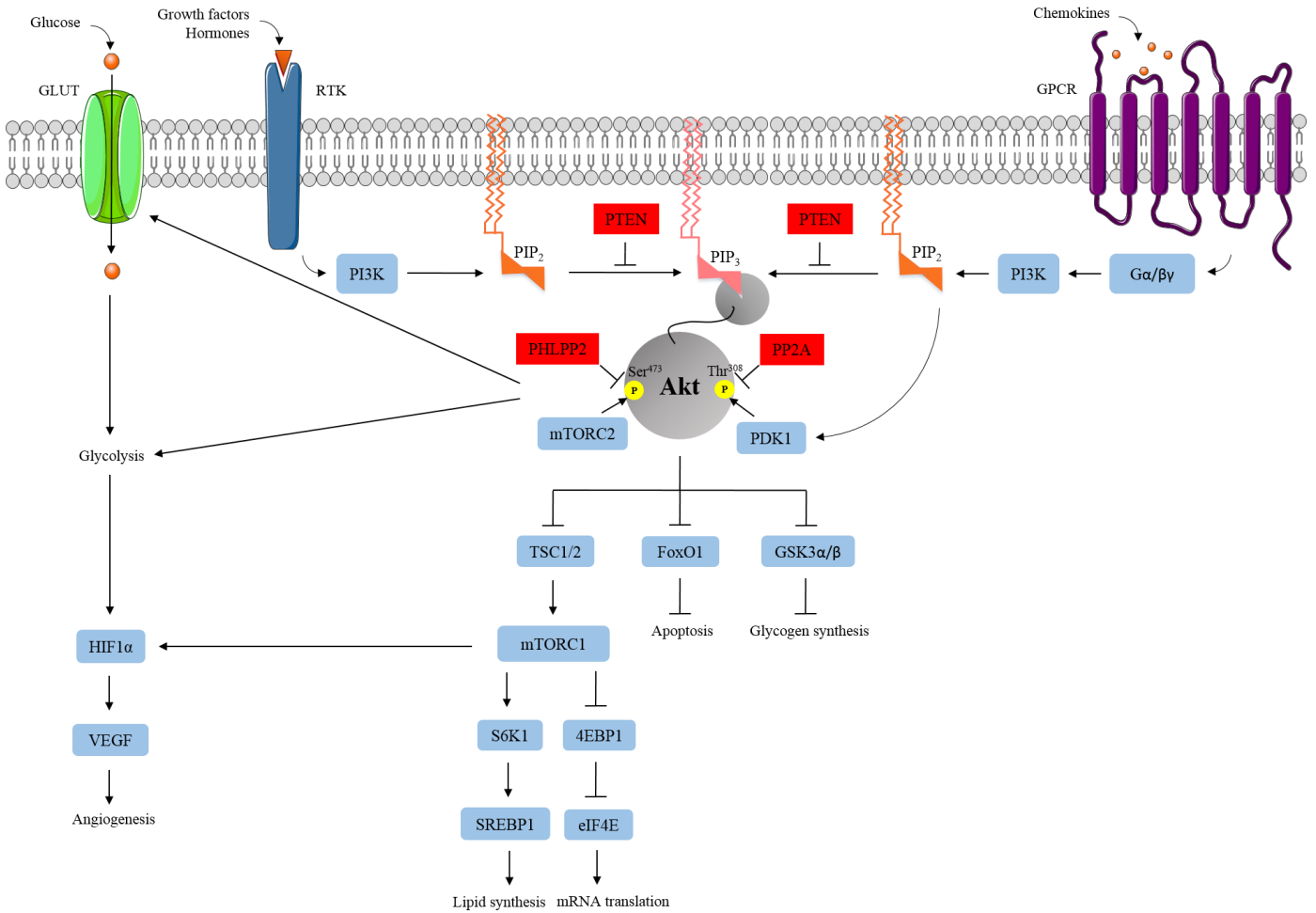

Figure 1.1 The PI3K/Akt/mTOR cell signalling cascade.
This signalling pathway is stimulated by ligands (e.g. chemokines, glucose, growth factors, hormones) activating extracellularly at the plasma membrane. PI3K phosphorylates PIP_2 to PIP_3. PTEN regulates PI3K activity. Akt translocates to the plasma membrane and binds to PIP_3. Akt is phosphorylated by PDK1 and mTORC2. Akt directly phosphorylates downstream substrates FoxO1, GSK3α/β, TSC2 responsible for cell proliferation and survival, angiogenesis, lipid synthesis, mRNA translation and metabolism. Akt dissociates from the plasma membrane into the cytosol and is dephosphorylated by PP2A and PHLPP2.

- Angiogenesis

Akt upregulates the translation of hypoxia-inducible factor 1 (HIF1) in response to increased glucose and oxygen availability in solid cancers (Harada et al., 2009). Radiotherapy of tumours induces formation of free radicals; HIF1 accumulates in the nucleus to be activated in response to reactive oxygen species (ROS) (Moeller et al., 2004). HIF1 is a heterodimer that consists of the α and β-subunit. HIF1β is constitutively active and insensitive to changes in oxygenation, however, hydroxylation of the HIF1α at Pro^{564} and Pro^{402} is oxygen-dependent (Niecknig et al., 2012). Under normoxic conditions, prolyl hydroxylases tag HIF1α for ubiquitination and proteolysis (Lee et al., 2015). In hypoxic conditions – especially in a tumour setting, HIF1α escapes degradation, accumulating to dimerise with HIF1β in the nucleus; thereby activating vascular endothelial growth factor (VEGF) to initiate angiogenesis and inhibit apoptosis (Krock et al., 2011; Lee et al., 2015).

- Lipid synthesis

Cancer cells exhibit high rates of *de novo* lipid synthesis; used as building blocks for biological processes (Santos & Schulze, 2012). Akt affects the synthesis and degradation of lipids involved in signalling for cell growth and survival, thus aberrant changes to lipid metabolism contribute to oncogenesis (Santos & Schulze, 2012). The primary mechanism of Akt-mediated activation of mammalian target of rapamycin complex 1 (mTORC1) is through the disruption of the tumour suppressor TSC1/TSC2 complex. Insulin-mediated Akt directly phosphorylates TSC2 at Ser^{939} and Thr^{1462} residues, triggering the release and degradation of TSC2 from TSC1 to activate mTORC1 (Huang & Manning, 2008). However, through negative feedback mechanisms, mTORC1 also inhibits PI3K activation (Huang & Manning, 2009). Akt-mediated degradation of TSC2 activates the mammalian target of rapamycin complex 1 (mTORC1) (Manning & Toker, 2017). In response to Akt activation, nuclear transcription factor sterol

regulatory element-binding protein 1 (SREBP1) activity is dependent on mTORC1 signalling (Porstmann et al., 2008). SREBP1 and ATP citrate lyase are activated; leading to induction of cholesterol synthesis, fatty acid synthase and low density lipoprotein (LDL)-receptors (Krycer et al., 2010; Laplante & Sabatini, 2009).

- Protein synthesis

Phosphorylation of the eIF4E-binding protein 1 (4EBP1) via the PI3K/Akt pathway also requires activation by mTORC1 (Gingras et al., 1998). Supplementary to the PI3K/Akt pathway, mitogen-activated protein kinase (MAPK) pathway also regulates eukaryotic translation initiation factor 4E (eIF4E). mTORC1 phosphorylates 4EBP1 to relieve its inhibitory binding of eIF4E (Siddiqui & Sonenberg, 2015). eIF4E (along with eIF4A, eIF4G) forms a subunit of the larger complex eIF4F; it binds the 5' cap of mRNA and recruits the 40S ribosomal subunit, initiating mRNA translation (Lazaris-Karatzas et al., 1990; Siddiqui & Sonenberg, 2015; Wendel et al., 2007). Phosphorylated eIF4E at Ser^{209} (previously thought to be at Ser^{53}) is essential for oncogenesis. Malignant transformation by overexpressing eIF4E was first observed in NIH/3T3 mouse fibroblast cells *in vitro* (Lazaris-Karatzas et al., 1990), followed by mouse models *in vivo* (Wendel et al., 2007). Overexpression of eIF4E has also been observed in human cancers (Siddiqui & Sonenberg, 2015).

- Glucose and glycogen metabolism

GSK3 was the first downstream substrate of Akt to be reported (Cross et al., 1995). Insulin-mediated Akt directly phosphorylates the two isoforms, GSK3α/β, at Ser^{21}/Ser^{9} residues at the N-terminus (Jiang et al., 2003; Pap & Cooper, 1998), GSK3 in turn, can regulate Akt activity by regulating PTEN expression (Maccario et al., 2007) or transporting Akt in close proximity to phosphatase PP2A (Beurel et al., 2015). Inhibition of GSK3 is implicated in the regulation

of glucose uptake and glucose transporter (GLUT) protein expression (Buller et al., 2008), glycogen and protein synthesis (Cross et al., 1995). In an Akt-independent setting, GSK3 is most notably involved in the Wnt–β-catenin pathway that regulates gene transcription (Yost et al., 1996). AXIN1/2, adenomatous polyposis coli and GSK3 form a destruction complex to trigger β-catenin destabilisation (MacDonald et al., 2009; Wu & Pan, 2010).

Constitutively active Akt directly increases the rate of glucose metabolism and aerobic glycolysis (Elstrom et al., 2004) by activating the metabolic enzyme, hexokinase. Akt phosphorylates hexokinase, which thereby stimulates phosphofructokinase activity to enhance production of ATP (Barthel et al., 1999; Buzzai et al., 2005)**.** Interestingly, inactive Akt inhibits insulin from transcribing GLUT mRNA, signifying that Akt plays a crucial role in glucose metabolism (Barthel et al., 1999).

1.2 Akt/Protein Kinase B

Akt or protein kinase B (PKB), was first identified by Staal and colleagues in 1977. A transforming retrovirus was isolated from an AKR mouse with T-cell lymphoma and named AKT-8 (Staal et al., 1977). Staal showed that *AKT* is an oncogene in humans (Staal, 1987). Activation of *AKT* drives the switch to aerobic glycolysis; thus tumour cells require a continuous supply of glucose – rendering them dependent on aerobic glycolysis to survive and proliferate (Elstrom et al., 2004).

1.2.1 Isoforms of Akt/PKB

Mammalian cells express three isoforms of Akt/PKB (Akt1/PKBα, Akt2/PKBβ, Akt3/PKBγ) and are members of the AGC family of protein kinases (Manning & Cantley, 2007). Akt1 is ubiquitously expressed in all tissues. Akt2 is expressed in metabolically active tissue, e.g. liver, adipose tissue and muscle. Akt3 is predominantly expressed in the brain and testes (Chan et al., 2014; Yang et al., 2004). Isoforms of human Akt are all similar in structure (**Figure 1.2A**). Akt consists of the N-terminus pleckstrin homology (PH) domain containing the phosphatidylinositol binding pocket, followed by the glycine rich linker, connected to the kinase domain containing the phosphorylation site threonine (Thr)^{30*}, and the C-terminus regulatory domain containing the second phosphorylation site serine (Ser)^{47*} (Alessi et al., 1996a). The kinase domain of Akt1 shares 85% identity with Akt2 and Akt3, whilst the PH domain of Akt1 shares 60% identity with Akt2 and Akt3 (Masure et al., 1999) (**Figure 1.2B**). The focus of my thesis is on the isoform Akt1.

A

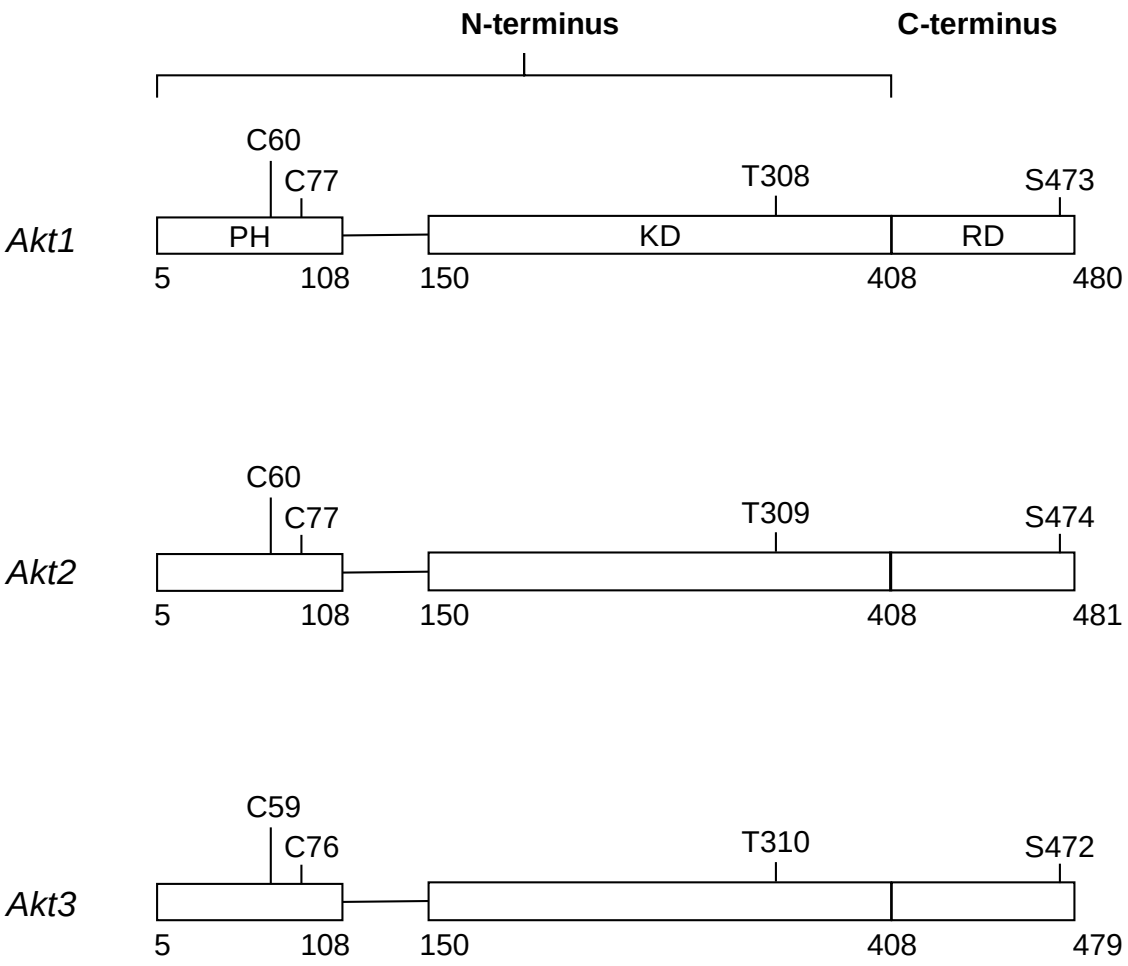
N-terminus
C-terminus
C60
C77
T308
S473
Akt1
PH
KD
RD
5
108
150
408
480
C60
C77
T309
S474
Akt2
5
108
150
408
481
C59
C76
T310
S472
Akt3
5
108
150
408
479

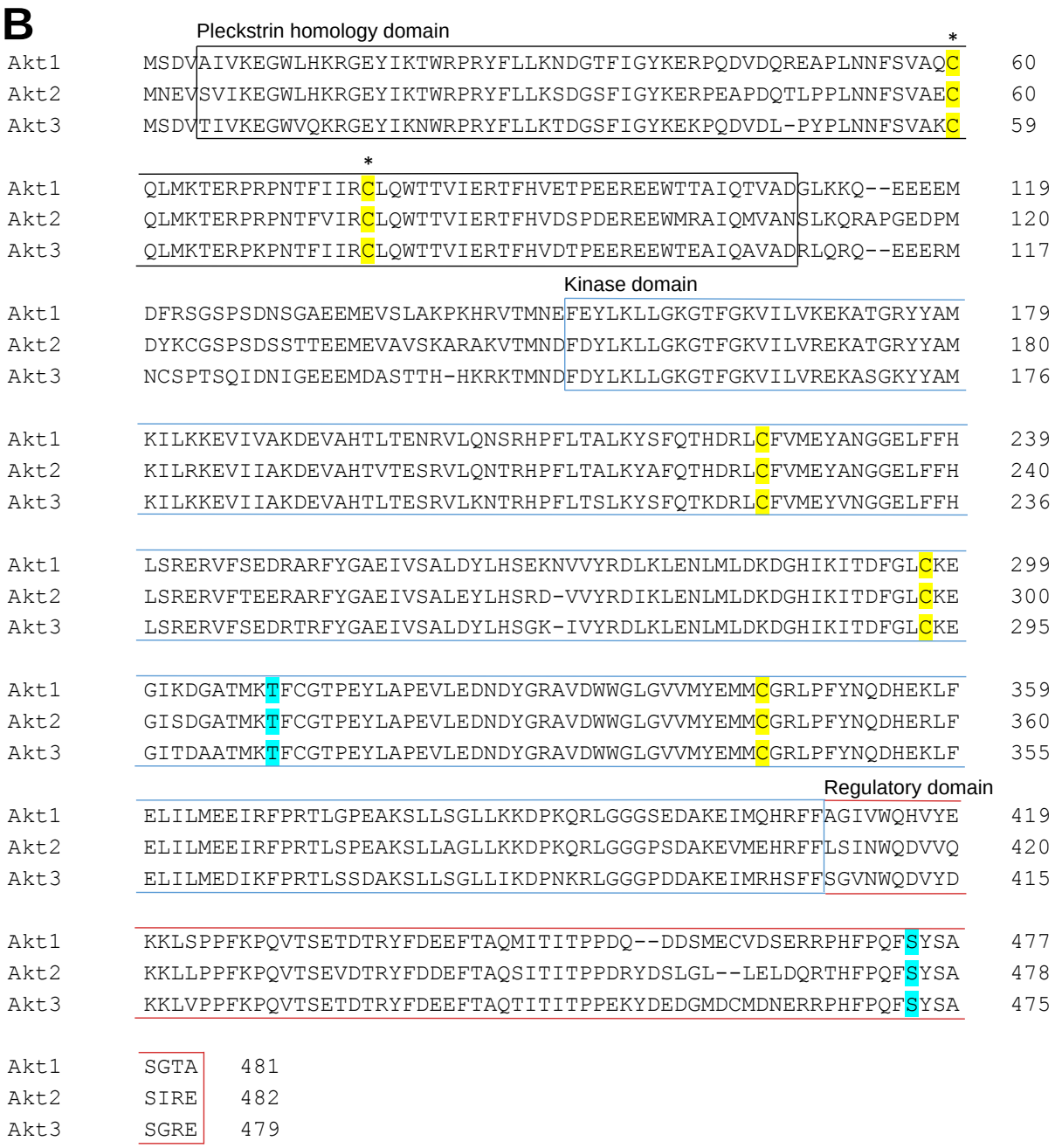

Figure 1.2 Structural domains and amino acid sequences of human Akt1, Akt2 and Akt3. **A.** Structure of Akt isoforms. N-terminus pleckstrin homology (PH) domain contains conserved cysteine (C) residues that form a disulphide bond, followed by the catalytic kinase domain (KD) containing the phosphorylation site threonine (T)[30*], and C-terminus hydrophobic motif regulatory domain (RD) containing the phosphorylation site serine (S)[47*]. **B.** Alignment of the amino acid sequences of human Akt isoforms. Pleckstrin homology domain sequence is shown in the black box. Kinase domain sequence is shown in the blue box. Regulatory domain sequence is shown in the red box. Conserved cysteine residues are highlighted in yellow. Residues of interest are marked with an asterisk above the sequence. Conserved threonine and serine residues that are phosphorylated after activation are highlighted in blue.

1.2.2 Akt1 membrane localisation and dissociation

It was reported recently that Akt1 is allosterically activated by PIP_3 at the plasma membrane by relieving autoinhibitory intramolecular interactions between the PH and kinase domains (Ebner et al., 2017). Upon binding of the positively charged PH domain of Akt1 to the negatively charged phospholipid PIP_3 at the plasma membrane, Akt1 is activated and undergoes a conformation change. The PH domain no longer interacts with the kinase domain, exposing Akt1 phosphorylation sites and access for substrate binding, but not nucleotide binding. Phosphoinositide-dependent kinase 1 (PDK1) interacts with the activation loop and phosphorylates Akt1 at Thr^{308} in the kinase domain (Calleja et al., 2009). Akt1 activity is restricted to membrane sites containing PIP_2 or PIP_3 (Lučić et al., 2018). Upon dissociation from PIP_3 at the plasma membrane, Akt1 briefly phosphorylates downstream nucleic and cytoplasmic proteins; the reported half-life of cytosolic active Akt1 is 3-5 min before dephosphorylation (Calleja et al., 2007). A suggested mechanism of membrane dissociation is the phosphorylation of Thr^{34}, dependent on the recruitment of PKCζ (Powell et al., 2003) or PDK1 (concurrent phosphorylation of Thr^{308}) (Huang et al., 2015) at the plasma membrane, resulting in a conformation change and inducing the detachment from the plasma membrane. Depending on the acquired mutation at Thr^{34}, there are differing outcomes of Akt1 membrane dissociation that have been reported. Mutant Thr34Ala (T34A) has the ability to bind to PIP_3 even in the presence of PKCζ (Powell et al., 2003), although conflicting observations of the mutant Thr34Asp (T34D) have been reported. This mutant was either reported to mimic phosphorylation, thus impairing the translocation of Akt1 to the plasma membrane (Huang et al., 2015); or conversely, was observed to prominently localise Akt1 at the plasma membrane (Várnai et al., 2005). The reformation of the interaction between PH and kinase domains promotes Akt1 membrane dissociation and subsequent dephosphorylation (Ebner et al., 2017).

1.2.3 Post-translational modifications of Akt1

- Phosphorylation

Phosphorylation and dephosphorylation of Akt1 is the most common post-translational modification (PTM) of the protein kinase. It is also the primary mechanism of regulating Akt1 activation and function (Chan et al., 2014). Receptors i.e. RTK, GPCR and GLUT are stimulated by extracellular ligands e.g. chemokines, hormones, or epidermal (EGF), fibroblast (FGF), insulin-like (IGF) growth factors; thereby activating intracellular PI3K at the plasma membrane. PI3K phosphorylates PIP_2 to PIP_3; PI3K activity is regulated by tumour suppressor PTEN (Chalhoub & Baker, 2009). Inactive Akt1 usually resides in the cytosol until its recruitment to the plasma membrane. Allosteric activation of Akt1 is initiated by the binding of its PH domain to PIP_3 (James et al., 1996), a docking phospholipid at the plasma membrane (Vivanco & Sawyers, 2002). Akt1 is primed for phosphorylation at the regulatory amino acid residues Thr^{308} in the kinase domain, and Ser^{473} in the regulatory domain, by phosphoinositide-dependent kinase-1 and 2 (PDK1 and PDK2 (commonly known as mTORC2)), respectively (Garcia-Echeverria & Sellers, 2008; Vivanco & Sawyers, 2002). Thr^{308} phosphorylation is necessary for Akt1 activation; ordering the activation loop and substrate binding access, whereas Ser^{473} phosphorylation is required for maximal activity and positioning of catalytic residues (Testa & Bellacosa, 2001; Yang et al., 2002). The minimal consensus sequence required for Akt1 phosphorylation is Arg-X-Arg-X-X-Ser/Thr-h, where X represents any amino acid and h is a bulky hydrophobic amino acid residue (Alessi et al., 1996b). Constitutively active phosphorylation site Thr^{450} in the regulatory domain is essential for folding and stability of the protein (Bellacosa et al., 1998). Active Akt1 detaches from the plasma membrane into the cytosol and phosphorylates downstream target proteins. Cytosolic Akt1 is rapidly dephosphorylated by protein phosphatase 2A (PP2A) and PH domain leucine-rich repeat-containing protein phosphatase 2 (PHLPP2), at Thr^{308} and Ser^{473}, respectively.

- Lysine modifications
  - Acetylation

Reversible acetylation of lysine (Lys) residues in Akt1 by histone acetyltransferases and deacetylases affect Akt1 membrane binding activity. Acetylation of Akt1 at Lys^{14} and Lys^{20} inhibits the PH domain from binding to PIP_3, thereby regulating its activity (Sundaresan et al., 2011). Mutants Lys14Arg, Lys14Gln and Lys20Gln are analogous to constitutive acetylation of Akt1, and thus the kinase remains inactive. Interestingly, Lys^{20} substituted with Arg deacetylates Akt1; it readily binds to PIP_3 to be phosphorylated (Sundaresan et al., 2011).

  - Ubiquitination

Ubiquitination of Akt1 plays a significant role in its stability and activation. Akt1 with no intact PH domain is unable to be ubiquitinated. Proteins usually undergo Lys^{48}-linked ubiquitination; resulting in protein degradation and termination of activity (Yang et al., 2010). Interestingly, Lys^{63}-linked ubiquitination of Akt1 at Lys^{8} and Lys^{14} residues does not induce degradation of the kinase, but mediate plasma membrane binding and increase phosphorylation of Akt1 (Yang et al., 2009).

  - SUMOylation

Covalent conjugation of the small ubiquitin-related modifier (SUMO) to an internal Lys residue in Akt1 is a reversible PTM that affects cell proliferation and apoptosis. SUMOylated Akt1 is usually localised in the nucleus (Risso et al., 2013). There are various different reports of SUMO-modification sites considered to be the major acceptors; Lys^{64} in the PH domain, Lys^{182}, Lys^{189} (de la Cruz-Herrera et al., 2015), Lys^{276} (Li et al., 2013; Lin et al., 2016) and Lys^{301} (Risso et al., 2013) within the kinase domain of Akt1. When these Lys residues are mutated, a significant reduction of SUMOylation is observed, thus perturbing Akt1 activity (de

la Cruz-Herrera et al., 2015). SUMOylation of Akt1 *in vivo* was detected under heat-shock stress conditions; implying Akt1 is not constitutively modified by SUMO (de la Cruz-Herrera et al., 2015).

- Glycosylation

The *O*-linked *N*-acetylglucosamine modifications of serine and threonine residues in Akt1 are reversible PTMs that inhibit Akt1 phosphorylation (Gandy et al., 2006; Wang et al., 2012). The competitive relationship between glycosylation and phosphorylation of Akt1 at the same sites has been implicated in the progression of cancer (Costa et al., 2015).

- Methylation

DNA methylation in promoter CpG islands is an epigenetic modification that maintains gene silencing (Sun et al., 2012). The promoter region of *Akt1* was observed to be significantly hypomethylated in a study of breast cancer patients (Heng et al., 2017).

1.2.4 Akt1 mutations in cancer

Aberrant Akt expression has been observed in over 50% of human cancers (Catalogue of Somatic Mutations in Cancer, COSMIC). Mutations in Akt1 occur in 3-5% of human cancers and are relatively conserved throughout other isoforms of Akt (Yi & Lauring, 2015) (**Table 1.1**). The PH domain of Akt1 plays a regulatory role in its function; hence the disruption of the PH–kinase domain interaction is implicated in cancer progression (Carpten et al., 2007). Somatic mutations in the PH domain of Akt1 have frequently been observed to disrupt membrane binding and dissociation. These residues are located near the lipid binding pocket of Akt1, therefore aberrant structural changes are direct attributes to these mutations.

The most common somatic missense mutation is Glu^{17} to Lys (E17K) in the PH domain of Akt1 near the lipid binding pocket, accounting for 36% of all Akt1 mutations (cBioPortal for Cancer Genomics) (Cerami et al., 2012; Gao et al., 2013; Yi & Lauring, 2015). E17K mutations have been observed in cancers of the breast (Carpten et al., 2007; Stephens et al., 2012; Yi et al., 2012), endometrium (Cohen et al., 2010), prostate (Boormans et al., 2010), bladder (Askham et al., 2010), non-small cell lung cancer (NSCLC) (De Marco et al., 2015; Ding et al., 2008), blood (Kim et al., 2008) and melanoma (Davies et al., 2008). The E17K mutation of Akt1 perturbs the interaction between the PH–kinase domains, inducing hyperactivation of Akt1; with or without insulin stimulation (Yang et al., 2009). Other missense activating mutations in the PH domain of Akt1 include Leu^{52} to Arg (L52R) and Gln^{79} to Lys (Q79K). They represent 1.2% of all Akt1 mutations (cBioPortal for Cancer Genomics) (Cerami et al., 2012; Gao et al., 2013) in colorectal and breast cancers (Parikh et al., 2012; Stephens et al., 2012; Yi et al., 2012).

Located in the PH domain of Akt1, the Cys^{77} mutation was also detected in cancer patients (COSMIC). The Cys^{77} to Phe (C77F) missense mutation in breast luminal carcinoma (Ellis et al., 2012; Yi et al., 2012), Cys77_Lys78ins10 (insertion of 10 amino acids, in breast ductal carcinoma (Zehir et al., 2017), and Cys77_Lys78ins12 (insertion of 12 amino acids, in frame) in ovarian granulosa cell tumour (Bessière et al., 2015).

Inactivating mutations are also located on the PH domain of Akt1. The Arg^{15} to Ala (R15A) and Lys^{20} to Ala (K20A) mutations inhibit the translocation of Akt1 to the plasma membrane; despite the presence of insulin stimulation (Akbar et al., 2005; Huang et al., 2011). The R15Q mutation has also been detected in cervical cancer (COSMIC). In autoinhibited Akt1, the PH domain of Akt1 interacts with the C-lobe of the kinase domain near Asp^{323} and Asp^{325} residues, as well as the unphosphorylated activation loop, where phosphorylation site Thr^{308} is located (Lučić et al., 2018). Double mutation of Asp^{323} and Asp^{325} to Ala (D323AD325A) reportedly disrupts the PH domain-mediated autoinhibition by permanently exposing the kinase domain for phosphorylation and substrate access, thus constitutively activating Akt1 (Lučić et al., 2018).

Table 1.1 Spectrum of recurrent mutations in Akt1 are relatively conserved in Akt2 and Akt3.

Domain	Akt1	Akt2	Akt3
Pleckstrin homology domain	E17K	E17K	E17K
	D32N/Y	D32H/N	D32N
	D46E	D46N	D46H
	P51L/S		P50L/S
	L52F/H/R		L51L/R
	Q79K/R		Q78K
	W80R	W80C/L	
Glycine rich linker	R121W		
Kinase domain	D221N		D219N
	S266N/S		S264F
	D323G/H/N/Y	D324G/H/N	D320H
	R367C	R368C/H/N	
	R370C/H	R371C/H/L	R367Q

Adapted from: Yi, K. H. & Lauring, 2015 and the Catalogue of Somatic Mutations in Cancer (COSMIC).

1.2.5 Akt1 inhibitors in cancer treatment

Akt has long been an attractive target for cancer therapeutics. So far, Akt-targeting molecules are limited by their lack of specificity, poor solubility and moderate potency. Current Akt inhibitors have shown limited success in the clinic due to toxicity or development of resistance (Nitulescu et al., 2016). ATP-competitive Akt inhibitors act as orthosteric ligands that occupy the ATP binding pocket (Chan et al., 2011); an active site that is the same throughout the isoforms of Akt (Yang et al., 2002). ATP-competitive Akt inhibitors lack efficacy and specificity against the isozymes as well as other kinases e.g. the AGC kinase family, in pre-clinical studies and in the clinic (Nitulescu et al., 2016); unexpectedly inducing hyperphosphorylation (Okuzumi et al., 2009). Development of Akt isozyme-selective therapies that are well-tolerated in the clinic has long been a challenge due to high sequence homology between the isoforms of Akt (Wu et al., 2010). Known allosteric Akt1 inhibitors target the PH domain of Akt1 to prevent plasma membrane localisation and activation of Akt1 (Barnett et al., 2005; Berndt et al., 2010; Calleja et al., 2009; Jo et al., 2011; Joh et al., 2012; Nitulescu et al., 2016). Effectiveness however, is dependent on the PH–kinase domain interface; once compromised, drug sensitivity is lost and Akt1 remains active (Parikh et al., 2012). Moreover, the phosphatidylinositol binding pocket in the PH domain of Akt1 is an unideal target due to its shallow, highly charged nature (Kumar & Madison, 2005). We therefore proposed a different approach by targeting an allosteric disulphide bond identified in the PH domain of Akt1.

1.3 Allosteric Disulphide Bond

Protein disulphide bonds are covalent linkages between the sulphur atoms of two cysteine (Cys) amino acids within or across different proteins. There are two types of disulphide bonds: structural and functional (**Figure 1.3A**). Structural disulphide bonds form during protein folding to stabilise protein conformation, withstanding changes in cellular environment and remain inert for the life of the protein (Hogg, 2003, 2013). Catalytic disulphide bonds are usually found in the active sites of enzymes that mediate thiol/disulphide exchange in other proteins. My focus is on the allosteric disulphide bond, defined as a bond that controls the function of the mature protein in which they reside. Conformational change of the protein is triggered by the formation or cleavage of the allosteric disulphide bond, altering protein function (Chiu & Hogg, 2019; Schmidt et al., 2006) (**Figure 1.3B**).

1.3.1 Cleavage of the allosteric disulphide bond

Disulphide bonds can be cleaved by oxidoreductases, thiol/disulphide exchange or hydrolysis (**Figure 1.4**). Thioredoxin, protein disulphide isomerases, glutaredoxin and peroxiredoxin are examples of oxidoreductases in cells and blood known to catalyse the reduction of disulphide bonds (Arnér & Holmgren, 2000; Butera et al., 2014; Cremers & Jakob, 2013; Holmgren, 1995). The active sites of oxidoreductases contain a reactive dithiol/disulphide that reduces or oxidises a protein disulphide bond (**Figure 1.4A**). Cleavage of disulphide bonds by thiol/disulphide exchange occurs within the same protein or between proteins, or between proteins and small molecules, however, unlike oxidoreductases, do not require additional electrons (**Figure 1.4B**). Cleavage of disulphide bonds by hydrolysis is an irreversible reaction resulting in a sulfenic acid/thiol pair (**Figure 1.4C**). Cleavage of disulphide bonds also depends on geometry of the atoms involved, spatial (right place) and temporal (right time)

considerations and energetics of the disulphide bond that is to be reduced (Chiu & Hogg, 2019; Cook & Hogg, 2013).

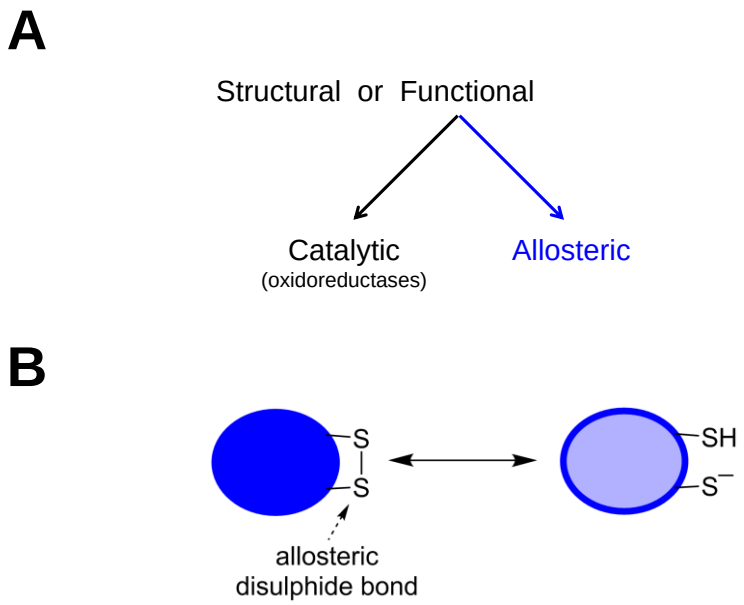

Figure 1.3 Types of protein disulphide bonds.
Disulphide bonds have structural or functional roles in mature protein. **A.** There are two types of functional disulphides. Catalytic disulphide bonds, usually in oxidoreductases, alter the redox state of disulphide bonds in other proteins. Allosteric disulphide bonds control function of the protein in which they reside. **B.** Formation or cleavage of the allosteric disulphide bond induces a conformational change and alters function of the protein.

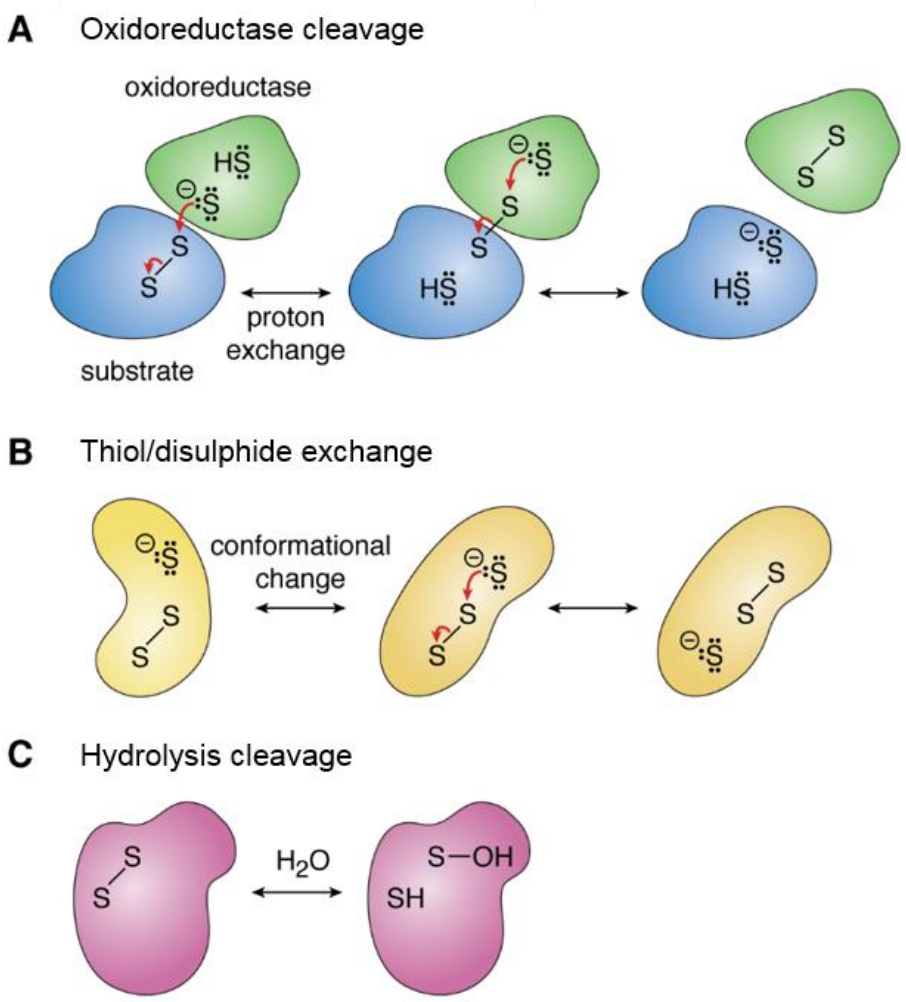

Figure 1.4 Mechanisms of cleavage of allosteric disulphides bonds.
A. An unpaired sulphur ion in an oxidoreductase (green) attacks one of the allosteric disulphide sulphur atoms in the substrate (blue). An intermediate bond between the sulphurs form temporarily. The allosteric disulphide bond in the substrate is reduced and the oxidoreductase sulphurs become oxidised. **B**. Conformational change brings an unpaired sulphur ion close to an allosteric disulphide bond in the same protein or between proteins. The sulphur ion attacks the allosteric disulphide and is reduced. **C**. Hydrolysis cleavage of the allosteric disulphide bond results its reduction and formation of a sulfenic acid/thiol pair. Source from: Chiu & Hogg, 2019.

1.3.2 Features of the allosteric disulphide bond

A classification system for disulphide bonds was designed when allosteric disulphides were first described (Schmidt et al., 2006) (**Figure 1.5**). Unlike protease cleavage sites, disulphide bonds are not readily identified from positions of cysteine residues in primary protein sequences. Instead, they can be identified from three-dimensional X-ray structures of the protein; disulphide bonds adopt certain configurations (Schmidt et al., 2006). Geometry of a disulphide bond is defined by two sets of three atoms linking two Cα atoms of the cystine residue, i.e. Cα–C$_\beta$–Sγ–Sγ'–C$_\beta'$–Cα', and five dihedral (χ) angles. The signs of the central three χ angles define whether the bonds are spirals (–,–,– or +,+,+), hooks (+,–,– or +,+,–) or staples (–,+,– or +,–,+). The sulphur–sulphur (S–S) bond χ angle determines whether the conformation is right-handed (+) (RH) or left-handed (–) (LH). As a result, there are 20 possible configurations for the disulphide bond (Chiu & Hogg, 2019; Chiu et al., 2015; Wong & Hogg, 2010) (**Figure 1.5A**). The –LHspiral configuration accounts for around one quarter of all disulphide bonds identified in the PDB and is associated with structural disulphide bonds. There are three emerging allosteric configurations, –RHstaple, –LHhook and –/+RHhook, which account for approximately 20% of all non-redundant disulphide bonds in the PDB (Schmidt et al., 2006), and approximately 80% of structurally defined allosteric disulphide bonds (**Figure 1.5B**). The tensile prestress in –RHstaple (-135 pN) and –/+RHhook (-221 pN) configurations was found to be relevant to disulphide reactivity (Schmidt et al., 2006; Zhou et al., 2014) (**Figure 1.5C**). The prestress is attributed to the stretching of the S–S bond and neighbouring α angles, indicative of disulphide reactivity and propensity for cleavage, and moreover, function of the protein (**Figure 1.5D**).

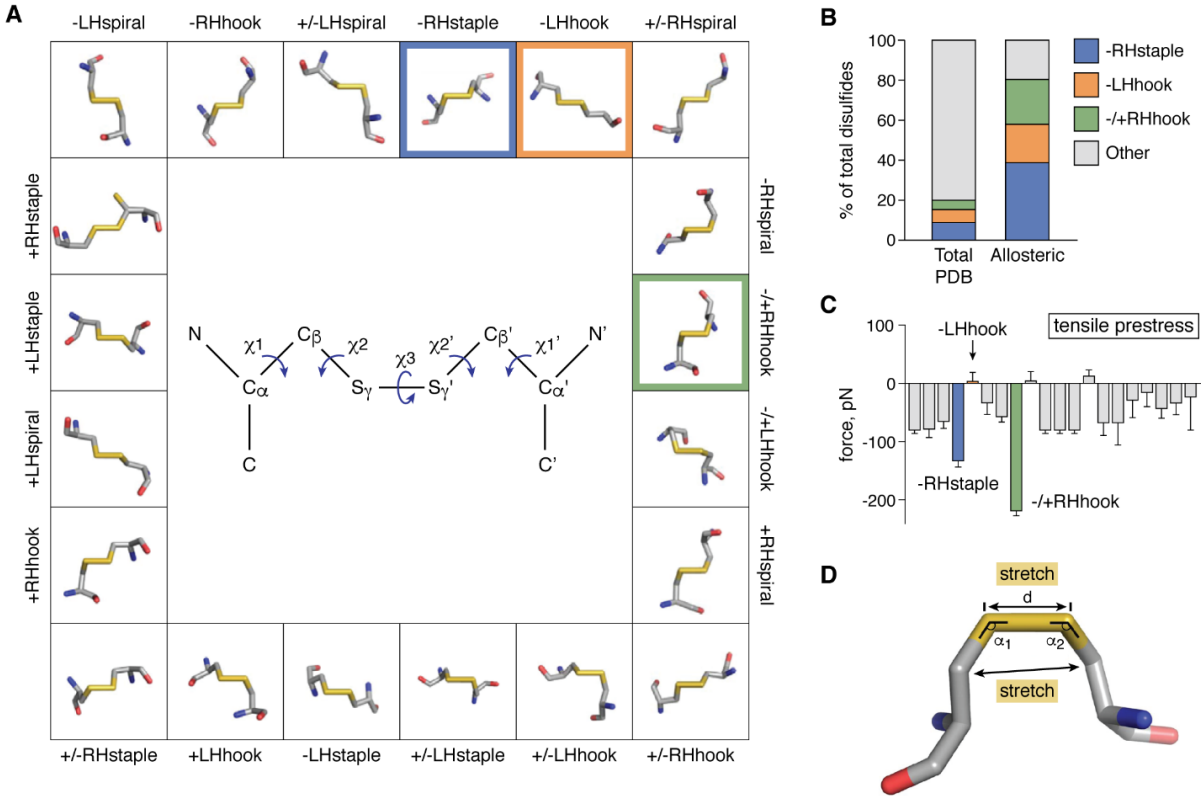

Figure 1.5 Classification of disulphide bonds and allosteric configurations.
A. Classification system of disulphide bonds using 5 dihedral (χ) angles of the cystine residue. There are 20 possible disulphide configurations. **B**. Incidence of the three allosteric disulphide conformations. The –RHstaple, –LHhook, and –/+RHhook configurations constitute approximately 20% of all disulphide bonds in the PDB, but approximately 80% of structurally defined allosteric bonds (n=32, (Pijning et al., 2018)). **C**. Mean tensile prestress of the 20 configurations was calculated using force distribution analysis (Zhou et al., 2014). The tensile prestresses on allosteric –RHstaple and –/+RHhook bonds are significantly higher than the other 18 configurations. **D**. Tensile prestress of –RHstaple and –/+RHhook disulphide bonds is the result of stretching of sulphur-sulphur bond length (d) and neighbouring α angles. Source from: Chiu & Hogg, 2019.

1.3.3 Disulphide bonds in Akt1

So far, about 40 allosteric disulphide bonds have been identified (Chiu & Hogg, 2019) (**Table 1.2**). Crystal structures of Akt1 show two disulphide bonds in the protein: one in the PH domain (Cys^{60}–Cys^{77}) and one in the kinase domain (Cys^{296}–Cys^{310}). The Cys^{296}–Cys^{310} disulphide bond is located in the kinase activation loop of Akt1, flanking the Thr^{308} phosphorylation site. Bioinformatic analyses of the Cys^{296}–Cys^{310} disulphide bond revealed a –LHspiral configuration, typical of a structural disulphide bond (Schmidt et al., 2006). Studies have shown oxidation of Cys^{296} and Cys^{310} residues led to Akt1 dephosphorylation through increased interaction with phosphatase PP2A; however, mutations of Cys^{296} and Cys^{310} to Ser did not affect Akt1 phosphorylation and downstream activity (Ahmad et al., 2014). The phospholipid binding region in the PH domain of Akt1 revealed the presence of another disulphide bond between Cys^{60} and Cys^{77} residues, adopting an archetypal allosteric –RHstaple configuration (Schmidt et al., 2006). As previously mentioned, the tensile prestress on the –RHstaple disulphide bond increases susceptibility to cleavage, suggesting its involvement in the function of Akt1 protein.

Table 1.2 Allosteric disulphide bonds that alter protein function in response to cleavage. Cleavage of allosteric disulphide bonds increases or decreases efficiency of ligand binding, substrate hydrolysis, proteolysis or formation of intermolecular disulphide bonds and homo- or hetero-oligomerisation of the protein.

Change	Protein	Disulphide Cys	Reference
Ligand binding	β2-glycoprotein I	288–326	(Ioannou et al., 2010)
	β3 integrin	177–184	(Passam et al., 2018)
	HIV gp120	126–196 296–331 385–418	(Auwerx et al., 2009; Azimi et al., 2010; Barbouche et al., 2003; Gallina et al., 2002; Ou & Silver, 2006; Reiser et al., 2012)
	CD4	130–159	(Matthias et al., 2002)
	CD44	81–101	(Kellett-Clarke et al., 2015)
	Glycoprotein 1b	4–17 209–248	(Li et al., 2018)
	Interleukin 4	46–99	(Plugis et al., 2018)
	Interleukin receptor subunit gamma	160-209	(Metcalfe et al., 2012)
	Thrombospondin 1	974–?	(Dieterich et al., 1997; Jin et al., 2011; Pinkas et al., 2007; Plugis et al., 2017; Yi et al., 2018)
	Tissue Factor	186–209	(Ahamed et al., 2006; Chen et al., 2006)
	Vitronectin	137–161 274–453	(Bowley et al., 2017)
	von Willebrand factor	1669–1670	(Butera et al., 2018)
Substrate hydrolysis	Adenosine-5'-phosphosulfate kinase	86–119	(Ravilious et al., 2012)
	Arylsulfate sulfotransferase	418–424	(Malojcić & Glockshuber, 2010)
	Botulinum neurotoxins	436–445	(Swaminathan & Eswaramoorthy, 2000)
	QueF	55–99	(Mohammad et al., 2017)
	Thiolase	88–378	(Kim et al., 2015)
	hTryptaseβ	191–220	(Cook et al., 2013)
	Methionine aminopeptidase 2	228–448	(Chiu et al., 2014b)
	Prolyl cis-trans isomerase, AtFKBP13	106–111	(Gopalan et al., 2004)
	Transglutaminase 2	370–371 230–370	(Pinkas et al., 2007)
	Lon protease	617–691	(Nishii et al., 2015)
	CgDapF	83–221	(Sagong & Kim, 2017)
	SAMHD1	341–350	(Mauney et al., 2017)

Proteolysis	Angiotensinogen	18–138	(Zhou et al., 2010)
	Factor XI	362–482	(Giannakopoulos et al., 2012)
	major histocompatibility complex class I chain-related A (MICA)	202–259	(Kaiser et al., 2007)
	Plasmin(ogen)	512–536 462–541	(Butera et al., 2014)
Oligomerisation	CD4	130–159	(Matthias et al., 2002)
	Vascular endothelial growth factor C & D	156–165	(Chiu et al., 2014a)
	LYVE-1	201–201	(Banerji et al., 2016)

Source from: Chiu & Hogg, 2019.

1.4 Hypothesis

Akt plays a central role in glucose metabolism, cell survival and angiogenesis and is often hyper-activated in cancer cells. Akt is activated at the plasma membrane via binding to PIP_3 through its PH domain. Dissociation of Akt from the plasma membrane leads to PH domain-mediated autoinhibition of the kinase by a mechanism that is currently unknown. This thesis aims to clarify the mechanism of Akt1 autoinhibition and further expand our knowledge of regulation of Akt1 activity. A potential allosteric Cys^{60}–Cys^{77} disulphide bond was identified in the PH domain of Akt1. I hypothesise that the PH domain Cys^{60}–Cys^{77} disulphide is an allosteric bond that regulates autoinhibition and functioning of the kinase. My goal was to characterise the role of the Cys^{60}–Cys^{77} disulphide bond in Akt1 function.

1.5 Specific Aims

- Characterise the features of the Akt1 Cys^{60}–Cys^{77} disulphide bond in existing crystal structures of the protein.

- Elucidate the role of the Akt1 Cys^{60}–Cys^{77} disulphide bond in PIP_3 and plasma membrane binding.

- Elucidate the role of the Akt1 Cys^{60}–Cys^{77} disulphide bond in Akt1 phosphorylation, Akt1 substrate activation, and transformation of mouse fibroblasts.

- Elucidate the role of the Akt1 Cys^{60}–Cys^{77} disulphide bond for angiogenesis, survival and development in zebrafish embryos.

2. Materials & Methods

2.1 Bioinformatics and Structural Biology

2.1.1 Analysis of missing labile disulphide bonds in X-ray structures

All X-ray structures released in the PDB as of June 2017 were assembled. The list was culled to exclude all structures with a resolution >2.5 Å. Structures that had been prepared and crystallised in the presence of 1,4-dithiothreitol (DTT) or any other reducing agent were removed from the analysis.

To identify missing disulphide bonds, each PDB chain was first mapped to a corresponding UniProtKB accession and protein sequence using the PDBSWS tool (Martin, 2005). Subsequently for each UniProtKB accession, a list of corresponding PDB chains and disulphide bonds present in any of these PDB chains were recorded. Disulphide bonds in structures were determined by the presence of an SSBOND line in the PDB file. Finally, for each disulphide bond that has now been associated with each UniProtKB protein, all PDB chains mapped to this corresponding UniProtKB accession were analysed to determine whether the disulphide bond is present or missing. If the disulphide bond is missing within a particular PDB chain, that structure was further analysed to establish whether the bond is missing due to a truncated or mutated PDB chain protein sequence. The annotation of each disulphide bond was performed as described previously (Schmidt et al., 2006). If the sequence is not truncated or mutated, the PDB chain was annotated as missing in the same crystal structure if the disulphide bond is present in another chain in the same PDB file. Otherwise, it was annotated as missing in a different crystal structure if the disulphide bond is only present in a different PDB file. A schematic diagram illustrating the analysis is shown in **Figure 2.1**. For the analysis of disulphide bond features, a list of culled disulphide bonds from all PDB structures was used. To define the set of culled disulphide bonds, the PISCES PDB culling server was used with a

cut-off of 90% homology, maximum resolution of 2.5 and R value of 1.0. Subcellular localisation of proteins were obtained from the UniProtKB database. Pathways enriched in human proteins containing labile disulphide bonds were identified using the DAVID Functional Annotation Tool and KEGG pathway analysis (Huang et al., 2009a, 2009b). A Python script was developed implementing the above analysis and can be downloaded from: https://github.com/jwon7011/missing_disulfide

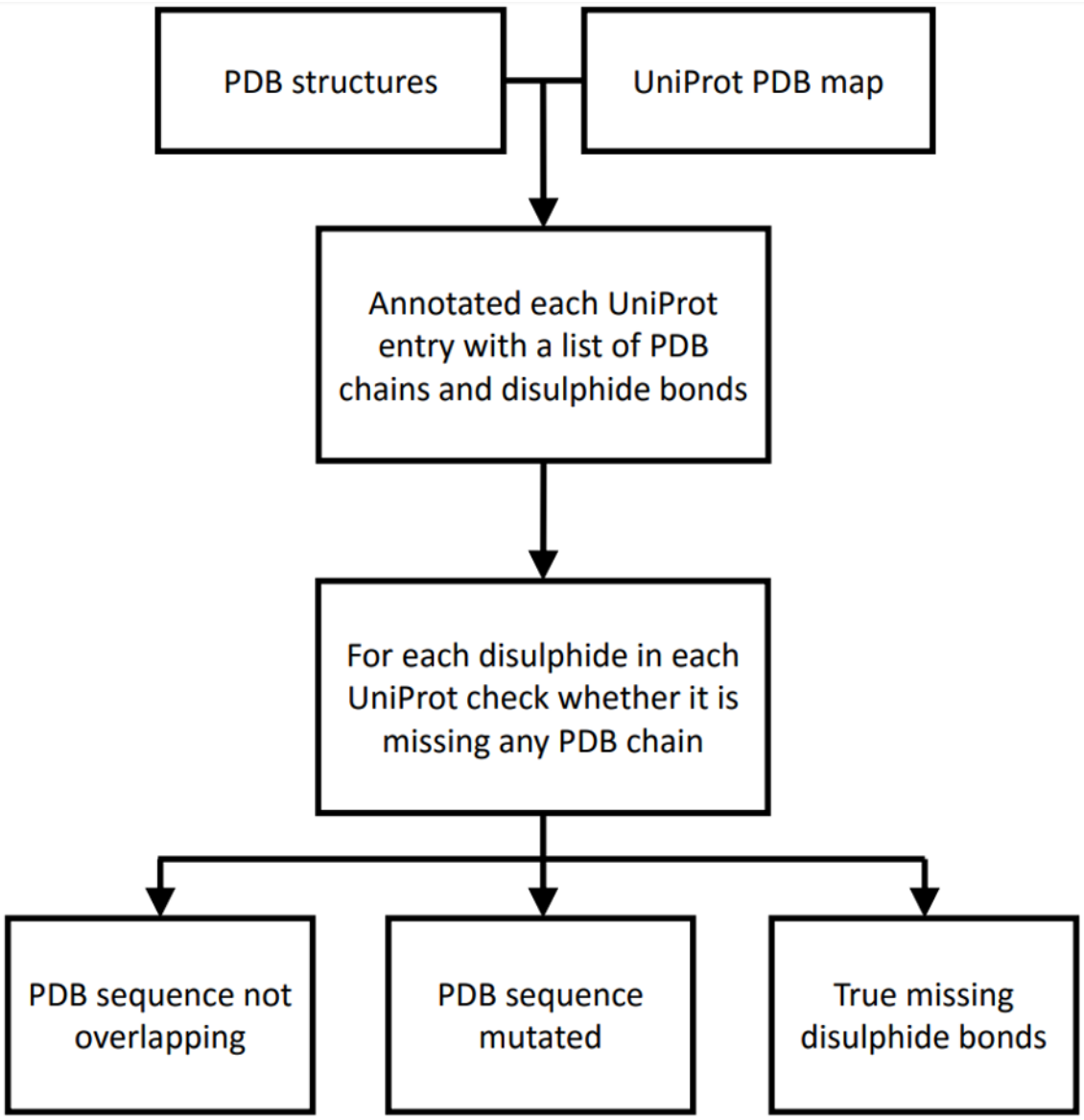

Figure 2.1 Flow chart for mining of PDB X-ray structures for labile disulphide bonds.

2.2 Molecular Cloning

Aerosol Barrier Tips were purchased from Interpath Services. Greiner Bio-One™ EasyLoad™ Refill Universal Pipette Tips were purchased from Greiner Bio-One. BD Falcon™ Conical Tubes were purchased from In Vitro Technologies. Microcentrifuge Tubes were purchased from Scientific Specialties Inc. (SSIbio). Corning® Costar® Stripette® serological pipettes and custom designed oligonucleotides were purchased from Sigma-Aldrich. Restriction digest enzymes and polymerase chain reaction (PCR) reagents were purchased from NEB. cOmplete™, Mini, ethylenediaminetetraacetic acid (EDTA)-free, Protease Inhibitor Cocktail and PhosSTOP™ Phosphatase Inhibitor tablets were purchased from Roche. Gateway™ BP and LR Clonase™ II Enzyme mixes and proteinase K were purchased from Thermo Fisher Scientific.

Plasmid *pcDNA-DEST53–TagRFP-T–WTAkt1* DNA construct containing the WTAkt1 insert was kindly provided by the James laboratory (University of Sydney). Lentiviral gene ontology vector *LeGO-iG2* containing enhanced green fluorescent protein internal ribosome entry site (EGFP-IRES) expression (Weber et al., 2008; Weber et al., 2012) was kindly provided by the Pimanda laboratory (University of New South Wales). The C-terminal EGFP 8× His-tag vector *pWaldo-TEV-GFPe* was kindly provided by the Jormakka laboratory (Centenary Institute). Gateway *Tol2* transposon cloning vectors (Kwan et al., 2007): *pDONR™221, pDestTol2, p5E/ubb, p3E/p2a-tdTomato,* and *Tol2 transposase* DNA constructs were kindly provided by the Oehlers laboratory (Centenary Institute). DNA plasmids were generated in One Shot™ *ccd*B Survival™ 2 $T1^R$ (Invitrogen) and Alpha-Select Gold Efficiency *E. coli* competent cells (Bioline) with the appropriate antibiotic.

2.2.1 Construction of full-length WTAkt1 and MyrAkt1 plasmids

Design of *WTAkt1* (wild-type) and *MyrAkt1* (myristoylated) oligonucleotides containing a HA-epitope tag sequence at the 5' end, was based off cDNA (complementary deoxyribonucleic acid) cloning performed previously by Liu et al., 2004 (**Table 2.1**). Full-length *WTAkt1* was inserted into the empty lentiviral *LeGO-iG2* vector. Each PCR reaction contained 10 pmol of the appropriate forward and reverse oligonucleotide, 5 ng of *pcDNA-DEST53–TagRFP-T–WTAkt1* DNA template, 1× Phusion® HF (high-fidelity) buffer containing 50 mM $MgCl_2$, 200 µM deoxyribose nucleoside triphosphate (dNTP) mix, amplification was started by the addition of 2 U/µl of Phusion® Hot Start II DNA Taq Polymerase and subjected to 15 s denaturation at 98°C, 20 s annealing at 66°C and 1 min extension at 72°C for 25 cycles on the Mastercycler nexus gradient (Eppendorf). PCR products were purified with Wizard® SV Gel and PCR Clean-Up System (Promega). Purified product of 1 µg of *WTAkt1* insert and 3 µg of empty *LeGO-iG2* vector were digested at 37°C for 2 h with 10 U of high fidelity enzymes BamHI and EcoRI, 1× bovine serum albumin (BSA), 1× CutSmart Buffer in MilliQ H_2O. Digested products were purified with SV Gel and PCR Clean-Up System. *LeGO-iG2* vector and *WTAkt1* insert were ligated using T4 DNA ligase, 10× T4 ligase buffer in MilliQ H_2O. Reaction was repeated with forward and reverse Lck-tag sequence oligonucleotides to construct *LeGO-iG2–MyrAkt1*.

Table 2.1. Oligonucleotides designed for lentiviral full-length *LeGO-iG2–Akt1* plasmids.
BamHI and EcoRI restriction enzymes are underlined. HA-epitope tag sequence is indicated in orange. Lck-tag sequence is highlighted in yellow. Design adapted from Liu et al., 2004.

DNA template	Oligonucleotide	Sequence 5’ to 3’
pcDNA-DEST53–TagRFP-T–*WTAkt1*	WTAkt1F (BamHI)	CCGGGATCCATGGCCGCTTATCCCTATGACGTCCCGGACTATGCA CCCATGAGCGACGTGGCTATTGTGAA
	MyrAkt1F (BamHI)	CCGGGATCCATGGGCTGTGGCTGCAGCTCACACCCGGAAGATGAC GCCGCTTATCCCTATGACGTCCCGGACTATGCACCCATGAGCGAC GTGGCTATTGTGAA
	Akt1R (EcoRI)	ATAAGAATGAATTCTCAGGCCGTGCTGCTGGCC

2.2.2 Construction of full-length disulphide bond Akt1 mutant plasmids by site-directed ligase independent mutagenesis (SLIM) hybridisation

Mutagenic oligonucleotides were designed to contain the point mutation of cysteine to serine at codon 60 (Cys60Ser), cysteine to serine at codon 77 (Cys77Ser), threonine to alanine at codon 308 (Thr308Ala) and serine to alanine at codon 473 (Ser473Ala) (**Table 2.2**). In two separate PCR reactions, 10 pM of each pair of tailed ($_T$) and non-tailed ($_S$) oligonucleotides hybridised to 5 ng *LeGO-iG2–WTAkt1* DNA template in 5× HF buffer containing 50 mM $MgCl_2$, 200 µM dNTP mix, amplification was started by the addition of 2 U/µl of DNA Taq Polymerase and subjected to 15 s denaturation at 98°C, 20 s annealing at 68°C and 5.5 min extension at 72°C for 25 cycles on the Mastercycler nexus gradient. This resulted in un-methylated mutant plasmids. 5 U of DpnI, a type IIM restriction enzyme was incubated for 2h at 37°C targeting and cutting methylated parental plasmids. SLIM hybridisation reactions contained both PCR products, 1× H-buffer (300 mM NaCl, 50 mM Tris, pH 9.0, 20 mM EDTA, pH 8.0) in MilliQ H_2O (Chiu et al., 2004; Chiu et al., 2008). Control group reactions contained only the single PCR product in H-buffer. Conditions for optimal hybridisation were denaturation at 99°C for 3 min, followed by two cycles of 5 min at 65°C and 15 min at 30°C.

Table 2.2 Oligonucleotides designed for site-directed ligase-independent mutagenesis hybridisation.
The overhang of 18 nucleotides is underlined. Site-directed mutagenesis is bolded. *LeGO-iG2* vector is highlighted in blue.

DNA template	Modification	Oligonucleotide	Sequence 5' to 3'
LeGO-iG2–WTAkt1	Point mutation of Cys^{60} to Ser	Cys60SerF	**A**GCCAGCTGATGAAGACGGAGCG
		Glu66F	GAGCGGCCCCGGCCCAACA
		Cys60SerR	CGTCTTCATCAGCTGGC**T**CTGCGCCACAGAGAAGTTGTTG
		Leu52R	CTGCGCCACAGAGAAGTTGTTG
	Point mutation of Cys^{77} to Ser	Cys77SerF	**A**GCCTGCAGTGGACCACTGTCAT
		Val83F	GTCATCGAACGCACCTTCCATG
		Cys77SerR	AGTGGTCCACTGCAGGC**T**GCGGATGATGAAGGTGTTGGG
		Pro70R	GCGGATGATGAAGGTGTTGGG
	Point mutation of Thr^{308} to Ala	Thr308AlaF	**G**CCTTTTGCGGCACACCTGAGTA
		Tyr326F	GAGTACCTGGCCCCCGAGGT
		Thr308AlaR	AGGTGTGCCGCAAAAGGCCTTCATGGTGGCACCGTCCTTG
		Lys307R	CTTCATGGTGGCACCGTCCTTG
	Point mutation of Ser^{473} to Ala	Ser473AlaF	**G**CCTACTCGGCCAGCAGCAC
		Thr479F	ACGGCCTGAGAATTCCTGCAGG
		Ser473AlaR	GCTGCTGGCCGAGTAGGCGAACTGGGGGAAGTGGGGCCT
		Phe472R	GAACTGGGGGAAGTGGGGCCT

2.2.3 Construction of truncated Akt1-PH plasmids for protein expression

To construct truncated PH domain of Akt1 plasmids (Akt1-PH), oligonucleotides were designed to contain amino acid residues 1-121 (**Table 2.3**). Wild-type Akt1-PH (WT-PH) was first to be constructed. Each PCR reaction contained 10 pM of the appropriate forward and reverse oligonucleotide, 5 ng of *pWaldo-TEV-GFPe* DNA template, 1× Phusion® HF buffer containing 50 mM $MgCl_2$, 200 µM dNTP mix, amplification was started by the addition of 2 U/µl of Phusion® Hot Start II DNA Taq Polymerase and subjected to 30 s at 98°C, followed by 25 cycles of 15 s denaturation at 98°C, 20 s annealing at 62°C and 1 min extension at 72°C, and then a further 10 min at 72°C on the Mastercycler nexus gradient (Eppendorf). PCR products were purified with Wizard® SV Gel and PCR Clean-Up System (Promega). Purified product of 1 µg of the *WT-PH* insert and 3 µg of empty *pWaldo-TEV-GFPe* vector were digested at 37°C for 2 h with 10 U of high fidelity enzymes EcoRI and XhoI, 1× BSA, 1× CutSmart Buffer in MilliQ H_2O. Digested products were purified with SV Gel and PCR Clean-Up System. *pWaldo-TEV-GFPe* vector and *WT-PH* insert were ligated using T4 DNA ligase, 10× T4 ligase buffer in MilliQ H_2O to construct *pWaldo-TEV-GFPe–WT-PH*. Truncated reduced Akt1-PH mutants *pWaldo-TEV-GFPe–C60S-PH, pWaldo-TEV-GFPe–C77S-PH* and *pWaldo-TEV-GFPe–C60SC77S-PH* plasmids were constructed by SLIM hybridisation as previously described using the *pWaldo-TEV-GFPe–WT-PH* DNA template (**Section 2.2.2**).

Table 2.3 Oligonucleotides designed for truncated *Akt1-PH* plasmids.
EcoRI and XhoI restriction enzymes are underlined. Start and stop codons are italicised.

Destination vector	Oligonucleotide	Sequence 5’ to 3’
pWaldo-TEV-GFPe	Akt1-PHF (XhoI)	CGCTCGAGCGGCTCGAG*ATG*AGCGACGTGGCTATTGTGA
	Akt1-PHR (EcoRI)	CCGGAATTC*TTA*CCGGAAGTCCATCTCCTCCT

2.2.4 Gateway™ BP and LR cloning

Recombinant Gateway™ BP and LR cloning was used to generate *Tol2* transposon gene transfer plasmids designed for zebrafish embryo microinjections. Gateway *Tol2* transposon cloning vectors (Kwan et al., 2007) *pDONR™221, pDestTol2, p5E/ubb, p3E/p2a-tdTomato,* and *Tol2 transposase* were generously provided by the Oehlers laboratory (Centenary Institute). DNA plasmids were generated in One Shot™ *ccd*B Survival™ 2 $T1^R$ (Invitrogen) and Alpha-Select Gold Efficiency *E. coli* competent cells (Bioline). Gateway™ BP and LR Clonase™ II Enzyme mixes and proteinase K were purchased from Thermo Fisher Scientific.

Designed oligonucleotides of Gateway™ *att*B sequences flanking *Akt1* to construct middle-entry *Akt1* (*pME/Akt1*) clones (**Table 2.4**). Each PCR reaction contained 10 pM of the appropriate forward and reverse *att*B oligonucleotides, 5 ng of *LeGO-iG2–WTAkt1* DNA template, 1× HF buffer containing 50 mM $MgCl_2$, 200 µM dNTP mix; amplification was started by the addition of 2 U/µl of DNA Taq Polymerase and subjected to 15 s denaturation at 98°C, 20 s annealing at 66°C and 1 min extension at 72°C for 25 cycles on the Mastercycler nexus gradient. PCR product (50-150 ng) and donor vector *pDONR™221* (100 ng) were combined with BP clonase mix in TE buffer (10 mM Tris-HCl, pH 8.0, 1 mM EDTA) to generate *att*L recombination sites (**Figure 2.2A**). Reaction mix was incubated for 1 h at 25°C. Reaction was stopped by addition of proteinase K at 37°C for 10 min. Mix was transformed in Alpha-Select Gold Efficiency *E. coli* competent cells and selected with 50 µg/ml kanamycin. Plasmids were sequenced by Ramaciotti Centre for Genomics and confirmed with DNA Baser Sequence Assembler. Experiment was repeated to generate full-length constitutively active mutant *pME/MyrAkt1*, disulphide bond mutants *pME/C60S-Akt1*, *pME/C77S-Akt1* and *pME/C60SC77S-Akt1* and constitutively inactive mutant *pME/T308AS473A-Akt1* middle-entry *Akt1* clones.

Transfer of the *WTAkt1* insert from the middle-entry *pME/WTAkt1* clone into the destination vector required a second recombination reaction. Destination vector *pDestTol2* (41 ng) containing *att*R recombinant sites, *Tol2* transposon backbone and *ccdB* toxin gene, was mixed with *pME/WTAkt1* (41 ng) containing *att*L sites from the BP clonase reaction, 5'-entry clone *p5E/ubb* (41 ng) containing *att*L/R recombinant sites and the ubiquitin zebrafish promoter and 3'-entry clone *p3E/p2a-tdTomato* (26 ng) containing *att*R/L recombinant sites and fluorescent protein marker tandem tomato polyadenylation tailing (**Figure 2.2B**). Recombination of the transgenic DNA construct was executed with the addition of LR clonase mix in TE buffer to generate *pDestTol2/ubb:WTAkt1-p2a-tomato*. Reaction was incubated overnight at 25°C. Reaction was stopped by the addition of proteinase K at 37°C for 10 min. Mix was transformed in Alpha-Select Gold Efficiency *E. coli* competent cells and selected with 100 µg/ml ampicillin. Experiment was repeated to generate full-length constitutively active mutant *pDestTol2/ubb:MyrAkt1-p2a-tomato*, disulphide bond mutants *pDestTol2/ubb;C60S-Akt1-p2a-tomato, pDestTol2/ubb:C77S-Akt1-p2a-tomato* and *pDestTol2/ubb:C60SC77S-Akt1-p2a-tomato* and constitutively inactive mutant *pDestTol2/ubb:T308AS473A-Akt1-p2a-tomato* gene transfer constructs.

Table 2.4 Designed *att*B oligonucleotides for Gateway™ BP cloning.
Lck-tag sequence is highlighted yellow. *att*B sequences are underlined. Start codon is italicised. Stop codon is omitted.

Donor vector	Oligonucleotide	Sequence 5' to 3'
pDONR™221	attB1 Akt1F	GGGGACAAGTTTGTACAAAAAAGCAGGCTTC*ATG*AGCGACGTGGCTATTGTGAA
	attB1 MyrAkt1F	GGGGACAAGTTTGTACAAAAAAGCAGGCTTCATGGGCTGTGGCTGCAGCTCA
	attB2 Akt1R	GGGGACCACTTTGTACAAGAAAGCTGGGTCGGCCGTGCTGCTGGCCGAG

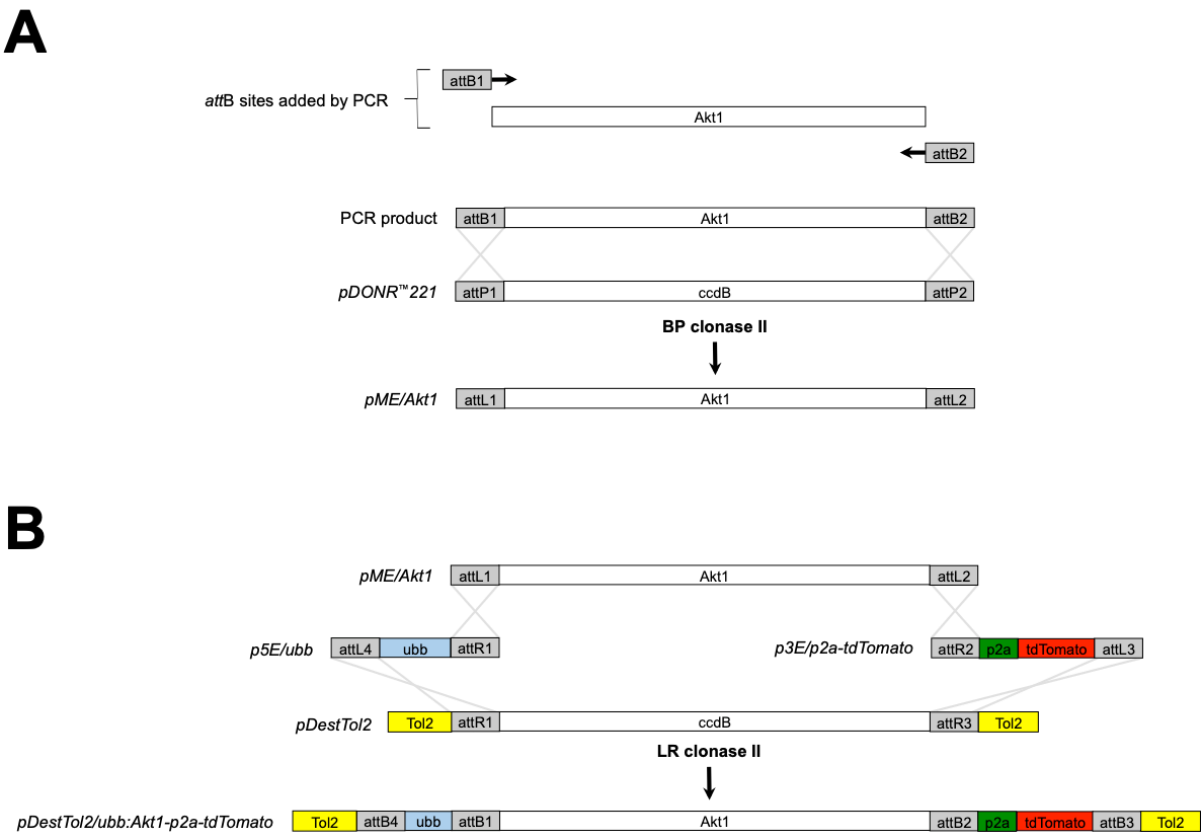

Figure 2.2 Gateway™ BP and LR recombination cloning of middle-entry *pME/Akt1* and transgenic *pDestTol2/ubb:Akt1-p2a-tomato* constructs.
A. Construction of middle-entry *Akt1* (*pME/Akt1*) clones. *att*B recombination sites flanking *Akt1* was added by PCR. Gateway™ recombination cloning of PCR product and donor vector *pDONR™221* by BP clonase II. **B.** Construction of *pDestTol2/ubb:Akt1-p2a-tomato* transgenic clones for zebrafish injections. Gateway™ recombination cloning of *pME/Akt1*, 5'entry ubiquitin zebrafish promoter *p5E/ubb*, 3'entry tandem-Tomato polyadenylation tailing *p3E/p2a-tdTomato* and gene transfer vector backbone *pDestTol2* by LR clonase II.

2.2.5 Heat shock transformation of E. coli

DNA plasmids were transformed into *E. coli* competent cells and a selective pressure as directed by *Curr Protocols Mol Biol* (Seidman et al., 2001). 1 µg of DNA plasmid was mixed with the appropriate *E. coli* competent cells and incubated on ice for 25 min. Competent cells were heat-shocked at 42°C in a water bath for 45 s and immediately incubated on ice for 2 min. Competent cells were topped-up with sterilised Luria-Burtani (LB) broth, Miller (BD Difco™) and resuscitated for 45 min at 37°C in the Bioline Incubator Shaker, Bench Top Style With Hinged Lid (Bioline) at 250 rpm. Competent cells were plated on sterile LB (BD Difco™) agar (Sigma-Aldrich) petri dishes (Greiner Bio-One) containing the appropriate antibiotic (100 µg/ml ampicillin, 50 µg/ml kanamycin and/or 20 µg/ml chloramphenicol) and incubated overnight at 37°C. A single colony was picked with a clean pipette tip and ejected into LB broth containing the appropriate antibiotic and grown overnight at 37°C in the Bioline Incubator Shaker at 250 rpm. Plasmids were extracted and purified from the competent cells using the Wizard® Plus SV Minipreps DNA Purification System (Promega). DNA plasmids were sequenced by Ramaciotti Centre for Genomics (University of New South Wales) and confirmed with Align Sequence Nucleotide BLAST (National Center for Biotechnology Information [NCBI]) and DNA Baser Sequence Assembler.

2.2.6 Protein expression in E. coli

Truncated *pWaldo-TEV-GFPe–Akt1-PH* plasmids were transformed into Rosetta-gami™ 2 (DE3) *E. coli* competent cells (Novagen) as previously described. Culture was grown in LB broth containing 50 µg/ml kanamycin and 20 µg/ml chloramphenicol in the Bioline Incubator Shaker at 37°C until OD_{600} reached 0.5. Protein expression was induced with 250 µM isopropyl β-D-1-thiogalactopyranoside (IPTG) (Sigma-Aldrich) and incubated at 20°C in the Bioline Incubator Shaker 250 rpm for 20 h. Induced cells were centrifuged at 2,500 × *g* for 10 min at 4°C and supernatant was removed. Cells were lysed in lysis buffer (50 mM Tris-HCl, pH 7.5, 300 mM NaCl), supplemented with 5 mM phenylmethylsulfonyl fluoride (PMSF) and 1× cOmplete™, Mini, EDTA-free, Protease Inhibitor Cocktail (Roche). Cell lysates were obtained by sonication (Branson Digital Sonifier), sonicated 3× with 1 min intervals at 4°C. Lysates were centrifuged to separate soluble and insoluble fractions at 13,000 × *g* for 10 min at 4°C. Supernatant was collected and adsorbed onto 0.15 ml TALON Metal Affinity Resin (GE Healthcare Life Sciences). The beads were washed with wash buffer (50 mM Tris, pH 7.5, 300 mM NaCl, 100 mM imidazole), first wash 3 ml and subsequent washes (2×) 1 ml. Akt1-PH EGFP recombinant proteins were eluted in elution buffer (50 mM Tris, pH 7.5, 300 mM NaCl, 250 mM imidazole) and a total of 150 µl protein fraction was collected. Fraction was analysed by SDS-PAGE (method below) on the 4-12% polyacrylamide gel. Protein fractions were pooled and transferred into Amicon Ultra-0.5 Centrifugal Filter Unit (Merck) and centrifuged at 14,000 × *g* for 20 min at 4°C. Protein was centrifuged at 1,000 × *g* for 2 min at 4°C in a clean microcentrifuge tube. Filtered elutions were dialysed with Slide-A-Lyzer Mini Dialysis Devices (Thermo Fisher Scientific) against 1× Dulbecco's phosphate-buffered saline (PBS) (Gibco) overnight. Truncated Akt1-PH recombinant proteins were stored at −80°C.

2.2.7 RNA transcription

Tol2 transposase DNA plasmid was linearised with restriction enzyme NotI at 37°C for 2 h. Digested DNA product was purified using the SV Gel and PCR Clean-Up System. Messenger RNA (mRNA) was transcribed from digested DNA product using the mMESSAGE mMACHINE SP6 Transcription Kit (Invitrogen). Capped reactions were purified using the NucleoSpin® RNA clean-up (Macherey-Nagel) and resuspended in RNase-free H_2O.

2.2.8 Nucleic acid quantitation

Purity and concentration of DNA, RNA or proteins were measured by the NanoDrop 1000 Spectrophotometer (Thermo Fisher Scientific). Ratio of absorbance was measured at 260/280 nm; calculated ratio of >1.8 was accepted as pure DNA and calculated ratio of >2.0 was accepted as pure RNA. A secondary purity absorbance ratio was measured at 260/230 nm; calculated ratio between the range of 1.8-2.2 was accepted as pure. Absorbance of protein was measured at 280 nm.

2.3 Tissue Culture

Corning® Cell Culture Flasks, Corning® tissue-culture treated culture microplates and dishes, flat bottom were purchased from Sigma-Aldrich. BD Falcon™ 12 x 75 mm Tube with Cell Strainer Cap were purchased from In Vitro Technologies. Nunc® CryoTubes® cryogenic vials were purchased from Nunc.

NIH/3T3 mouse embryonic fibroblast cells, HEK293T human embryonic kidney cells and 3T3-L1 mouse embryonic fibroblast cells were purchased from the American Type Culture Collection (ATCC) and cleared of any contamination or mycoplasma.

Third generation lentiviral packaging and envelope plasmids *pMDLg/pRRe, pRSVRev* and *pMD2.VSV-G* were generously provided by the Rasko lab (Centenary Institute).

2.3.1 Tissue culture maintenance

Unless otherwise specified, cells were cultured in Dulbecco's Modified Eagle Media (DMEM) (Gibco) with high glucose, supplemented with 1× GlutaMAX™ (Gibco) and 10% (v/v) fetal bovine serum (FBS) (Gibco), containing 1% (v/v) penicillin-streptomycin solution (Thermo Fisher Scientific) at 37°C with 95% air atmosphere and 5% CO_2. Cells were washed with 1× PBS. Cells were passaged at 80-90% confluency and detached with 1× TrypLE Express, phenol red (Thermo Fisher Scientific) for 1 min at 37°C, and quenched with fresh DMEM. Cells (1.0×10^6) were frozen down in 10% (v/v) dimethyl sulfoxide (DMSO) and 20% (v/v) FBS in DMEM into cryogenic vials to be stored in liquid nitrogen for later use.

2.3.2 Lentiviral production and cell transduction

HEK293T cells (8.0×10^5 cells/T25 cm^2 flask) were co-transfected with 1.13 µg of DNA plasmid: *LeGO-iG2* (vector control), *LeGO-iG2–WTAkt1*, *LeGO-iG2–MyrAkt1*, *LeGO-iG2–C60S-Akt1*, *LeGO-iG2–C77S-Akt1*, *LeGO-iG2–C60SC77S-Akt1* or *LeGO-iG2–T308AS473A-Akt1*; with packaging and envelope plasmids *pMDLg/pRRe*, *pRSVRev* and *pMD2.VSV-G* in Opti-MEM Reduced Serum Media (Gibco), containing 30 µg polyethylenimine (PEI) for 24 h. Opti-MEM was removed, and cells were replenished with DMEM. Lentiviral particles produced in the media were collected after 72 h and purified with a 0.45 µm membrane filter (EMD Millipore) before infecting NIH/3T3 fibroblasts (6.0×10^5 cells/T75 cm^2 flask) in the presence of 4 µg/ml Polybrene (hexadimethrine bromide). Viral particles were removed from the fibroblasts and replenished with DMEM. Cells were grown in a T175 cm^2 flask up to 80% confluency. Transduced NIH/3T3 fibroblasts were sorted with the BD FACSAria™ II Flow Cytometer (Becton Dickinson Biosciences). NIH/3T3 fibroblasts expressing EGFP were collected and re-seeded in a T25 cm^2 flask in DMEM.

2.3.3 alamarBlue™ cell proliferation assay

NIH/3T3 fibroblasts were seeded at 2.0×10^4 cells/96-well clear-bottom plate in DMEM. At 72 h, alamarBlue™ reagent (1:2) was directly added to the cells and incubated for a further 2 h at 37°C. Fluorescence was read at Ex/Em 530/590 nm on the Infinite M1000 PRO plate reader (TECAN).

2.3.4 Soft agar colony formation

Agar powder (Sigma-Aldrich) dissolved in MilliQ H_2O was sterilised before use. Sterilised 1.6% (w/v) agar was melted in the microwave and cooled in the 37°C water bath right before use. The first layer of agar was prepared by mixing 1.6% (w/v) agar and 2× DMEM (1:1), and deposited into a 6-well flat-bottom plate. This layer was left to solidify for 30 min at room temperature. Sterilised 0.6% (w/v) agar was melted in the microwave and cooled in the 37°C water bath right before use. The upper layer containing NIH/3T3 fibroblasts was prepared by mixing 0.6% agar (w/v) and 2× DMEM (1:1), and was deposited into each well (2.0×10^4 cells/well). This layer was left to solidify for 30 min at room temperature and then incubated at 37°C with 90% air atmosphere and 5% CO_2. DMEM was carefully added on top of the agar twice weekly to prevent desiccation. 21 days after seeding, cells were fixed in 4% (v/v) formaldehyde for 30 min at room temperature and imaged on the Axio Vert.A1 microscope (ZEISS).

2.3.5 Insulin stimulation

NIH/3T3 fibroblasts were seeded at 2.5×10^6 cells/100 mm dishes in DMEM. At 24 h, cells were gently washed with 1× PBS, serum-starved with DMEM supplemented with 1× GlutaMAX™, no FBS for 2 h at 37°C and then stimulated with 10 nM of human recombinant

insulin (Sigma-Aldrich) for 20 min. DMEM and insulin was removed and cells were washed with 1× PBS.

2.3.6 Preparing Matrigel®

Sterile dishes, plastics and reagents were pre-chilled in the fridge the night before preparation. Corning® Matrigel® Matrix (Sigma-Aldrich) was thawed and diluted with ice-cold 1× PBS (1:50). 6-well plates and 35 mm glass-bottom dishes were coated with Matrigel® and then incubated for 2 h at room temperature. Coated plates were washed twice with room temperature 1× PBS prior to use.

2.3.7 Electroporation

3T3-L1 fibroblasts were seeded in 100 mm dishes at 37°C with 90% air atmosphere and 10% CO_2. Confluent dishes of fibroblasts were reseeded into Matrigel® coated 6-well plates. At 120 h, cells were differentiated in DMEM supplemented 0.22 µM dexamethasone, 100 ng/ml biotin, 2 µg/ml insulin and 500 µM 3-isobutyl-1-methylxanthine (IBMX) for 72 h. Media was replaced with DMEM supplemented with 2 µg/ml insulin for 72 h. Differentiated 3T3-L1 adipocytes were replenished with fresh DMEM daily. At 7 days post-differentiation, 3T3-L1 adipocytes were trypsinised with 5× trypsin-EDTA for 5-10 min at 37°C, and quenched with fresh DMEM. 3T3-L1 adipocytes were centrifuged at 150 × *g* for 5 min and washed twice with 1× PBS. Cell pellets were resuspended in Electroporation Buffer (20 mM HEPES, 135 mM KCl, 2 mM $MgCl_2$, 0.5% (v/v) Ficol 400, 1% (v/v) DMSO, 2 mM ATP and 5 mM glutathione, pH 7.6) and 5-10 µg of DNA plasmid: *pcDNA-DEST53–TagRFP-T–WTAkt2*, *pcDNA-DEST53–TagRFP-T–C60S-Akt2*, *pcDNA-DEST53–TagRFP-T–C77S-Akt2* or *pcDNA-DEST53–TagRFP-T–C60SC77S-Akt2*. 3T3-L1 adipocytes were electroporated at 200 mV for 20 ms and then plated on 35 mm glass-bottom dishes coated with Matrigel®.

2.3.8 Total internal reflection fluorescence (TIRF) microscopy

Live-cell imaging experiments were performed 48 h post-electroporation as described by Norris and colleagues (Norris et al., 2017). TIRF microscopy was performed on the Nikon Ti-LAPP H-TIRF module (Nikon), equipped with an Okolab Cage Incubator (Okolab) and temperature control. 3T3-L1 adipocytes expressing *pcDNA-DEST53–TagRFP-T–WTAkt2, pcDNA-DEST53–TagRFP-T–C60S-Akt2, pcDNA-DEST53–TagRFP-T–C77S-Akt2* and *pcDNA-DEST53–TagRFP-T–C60SC77S-Akt2* were serum-starved in FluoroBrite DMEM (Gibco) supplemented with 0.2% (v/v) BSA and GlutaMAX™ for 2 h at 37°C in 10% CO_2 before stimulation with 1 nM and 100 nM insulin at 10 and 20 min time points, respectively, using a custom-made perfusion system. The system was standardised by testing delivery of 3 ng/ml fluorescein isothiocyanate (FITC) (Thermo Fisher Scientific) and 100 ng/ml Alexa Fluor 647-labelled goat anti-rabbit F(ab')2 antibody (Thermo Fisher Scientific), to mimic the delivery of large proteins. Delivery to the edge and middle of the cell membrane was then measured by TIRF. Image and statistical analyses were performed using custom analysis pipelines developed in FIJI (Schindelin et al., 2012) and R programming (GNU General Public Licence).

2.4 Protein Analyses

Bovine Serum Albumin (BSA) heat shock fraction pH 7.0, ≥ 98% and TWEEN® 20 was purchased from Sigma-Aldrich. Pierce™ 20× Tris-buffered saline (TBS) Buffer and Pierce™ ECL (enhanced chemi-luminescence) Western Blotting Substrate were purchased from Thermo Fisher Scientific. Total and phosphorylated (Thr^{308} and Ser^{473}) Akt (60 kDa), total and phosphorylated (Ser^{256}) FoxO1 (82 kDa), total and phosphorylated (Ser^{21}/ Ser^{9}) GSK3α/β (51/46 kDa) monoclonal primary antibodies were purchased from Cell Signalling Technology. HA-epitope tag monoclonal primary antibody was purchased from Thermo Fisher Scientific. β-actin (42 kDa) polyclonal primary antibody was purchased from Abcam. Mouse anti-rabbit and goat anti-mouse immunoglobulin/HRP (horseradish peroxidase) secondary antibodies were purchased from Dako.

2.4.1 Protein extraction and quantification

Cells were washed with 1× PBS and lysed in lysis buffer (5 mM EDTA, 1% (v/v) Triton X-100 in 1× PBS), supplemented with 1× Protease Inhibitor Cocktail, 1× Phosphatase Inhibitor and 1 mM PMSF. Whole cell lysates were incubated on ice for 30 min. Whole cell lysates were centrifuged at 18,000 × *g* for 5 min, supernatant was transferred into a new microcentrifuge tube. The bicinchoninic acid (BCA) method (Thermo Fisher Scientific) was performed for colourimetric quantitation of total proteins in collected lysates. Absorbance was read at 562 nm on the plate reader. Lysates were diluted into appropriate concentrations (25-50 µg) and terminated with 1× NuPAGE™ LDS Sample Buffer (Thermo Fisher Scientific) and incubated for 5 min at 95°C.

2.4.2 Immunoprecipitation

Whole cell lysates were diluted in dilution buffer (5 mM EDTA in 1× PBS, supplemented with 1× Protease Inhibitor Cocktail, 1× Phosphatase Inhibitor and 1 mM PMSF) to 1 mg/ml for immunoblotting or 3 mg/ml for mass spectrometry analyses. Dynabeads™ Protein G (Invitrogen) were added directly to preclear the lysate. Mixture was incubated with rotation for 1h at 4°C. Dynabeads™ were separated with a magnet and discarded. Precleared lysate was transferred to a fresh microcentrifuge tube. The HA-epitope tag antibody (2 µg for immunoblotting, 20 µg for mass spectrometry) was directly added to the lysate. Mixture was incubated with rotation for 1h at 4°C. Fresh Dynabeads™ were added; mixture was incubated on rotation overnight at 4°C. Dynabeads™ were separated with a magnet and supernatant was discarded. Dynabeads™ were washed 3× with 1× PBS. Proteins on the Dynabeads™ were terminated with 2× LDS Sample Buffer and incubated for 5 min at 95°C.

2.4.3 Akt downstream activity assay

Downstream substrate activation of immunoprecipitated Akt1 recombinant protein was determined by the Akt activity assay kit (Abcam). Kinase Assay Buffer and recombinant GSK3α substrate/ATP mixture was added to Dynabeads™ bound to Akt1 and incubated at 30°C for 4 hours. Dynabeads™ were separated with a magnet and supernatant was discarded. Dynabeads™ were 3× washed with Kinase Assay Buffer. Dynabeads™ were separated with a magnet and supernatant was discarded. Proteins on the Dynabeads™ were terminated with 2× LDS Sample Buffer and incubated for 5 min at 95°C.

2.4.4 Treatment of truncated Akt1-PH protein with thioredoxin protein

Thioredoxin (Trx) protein was reduced with 10 mM DTT at room temperature for 30 min. Unreacted DTT was removed by Zeba™ Spin Desalting Columns, 7K MWCO, 0.5 ml (Thermo

Fisher Scientific) at 1,500 × *g* for 2 min. 3 µg of WT-PH EGFP protein was incubated with 10 µM of reduced Trx at room temperature for 30 min. Reduced WT-PH EGFP protein was alkylated with 5 mM of carbon-12 ring linked to 2-iodo-*N*-phenylacetamide (^{12}C-IPA) (Cambridge Isotopes) for 1 h at room temperature. Proteins were added to 1× LDS Sample Buffer and incubated for 5 min at 95°C.

2.4.5 Protein separation by sodium dodecyl sulphate-polyacrylamide gel electrophoresis (SDS-PAGE)

Protein samples were loaded into the NuPAGE™ Novex™ 4-12% Bis-Tris Gel (Thermo Fisher Scientific) and separated by SDS-PAGE in 1× NuPAGE 3-(*N*-morpholino)propanesulfonic acid (MOPS) SDS Running Buffer (Thermo Fisher Scientific) using the Invitrogen™ Mini Gel Tank (Thermo Fisher Scientific) connected to the PowerPac™ Basic Power Supply (Bio-Rad) at 150 V for 1 h.

2.4.6 Dry protein transfer onto polyvinylidene fluoride (PVDF) membrane

Separated proteins in the 4-12% Bis-Tris Gel was transferred onto PVDF membrane using the iBlot Dry Blotting System (Thermo Fisher Scientific) at 22 V for 10 min. Dried PVDF membrane was reactivated with methanol and washed with 1× TBS and 0.1% (v/v) TWEEN® 20 (TBST).

2.4.7 Immunoblotting and densitometry analyses

PVDF membranes were blocked with 5% (w/v) BSA in 1× TBST for 1 h at room temperature on a rocker. Membranes were probed with total and phospho-Akt (1:1000), total and phospho-GSK3α/β (1:1000), and total and phospho-FoxO1 (1:1000) antibodies diluted with 5% (w/v) BSA in 1× TBST overnight at 4°C on a rocker. Membranes probed with β-actin (1:5000)

antibody were incubated for 1 h at room temperature on a rocker. Membranes were washed 3× with 1× TBST in 5 min intervals at room temperature on a rocker. Membranes were probed with appropriate HRP-conjugated secondary antibody diluted with 5% (w/v) skim milk powder in 1× TBST (1:2000) for 1 h at room temperature on a rocker. Membranes were washed 3× with 1× TBST in 5 min intervals on a rocker. Membranes were soaked in a tray of 1:1 ECL solution for 2 min at room temperature. Membranes were imaged on the ChemiDoc Touch Imaging System (Bio-Rad). Densitometry was analysed using Image Lab Software (Bio-Rad).

2.4.8 Differential cysteine labelling and mass spectrometry analysis

The 4-12% Bis-Tris Gel containing protein of interest was covered in fixing solution (10% (v/v) methanol, 7% (v/v) acetic acid in MilliQ H_2O) for 30 min at room temperature on a rocker. Gel was stained with SYPRO® Ruby Gel Stain (Thermo Fisher Scientific) in the dark for 30 min at room temperature on a rocker. Gel was imaged on the ChemiDoc Touch Imaging System before the excision of Akt1 protein. Gel pieces were vortexed 3× using a thermomixer in wash buffer (25 mM ammonium bicarbonate, 50% (v/v) acetonitrile) in 10 min intervals at room temperature. Unpaired Cys thiols in Akt1 were alkylated with 5 mM ^{12}C-IPA for 1 h at room temperature, and washed. Gel slices were incubated with 40 mM DTT for 30 min at 56°C, and washed. Fully reduced disulphide bonded Cys thiols in Akt1 were alkylated with 5 mM of carbon-13 ring linked to 2-iodo-*N*-phenylacetamide (^{13}C-IPA) (Cambridge Isotopes) for 1 h at room temperature in the dark, and washed. Samples were dried with 100% (v/v) acetonitrile and placed in the Speedivac for 20 min at 55°C. Akt1 was digested with 12.5 ng/µl of trypsin (Roche) in 25 mM ammonium bicarbonate, overnight at 25°C. Peptides were eluted from gel slices with 5% (v/v) formic acid/50% (v/v) acetonitrile, vortexed for 15 min at room temperature. Peptides were separated by liquid chromatography-mass spectrometry (LC-MS). Peptides covering both Cys^{60} and Cys^{77} residues were quantified (**Table 2.5**). Levels of reduced

and oxidised cysteines were compared by relative ion abundance of the peptides labelled with ^{12}C-IPA (reduced) and ^{13}C-IPA (oxidised). Extracted ion chromatograms were analysed using Xcalibur™ Qual Browser Software v2.1.0 (Thermo Fisher Scientific). The area was calculated using automated the peak detection function.

Table 2.5 Peptide sequences of Cys^{60} and Cys^{77} in Akt1 generated from trypsin digest. Disulphide bonded and free thiols were differentially labelled and analysed by tandem mass spectrometry.

Protein	Cysteine residue	Protease	Peptide sequence
Akt1	60	Trypsin	EAPLNNFSVAQCQLMK
	77		CLQWTTVIER

2.4.9 Protein–lipid binding interaction assay

Lyophilised phospholipid PIP_3 diC16 (Sapphire Bioscience) was reconstituted in methanol−chloroform solution (1:1) to a working concentration of 1 mM and stored at −80°C. PIP_3 was diluted in a methanol, chloroform and MilliQ H_2O solution (2:1:0.8) to various concentrations of 1, 5, 10, 25, 50 and 100 μM. 1 μl aliquots of selected PIP_3 dilutions (1 to 100 pM) were spotted onto Amersham Protran 0.45 μm nitrocellulose supported Western blotting membranes (GE Healthcare Life Sciences) and dried at room temperature for 1 h. Membranes were incubated in blocking buffer (20% (w/v) Bovine Serum Albumin (BSA) Fatty Acid-Free (Sigma-Aldrich) in 50 mM Tris-HCl, pH 7.5, 150 mM NaCl, 0.1% (v/v) TWEEN® 20 (Sigma-Aldrich) in MilliQ H_2O) at room temperature for 1 h. Membrane was incubated with 10 nM WT-PH EGFP or reduced C60AC77A-PH EGFP protein in fresh blocking buffer overnight at 4°C. Membranes were washed 5× in 10 min intervals with 1× TBST at room temperature. Membranes were probed with GFP (FL) polyclonal antibody (Santa Cruz Biotechnology) diluted in fresh blocking buffer (1:1000) for 1 h at room temperature. Membranes were washed 5× in 10 min intervals with 1× TBST at room temperature. Membranes were probed with appropriate HRP-conjugated secondary antibody diluted with 5% (w/v) skim milk powder in 1× TBST (1:2000) for 1 h at room temperature. Membranes were washed 4× in 8 min intervals with 1× TBST at room temperature. Membranes were soaked in a tray of ECL solution (1:1) for 2 min at room temperature. Membranes were imaged on the ChemiDoc Touch Imaging System (Bio-Rad).

2.4.10 Enzyme-linked immunosorbent assay (ELISA)

The ELISA protocol was based off a procedure curated by Rowland et al., 2012. 96-well ELISA Microplates (Greiner Bio-One) were washed with Coating Buffer (20 mM Tris, pH 8.0, 0.05% (v/v) TWEEN® 20) for 30 min on a plate shaker at room temperature. Coating Buffer was removed from the wells and dried. 500 nM of 1-oleoyl-2-[12-biotinyl(aminododecanoyl)]-sn-glycero-3-PIP_3 (18:1 – 12:0 Biotin-PIP_3) (Avanti) was added to each well and incubated on a plate shaker for 1 h at room temperature. Biotin-PIP_3 was removed from the wells and washed with Coating Buffer 3× in 10 min intervals on a plate shaker at room temperature. Serial dilutions of WT-PH EGFP (untreated), reduced WT-PH EGFP (treated with 10 mM DTT for 30 min, desalted in Zeba™ Spin Desalting Columns, 7K MWCO, 0.5 ml) and reduced C77S-PH EGFP proteins were prepared in Protein Buffer solution (1× PBS, 0.05% (v/v) TWEEN 20) to concentrations of 1, 5, 10, 25, 50, 100 nM. Protein solutions were added to each well and incubated on a plate shaker for 1 h at room temperature. Wells were washed with Protein Buffer solution 3× in 10 min intervals on a plate shaker at room temperature and resuspended in Protein Buffer solution. Bound fluorescent Akt1-PH EGFP proteins were read at Excitation/Emission 485/535 nm on the plate reader.

2.5 Zebrafish Analyses

2.5.1 Zebrafish maintenance

Zebrafish (*Danio rerio*) husbandry and experimental procedures were performed adhering to the Australian code of animal ethics. Adult zebrafish were housed at the Garvan Institute. Transgenic zebrafish line *Tg(fli1a:EGFP)* was utilised for this project. Clutches of embryos were collected from natural spawning. Microinjections of *pDestTol2/ubb:Akt1-p2a-tdTomato* (**Figure 2.2B**) were performed at the Garvan Institute. Embryos were incubated at 28°C in E3 media (5 mM NaCl, 0.17 mM KCl, 0.33 mM $CaCl_2$, 0.33 mM $MgSO_4$, 0.1% (v/v) methylene blue in MilliQ H_2O) at the Centenary Institute. Pigment development was prevented with the addition of 45 μg/ml phenylthiourea (PTU) solution (Sigma-Aldrich). *In vivo* imaging of zebrafish embryos were performed at the Centenary Institute.

2.5.2 Microinjection and imaging

Tg(fli1a:EGFP) zebrafish embryos were injected with 2 nl of *pDestTol2/ubb:Akt1-p2a-tdTomato* (150 ng), Tol2 transposase mRNA (20 ng) and phenol red into the animal pole at the one-cell stage under the SMZ1270 microscope with P-DSL32 LED Diascopic Illumination Stand (Nikon) at the 40× objective (**Figure 2.3**). Dead or unfertilised embryos were removed 3 hours post-fertilisation (hpf). Embryos were dechorionated with 1× Pronase for 2 min at 24 hpf. Embryos overexpressing *Akt1* (tdTomato) were anesthetised with 10× Tricaine mesylate and mounted on 3% (w/v) methylcellulose in E3 media at 48 hpf. *In vivo* imaging was performed on the M205 FA fluorescent stereomicroscope (Leica). A new channel was applied to label the EGFP (green) and Cy5 (red) fluorophores. Images were processed using ImageJ (National Institute of Health). Completeness of intersegmental vessels (ISV) and length of zebrafish embryos were evaluated.

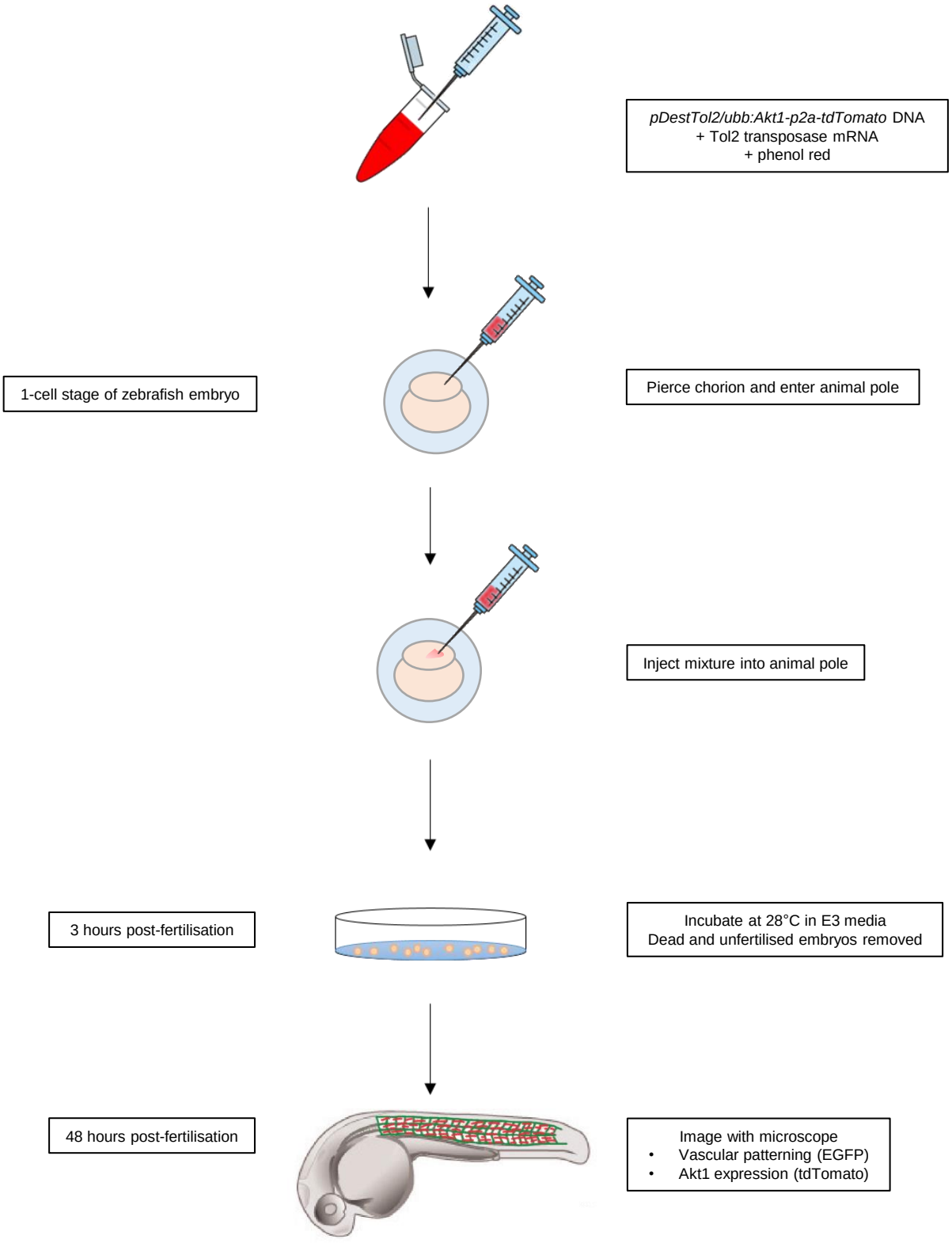

Figure 2.3 Timeline of *Tg(fli1a:EGFP)* zebrafish embryo injection and imaging. Vasculature (green) of *Tg(fli1a:EGFP)* embryos injected with mutant *Akt1* (red) constructs imaged 48 hours post-fertilisation.

2.5.3 Protein extraction and quantification

Embryos were centrifuged at 18,000 × *g* for 2 min and supernatant was discarded. Embryos were resuspended in Ringer's solution (58 mM NaCl, 4 mM KCl, 4.8 mM $NaHCO_3$, pH 7.0 in MilliQ H_2O) and centrifuged at 18,000 × *g* for 2 min, supernatant was discarded. Embryos were washed 1× PBS and centrifuged at 18,000 × *g* for 2 min, supernatant was discarded. Embryos were harvested in RIPA buffer (1 mM EDTA, 1% (v/v) Triton X-100, 0.1% (w/v) sodium deoxycholate, 0.1% (w/v) SDS, 10 mM Tris-Cl, pH 8.0 in MilliQ H_2O), supplemented with 1× Protease Inhibitor Cocktail, 1× Phosphatase Inhibitor and 1 mM PMSF. Embryo lysates were incubated on ice for 30 min. Lysates were centrifuged at 18,000 × *g* for 5 min, supernatant was transferred into a new microcentrifuge tube. The BCA method was performed for colourimetric quantitation of total proteins in collected embryo lysates. Absorbance was read at 562 nm on the plate reader. Method of protein separation and immunoblotting analyses were previously described (**Section 2.4.4-2.4.7**).

2.5.4 RNA extraction

Zebrafish larvae were lysed with TRIzol® Reagent (Invitrogen) in E3 media (3:1) and incubated for 5 min at room temperature. Chloroform (Sigma-Aldrich) (2:1) was added to the mixture and incubated for 2 min at room temperature. Lysates were centrifuged at 12,000 × *g* for 15 min at 4°C. Aqueous phase (top layer) containing total RNA was aliquoted into a fresh microcentrifuge tube. Isopropanol (2:1) was added and incubated for 10 min at room temperature to precipitate RNA. Reaction was centrifuged at 12,000 × *g* for 15 min at 4°C, supernatant was removed. RNA pellet was washed with 75% (v/v) ethanol and centrifuged at 7,500 × *g* for 5 min at 4°C. Supernatant was removed and the RNA pellet was air-dried before resuspension in RNase-free H_2O.

2.5.5 Real-time quantitative polymerase chain reaction (RT-qPCR)

RNA (1 µg) was mixed with 1× reverse transcriptase, 1× RT buffer, 60 µM random primers and 10 mM oligo(dT) primers in RNase-free H_2O. Reaction mix was subjected to 10 min of primer extension at 25°C, synthesis of cDNA at 37°C for 2 h and termination at 85°C for 1 min on the Mastercycler nexus gradient. cDNA product was diluted in MilliQ H_2O (1:6). Diluted cDNA was mixed with SYBR® Green master mix (Thermo Fisher Scientific) and the appropriate forward and reverse oligonucleotides of downstream *Akt1* genes in zebrafish required for neuronal differentiation and angiogenesis (**Table 2.6**). Each reaction was loaded into a Non-skirted Flat Top Low Profile 96-well Plate, Clear (SSIbio) and read on the CFX96™ Real-Time PCR Detection System (Bio-Rad). Reaction mix was subjected to 3 min at 95°C, followed by 40 cycles of 10 s denaturation at 95°C, 30 s annealing at 55°C, data was recorded at each annealing step. Melt curve protocol followed by 0.5 s at 65°C to 95°C, in 0.5°C increments, data was recorded at each increment of the melt curve. Melt and standard curves were generated by the CFX Manager™ Software v2.0 (Bio-Rad).

Table 2.6 Oligonucleotides designed for RT-qPCR of selected genes downstream targets of *Akt1* in the zebrafish model.
Differentiated and progenitor neuronal markers downstream of *Akt1*.

Oligonucleotide	Sequence 5'-3'
TbpF	CGGTGGATCCTGCGAATTA
TbpR	TGACAGGTTATGAAGCAAAACAACA
Elavl3F	GTCAGAAAGACATGGAGCAGTTG
Elavl3R	GAACCGAATGAAACCTACCCC
DeltaAF	ACCGGGTGAAGCTTGTGAAC
DeltaAR	CGTCATGCYCGTCCAGAAGTT
Her8aF	GTAACGGGGAGACGCGTCTGCAGCG
Her8aR	GATTATTCCCACGATGACGGCGGCG
Ngn1F	CGCACACGGATGATGAAGACTCGCG
Ngn1R	CGGTTCTTCTTCACGACGTGCACAGTGG

Tbp TATA-box binding protein is the housekeeping gene. *Elavl3* ELAV-like neuron-specific RNA-binding protein 3; *Her8a* hairy-related 8a; *Ngn1* neurogenin 1.

2.6 Statistical Analyses

2.6.1 GraphPad Prism

Unless otherwise specified, statistical significance was assessed in GraphPad Prism 7 (GraphPad Software) using Student's *t*-tests or analysis of variance (ANOVA); comparing the mean of each group against the mean of every other group using Tukey's multiple comparison test. Data are expressed as mean ± standard deviation (s.d.). Experiments were performed in duplicate or triplicate, with a minimum of n=3 independent biological experiments. *$p<0.05$ was considered statistically significant.

3. Identification of the Cys^{60}-Cys^{77} disulphide bond in the PH domain of Akt1

3.1 Declaration

This thesis chapter contains an edited version of a published manuscript prepared in a format for publication, using the final accepted version. Material & Methods in this publication appear elsewhere in this thesis (**Section 2.1**).

Chapter 3 of this thesis is published as:

Pijning AE, Chiu J, Yeo RX, Wong JWH, Hogg PJ 2018 Identification of allosteric disulfides from labile bonds in X-ray structures. *R. Soc. open sci*. **5**:171058.

http://dx.doi.org/10.1098/rsos.171058

Authorship contribution statement:

The author of this thesis R.X.Y. participated in data analysis and writing of the manuscript specific to protein kinase B/Akt.

A.E.P. participated in data analysis, design of the study and drafted the manuscript; J.C. participated in data analysis; J.W.H.W. participated in data analysis and designed the study; P.J.H. conceived and designed the study and drafted the manuscript. All authors gave final approval for publication.

Authorship attribution statement:

As supervisor for the candidature upon which this thesis is based, I can confirm that the authorship attribution statements above are correct.

Philip J. Hogg

February 2019

Permission:

As corresponding author for this manuscript, I give permission for it to be included in this thesis and confirm that appropriate acknowledgement of authorial contributions has been stated.

Philip J. Hogg

February 2019

3.2 Manuscript: Identification of allosteric disulfides from labile bonds in X-ray structures

Aster E. Pijning[1], Joyce Chiu[1,2], Reichelle X. Yeo[1], Jason W. H. Wong[3] and Philip J. Hogg[1,2]

Affiliations:

[1]The Centenary Institute, Camperdown, New South Wales 2050, Australia; [2]National Health and Medical Research Council Clinical Trials Centre, University of Sydney, Sydney, New South Wales 2006, Australia; [3]Prince of Wales Clinical School and Lowy Cancer Research Centre, UNSW Sydney, Sydney, New South Wales 2052, Australia.

Correspondence:

Philip J. Hogg. ACRF Centenary Cancer Research Centre, The Charles Perkins Centre – D17, The University of Sydney, NSW, Australia, 2006. E-mail: phil.hogg@sydney.edu.au

Competing interests:

We declare we have no competing interests.

Acknowledgements:

This study was supported by the National Health and Medical Research Council of Australia (P.J.H.), Helen and Robert Ellis Postdoctoral Fellowship and Sydney Medical School Foundation Fellowship (J.C.), Australian Postgraduate Award (R.X.Y.) and Australian Research Council Future Fellowship (FT130100096) (J.W.H.W.).

3.3 Abstract

Protein disulphide bonds link pairs of cysteine sulphur atoms and are either structural or functional motifs. The allosteric disulphides control the function of the protein in which they reside when cleaved or formed. Here, we identify potential allosteric disulphides in all Protein Data Bank X-ray structures from bonds that are present in some molecules of a protein crystal but absent in others, or present in some structures of a protein but absent in others. We reasoned that the labile nature of these disulphides signifies a propensity for cleavage and so possible allosteric regulation of the protein in which the bond resides. A total of 511 labile disulphide bonds were identified. The labile disulphides are more stressed than the average bond, being characterised by high average torsional strain and stretching of the sulphur–sulphur bond and neighbouring bond angles. This pre-stress likely underpins their susceptibility to cleavage. The coagulation, complement and oxygen-sensing hypoxia inducible factor-1 pathways, which are known or have been suggested to be regulated by allosteric disulphides, are enriched in proteins containing labile disulphides. The identification of labile disulphide bonds will facilitate the study of this post-translational modification.

3.4 Introduction

Allosteric disulphide bonds are defined by their ability to affect the functioning of the protein in which the bond resides. Reduction or oxidation of allosteric disulphide bonds leads to conformational transitions in the residing protein, that result in a change in either ligand binding, enzyme activity, proteolysis or oligomerisation of the protein (Cook & Hogg, 2013). Since the identification of this type of posttranslational control of protein function, over 30 examples have been described. The extent to which biological processes are controlled by allosteric disulphides has not yet been fully elucidated. However, certain processes are highly regulated by this form of protein control. In humans, thrombosis and hemostasis is an example of a system that is regulated by allosteric disulphides (Butera et al., 2014). Disease processes regulated by allosteric disulphide bonds include cancer (Hogg, 2013) and viral infection (Wouters et al., 2004). Clinical relevance lies in the fact that these disulphide bonds can be targeted with inhibitors of the factors that cleave the bonds, such as protein disulphide isomerase (PDI). Small molecule PDI inhibitors are being developed (Bekendam et al., 2016) and a first generation molecule is currently being tested as an anti-thrombotic in a Phase II cancer clinical trial (Stopa et al., 2017).

Studies of the biophysical properties of allosteric disulphides have led to the recognition of defining features of these bonds. Firstly, a conformational signature for allosteric disulphides has been identified based on the sign of the five dihedral angles which define the cystine residue (Schmidt et al., 2006). There are 20 different disulphide bond configurations based on this classification and 3 of the 20 are emerging as allosteric configurations; the –RHstaple, –LHhook and –/+RHhook bonds. Secondly, the –RHstaple and –/+RHhook bonds are more stressed than the other 18 disulphide types (Zhou et al., 2014), which is primarily due to stretching of the sulphur-sulphur bond and neighboring bond angles. Stretching of sulphur-

sulphur bonds is known to accelerate their cleavage (Baldus & Gräter, 2012; Li & Gräter, 2010; Wiita et al., 2006; Wiita et al., 2007), so the pre-stress of the –RHstaple and –/+RHhook configurations is very likely important for their reduction and has probably influenced their evolution as allosteric bonds.

The three allosteric configurations constitute approximately 20% of all disulphide bonds in X-ray structures from the PDB (Schmidt et al., 2006). While bond configuration has proven useful for identifying allosteric disulphides in proteins, it is likely that many, if not most, bonds with allosteric configurations will not have a functional role. Additional methods are needed to identify this post-translational modification. Here we identify 511 labile disulphide bonds in PDB X-ray structures from bonds that are present in some molecules of a protein crystal or in some structures of a protein, but absent in others. A notable feature of the labile bonds is their pre-stress that likely underlies their facile nature. A biological pathway enriched in proteins containing labile disulphides is the cytoplasmic oxygen-sensing HIF1 system. Potential allosteric disulphide bonds in this pathway are presented.

3.5 Results

A total of 1,361 unique labile disulphide bonds were identified from the PDB as of June 2017. The reference dataset consisted of all 14,033 unique disulphide bonds in the PDB. To eliminate poorly defined or erroneous bonds, criteria of a structure resolution <2.5 Å and sulphur–sulphur distances <10% from the disulphide bond equilibrium length of 2.038 Å (Zhou et al., 2014) were applied. The datasets were refined to present each unique disulphide bond as a single entry. The final list contains 511 labile disulphides and 13,030 total disulphides.

In X-ray crystallography, the B factor is a measure of the degree to which the electron density of an atom is dispersed. To ensure that the missing disulphide bonds that we detected were not due to uncertainty in the position of cysteines, we compared the average B factor of disulphide-bonded cysteines with those of matched missing disulphide bonds. The B factor for each atom of each cysteine involved in disulphide bond formation (present or missing) was extracted from corresponding PDB structure. The B factor for each disulphide bond was calculated as the average of the 12 atoms per cysteine pair. To compare the B factor of present and missing disulphide bonds, the average disulphide bond B factors for all redundant structures were further averaged, respectively. There was no significant difference between the B factor of present (37.58±21.78, s.d.) and missing (36.24±21.02, s.d.) disulphide bonds ($p=0.0736$, paired *t*-test).

3.5.1 Structural and functional features of the labile disulphide bonds

By comparing the distribution of the 20 disulphide configurations between the entire PDB and labile disulphides, two differences were notable (**Figure 3.1A**). Within the labile disulphide bonds, an increase in the +/–RHhook and +/–LHstaple configurations was observed (χ^2 test, $p<0.0001$). The –LHspiral, which is the main structural disulphide, as well as the +RHspiral configurations were decreased in the labile disulphides compared with the total PDB (χ^2 test, $p<0.0001$). The +/–RHhook is the predominant configuration of the catalytic disulphide bonds of oxidoreductases (Schmidt et al., 2006), such as PDI. This reflects the conserved position of this bond at the end of an α-helix in a thioredoxin fold. The catalytic disulphides of oxidoreductases undergo cycles of reduction and oxidation and there are several examples of oxidised and reduced structures in the PDB, hence their prevalence in the labile disulphide dataset. Of the 67 proteins in the labile disulphide dataset that have a +/–RHhook configuration, 22 are oxidoreductases.

The secondary structures that a disulphide links can be informative. For instance, allosteric –RHstaple bonds often link adjacent strands in the same antiparallel β-sheet or constrain β-loops (Matthias et al., 2002; Wouters et al., 2004). Also, the catalytic disulphide bonds of oxidoreductases link an α-helix to another or a loop structure. For the total PDB, disulphide bonds linking two β-strands were the most common, followed by linking of β strands and loops (**Figure 3.1B**). For labile disulphide, enrichment of bonds linking α-helices and loops was observed (χ^2 test, $p<0.0001$) (**Figure 3.1B**), which reflects the higher relative number of catalytic +/–RHhook configurations.

As anticipated, oxidoreductases were enriched in proteins containing labile disulphide bonds (**Figure 3.1C**). Transferases, which include kinases, methyltransferases and other enzyme that

transfer functional groups, were also enriched in proteins containing labile disulphide bonds (**Figure 3.1C**). Hydrolases and proteins involved in immune function were the largest category of disulphide-containing proteins in the PDB. Immune function proteins contain relatively fewer labile disulphides in this analysis. Overall, labile disulphide bonds were found in proteins of diverse functionalities.

The subcellular localisation of proteins containing disulphide bonds was examined using the UniProt designation of the protein. A high proportion of cytoplasmic and nuclear proteins contained labile disulphide bonds (**Figure 3.1D**). The cytoplasm and nucleus are environments traditionally thought not to be conducive to disulphide bond formation. This is not the case, however, as 509 disulphide bonds have been structurally defined in cytoplasmic proteins. A high proportion of these disulphides (113 disulphides) have been characterised in oxidised and reduced states, indicating that they are unusually labile.

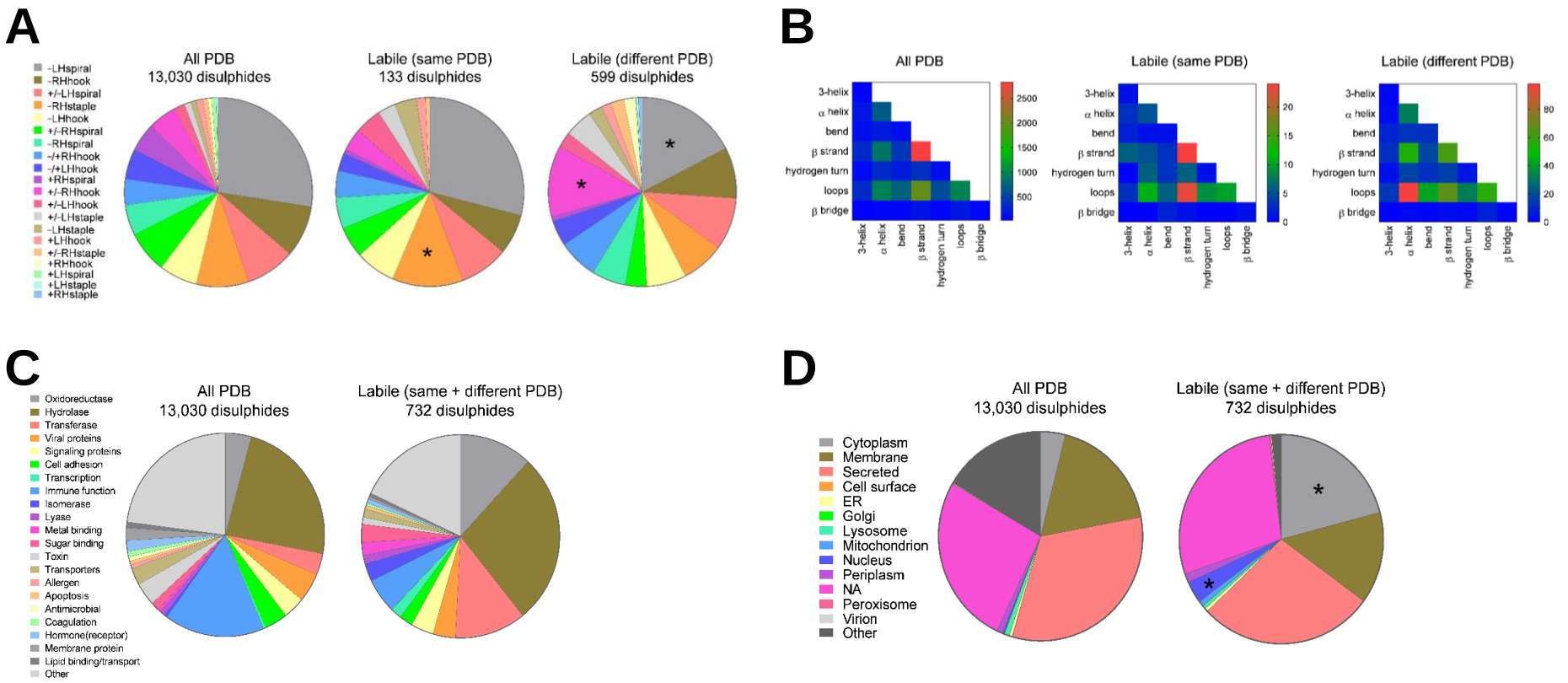

Figure 3.1 Structural and functional features of the labile disulphide bonds.
A. Distribution of the 20 disulphide bond configurations in unique disulphide bonds in PDB protein X-ray structures (13,030 disulphides) and in labile bonds (511 disulphides). Compared with the total PDB, the labile bonds in are enriched in +/–RHhook and +/–LHstaple bonds (χ^2 test, $p<0.0001$) and have relatively fewer –LHspiral and+RHspiral bonds (χ^2 test, $p<0.0001$) (indicated by *). **B**. Heatmap displaying the frequency of the secondary structures linked by disulphide bonds in all PDB protein structures and by labile disulphide bonds. There is enrichment of disulphides linking α-helices and loops in labile disulphide bonds (χ^2 test, $p<0.0001$). **C**. Distribution of the functional classification of all proteins containing disulphide bonds and proteins containing labile disulphide bonds. Compared to the total PDB, there was a significant increase in oxidoreductases, transferases and isomerases (indicated by *). .A significant decrease in disulphide bonds in proteins involved in signalling and immune function was observed (χ^2 test, $p<0.0001$). **D**. Subcellular localisation of all proteins containing disulphide bonds and proteins containing labile disulphide bonds. Compared to the total PDB, a significant increase in cytoplasmic proteins, as well as a decrease in membrane associated and secreted proteins was observed (χ^2 test, $p<0.0001$) (indicated by *).

3.5.2 Labile disulphides are characterised by high strain

The conformational constraints on allosteric disulphides imposed by secondary structural features stress the bonds. The stresses fine tune their cleavage and thus the function of the protein. The stresses of the labile disulphides have been compared and contrasted with the average disulphide. There are different measures of disulphide bond stress (Schmidt et al., 2006; Zhou et al., 2014).

DSE (dihedral strain energy) is an indicator of bond strain. The DSE is defined in terms of the torsion of the five dihedral or χ angles (**Figure 3.2A**) of the cystine residue (Katz & Kossiakoff, 1986; Weiner et al., 1984) , and has been shown experimentally to reflect the amount of strain in a disulphide bond (Kuwajima et al., 1990; Pjura et al., 1990; Wells & Powers, 1986; Wetzel et al., 1988). The length of the sulphur-sulphur bond and magnitude of the neighbouring angles (**Figure 3.2A**) also reflect the stress in a disulphide (Zhou et al., 2014). The allosteric −RHstaple and−/+RHhook disulphide configurations carry tensile pre-stress in the bond due to direct stretching of the sulphur-sulphur bond and α angles, rather than by dihedral angle torsions (Zhou et al., 2014). This was shown using force distribution analysis, a technique for calculating atom-atom and residue-residue forces from molecular-dynamics simulations. As mechanical stretching of sulphur-sulphur bonds increases their redox potential (Baldus & Gräter, 2012; Li & Gräter, 2010; Wiita et al., 2006; Wiita et al., 2007), the pre-stressed bonds are more susceptible to cleavage.

The mean DSE of labile disulphide bonds (different PDB) was significantly higher than that of all disulphide bonds in the PDB (**Figure 3.2B**). The mean DSE for all disulphide bonds was 12.48 kJ mol^{-1}, whereas that of labile disulphide bonds was 17.64 kJ mol^{-1}. The mean sulphur-sulphur bond length (**Figure 3.2C**) and α angle magnitude (**Figure 3.2D**) were also

significantly higher than those for all disulphide bonds. The mean sulphur-sulphur bond length of all disulphides was 2.046 Å, whereas for the labile disulphide bonds it was 2.055 Å. While the increased bond length is small at approximately 1 pm, the high stiffness of sulphur-sulphur bonds means that this change can entail substantial stress. The mean α angle of all disulphide bonds was 104.7°, whereas for the labile disulphide bonds it is 106.1°. Between 1 and 2° of stretching is also seen for the allosteric −RHstaple and −/+RHhook disulphide configurations (Zhou et al., 2014). Thus, the labile disulphide bonds are more stressed than the average bond based on three measures of strain.

Correlations between the measures of strain on disulphides was examined (**Figure 3.3**). DSE positively correlated with stretching of the α-angles for both labile ($p < 0.0001$) and total ($p < 0.0001$) disulphides. There was no correlation between DSE and sulphur-sulphur bond length, or between sulphur-sulphur bond length and α angles for both labile and total disulphides. This indicates that stretching of the α-angles is associated with high overall torsional strain, whereas sulphur-sulphur bond length is independent of the α-angles.

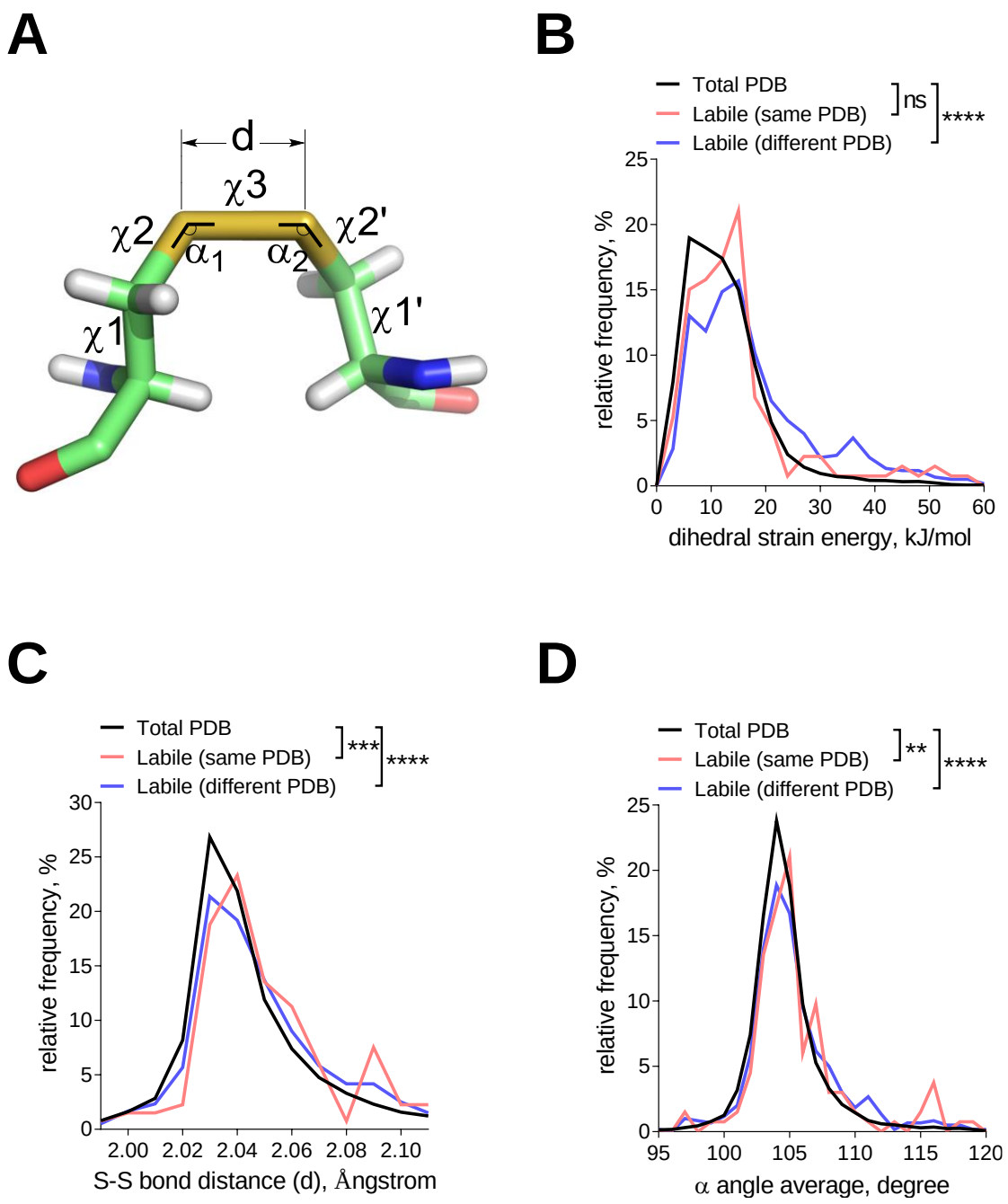

Figure 3.2 The labile disulphides are characterised by high dihedral strain energy, elongation of the sulphur-sulphur bond distance and stretching of the neighbouring bond angles.

A. Angles and distances of the cystine residue. The values α_1 and α_2 represent the two relevant bending angles of the disulphide, and the five dihedral angles are χ^1, χ^2, χ^3, $\chi^{2'}$, and $\chi^{1'}$. d is the sulphur-sulphur bond length. **B.** Relative frequency of DSE ranging from 0 to 60 kJ mol^{-1}. The DSE was significantly increased for labile disulphides from different PDB compared to the total PDB with ****p<0.0001. **C.** The relative frequency of the sulphur-sulphur bond distance ranging from 1.96 to 2.14 Å is shown. An increase in sulphur-sulphur bond distance is observed for labile disulphide bonds (****p<0.0001). **D.** The average of both α angles was calculated for each disulphide bond. Shown is the relative frequency of the average angle ranging from 95 to 120°. Angles are increased for labile disulphide bonds (****p<0.0001). *T*-tests were used to compare total PDB to labile disulphides.

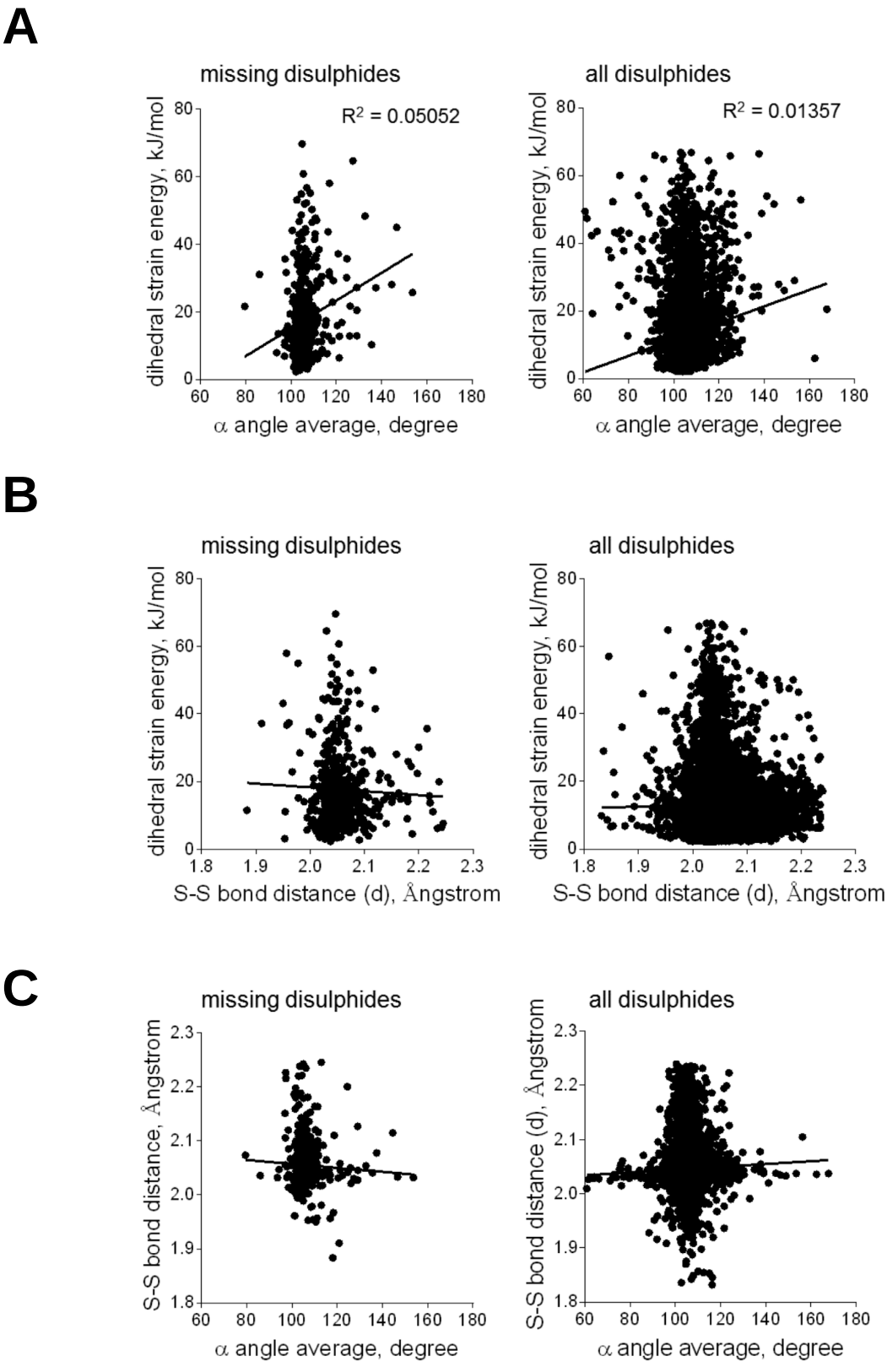

Figure 3.3 Correlations of the measures of strain of the missing and all disulphides.
A. Positive correlation of DSE with stretching of the α angle for both missing and all disulphides. **B**. No correlation between DSE and length of the sulphur-sulphur bond of disulphides for both missing and all disulphides. **C**. No correlation between sulphur-sulphur bond length and α angle for both missing and all disulphides.

3.5.3 Labile disulphides with allosteric configurations have higher dihedral strain

The allosteric –RHstaple, –LHhook, and –/+RHhook configurations represent 9%, 6.5%, and 4.5% of all disulphide bonds in the PDB (**Figure 3.4A**). For those allosteric disulphide bonds where there are high resolution crystal structures (n = 29), these percentages increase to 39%, 16%, and 16%, respectively (**Figure 3.4A**). The labile disulphides with allosteric configurations have a higher mean DSE than for all disulphide bonds (18.11 versus 12.74 kJ mol^{-1}, $p<0.0001$, Mann-Whitney test) (**Figure 3.4B**), which is consistent with the known properties of two (−RHstaple and −/+RHhook) of the three allosteric configurations.

3.5.4 Labile disulphide bonds are enriched in certain biological pathways

Five known allosteric disulphides are amongst the 511 labile bonds, which is a validation of this approach for identifying functional disulphides. These are the –RHstaple bonds in methionine aminopeptidase 2 (Chiu et al., 2014b), botulinum neurotoxins (Swaminathan & Eswaramoorthy, 2000) and transglutaminase 2 (Pinkas et al., 2007), the –/+RHhook disulphides in plasminogen (Butera et al., 2013) and Lon protease (Nishii et al., 2015), and the –LHhook bonds in DNA repair protein XRCC1 (Cuneo & London, 2010) and plasminogen (Butera et al., 2013) (**Table 3.1**).

To determine whether specific biological processes or pathways are enriched among human labile disulphides, the labile dataset was analysed using the DAVID Functional Annotation Tool (Huang et al., 2009a, 2009b). The oxygen-sensing HIF1 pathway is significantly enriched in proteins containing labile disulphide bonds (**Table 3.2**). My focus was on protein kinase B/Akt involved in the PI3K/Akt/mTOR cell signalling cascade.

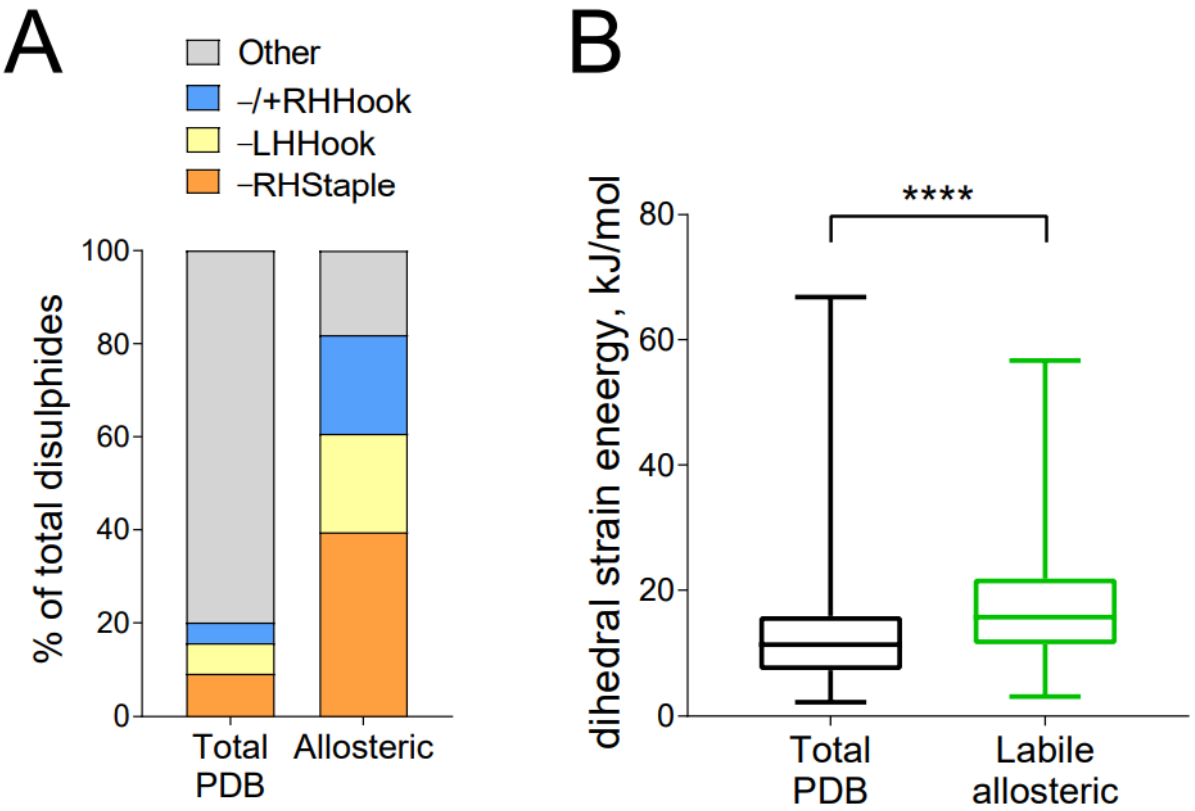

Figure 3.4 The labile disulphides with allosteric configurations have higher dihedral strain energy.

A. The –RHstaple, –LHhook, and –/+RHhook configurations represent 9%, 6.5%, and 4.5% of all disulphide bonds in the PDB. For the structurally defined allosteric disulphide bonds (n = 29), these percentages increase to 39%, 16%, and 16%, respectively. **B**. The labile disulphide bonds with allosteric configurations (n = 158) have an increased DSE compared to the total PDB (****p<0.0001, Mann-Whitney test).

Table 3.1 Allosteric disulphides with known configurations.

Protein	Species	Disulphide Cys	PDB	Configuration
Methionine aminopeptidase 2	*Homo sapiens*	228–448	1B59	–RHstaple
Tissue Factor	*Homo sapiens*	186–209	1BOY	–RHstaple
Botulinum neurotoxins	*Clostridium botulinum*	436–445	1EPW	–RHstaple
Prolyl cis-trans isomerase, AtFKBP13	*Arabidopsis thaliana*	106–111	1Y0O	–RHstaple
HIV gp120	*Human immunodeficiency virus type 1*	126–196	1YYM	–RHstaple
		296–331		–RHstaple
		385–418		–RHstaple
Transglutaminase 2	*Homo sapiens*	370–371	2Q3Z	–RHstaple
CD4	*Homo sapiens*	130–159	3CD4	–RHstaple
Arylsulfate sulfotransferase	*Escherichia coli*	418–424	3ELQ	–RHstaple
C-reactive protein	*Homo sapiens*	36–97	3L2Y	–RHstaple
von Willebrand factor	*Homo sapiens*	2451–2468	3BK3	–RHstaple
β2-glycoprotein I	*Homo sapiens*	288–326	1C1Z	–/+RHhook
Factor XI	*Homo sapiens*	362–482	2F83	–/+RHhook
Angiotensinogen	*Homo sapiens*	18–138	2WXW	–/+RHhook
Lon protease[1]	*Homo sapiens*	617–691	3WU4	–/+RHhook
Plasmin(ogen)	*Homo sapiens*	462–541	4DUR	–/+RHhook
Interleukin receptor subunit gamma	*Homo sapiens*	160–209	2ERJ	–LHhook
CD44	*Mus musculus*	81–101	2JCP	–LHhook
Vascular endothelial growth factors C & D	*Homo sapiens*	156–165	2X1W	–LHhook
XRCC1	*Homo sapiens*	12–20	3LQC	–LHhook
Plasmin(ogen)	*Homo sapiens*	512–536	4DUR	–LHhook
QueF	*Bacillus subtilis*	55–99	5UDG	–LHhook
CgDapF	*Corynebacterium glutamicum*	83–221	5H2G	–LHhook
C-terminal Src kinase[2]	*Homo sapiens*	122–164	3EAC	+LHhook
Transglutaminase 2	*Homo sapiens*	230–370	3LY6	+RHstaple
hTryptaseβ[3]	*Homo sapiens*	191–220	2FPZ	–RHhook
Thiolase	*Clostridium acetobutylicum*	88–378	4XL2	+/–LHspiral
MICA	*Homo sapiens*	202–259	1HYR	–/+LHhook
PAI-2	*Homo sapiens*	79–161	1BY7	Undetermined

1. Also exists in a +/–LHspiral configuration (PDB 3WU4, chain A)
2. Also exists in a +/–RHspiral configuration (PDB 3EAC, chain A)
3. Also exists in a –RHspiral configuration (PDB 2FPZ, chain B)

Table 3.2 Labile disulphide bonds in the HIF1 signalling pathway.
The first four characters are the PDB identifier followed by the strain. Underlined PDB identifiers of Akt1 are shown as examples in Figure 3.5.

Protein	Disulphide Cys	PDB with bond	PDB missing bond	Configuration
Akt/PKB	60–77	4EJNA, 3O96A, 5KCVA, 2UZRA, 1UNPA, 1UNRA	1UNQA, 1H10A, 2UZSA, 2UVMA	–RHstaple
EGF	133–216	4KRPA	3NJPA, 3NJPB, 1MOXA, 1MOXB, 1NQLA, 3QWQA, 1IVOA, 1IVOB, 4UV7A, 4KROA, 4UIPA, 1YY9A	–/+LHhook
Egl 9 homolog 1 (or PHD2)	201–208	4BQYA, 3OUIA, 4BQXA, 4JZRA, 5LATA, 4BQWA, 3OUHA, 2Y33A, 3HQRA, 5LBEA, 5LBFA, 2HBTA, 5LBBA, 5LB6A	4UWDA, 5L9RA, 3HQUA, 5A3UA, 5A3UB, 5A3UC, 4KBZA, 3OUJA, 2HBUA, 5LBCA, 2G19A, 2G1MA, 5L9BA, 5L9BB, 2Y34A	+/–LHspiral
EP300	1796–1806 1796–1801	3P57P	3IO2A, 2MZDA, 2MH0B, 2K8FA	+LHspiral +/–RHspiral
	1177–1201 1177–1183	4BHWA, 4BHWB	5LKUA, 5LKTA, 5LKZA, 5LKXA	+/–LHstaple +/–RHstaple
PI3K	357–524	4FULA	3DPDA, 2A4ZA, 3PRZA, 3TJPA, 4ANVA, 3ML8A, 3ML9A, 3OAWA, 3R7QA, 4FA6A, 3TL5A, 5G55A, 1HE8A	–LHstaple
TEK	1040–1118	2WQBA	3L8PA, 1FVRA, 1FVRB	–RHhook
VEGFA	188–207	4DEQB	4DEQA	–LHspiral

3.5.5 Identification of the Cys^{60}–Cys^{77} disulphide bond in crystal structures of the PH domain of Akt1

The PH domain of Akt1 (Akt1-PH) contains a labile disulphide bond that links Cys^{60} and Cys^{77} residues near the lipid binding pocket. The Cys^{60}–Cys^{77} disulphide bond is formed in all apo structures of truncated Akt1-PH (**Figure 3.5A**), but is absent in all Akt1-PH structures bound to inositol 1,3,4,5-tetrakis-phosphate (IP_4); the head group of phospholipid PIP_3 (**Figure 3.5B**). In addition, the Cys^{60}–Cys^{77} disulphide bond has the archetypal –RHstaple allosteric configuration (Schmidt et al., 2006). Reduction of the Cys^{60}–Cys^{77} disulphide bond results in movement of variable loop (VL) 3 adjacent to the disulphide bond and VL1 that lines the phosphatidylinositol binding pocket, suggesting it may be involved in PIP_3 membrane binding. Additionally, a short acidic α-helix in VL2 is present when the disulphide is intact but not when the bond is cleaved. Structurally, alignment of the oxidised and reduced crystal structures show that there is a distinct conformational change of Akt1-PH depending on the redox state of the labile disulphide bond (**Figure 3.5C**); suggesting it may be an allosteric disulphide.

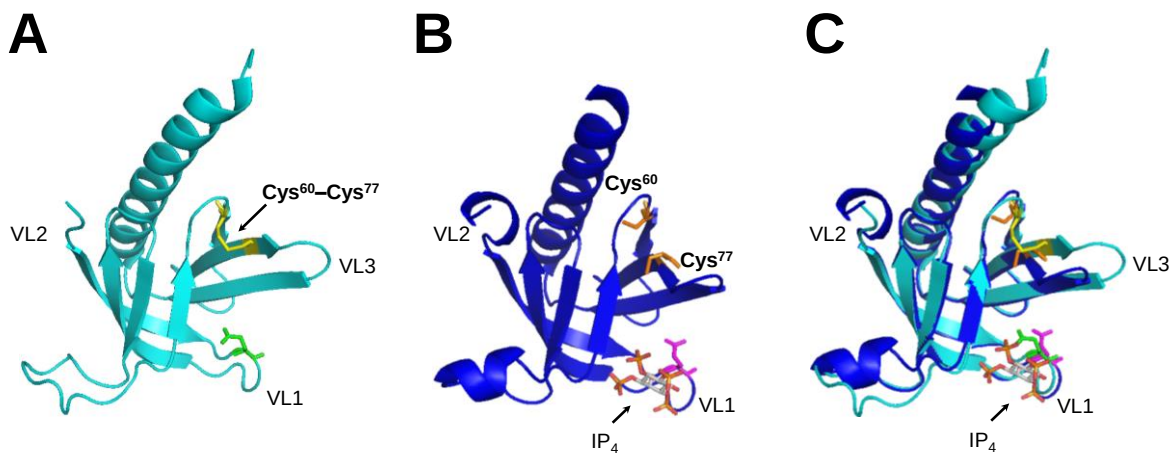

Figure 3.5 Conformational change in the PH domain of Akt1 from cleavage of a labile disulphide bond.
Crystal structures of oxidised (PDB identifier 1UNPA) and reduced (PDB identifier 1UNQA) PH domains of Akt1 (Akt1-PH) adapted from Milburn et al., 2013. **A.** The apo structure (cyan) contains an oxidised Cys^{60}–Cys^{77} disulphide bond that has an archetypal allosteric –RHstaple configuration. **B.** The Cys^{60}–Cys^{77} disulphide bond is reduced (blue) in structures of the Akt1-PH bound to inositol 1,3,4,5-tetrakisphosphate (IP_4). **C.** Conformational differences in oxidised versus reduced Akt1-PH structures. The oxidised (A) and reduced (B) structures have been overlayed. Positions of variable loops (VL) 1, 2 and 3 differ depending on the redox state of the disulphide bond.

3.6 Discussion

External mechanical forces regulate cleavage of protein disulphide bonds (Ainavarapu et al., 2008; Baldus & Gräter, 2012; Garcia-Manyes et al., 2009; Keten et al., 2012; Li & Gräter, 2010; Liang & Fernandez, 2009; Ribas-Arino & Marx, 2012; Wiita et al., 2006; Wiita et al., 2007). Rates of thiol/disulphide bond exchange are subject to mechano-chemical coupling. That is, the reactivity of a disulphide bond can be increased or decreased by mechanical forces that stretch, bend and twist the sulphur-sulphur and neighbouring bonds. For example, stretching of the sulphur-sulphur bond enhances cleavage of the disulphide.

Internal mechanical forces also control cleavage of protein disulphide bonds in an analogous fashion (Zhou et al., 2014). Two of the twenty disulphide bond configurations; –RHstaple and –/+RHhook bonds, are particularly subject to topological stresses and allosteric function has been reported for seventeen of these bonds thus far. The –LHhook configuration is also being associated with allosteric function with seven examples thus far, although these bonds are no more stressed than the other eighteen configurations and it remains to be determined the reason for this functional association.

While these biophysical properties are informative and have proven useful for identifying new allosteric bonds, it is likely that the majority of the approximately 2,800 disulphide bonds with allosteric configurations in known protein structures will not be redox active. To facilitate identification of this post-translational control of protein function, we mined X-ray structures for labile disulphide bonds that exist in some structures of a protein but are reduced in others. Our hypothesis is that the facile nature indicates a propensity for cleavage and so possible allosteric regulation of the protein in which the disulphide resides.

The limitations of this analysis are the availability of crystal structures, potential differences in the qualities of the structures themselves, and the non-native conditions that may have been employed to obtain the crystals and structures. For example, purifying and crystallising cytosolic proteins in oxidising conditions. It is also possible that some of the identified labile bonds are the result of cleavage by X-rays during data collection (Sutton et al., 2013), or inefficient formation during maturation of the protein. This does not exclude an allosteric function for these particular bonds, although they may have no functional role in the protein.

Five hundred and eleven labile disulphide bonds were identified and we suggest that these bonds are enriched in allosteric disulphides. This conclusion is supported by the finding that the labile bonds are stressed based on high average dihedral strain coupled with an average elongated sulphur-sulphur bond length and extended bond angles. As stretching of the sulphur-sulphur bond makes disulphides easier to cleave (Baldus & Gräter, 2012), this feature is likely a major reason why the identified bonds are labile. Five known allosteric disulphides are captured in the labile bonds and visual inspection of some of the labile bonds suggest an allosteric function, which further supports the conclusion that the labile bonds are enriched in allosteric disulphides.

A high proportion of labile disulphide bonds occur in proteins that reside in the cytoplasm or nucleus. This finding implies that these intracellular compartments are conducive to this post-translational protein control. Cleavage and/or formation of the labile disulphides are presumably enabled by the precise redox buffering mechanisms of the cytoplasm/nucleus. Pathway analysis showed that proteins involved in the HIF1 oxygen homeostasis system were enriched among human proteins containing labile disulphides. Notably, reversible disulphide

bond formation has been speculated to be a common regulatory mechanism of oxygen sensors (Cremers & Jakob, 2013).

Among the list of human proteins involved in the HIF1 signalling pathway, the Cys^{60}–Cys^{77} disulphide bond in the PH domain of Akt1 was of interest due its –RHstaple allosteric configuration (Schmidt et al., 2006). Cleavage of the Cys^{60}–Cys^{77} disulphide bond induced a significant conformational change of the lipid-bound Akt1 PH domain. In this thesis, I investigate whether the redox state of the Cys^{60}–Cys^{77} disulphide bond has a functional role in Akt1 function.

4. The Cys^{60}–Cys^{77} disulphide bond is involved in plasma membrane localisation of Akt1

4.1 Introduction

Akt is a highly conserved human serine/threonine protein kinase. Mammalian cells express three isoforms; Akt1/PKBα, Akt2/PKBβ and Akt3/PKBγ. Isoforms of human Akt are similar in structure, consisting of an N-terminus PH domain, followed by the catalytic kinase domain and the C-terminus regulatory domain. The focus of this study is primarily on the Akt1 isoform.

Growth factor stimulation recruits PI3K to the plasma membrane catalysing the phosphorylation of PIP_2 to generate PIP_3. Allosteric activation of Akt1 is initiated by its PH domain binding to PIP_3 (Ebner et al., 2017), resulting in a significant conformational change in Akt1 to expose its activation loop (Milburn et al., 2003). Akt1 is subsequently phosphorylated at Thr^{308} and Ser^{473} residues by PDK1 and mTORC2, respectively. Upon Akt1 membrane dissociation, allosteric communication between the PH and kinase domains promotes autoinhibition; the rate limiting step for Akt1 dephosphorylation (Ebner et al., 2017).

Akt1 is often overexpressed and hyperactivated in cancers to promote tumour growth and survival (Bellacosa et al., 2005; Hers et al., 2011; Manning & Cantley, 2007; Staal et al., 1977; Sun et al., 2001). The autoinhibitory role of the membrane binding PH domain is to maintain the inactive conformation of Akt1. The common somatic mutation of Glu^{17} to Lys (E17K-Akt1) in the PH domain of Akt1 weakens the PH–kinase domain interaction, leading to oncogenic activation of Akt1 (Carpten et al., 2007; Parikh et al., 2012). Exposure of the PH and kinase domains constitutively activates Akt1 by promoting PIP_3 membrane localisation and phosphorylation of the kinase. The somatic mutation of Cys^{77} to Phe (C77F-Akt1) in the

PH domain of Akt1 was identified in clinical samples (Cerami et al., 2012; Ellis et al., 2012; Gao et al., 2013; Yi et al., 2012). This suggested that the Cys^{77} mutation may similarly perturb Akt1–PIP_3 membrane localisation by interfering with the PH–kinase domain interface.

In chapter 3, bioinformatic analyses revealed crystal structures of the PH domain of Akt1 contain a labile Cys^{60}–Cys^{77} disulphide bond with a distinct –RHstaple allosteric configuration (**Figure 3.5A**). The Cys^{60}–Cys^{77} disulphide bond is formed in all apo structures of PH domain, but is notably reduced in PH domain structures with IP_4 (Milburn et al., 2003). In this chapter, I investigate the effect of the Cys^{60}–Cys^{77} disulphide bond on Akt1 membrane localisation. I also examine the redox state of the Cys^{60}–Cys^{77} disulphide bond in truncated wild-type Akt1 PH domain and full-length WTAkt1 recombinant proteins.

The PH domain of Akt1 plays a critical role in the translocation and localisation of Akt1 at the plasma membrane (Andjelkovic et al., 1997). Moreover, mutations near the lipid binding site of the PH domain have been linked to cancer progression and may indicate a functional role, therefore justifying my investigation of the Cys^{60}–Cys^{77} disulphide bond. I hypothesise that the Cys^{60}–Cys^{77} disulphide bond in the PH domain of Akt1 is an allosteric disulphide bond that regulates Akt1 membrane localisation.

4.2 Results

To examine the effect of the redox state of the Cys^{60}–Cys^{77} disulphide bond in the PH domain of Akt1 on plasma membrane localisation, I designed truncated *Akt1-PH* DNA constructs to investigate the functional relevance of the Cys^{60}–Cys^{77} disulphide bond. Truncated *Akt1-PH* clones (Akt1 amino acid residues 1-121) constructed by PCR (**Figure 4.1A**) were based on constructs previously reported by Milburn and colleagues (Milburn et al., 2003). Disulphide bond *Akt1-PH* mutants were constructed by SLIM hybridisation (Chiu et al., 2004; Chiu et al., 2008). Cys^{60} and/or Cys^{77} residues in the PH domain were mutated to serine (Ser) (*C60S-PH, C77S-PH, C60SC77S-PH*), ablating formation of the Cys^{60}–Cys^{77} disulphide bond. Truncated wild-type (*WT-PH*) and *reduced-PH* DNA constructs (*C60S-PH, C77S-PH* and *C60SC77S-PH*) transformed in Rosetta-gami™ 2 (DE3) *E. coli* competent cells expressed recombinant Akt1-PH proteins. Crystal structures of WT-PH protein contain a mix of oxidised and reduced Cys thiols (Milburn et al., 2003), whilst the single or double cysteine mutant-PH protein is permanently in the reduced state and is lipid bound to IP_4 (**Figure 4.1B**).

In this chapter, disulphide bond Akt1 mutants (single or double Cys mutations) are denoted as reduced Akt1-PH (truncated) or reduced Akt1 (full-length) recombinant proteins. An EGFP tag was introduced at the C-terminus of designed truncated *Akt1-PH* DNA constructs to facilitate immunoblotting of truncated Akt1-PH protein.

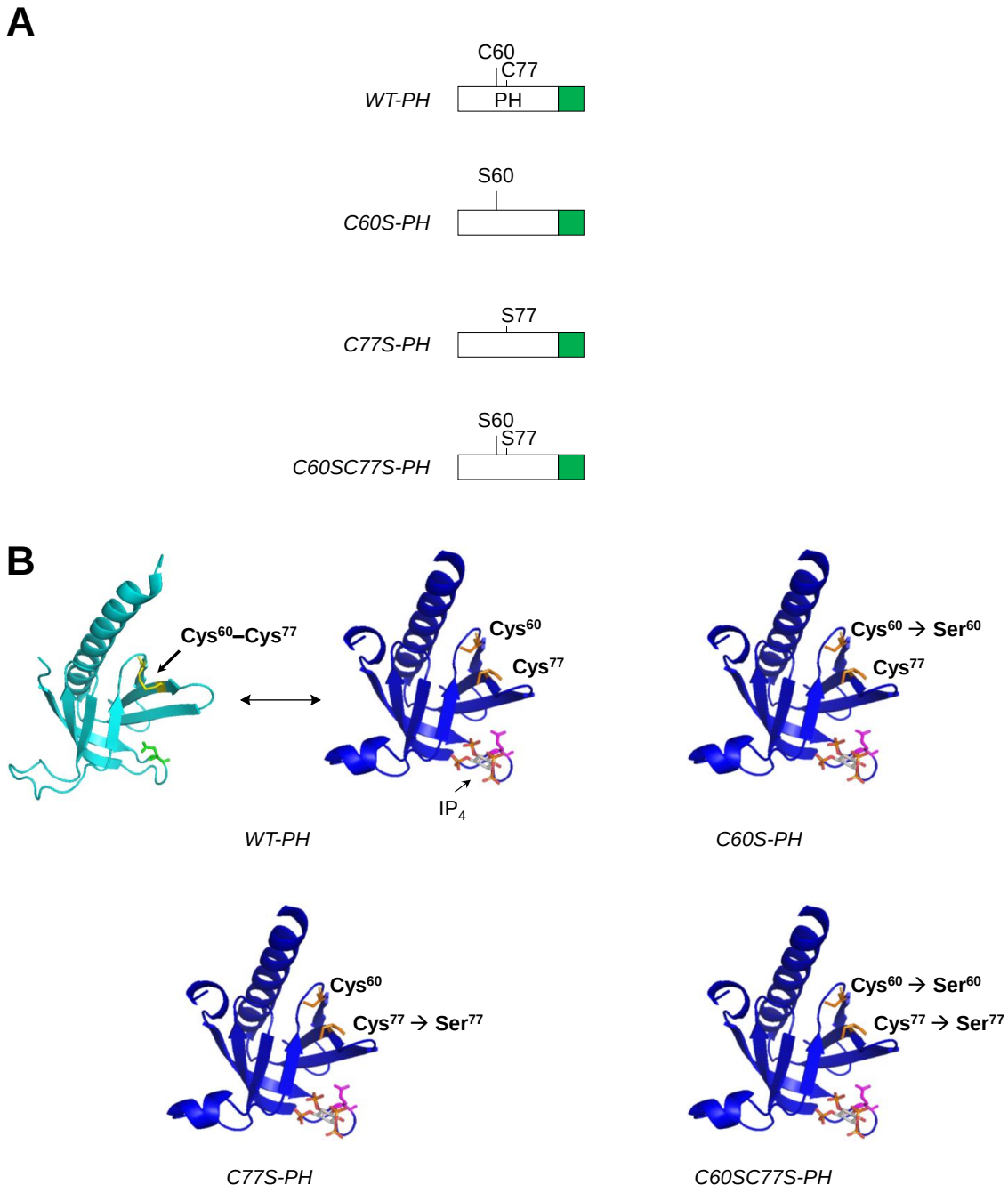

Figure 4.1 Schematic DNA and protein structures of designed truncated Akt1-PH.
A. Schematic structure of truncated oxidised and reduced *Akt1-PH* DNA constructs. Positions of functional or mutated amino acid residues in the pleckstrin homology (PH) domain of Akt1 are noted. EGFP tag is at the C-terminus of each construct. Reduced *Akt1-PH* constructs where cysteine (C) was replaced by serine (S) were generated by the PCR-based, SLIM hybridisation method (Chiu et al., 2004; Chiu et al., 2008). All *Akt1-PH* constructs were sub-cloned into the *pWaldo-TEV-GFPe* vector. **B.** Crystal structures of truncated wild-type (WT-PH) (PDB identifier 1UNPA) and reduced-PH (PDB identifier 1UNQA) recombinant proteins were adapted from Milburn et al., 2013. WT-PH contains both disulphide bonded and reduced Cys^{60} and Cys^{77} thiols. Single and double cysteine mutant-PH are permanently reduced. Oxidised-PH protein, defined by the Cys^{60}–Cys^{77} disulphide bond, is formed in all apo structures. Reduced-PH protein, defined by the cleavage of the disulphide bond, is lipid bound to inositol 1,3,4,5-tetrakisphosphate (IP_4) at the plasma membrane.

4.2.1 The Cys^{60}–Cys^{77} disulphide bond is oxidised in truncated WT-PH protein

The native state of the Cys^{60}–Cys^{77} disulphide bond in purified, truncated Akt1 wild-type PH domain (WT-PH) recombinant protein was investigated by differential cysteine alkylation and mass spectrometry analyses (Bekendam et al., 2016; Butera et al., 2018; Pasquarello et al., 2004; Passam et al., 2018). Protein expression of WT-PH detected by SDS-PAGE and SYPRO Ruby Gel staining (**Figure 4.2A**) was further verified by LC-MS. Reduced unpaired cysteine thiols in WT-PH were alkylated with ^{12}C-IPA; whilst the remaining oxidised disulphide bonded cysteines were reduced with 40 mM DTT and alkylated with ^{13}C-IPA (**Figure 4.2B**). Peptide sequences encompassing the disulphide Cys^{60} (EAPLNNFSVAQCQLMK) and Cys^{77} (CLQWTTVIER) in the PH domain of Akt1, generated from trypsin digest, were resolved and analysed. Peptides were validated by their relative retention time (RT) (**Figure 4.3**) and fragmentation spectra (**Figure 4.4A-D**). Quantification of Cys^{60} and Cys^{77} residues in WT-PH, in the presence or absence of the cellular oxidoreductase Trx, were calculated from the relative ion abundance of peptides alkylated with ^{12}C-IPA and/or ^{13}C-IPA molecules. The ratio of reduced (^{12}C-IPA) to oxidised (^{13}C-IPA) Cys^{60} and Cys^{77} residues represents the fraction of the disulphide bond in the population that is in the reduced state (**Figure 4.4E**). In untreated WT-PH, 20% of Cys^{60} and 15% of Cys^{77} residues were in the reduced state, indicating 75-80% of cysteines were oxidised and formed the Cys^{60}–Cys^{77} disulphide bond. Incubation of WT-PH with Trx resulted in a significant change in the redox state of the disulphide bond to an increase of 50% reduced, 50% oxidised of both Cys^{60} and Cys^{77} residues. This suggested Trx may potentially be involved in the reduction of the Cys^{60}–Cys^{77} disulphide bond of Akt1 in the cellular environment.

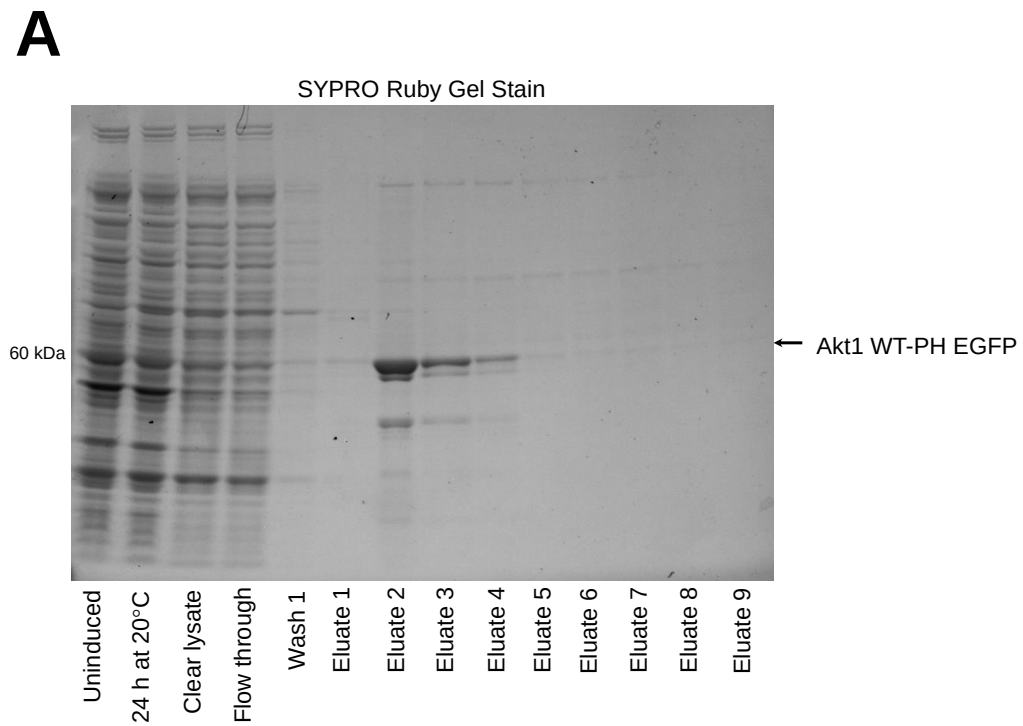

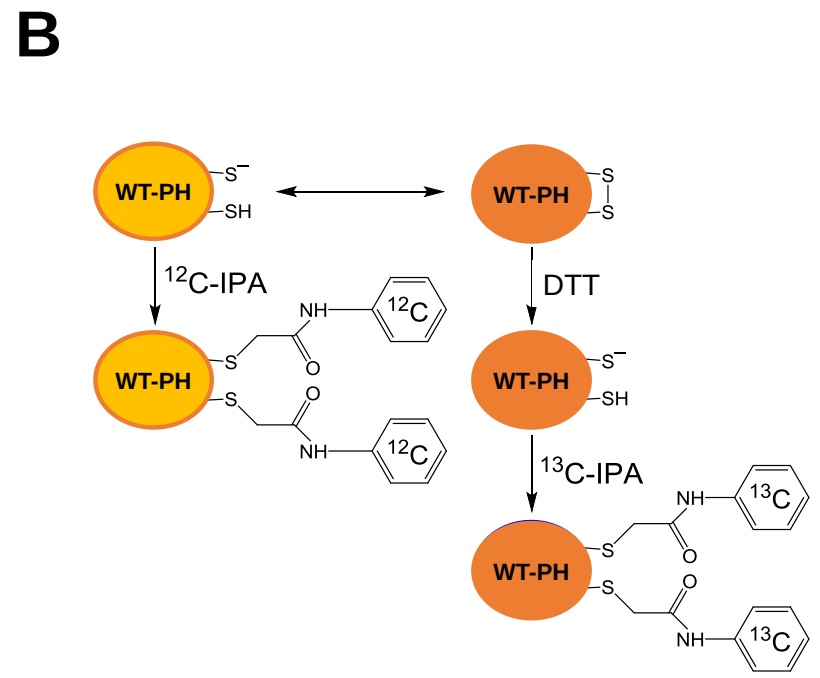

Figure 4.2 Redox state of the Cys^{60}–Cys^{77} disulphide bond in truncated Akt1 WT-PH recombinant protein determined by differential cysteine alkylation and mass spectrometry.
A. Eluates of WT-PH protein expressed in Rosetta-gami™ 2 (DE3) *E. coli* competent cells yielded 0.3 mg per 100 ml of culture. WT-PH protein was purified. **B.** Differential cysteine alkylation and mass spectrometry method of measuring the redox state of Cys^{60} and Cys^{77} in WT-PH protein. Unpaired Cys^{60} and Cys^{77} thiols are alkylated with carbon-12 isotope linked 2-iodo-*N*-phenylacetamide (^{12}C-IPA), whilst disulphide bonded thiols are alkylated with carbon-13 isotope linked 2-iodo-*N*-phenylacetamide (^{13}C-IPA) following reduction with dithiothreitol (DTT).

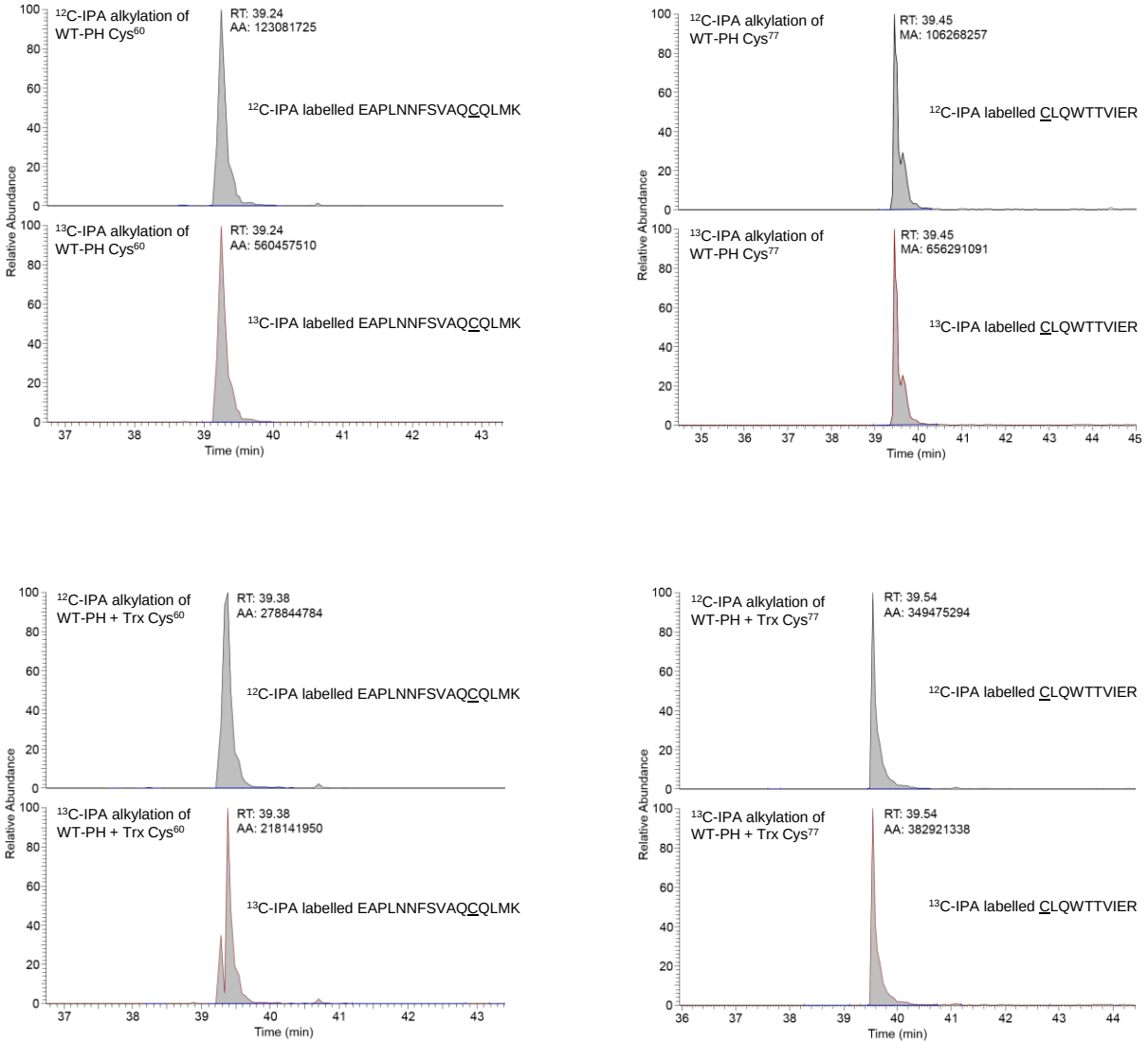

Figure 4.3 Retention time and area of Cys^{60} and Cys^{77} peptides in truncated Akt1 WT-PH recombinant protein following differential cysteine alkylation.
Relative elution times and peak areas of EAPLNNFSVAQCQLMK (Cys^{60}) and CLQWTTVIER (Cys^{77}) peptides labelled with carbon-12 isotope linked 2-iodo-*N*-phenylacetamide (^{12}C-IPA) and carbon-13 isotope linked 2-iodo-*N*-phenylacetamide (^{13}C-IPA) in WT-PH protein, either untreated or treated with thioredoxin (Trx).

A

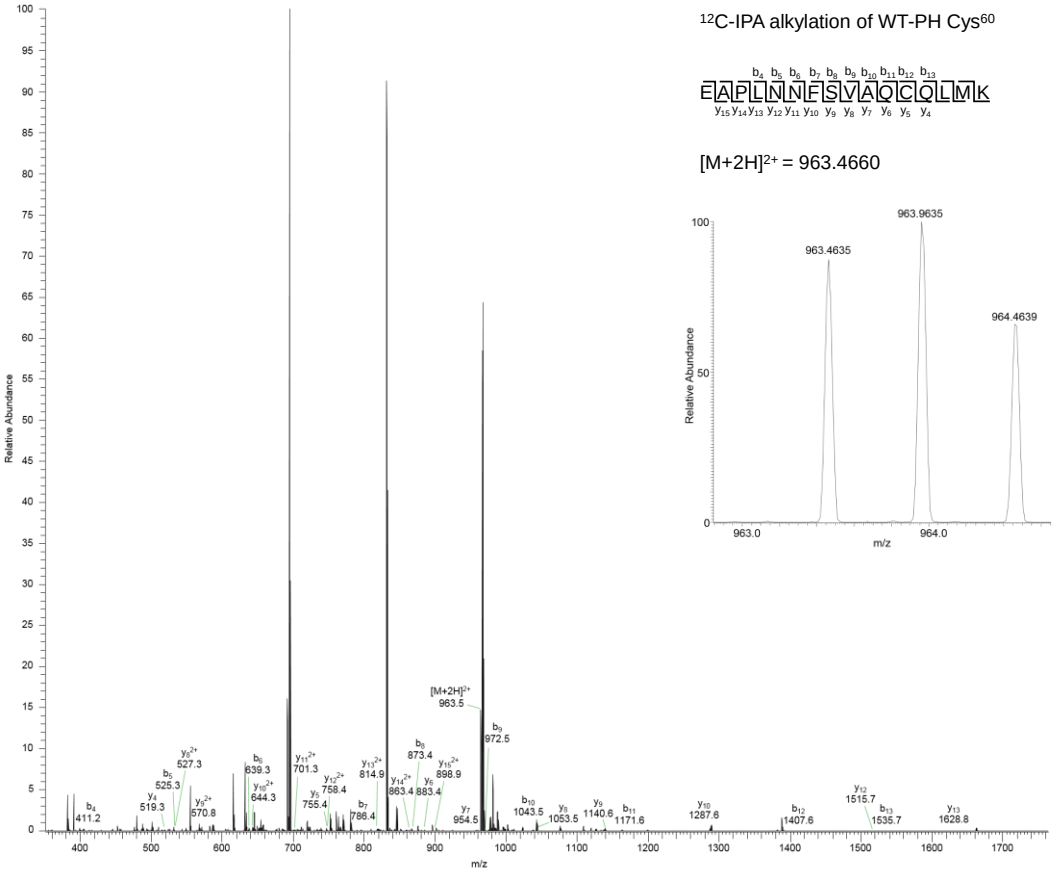
12C-IPA alkylation of WT-PH Cys60
EAPLNNFSVAQCQLMK
[M+2H]2+ = 963.4660
963.9635
963.4635
964.4639
Relative Abundance
m/z
[M+2H]2+
963.5

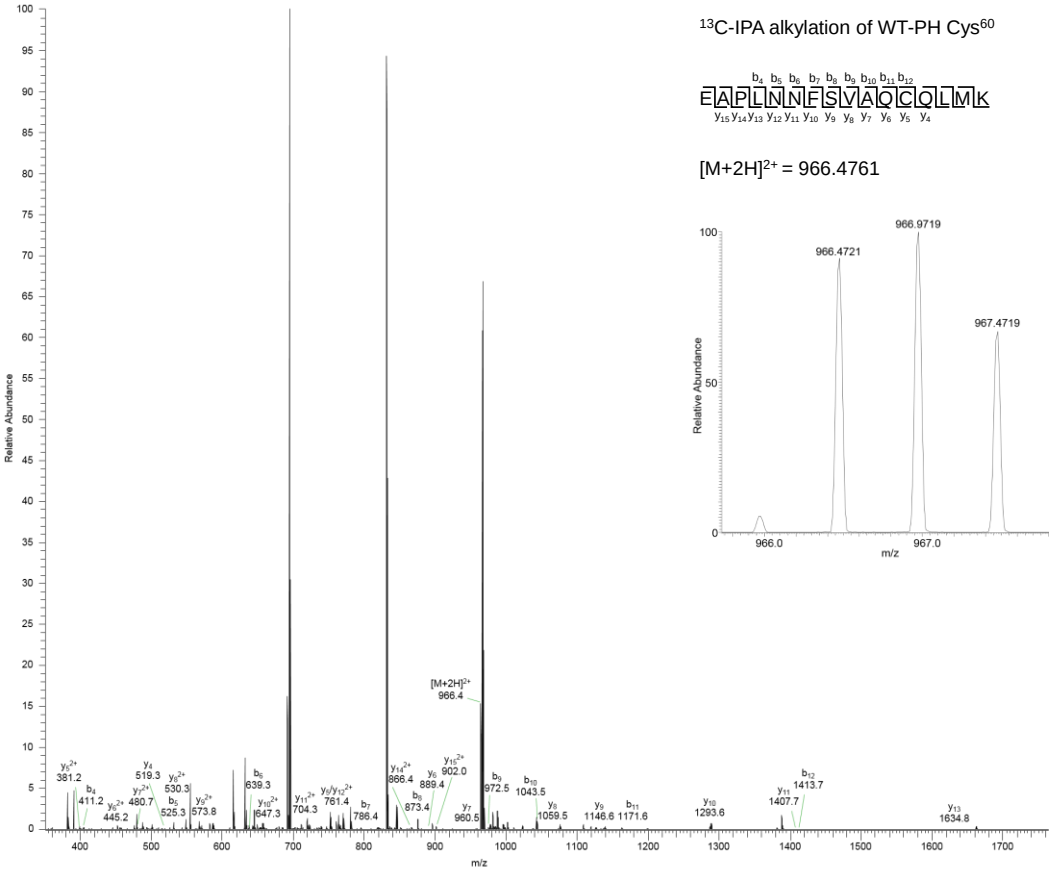
13C-IPA alkylation of WT-PH Cys60
EAPLNNFSVAQCQLMK
[M+2H]2+ = 966.4761
966.9719
966.4721
967.4719
Relative Abundance
m/z
[M+2H]2+
966.4

B

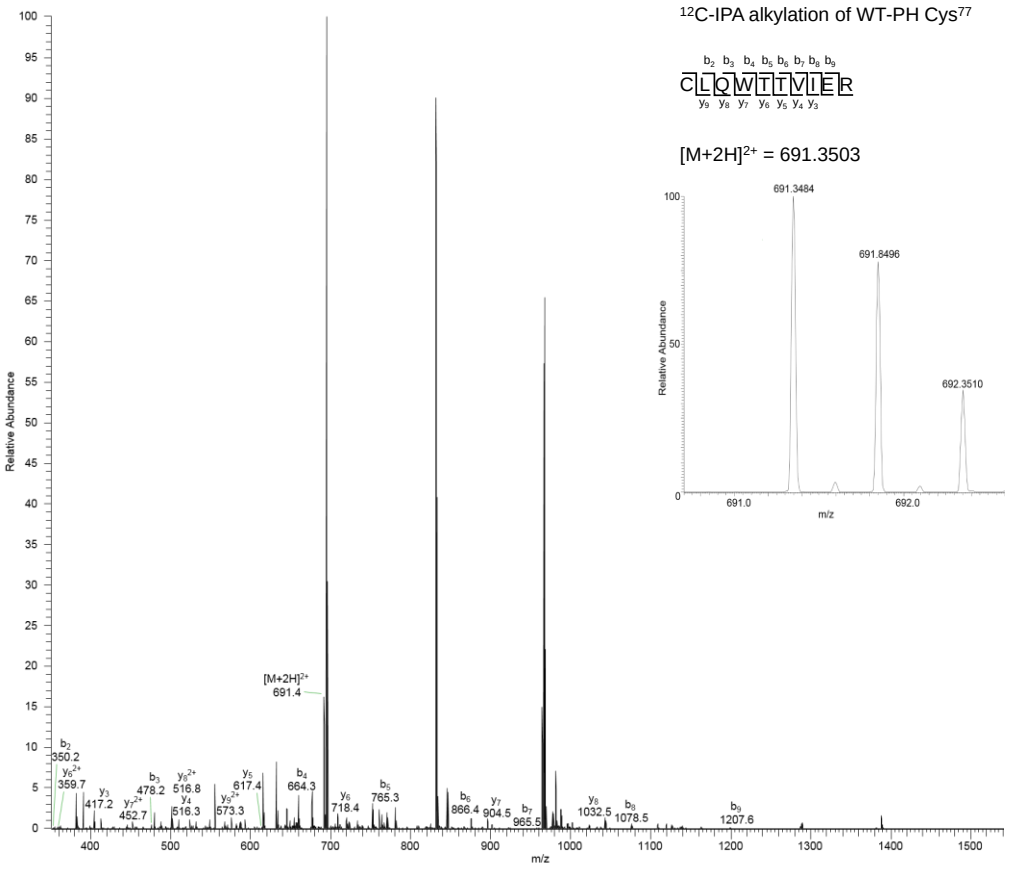
12C-IPA alkylation of WT-PH Cys77
C L Q W T T V I E R
[M+2H]2+ = 691.3503
691.3484
691.8496
692.3510
Relative Abundance
m/z
[M+2H]2+
691.4

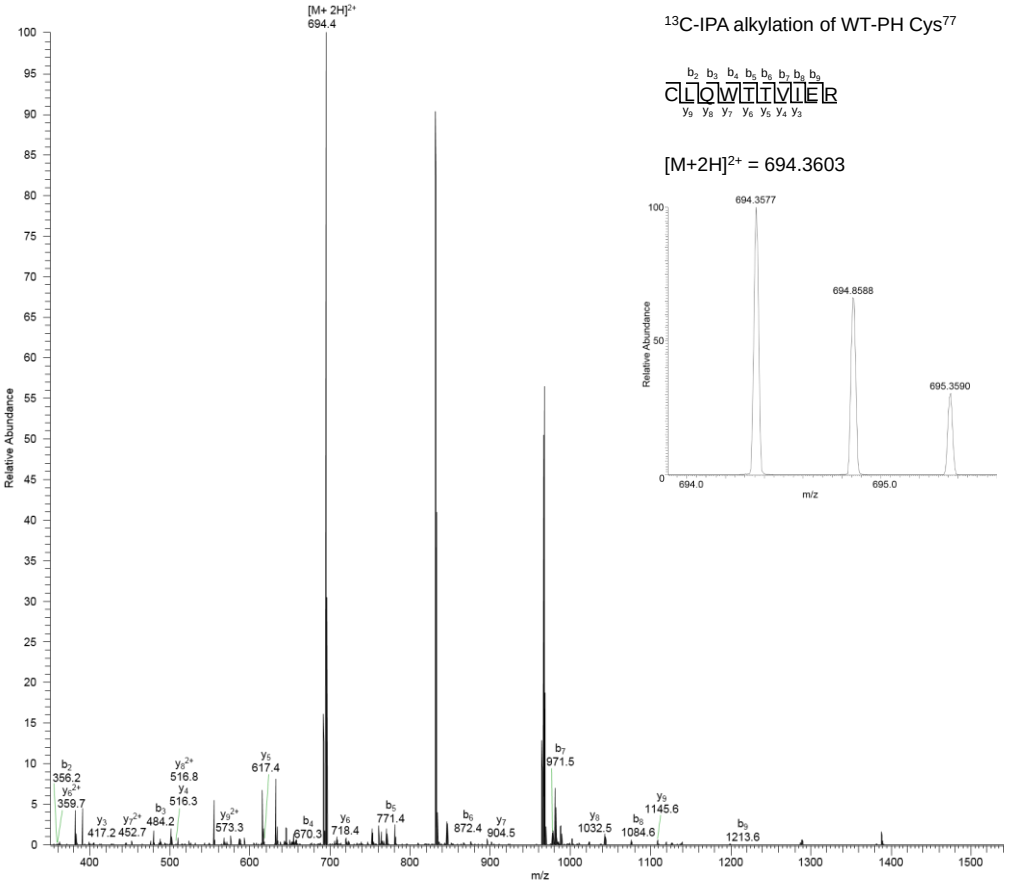
13C-IPA alkylation of WT-PH Cys77
C L Q W T T V I E R
[M+2H]2+ = 694.3603
694.3577
694.8588
695.3590
Relative Abundance
m/z
[M+ 2H]2+
694.4

C

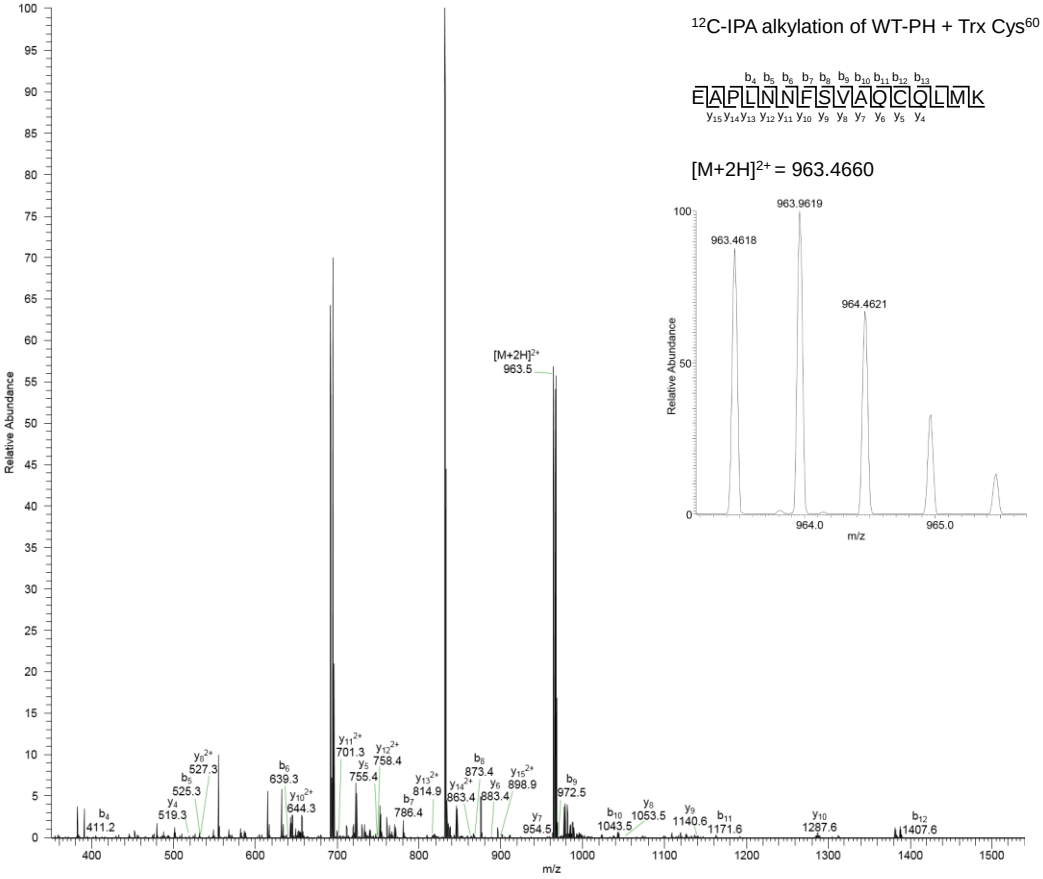
12C-IPA alkylation of WT-PH + Trx Cys60
b4 b5 b6 b7 b8 b9 b10 b11 b12 b13
EAPLNNFSVAQCQLMK
y15 y14 y13 y12 y11 y10 y9 y8 y7 y6 y5 y4
[M+2H]2+ = 963.4660
963.9619
963.4618
964.4621
Relative Abundance
m/z
[M+2H]2+
963.5

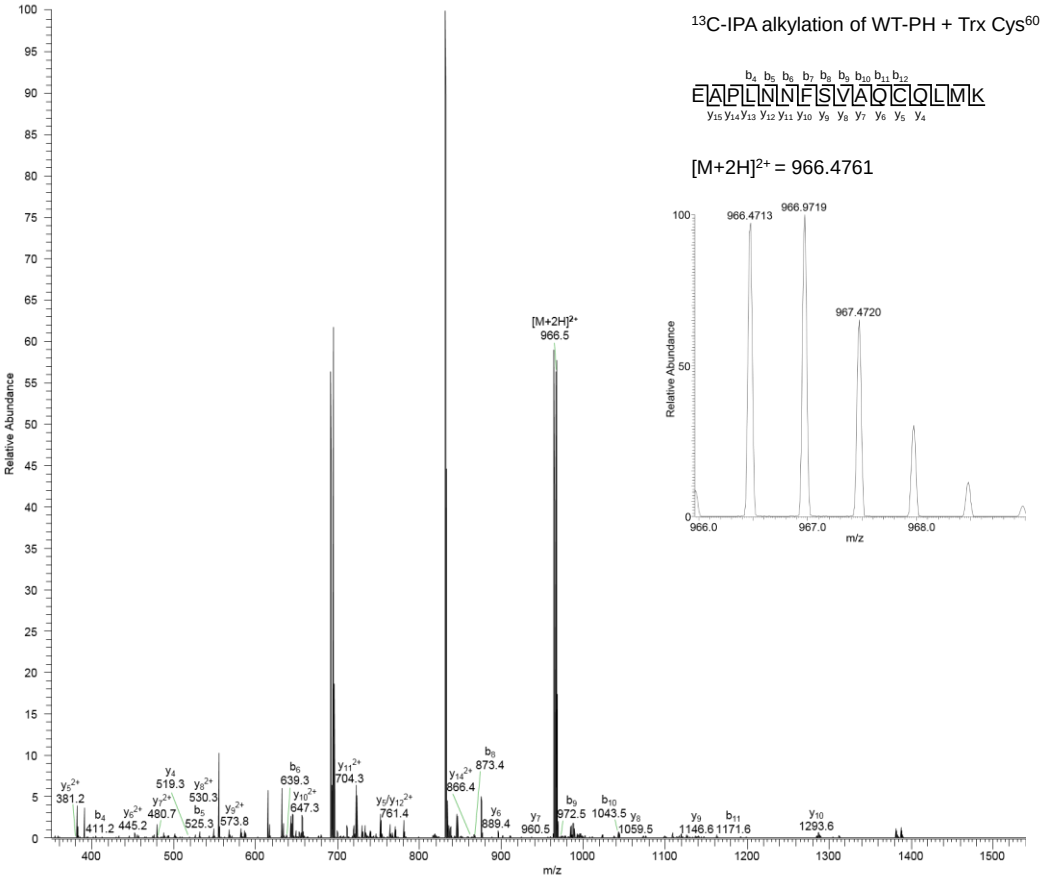
13C-IPA alkylation of WT-PH + Trx Cys60
b4 b5 b6 b7 b8 b9 b10 b11 b12
EAPLNNFSVAQCQLMK
y15 y14 y13 y12 y11 y10 y9 y8 y7 y6 y5 y4
[M+2H]2+ = 966.4761
966.4713
966.9719
967.4720
Relative Abundance
m/z
[M+2H]2+
966.5

D

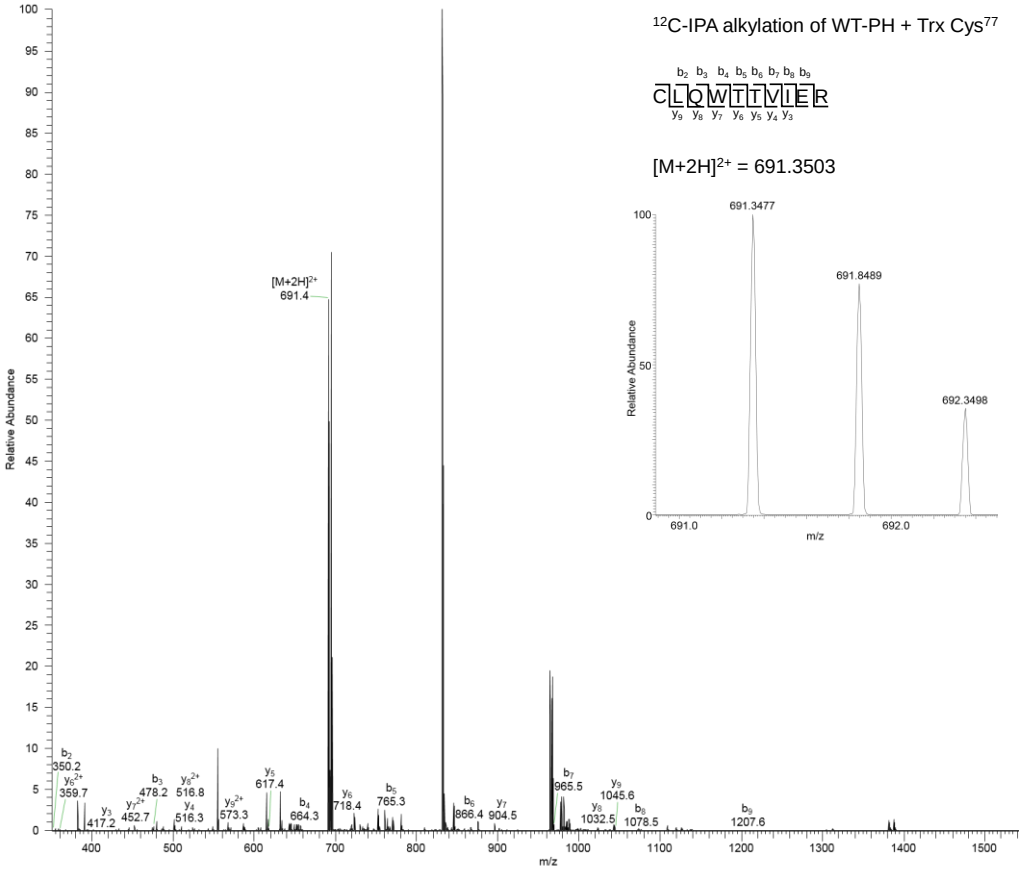
12C-IPA alkylation of WT-PH + Trx Cys77
b2 b3 b4 b5 b6 b7 b8 b9
C L Q W T T V I E R
y9 y8 y7 y6 y5 y4 y3
[M+2H]2+ = 691.3503
691.3477
691.8489
692.3498
Relative Abundance
m/z
[M+2H]2+
691.4

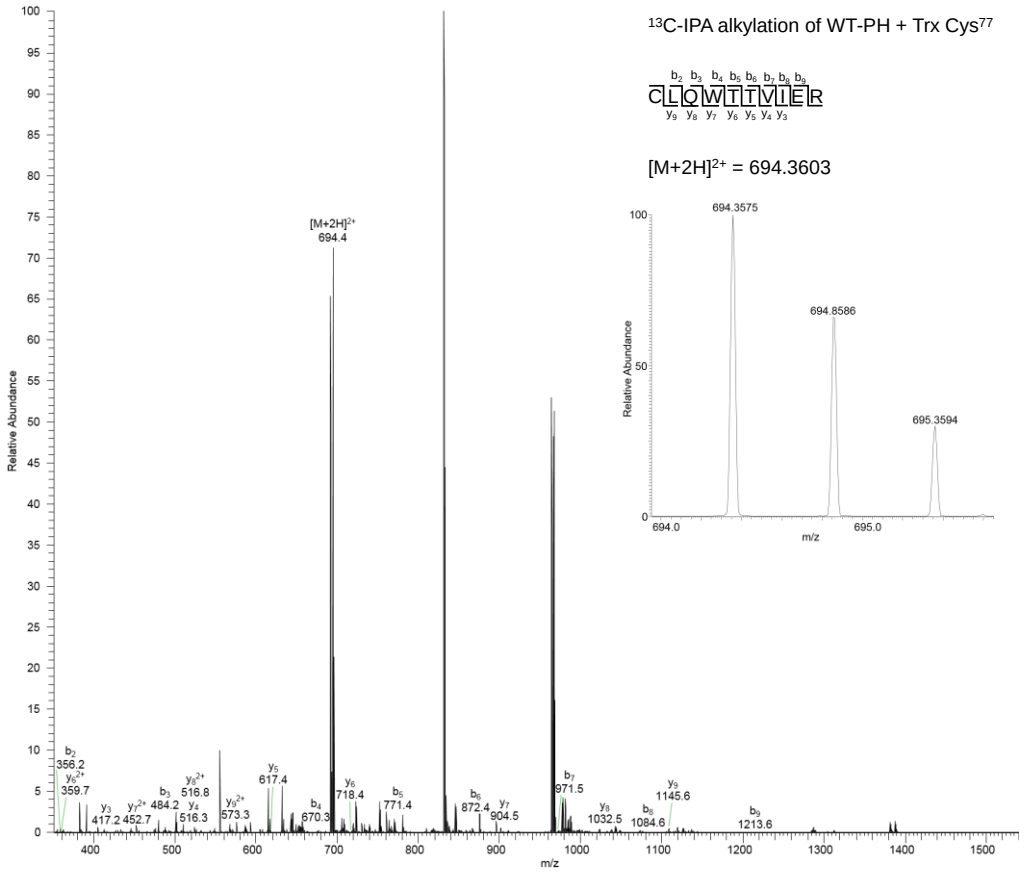
13C-IPA alkylation of WT-PH + Trx Cys77
b2 b3 b4 b5 b6 b7 b8 b9
C L Q W T T V I E R
y9 y8 y7 y6 y5 y4 y3
[M+2H]2+ = 694.3603
694.3575
694.8586
695.3594
Relative Abundance
m/z
[M+2H]2+
694.4

E

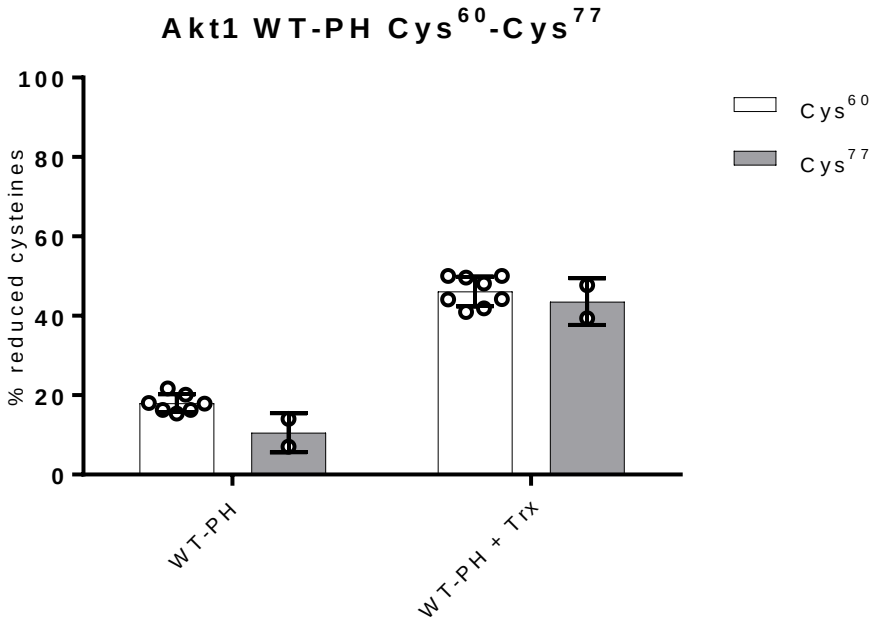

Figure 4.4 The Cys^{60}–Cys^{77} disulphide bond in truncated Akt1 WT-PH recombinant protein is oxidised.
Tandem mass spectra of the EAPLNNFSVAQCQLMK (Cys^{60}) and CLQWTTVIER (Cys^{77}) peptide sequence alkylated with labelling molecules carbon-12 isotope linked 2-iodo-*N*-phenylacetamide (^{12}C-IPA) and carbon-13 isotope linked 2-iodo-*N*-phenylacetamide (^{13}C-IPA) in WT-PH untreated or treated with thioredoxin (Trx). The EEWTTAIQTVADGLK peptide sequence (predicted: $[M + 2H]^{2+}$ = 831.4227 *m/z*) was not a peptide of interest. **A.** Accurate mass spectra of the Cys^{60} peptide labelled with ^{12}C-IPA (predicted: $[M + 2H]^{2+}$ = 963.4660 *m/z*, detected $[M + 2H]^{2+}$= 963.4635 *m/z*) and ^{13}C-IPA (predicted: $[M + 2H]^{2+}$ = 966.4761 *m/z*, detected $[M + 2H]^{2+}$= 966.4721 *m/z*) are displayed in the inset. **B.** Accurate mass spectra of the Cys^{77} peptide labelled with ^{12}C-IPA (predicted: $[M + 2H]^{2+}$ 691.3503 = *m/z*, detected $[M + 2H]^{2+}$ 691.3484 = *m/z*) and ^{13}C-IPA (predicted: $[M + 2H]^{2+}$ = 694.3603 *m/z*, detected $[M + 2H]^{2+}$= 694.3577 *m/z*). **C.** Accurate mass spectra of the Cys^{60} peptide labelled with ^{12}C-IPA (predicted: $[M + 2H]^{2+}$ = 963.4660 *m/z*, detected $[M + 2H]^{2+}$ 963.4618 = *m/z*) and ^{13}C-IPA (predicted: $[M + 2H]^{2+}$ = 966.4761 *m/z*, detected $[M + 2H]^{2+}$ 966.4713 = *m/z*). **D.** Accurate mass spectra of the Cys^{77} peptide labelled with ^{12}C-IPA (predicted: $[M + 2H]^{2+}$ 691.3503 = *m/z*, detected $[M + 2H]^{2+}$ 691.3477 = *m/z*) and ^{13}C-IPA (predicted: 694.3603 = *m/z*, detected $[M + 2H]^{2+}$ 694.3575 = *m/z*). **E.** Redox state of the Cys^{60} and Cys^{77} residues in WT-PH protein; in the presence or absence of Trx. Data are expressed as the mean ± s.d.

4.2.2 Ablation of the Akt1 Cys^{60}–Cys^{77} disulphide bond increases affinity of Akt1-PH domain for PIP_3

Allosteric activation of Akt1 is fundamentally dependent on the conformation of its membrane binding PH domain (Andjelkovic et al., 1997; Lučić et al., 2018). At the plasma membrane, phospholipid PIP_3 binds to the PH domain of Akt1 at its lipid binding site, thereby disrupting the PH domain-mediated autoinhibitory mechanism on the kinase domain (Ebner et al., 2017). Crystal structures show the Cys^{60}–Cys^{77} disulphide bond is located near the lipid binding pocket of the PH domain (**Figure 3.5A**). I therefore examined the effect of the Cys^{60}–Cys^{77} disulphide bond in truncated Akt1-PH recombinant protein on binding affinity for PIP_3 phospholipid by two independent methods.

The protein–lipid interaction assay was based on a method designed by Cho and colleagues (Cho et al., 2017). Previous reports have shown truncated Akt1-PH recombinant protein readily binds to pmol levels of PIP_3 (Frech et al., 1997; James et al., 1996). PIP_3 phospholipid was blotted onto nitrocellulose membrane and incubated with truncated WT-PH, transforming mutant E17K-PH and double cysteine mutant C60AC77A-PH recombinant proteins; followed by immunoblotting with an EGFP antibody (**Figure 4.5A-B**). Transforming mutant E17K-PH was utilised as a PIP_3 membrane binding positive control (**Figure 4.5A**). Reduced C60AC77A-PH prominently bound to PIP_3 from 5 to 100 pmol, while WT-PH lost its binding capacity at 10 pmol (**Figure 4.5B**). Lipid binding capacity of Akt1-PH was measured by densitometry analyses of EGFP (**Figure 4.5C-D**). Apparent Kd values of WT-PH indicated a lower affinity for PIP_3 than mutant C60AC77A-PH; but interestingly, a higher affinity for PIP_3 than transforming mutant E17K-PH (**Table 4.1**).

The ELISA Biotin-PIP_3 assay method was based on a procedure by Rowland and colleagues (Rowland et al., 2012). Similar to my protein–lipid overlay assays, transforming mutant E17K-PH was utilised as the positive control for Biotin-PIP_3 binding. Biotin-PIP_3 was incubated with untreated WT-PH, WT-PH treated with reducing agent DTT, single cysteine mutant C77S-PH and transforming mutant E17K-PH. Binding capacity of Akt1-PH to Biotin-PIP_3 was measured by EGFP fluorescent levels (**Figure 4.5E**). Apparent Kd values of E17K-PH indicated a higher binding affinity to Biotin-PIP_3 than all other Akt1-PH mutants (**Table 4.1**). Kd values of WT-PH showed lower affinity to Biotin-PIP_3 compared to that of DTT-treated WT-PH, suggesting reduction of the Cys^{60}–Cys^{77} disulphide bond influences Akt1 membrane binding. This was further supported by apparent Kd values of single cysteine mutant C77S-PH displaying higher affinity for PIP_3 than both untreated and DTT-treated WT-PH, possibly attributed to the mutant Ser^{77} residue causing a change in polarity at this position (the Ser hydroxyl is more polar than the Cys thiol) and altering the molecular conformation of the PH domain.

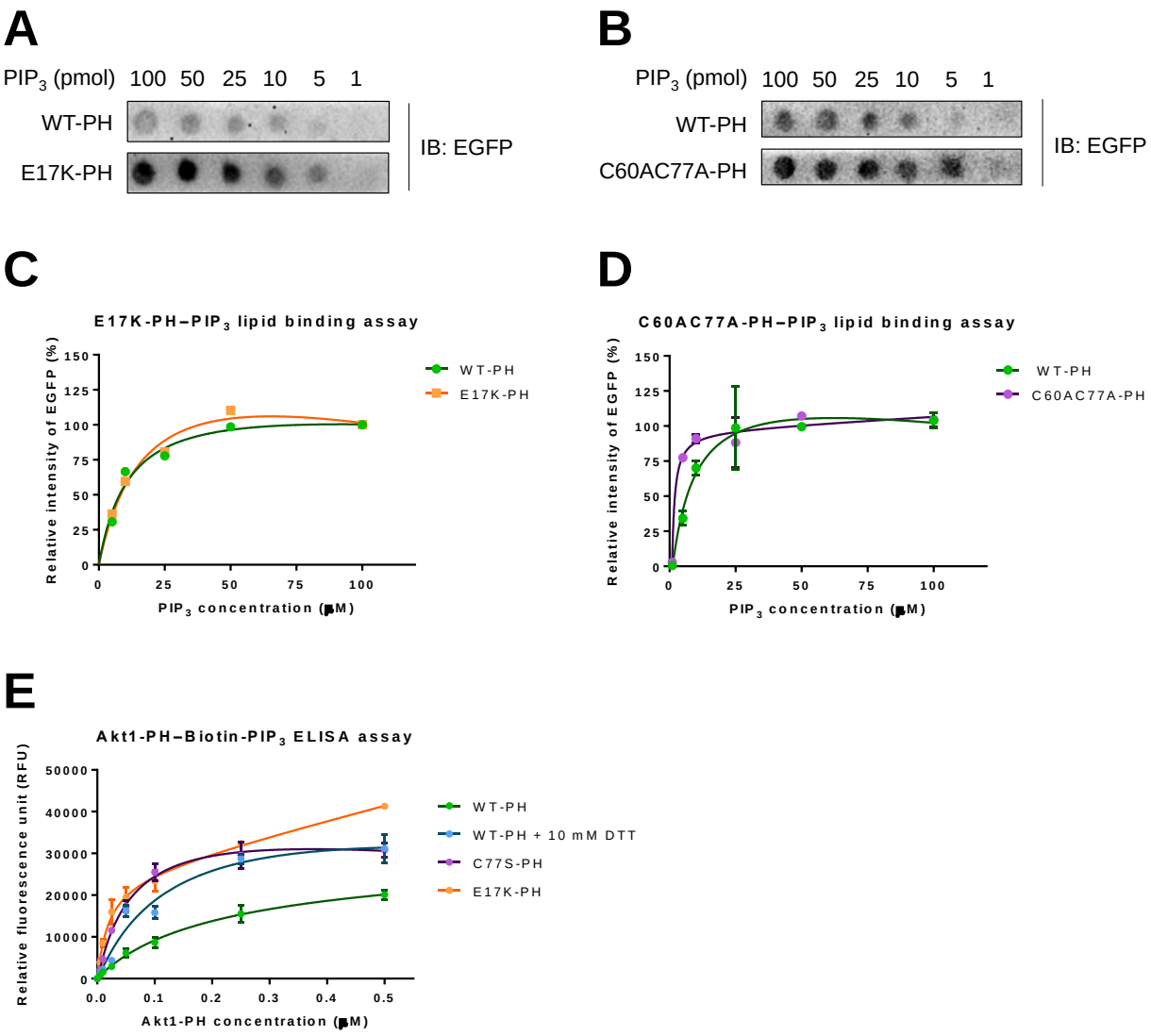

Figure 4.5 The Cys^{60}–Cys^{77} disulphide bond in truncated Akt1-PH recombinant protein affects phospholipid PIP$_3$ binding.
Binding affinity of truncated Akt1-PH proteins to phospholipid PIP$_3$ was measured by EGFP fluorescence. **A-D**. Protein–lipid overlay assays. Immunoblots (IB) detecting EGFP displayed in **A.** is of an individual experiment, and **B.** is representative of two independent experiments. **C-D**. Nonlinear regression in relative intensity (%) of blots displayed in A-B. Data are expressed as the mean ± s.d. **E.** Biotin-PIP$_3$ ELISA assay is representative of three independent experiments. Nonlinear regression of Akt1-PH protein fluorescence in relative fluorescent units (RFU). Data are expressed as the mean ± s.d.

Table 4.1 Apparent equilibrium binding constant measurements between truncated Akt1-PH recombinant proteins and phospholipid PIP_3.
Apparent Kd values of Akt1-PH–PIP_3 protein–lipid overlay assay and Akt1-PH–Biotin-PIP_3 ELISA assay displayed in Figure 4.5.

Method of detection	Akt1-PH	Apparent Kd, µM	Reference
Protein–lipid overlay assay	WT-PH	11.7 ± 0.14	Figure 4.5A,C
	E17K-PH	18.7 ± 0.47	
	WT-PH	8.15 ± 0.26	Figure 4.5B,D
	C60AC77A-PH	0.02 ± 0.11	
ELISA assay	WT-PH	193 ± 2.98	Figure 4.5E
	WT-PH + DTT	140 ± 13.1	
	C77S-PH	63.0 ± 14.2	
	E17K-PH	19.0 ± 34.9	

4.2.3 The Cys60–Cys77 disulphide bond is reduced in full-length WTAkt1 protein

The redox state of the Cys^{60}–Cys^{77} disulphide bond in immunoprecipitated full-length WTAkt1 recombinant protein was investigated in NIH/3T3 fibroblasts stably transfected with *WTAkt1*, in the absence or presence of insulin. WTAkt1 protein was immunoprecipitated from cell lysates by the HA-epitope tag engineered in the N-terminus of all full-length *Akt1* DNA constructs (**Figure 5.1**). Subsequently, I investigated the redox state of the Cys^{60}–Cys^{77} disulphide bond in response to insulin stimulation. Reduced unpaired Cys thiols in full-length WTAkt1 were alkylated with ^{12}C-IPA, whilst oxidised disulphide bonded Cys were reduced with DTT and alkylated with ^{13}C-IPA. Firstly, I confirmed that the full-length *WTAkt1* DNA constructs were effectively transfected into wild-type NIH/3T3 fibroblasts. Immunoprecipitated full-length WTAkt1 protein was verified by SDS-PAGE, followed by immunoblot detection of total Akt (**Figure 4.6A**) and SYPRO Ruby Gel staining (**Figure 4.6B**). Cysteine residues are sensitive targets of ROS generated by insulin stimulation (Goldstein et al., 2005). I therefore investigated whether oxidation of the Cys^{60}–Cys^{77} disulphide bond could be induced by insulin-stimulated ROS in the cell. NIH/3T3 fibroblasts expressing *WTAkt1* were stimulated with insulin (10 nM) for 20 min. Immunoprecipitated untreated or insulin-stimulated full-length WTAkt1 recombinant protein was verified by SDS-PAGE, followed by SYPRO Ruby Gel staining (**Figure 4.6C**). Reduced unpaired cysteine thiols in WTAkt1 were alkylated with ^{12}C-IPA; whilst the remaining oxidised disulphide bonded thiols were reduced with 40 mM DTT and alkylated with ^{13}C-IPA (**Figure 4.6D**). Peptide sequences encompassing the disulphide Cys^{60} (EAPLNNFSVAQCQLMK) and Cys^{77} (CLQWTTVIER) in the PH domain of Akt1, generated from trypsin digest, were resolved and analysed. Peptides were validated by their relative RT (**Figure 4.7**) and fragmentation spectra (**Figure 4.8A-D**). Quantification of Cys^{60} and Cys^{77} residues in untreated or insulin-stimulated WTAkt1 were calculated from the relative ion abundance of peptides alkylated with ^{12}C-IPA

and/or ^{13}C-IPA molecules. The ratio of reduced (^{12}C-IPA) to oxidised (^{13}C-IPA) Cys^{60} and Cys^{77} residues represent the fraction of the disulphide bond in the population that is in the reduced state (**Figure 4.8E**). Insulin stimulation was unable to induce Cys^{60}–Cys^{77} disulphide formation in immunoprecipitated full-length WTAkt1 protein; with >95% of both Cys^{60} and Cys^{77} residues reduced.

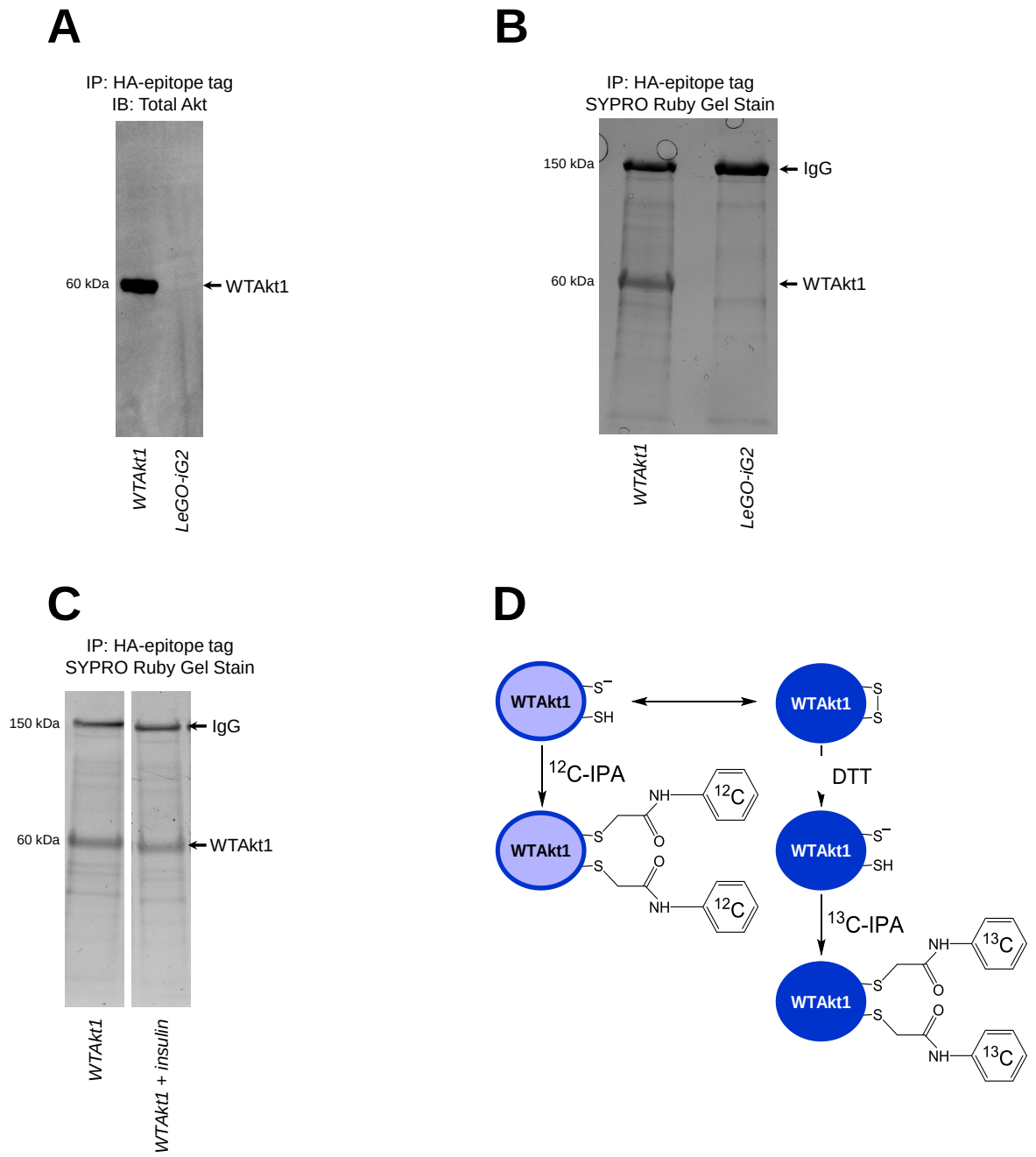

Figure 4.6 Redox state of the Cys^{60}–Cys^{77} disulphide bond in full-length WTAkt1 recombinant protein determined by differential cysteine alkylation and mass spectrometry.

Whole cell lysates were subjected to immunoprecipitation (IP) with a HA-epitope tag immunoglobulin G (IgG) antibody. Immunoprecipitated WTAkt1 was detected by **A.** immunoblotting (IB) for total Akt and **B.** SYPRO Ruby Gel staining. **C.** Immunoprecipitated untreated and insulin-stimulated WTAkt1 protein was subjected to differential cysteine (Cys) labelling. **D.** Differential cysteine alkylation and mass spectrometry method of measuring the redox state of Cys^{60} and Cys^{77} in WTAkt1. Unpaired Cys^{60} and Cys^{77} thiols are alkylated with carbon-12 isotope linked 2-iodo-*N*-phenylacetamide (^{12}C-IPA), whilst disulphide bonded thiols are alkylated with carbon-13 isotope linked 2-iodo-*N*-phenylacetamide (^{13}C-IPA) following reduction with dithiothreitol (DTT).

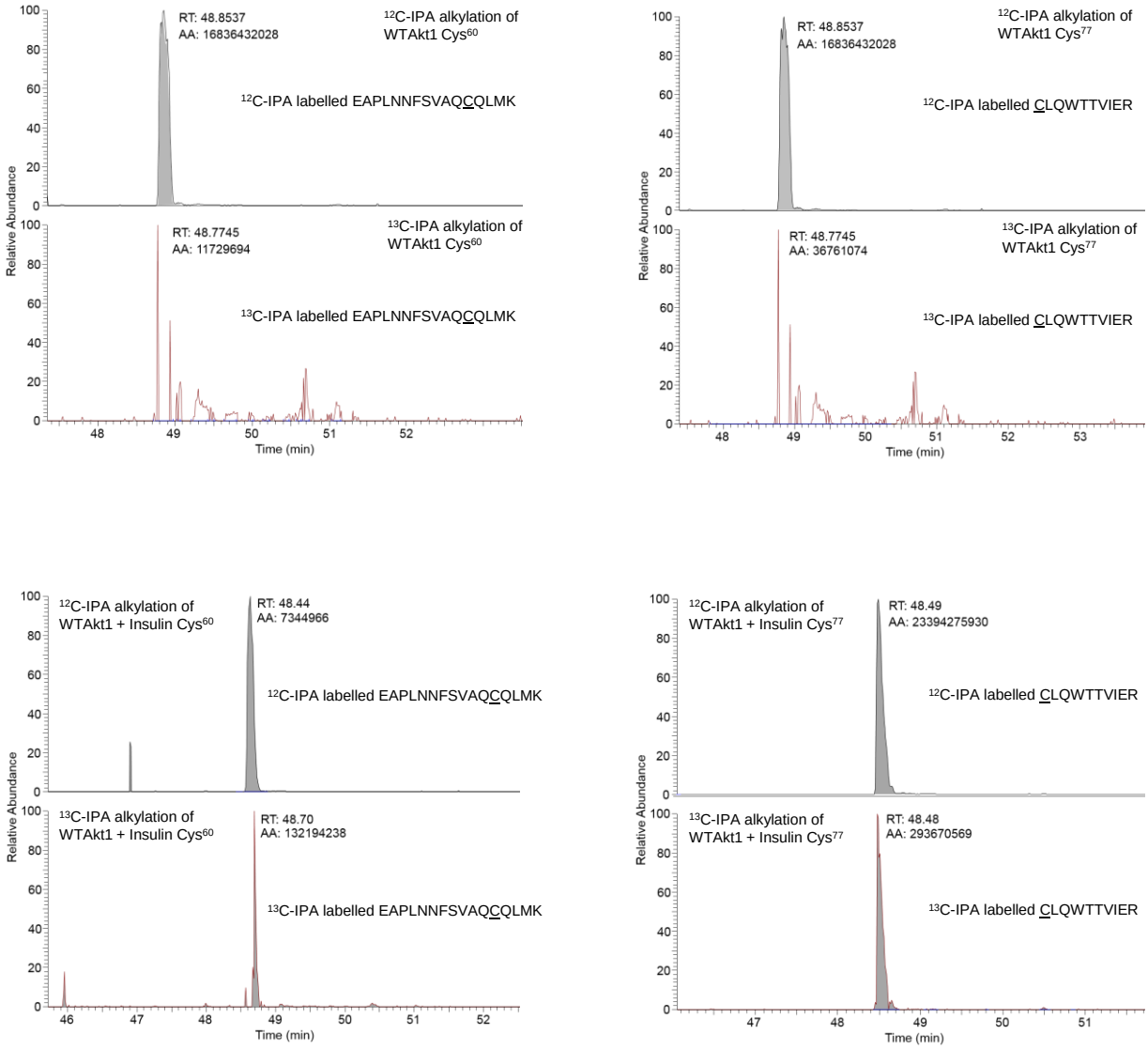

Figure 4.7 Retention time and area of Cys^{60} and Cys^{77} peptides in full-length WTAkt1 recombinant protein following differential cysteine alkylation.
Relative elution times and peak areas of EAPLNNFSVAQCQLMK (Cys^{60}) and CLQWTTVIER (Cys^{77}) peptides labelled with carbon-12 isotope linked 2-iodo-*N*-phenylacetamide (^{12}C-IPA) and carbon-13 isotope linked 2-iodo-*N*-phenylacetamide (^{13}C-IPA) in untreated or insulin-stimulated WTAkt1 protein.

A

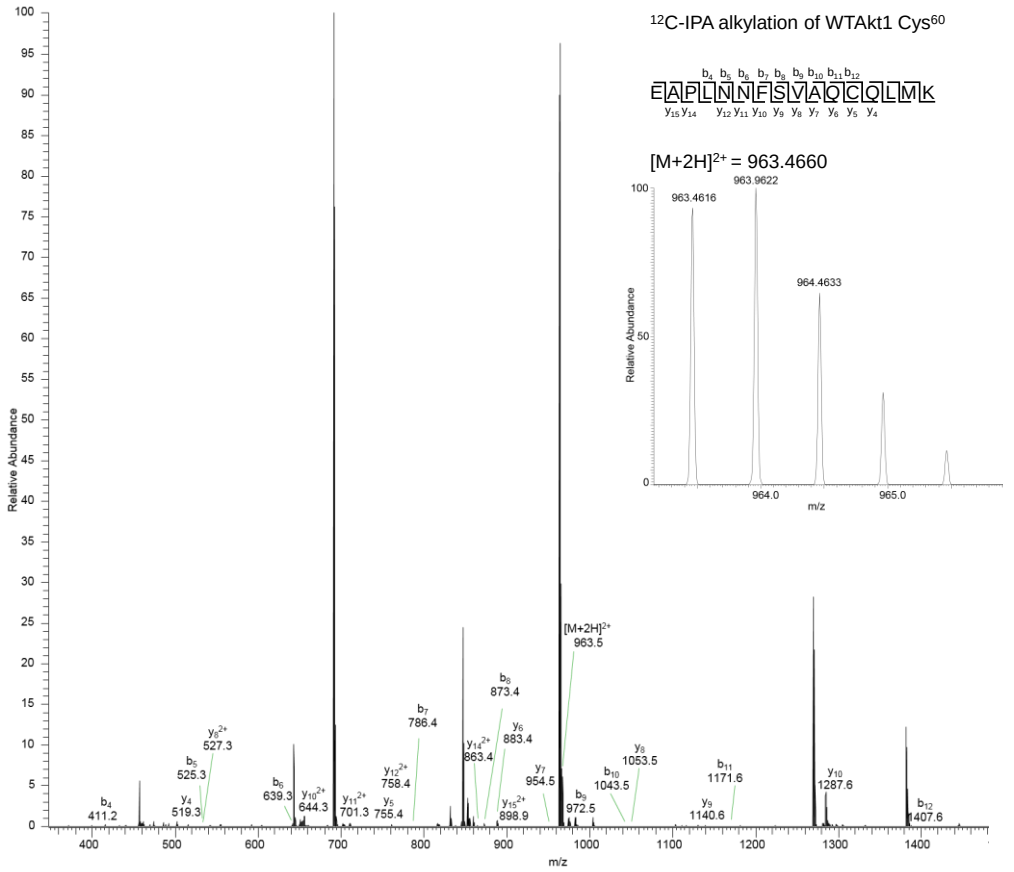
12C-IPA alkylation of WTAkt1 Cys60
EAPLNNFSVAQCQLMK
[M+2H]2+ = 963.4660
963.4616
963.9622
964.4633
Relative Abundance
m/z
[M+2H]2+
963.5
Relative Abundance
m/z

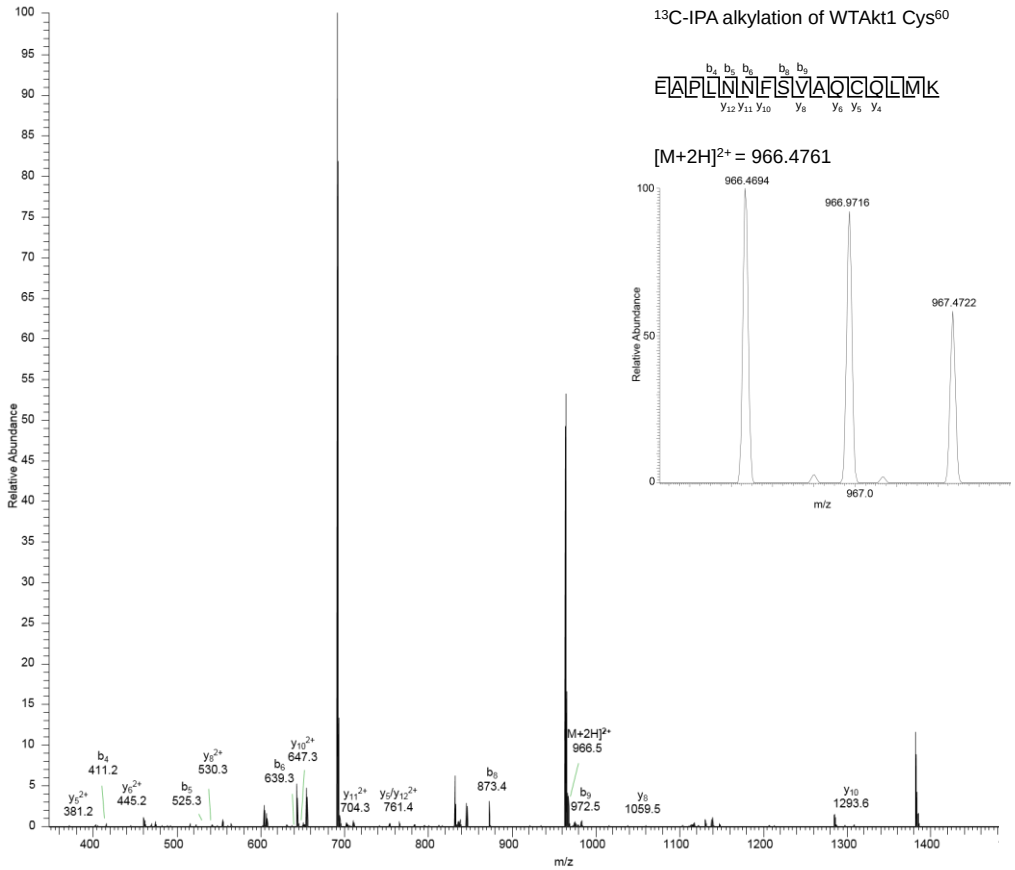
13C-IPA alkylation of WTAkt1 Cys60
EAPLNNFSVAQCQLMK
[M+2H]2+ = 966.4761
966.4694
966.9716
967.4722
Relative Abundance
m/z
[M+2H]2+
966.5
Relative Abundance
m/z

B

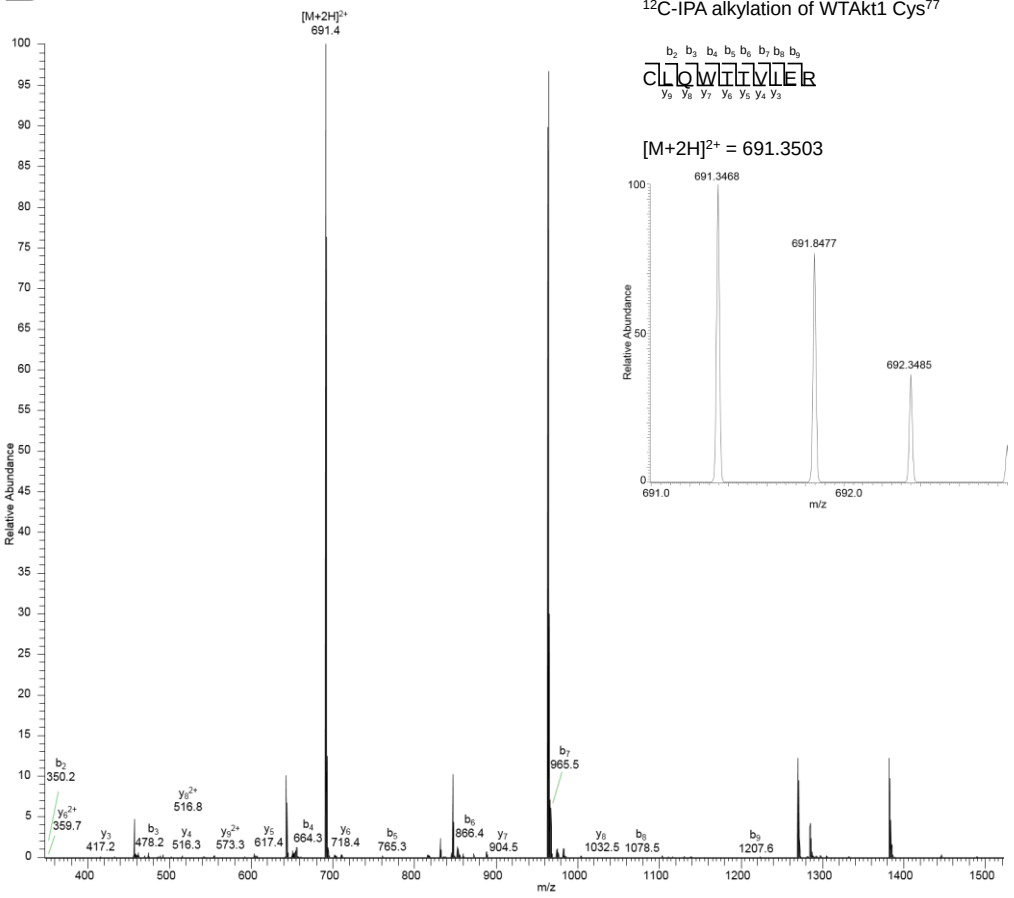

^{12}C-IPA alkylation of WTAkt1 Cys^{77}

$[M+2H]^{2+}$ = 691.3503

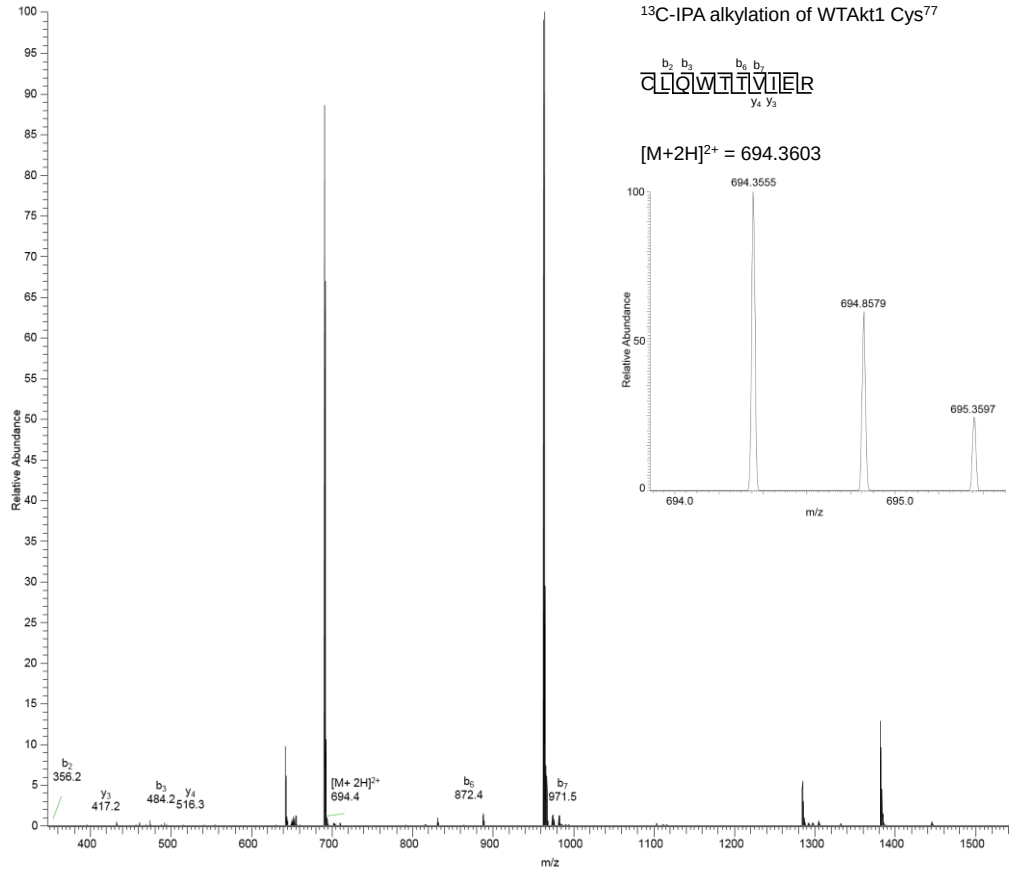

^{13}C-IPA alkylation of WTAkt1 Cys^{77}

$[M+2H]^{2+}$ = 694.3603

C

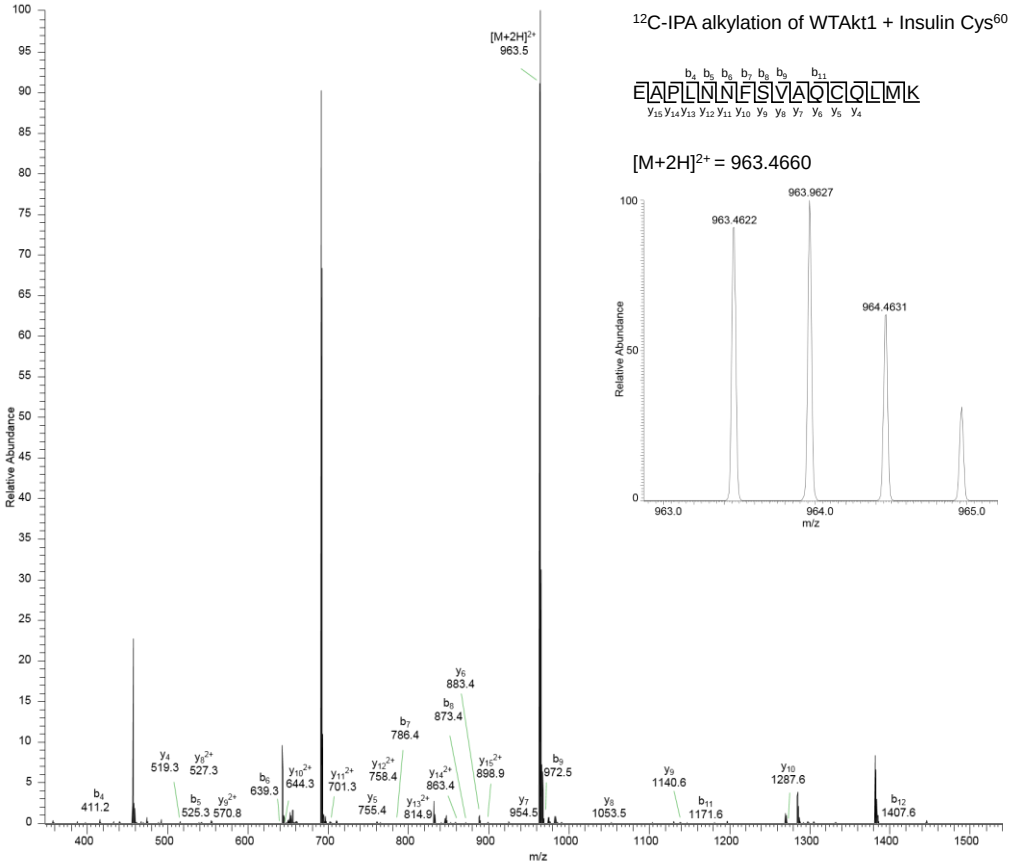

^{12}C-IPA alkylation of WTAkt1 + Insulin Cys^{60}

EAPLNNFSVAQCQLMK

$[M+2H]^{2+}$ = 963.4660

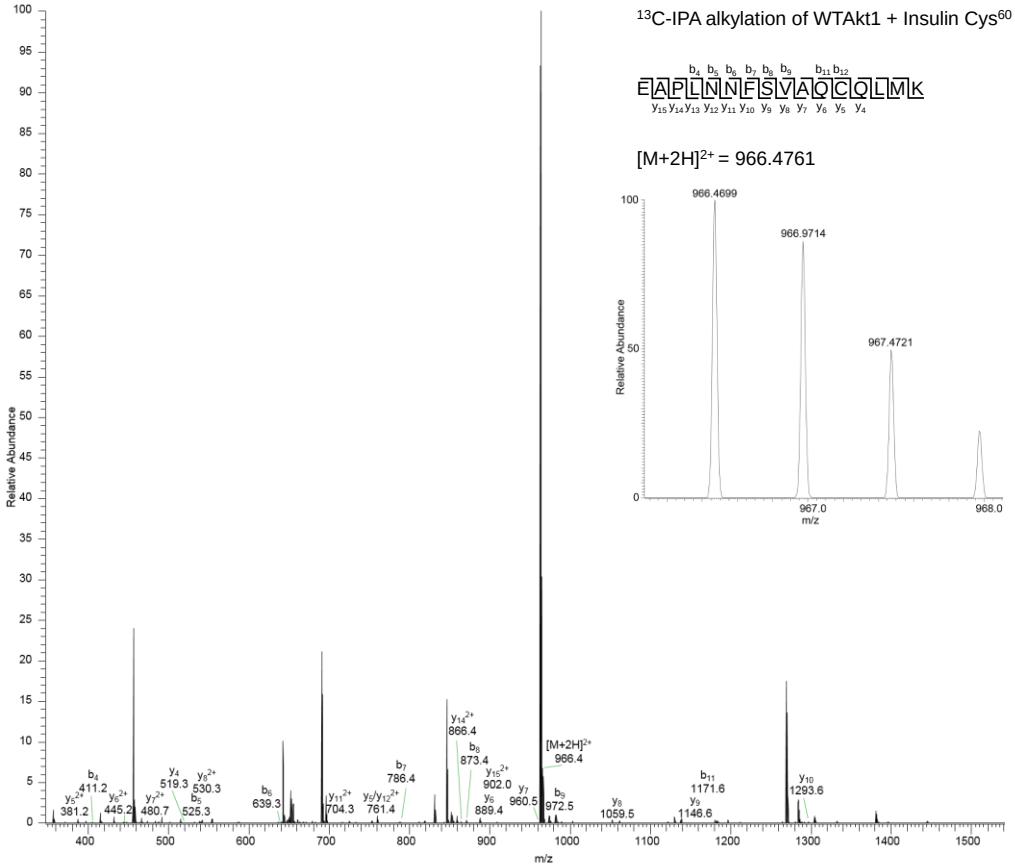

^{13}C-IPA alkylation of WTAkt1 + Insulin Cys^{60}

EAPLNNFSVAQCQLMK

$[M+2H]^{2+}$ = 966.4761

D

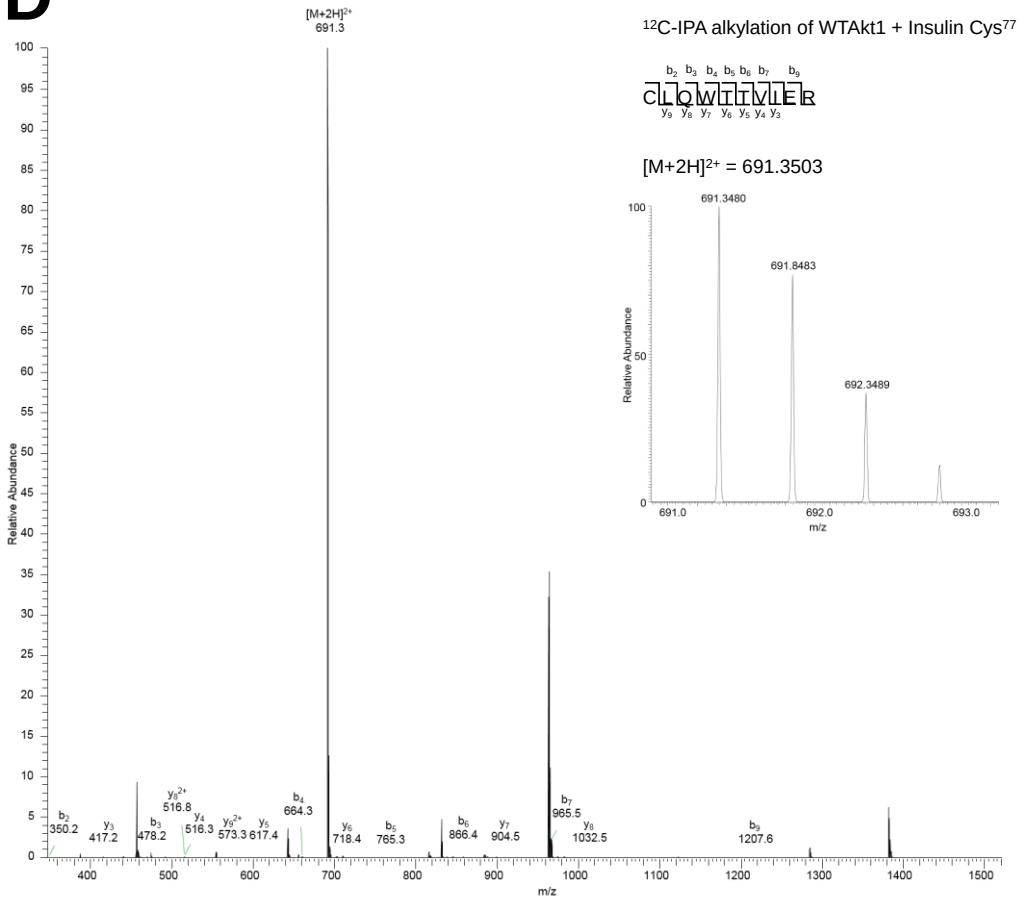

^{12}C-IPA alkylation of WTAkt1 + Insulin Cys^{77}

$[M+2H]^{2+}$ = 691.3503

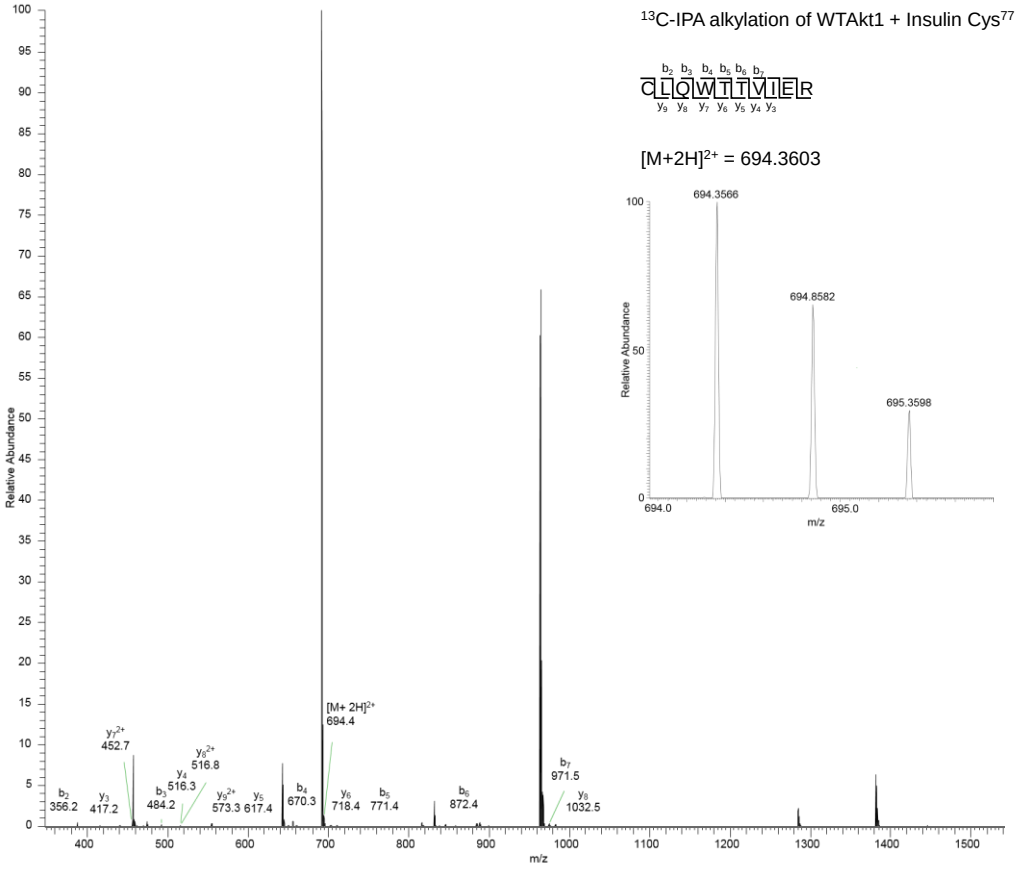

^{13}C-IPA alkylation of WTAkt1 + Insulin Cys^{77}

$[M+2H]^{2+}$ = 694.3603

E

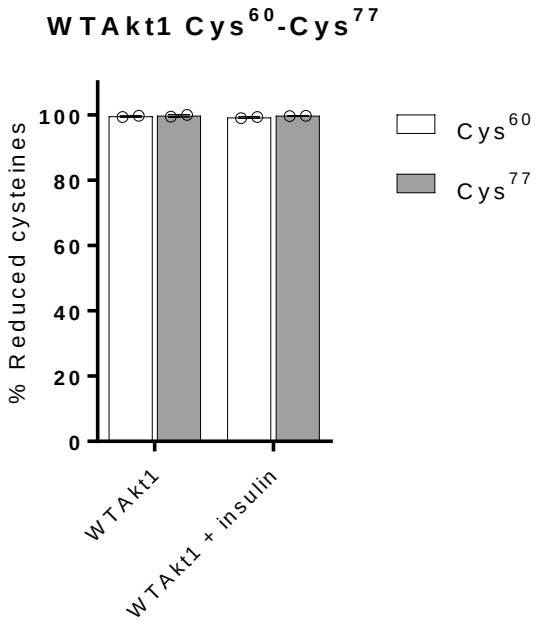

Figure 4.8 The Cys^{60}–Cys^{77} disulphide bond in full-length WTAkt1 recombinant protein is reduced.

Tandem mass spectra of the EAPLNNFSVAQCQLMK (Cys^{60}) and CLQWTTVIER (Cys^{77}) peptide sequence alkylated with labelling molecules carbon-12 isotope linked 2-iodo-*N*-phenylacetamide (^{12}C-IPA) and carbon-13 isotope linked 2-iodo-*N*-phenylacetamide (^{13}C-IPA) in insulin-stimulated WTAkt1. **A.** Accurate mass spectra of the Cys^{60} peptide labelled with ^{12}C-IPA (predicted: $[M + 2H]^{2+}$ = 963.4660 *m/z*, detected $[M + 2H]^{2+}$= 963.4616 *m/z*) and ^{13}C-IPA (predicted: $[M + 2H]^{2+}$ = 966.4761 *m/z*, detected $[M + 2H]^{2+}$= 966.4694 *m/z*) are displayed in the inset. **B.** Accurate mass spectra of the Cys^{77} peptide labelled with ^{12}C-IPA (predicted: $[M + 2H]^{2+}$ 691.3503 = *m/z*, detected $[M + 2H]^{2+}$ 691.3468 = *m/z*) and ^{13}C-IPA (predicted: $[M + 2H]^{2+}$ = 694.3603 *m/z*, detected $[M + 2H]^{2+}$= 694.3555 *m/z*).**C.** Accurate mass spectra of the Cys^{60} peptide labelled with ^{12}C-IPA (predicted: $[M + 2H]^{2+}$ = 963.4660 *m/z*, detected $[M + 2H]^{2+}$= 963.4622 *m/z*) and ^{13}C-IPA (predicted: $[M + 2H]^{2+}$ = 966.4761 *m/z*, detected $[M + 2H]^{2+}$= 966.4699 *m/z*) are displayed in the inset. **D.** Accurate mass spectra of the Cys^{77} peptide labelled with ^{12}C-IPA (predicted: $[M + 2H]^{2+}$ 691.3503 = *m/z*, detected $[M + 2H]^{2+}$ 691.3480 = *m/z*) and ^{13}C-IPA (predicted: $[M + 2H]^{2+}$ = 694.3603 *m/z*, detected $[M + 2H]^{2+}$= 694.3566 *m/z*). **E.** Redox state of the Cys^{60} and Cys^{77} residues in untreated or insulin-stimulated WTAkt1 protein. Data are expressed as the mean ± s.d.

4.2.4 Ablation of the Akt2 Cys^{60}–Cys^{77} disulphide bond impairs full-length Akt2 plasma membrane localisation in 3T3-L1 adipocytes

The Cys^{60} and Cys^{77} residues in the PH domain of Akt1 of interest are well-conserved functionally and structurally in the PH domain of Akt2 (Masure et al., 1999). Akt1 and Akt2 share a high degree of structural homology; amino acid sequence is 81% identical (Laine et al., 2002). Total internal reflection fluorescence (TIRF) microscopy analyses of protein membrane binding was previously well-established with Akt2 protein (Norris et al., 2017), therefore, data presented here are of isoform Akt2.

Conformational changes of the PH–kinase domains primarily govern Akt activation and inactivation by phosphorylation and dephosphorylation, respectively (Lučić et al., 2018). Inactive Akt is maintained by the autoinhibitory interaction between the membrane binding PH domain, and the catalytic kinase domain. Phospholipid PIP_3 drives the disruption of the PH–kinase domain interface to initiate Akt activation (Ebner et al., 2017). Once the PH domain binds to the lipid head group of PIP_3 at the plasma membrane and relieves the kinase domain from its hold, it exposes the substrate binding cleft of the kinase domain for phosphorylation (Milburn et al., 2003). We therefore examined whether the redox state of the Cys^{60}–Cys^{77} disulphide bond in full-length Akt affects plasma membrane recruitment.

Membrane translocation kinetics of full-length wild-type and reduced TagRFP-T–Akt2 recombinant proteins in response to insulin stimulation were examined by TIRF microscopy detecting the red fluorescent protein (RFP) fluorophore (**Figure 4.9**). Previous reports of Akt2 membrane recruitment in live-cell experiments have presented inconsistent observations (Calleja et al., 2007; Gonzalez & McGraw, 2009; Parikh et al., 2012), possibly due to EGFP as the chosen fluorescent protein marker and its affinity for nucleus localisation (Seibel et al.,

2007). An improved fluorescent Akt2 reporter was developed to emulate endogenous Akt2 plasma membrane localisation. EGFP-tagged Akt2 displayed impaired recruitment to the plasma membrane when compared to endogenous Akt2, however, TagRFP-T–Akt2 plasma membrane recruitment was observed to be comparable to endogenous Akt2 (Norris et al., 2017).

TIRF microscopy has allowed for the detection of full-length Akt2 localisation at the plasma membrane of 3T3-L1 adipocytes in response to insulin stimulation. Untreated wild-type and reduced TagRFP-T–Akt2 proteins were not detectable at the plasma membrane. Insulin stimulation rapidly altered TIRF signalling for TagRFP-T–Akt2 at the plasma membrane, which displayed a graded intracellular dose response to insulin (**Figure 4.10**). Insulin stimulation prominently increased TIRF fluorescent signalling of WTAkt2 protein when compared to disulphide bond Akt2 proteins, with a 2.8-fold and 3.7-fold increase at the plasma membrane in response to insulin at 1 and 100 nM, respectively. TIRF signalling for reduced C60S-Akt2 protein saw a moderate reduction of plasma membrane recruitment compared to WTAkt2 protein, with a 1.7-fold and 2.2-fold increase at the plasma membrane in response to insulin at 1 and 100 nM, respectively. Interestingly, TIRF signalling for reduced C77S-Akt2 and C60SC77S-Akt2 proteins were similar to untreated baseline measurements, suggesting the mutation of Cys^{77} to Ser in the PH domain significantly impaired Akt2 plasma membrane recruitment.

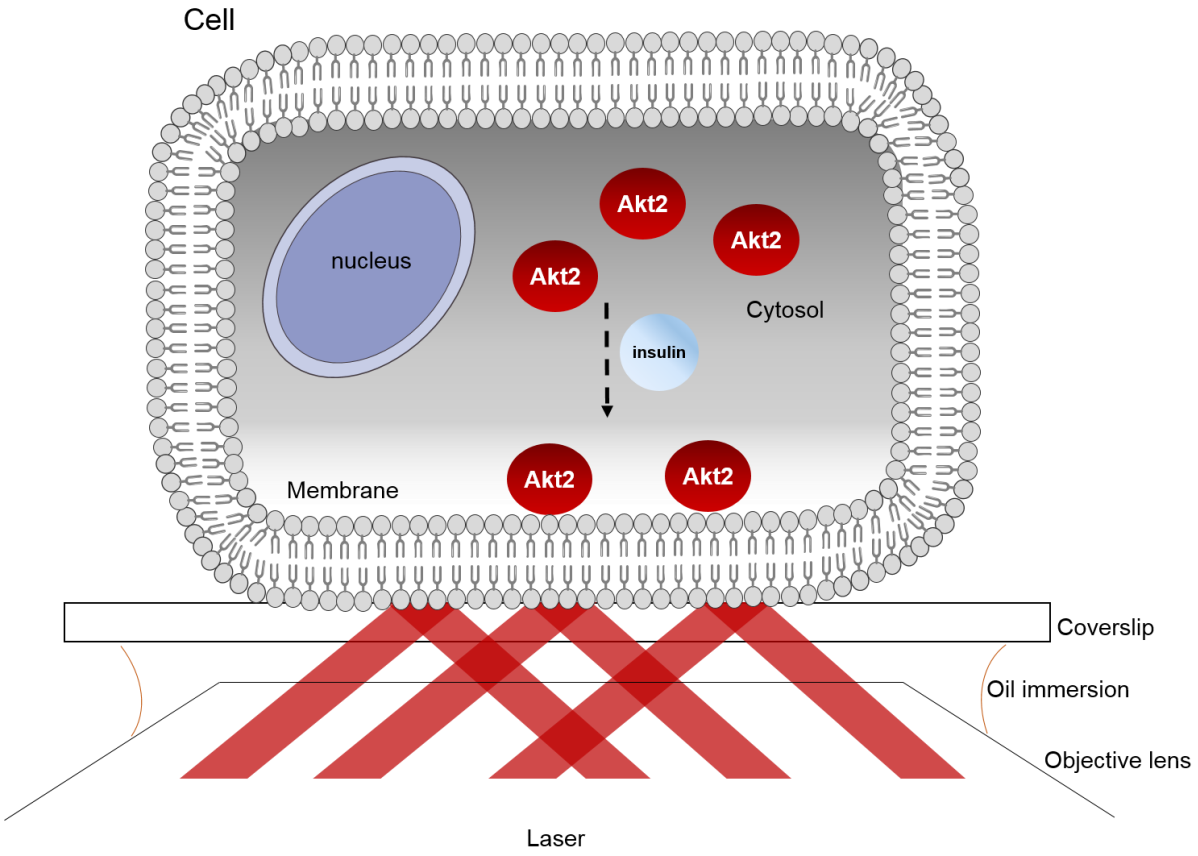

Figure 4.9 TIRF microscopy detecting full-length Akt2 recombinant proteins in 3T3-L1 adipocytes in response to insulin stimulation.
Translocation kinetics of full-length Akt2 proteins were examined by total internal reflection fluorescence (TIRF) microscopy. Laser light produces the evanescent wave that penetrates through the objective lens of the microscope, immersion oil and cover slip interface; reaching the plasma membrane but not the cytosol of the cell. Red fluorescent protein (RFP) fluorophores excited by the evanescent field at the plasma membrane were recorded. Insulin stimulation resulted in the translocation of Akt2 protein from the cytosol to the plasma membrane.

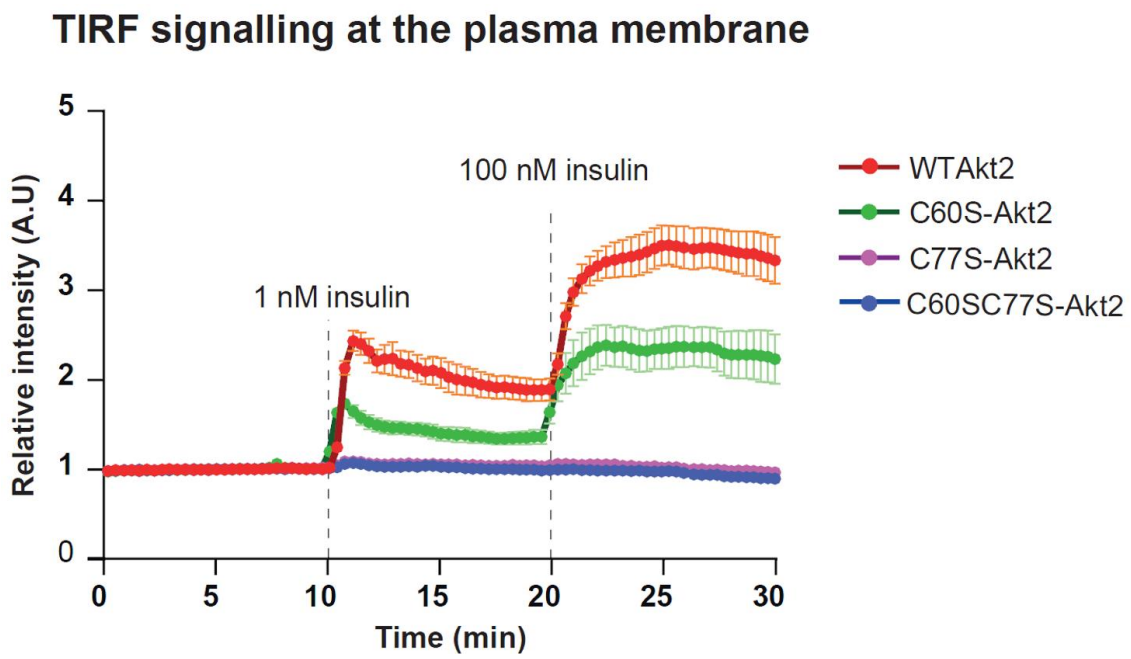

Figure 4.10 Ablation of the Akt2 Cys^{60}–Cys^{77} disulphide bond impairs full-length Akt2 plasma membrane localisation.
Quantification of time-lapse total internal reflection fluorescence (TIRF) signalling in response to 1 nM and 100 nM of insulin stimulation of 3T3-L1 adipocytes expressing *TagRFP-T–Akt2* mutants at 10 and 20 min, respectively. Data are expressed as the mean ± s.d. (Su et al., unpublished data).

4.3 Discussion

In the inactive state of Akt1, the PH domain occludes the phosphorylation of the Thr^{308} residue on the activation loop of the kinase domain (Lučić et al., 2018). Akt1 usually resides in the cytosol and nuclei and stimulation with insulin rapidly induces transient accumulation of cytosolic Akt1 at the plasma membrane (Ebner et al., 2017). Once recruited to the plasma membrane, the PH domain of Akt1 has strong affinity for phospholipid PIP_3. Engagement of the PH domain with PIP_3 stabilises Akt1 phosphorylation, attributed to relief of the PH domain-mediated autoinhibitory interaction with the kinase domain (Ebner et al., 2017). Upon membrane dissociation, reformation of the autoinhibitory PH–kinase domain interface promotes Akt1 dephosphorylation at Thr^{308} and Ser^{473} residues (Ebner et al., 2017).

The most common somatic mutation E17K-Akt1 is located near the lipid binding pocket of the PH domain of Akt1 and has been observed in cancers of the breast (Carpten et al., 2007; Stephens et al., 2012; Yi et al., 2012), endometrium (Cohen et al., 2010), prostate (Boormans et al., 2010), bladder (Askham et al., 2010), NSCLC (De Marco et al., 2015; Ding et al., 2008), blood (Kim et al., 2008) and melanoma (Davies et al., 2008). Through the disruption of the PH–kinase domain interface, this transforming mutation was noted to activate Akt1 (Parikh et al., 2012). Given that PIP_3 membrane attachment is facilitated by the configuration of the PH domain of Akt1, I postulated that the Cys^{60}–Cys^{77} labile disulphide bond in the PH domain of Akt1 is functional in nature. In the previous chapter, crystal structures of Akt1 PH domain show the different redox states of the Cys^{60}–Cys^{77} disulphide bond led to significant structural alterations of the lipid-binding pocket (**Figure 3.5**). Here I propose the Cys^{60}–Cys^{77} disulphide bond is a regulatory mechanism of Akt1 membrane recruitment.

The comparison in PIP_3 membrane binding behaviour between truncated Akt1-PH and full-length Akt1 recombinant proteins revealed notable differences. In two independent assays, truncated WT-PH was shown to have weaker binding affinity for PIP_3 when compared to truncated reduced-PH protein. This suggested that the reduction of the Cys^{60}–Cys^{77} disulphide bond promotes Akt1-PH domain binding affinity to PIP_3; consistent with the finding that crystal structures of IP_4 phospholipid were in complex with reduced-PH proteins (**Figure 4.1B**). However, my observations of the membrane binding behaviour of full-length reduced Akt2 revealed that Cys^{60} and/or Cys^{77} to Ser mutations profoundly impaired plasma membrane localisation when compared to full-length WTAkt2.

In this chapter, I show that the majority of Cys^{60} and Cys^{77} residues naturally form disulphide bonds in truncated WT-PH recombinant protein. The disulphide bonds in turn, are readily reduced by cellular oxidoreductase thioredoxin. Contrastingly, Cys^{60} and Cys^{77} residues in insulin-stimulated, full-length WTAkt1 recombinant protein were predominantly reduced. Akt1 is known to be sensitive toward insulin-stimulated reactive oxygen species i.e. H_2O_2 (Okoh et al., 2013; Ushio-Fukai et al., 1999; Zhang et al., 2016); despite minimal detection of Cys^{60}–Cys^{77} disulphide bonds in the protein. Cysteines residues are sensitive targets of H_2O_2, inducing disulphide bond formation (Goldstein et al., 2005; Paulsen & Carroll, 2013). Bursts of H_2O_2 generated from growth factor stimulation lasts for 10 min (Lee et al., 1998). To capture maximal oxidative effects, differential cysteine alkylators ^{12}C-IPA and ^{13}C-IPA would require a longer timeframe for internalisation and equilibration in NIH/3T3 fibroblasts post-stimulation (Abo & Weerapana, 2015).

I have shown that the redox state of the Cys^{60}–Cys^{77} disulphide bond in full-length Akt2 has a critical role in plasma membrane localisation. The ability of Akt2 membrane recruitment was

slightly decreased by the mutation of Cys^{60} to Ser compared to the wild-type, whereas the mutation of Cys^{77} to Ser completely impaired Akt2 membrane recruitment. Lack of Akt2 recruitment to the plasma membrane suggested that the Cys^{60}–Cys^{77} disulphide bond possibly causes a structure change at the lipid-binding pocket in the PH domain.

In this study, the redox state of the Cys^{60}–Cys^{77} disulphide bond was observed to have a functional role in Akt plasma membrane binding affinity. Activated cellular full-length Akt2 is predominantly membrane bound, and my research has indicated that the redox state of the Cys^{60}–Cys^{77} disulphide bond plays an influential role in membrane localisation. Differing results in PIP_3 membrane binding between the reduced forms of truncated Akt1-PH and full-length Akt2 recombinant proteins may possibly be attributed to the cysteine mutation affecting the configuration of the kinase domain; subsequently inhibiting the Akt phosphorylation loop. My data therefore suggests the Cys^{77} residue is especially critical for Akt membrane binding affinity. To investigate my findings in an *in vitro* model, I next examined the role of the Cys^{60}–Cys^{77} disulphide bond in Akt function in the NIH/3T3 mouse fibroblast cell line.

5. The Cys^{60}–Cys^{77} disulphide bond is involved in phosphorylation of Akt1 *in vitro*

5.1 Introduction

The PI3K/Akt/mTOR pathway is a critical signalling pathway that regulates various cellular processes; namely cell proliferation, survival and metabolism (Yu & Cui, 2016). Akt is often hyper-activated in cancer cells that facilitates catabolism and anabolism of nutrients to meet their increased demands of growth and survival (Ward & Thompson, 2012).

Inactive Akt resides in the cytoplasm and adopts an autoinhibitory conformation with its PH domain inhibiting the kinase domain, thereby preventing phosphorylation of the activation loop (Calleja et al., 2007). In response to extracellular stimulation, i.e. insulin, PI3K is activated and catalyses the phosphorylation of PIP_2 to PIP_3 at the plasma membrane. Akt subsequently translocates and localises at the plasma membrane through the interaction between the PH domain of Akt and PIP_3, therefore relieving the autoinhibitory function of the PH domain on the kinase domain (Ebner et al., 2017). Maximal activation of Akt requires phosphorylation of Ser^{473} in the hydrophobic motif by PDK1, which in turn stabilises phosphorylation of Thr^{308} by mTORC2 (Testa & Bellacosa, 2001; Yang et al., 2002).

A previously established model of Akt activation was that membrane recruitment and Akt phosphorylation of Thr^{308} and Ser^{473} impacts the protein–lipid binding interaction between the PH domain of Akt and PIP_3 at the plasma membrane. General consensus is that activated Akt dissociates from the plasma membrane in the cytosol; phosphorylating downstream substrates until its rapid dephosphorylation by PP2A and PHLPP2 at Thr^{308} and Ser^{473}, respectively (Calleja et al., 2007). A recent study however, shows mutating Thr^{308} and Ser^{473} residues to

either abolishing (T308AS473A) or mimicking (T308DS473D) phosphorylation had no effect on PIP_3 binding or plasma membrane localisation (Arauz et al., 2016). This suggests Akt binding affinity to PIP_3 is not dependent on the phosphorylation status of Akt, and thus Akt membrane dissociation is regulated by a different mechanism of action.

Ebner and colleagues recently proposed an alternative model of Akt activation. Active Akt is restricted to PIP_3-containing membranes to govern substrate selectivity (Ebner et al., 2017). Upon dissociation from PIP_3 at the plasma membrane, reformation of the PH–kinase domain interface is the rate-limiting step for Akt dephosphorylation (Ebner et al., 2017), with a short active half-life of 3-5 min in the cytosol (Calleja et al., 2007; Kunkel et al., 2005). Moreover, growth factor stimulation can prolong Akt activity in the cytosol to at least 1-2 h post-stimulation (Kubota et al., 2012; Kunkel et al., 2005).

In chapter 4, I showed the Cys^{60}–Cys^{77} disulphide bond in the PH domain of Akt is an important regulator of Akt membrane binding. My data showed the mutation of Cys^{60} to Ser decreases Akt2 localisation at the plasma membrane by 50%, whilst mutation of Cys^{77} to Ser abolishes all ability of Akt2 translocation to the plasma membrane. This suggests that the Cys^{60} and Cys^{77} residues are involved in Akt2 membrane localisation, which potentially impacts on Akt activity. In this chapter, the immortalised NIH/3T3 mouse embryonic fibroblast cell line was chosen to assess proliferative activity and oncogenic transformation (Liu et al., 2004; Parikh et al., 2012); the *Akt1* gene is catalytic inactive in serum-starved immortalised fibroblasts (The Human Protein Atlas). Here I show the effect of the Cys^{60}–Cys^{77} disulphide bond on the phosphorylation of Akt1 at Thr^{308} and Ser^{473} residues, in response to growth factor stimulation. Growth factor stimulation of Akt1 directly attenuates signalling of well-studied downstream targets; FoxO1 inhibits apoptosis and autophagy (Zhang et al., 2002; Zhang et al., 2011) and

GSK3α represses glycogen synthesis and glucose uptake (Buller et al., 2008; Pap & Cooper, 1998). And so, I further demonstrate its effect on the activation of Akt1 downstream substrates.

Further supporting our data, the somatic mutation Cys^{77} to Phe (C77F-Akt1) on the PH domain of Akt1 has previously been identified in clinical samples (Cerami et al., 2012; Ellis et al., 2012; Gao et al., 2013; Yi et al., 2012), suggesting the Cys^{77} mutation may induce malignancy. I propose that the Cys^{60}–Cys^{77} disulphide bond in the PH domain of Akt1 is the mechanism by which Akt1 is activated and autoinhibited *in vitro*.

5.2 Results

To investigate whether the Cys^{60}–Cys^{77} disulphide bond is an allosteric disulphide involved in Akt1 activation, I designed full-length *Akt1* DNA constructs to examine the functional relevance of the Cys^{60}–Cys^{77} disulphide bond on Akt1 activity *in vitro* **(Figure 5.1)**. Cys^{60} and/or Cys^{77} residues in the PH domain of Akt1 were mutated to Ser (C60S, C77S and C60SC77S), ablating formation of the disulphide bond. A constitutively active form of Akt1 (Myr) was constructed by inserting an N-terminus Lck tag sequence (MGCGCSSHPEDD) (Patwardhan & Resh, 2010). Myristoylation signalling promotes the permanent docking of Akt1 at the plasma membrane and was used as the positive control for oncogenic growth (Aicart-Ramos et al., 2011). Constitutively inactive *Akt1* mutant, with both phosphorylation residues Thr^{308} and Ser^{473} mutated to Ala (T308AS473A) was constructed to abolish Akt kinase activity (Kitamura et al., 1998; Kotani et al., 1999). Wild-type (*LeGO-iG2–WTAkt1*), constitutively active mutant (*LeGO-iG2–MyrAkt1*), disulphide bond mutants (*LeGO-iG2–C60S-Akt1*, *LeGO-iG2–C77S-Akt1*, *LeGO-iG2–C60SC77S-Akt1*), constitutively inactive mutant (*LeGO-iG2–T308AS473A-Akt1*) and vector control (*LeGO-iG2*) were stably transfected into NIH/3T3 fibroblasts by the lentiviral transduction system. NIH/3T3 fibroblasts positively expressing *Akt1* constructs were sorted using flow cytometry by green fluorescence arising from IRES–EGFP expression on the *LeGO-iG2* vector.

In this chapter, NIH/3T3 fibroblasts expressing *LeGO-iG2* served as the vector control, while NIH/3T3 fibroblasts expressing constitutively active *MyrAkt1* and constitutively inactive *T308AS473A-Akt1* were the positive oncogenic control and negative kinase-dead control, respectively. Disulphide bond *Akt1* mutants (single or double Cys mutations) are denoted as reduced *Akt1*. A HA-epitope tag in the N-terminus of designed constructs facilitated immunoprecipitation of Akt1 protein from NIH/3T3 fibroblasts.

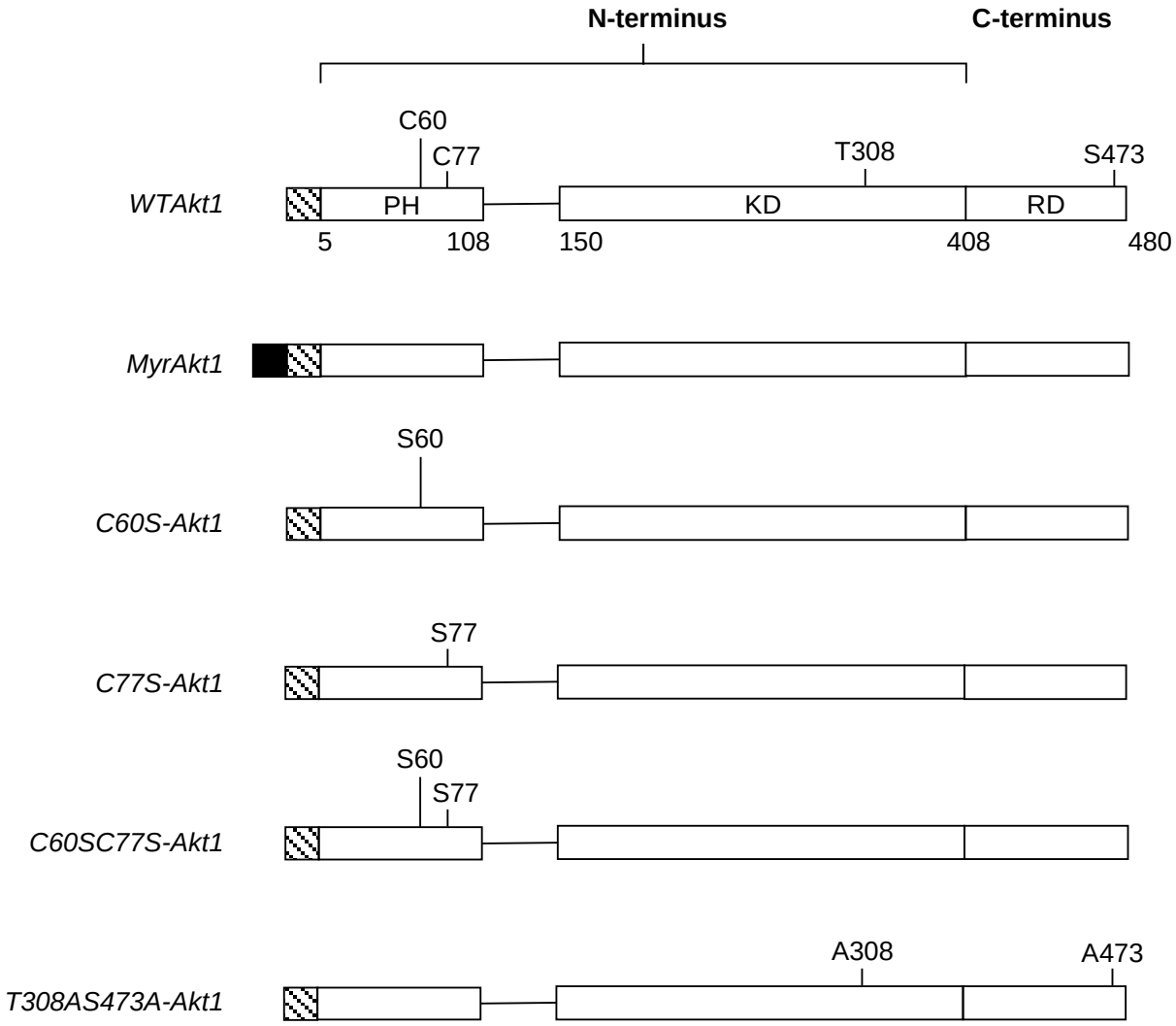

Figure 5.1 Schematic representation of designed full-length *LeGO-iG2–Akt1* constructs stably transfected into NIH/3T3 mouse fibroblasts.

The pleckstrin homology (PH), kinase (KD) and regulatory (RD) domains of Akt1 are indicated. Positions of functional or mutated amino acid residues in the domains are noted. HA-epitope tag is at the N-terminus of each construct. Lck tag encoding the myristoylation signal is indicated as a black box. Reduced *Akt1* mutant constructs where cysteine (C) was replaced by serine (S), and constitutively inactive *Akt1* where threonine (T) and serine (S) were replaced by alanine (A); were generated by the PCR-based, SLIM hybridisation method (Chiu et al., 2004; Chiu et al., 2008). All *Akt1* constructs were sub-cloned into the *LeGO-iG2* vector (Weber et al., 2008).

5.2.1 Ablation of the Akt1 Cys^{60}–Cys^{77} disulphide bond increases proliferation of mouse fibroblasts

The alamarBlue™ (resazurin) cell viability assay is an established, sensitive method of quantifying proliferation of animal cell lines that involves no cell lysis (O'Brien et al., 2000; Rampersad, 2012). We determined the effect of the Cys^{60}–Cys^{77} disulphide bond on the proliferative rate of stably transfected NIH/3T3 fibroblasts by measuring metabolic activity of viable cells (**Figure 5.2**). Viable cells metabolised resazurin into the red fluorescent resorufin, whilst non-viable cells do not metabolise the dye, and thus cannot generate fluorescence. Fluorescence exhibited from NIH/3T3 fibroblasts expressing *Akt1* constructs were normalised against the *LeGO-iG2* vector control. NIH/3T3 fibroblasts expressing disulphide bond mutant constructs *C60S-Akt1* (*p=0.02), *C77S-Akt1* (**p=0.007) and *C60SC77S-Akt1* (*p=0.01) showed significant proliferative activity compared to *WTAkt1*. Interestingly, NIH/3T3 fibroblasts expressing constitutively active *MyrAkt1* showed only moderate increase in cell proliferation, which was not statistically significant compared to *WTAkt1*.

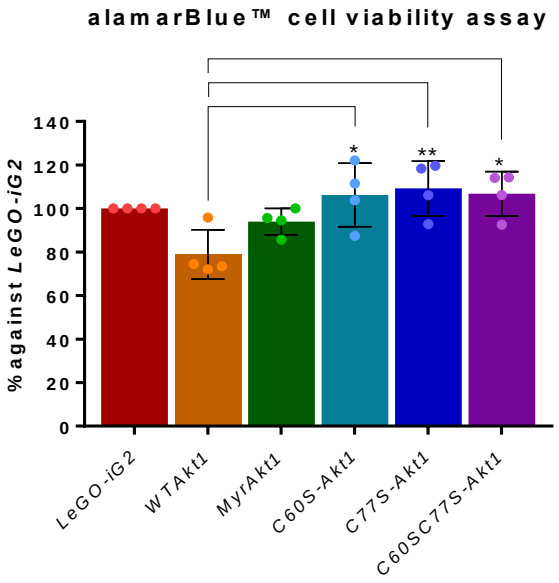

Figure 5.2 Ablation of the Akt1 Cys^{60}–Cys^{77} disulphide bond increases rate of cell proliferation.

Cell proliferation of NIH/3T3 fibroblasts were quantified by the alamarBlue™ assay after 72h of incubation. Fluorescence generated from viable cells were normalised to the *LeGO-iG2* vector control. Graph is representative of four independent experiments performed in triplicate. Data are expressed as the mean ± s.d (One-way ANOVA, *p<0.05; **p<0.01).

5.2.2 Ablation of the Akt1 Cys^{60}–Cys^{77} disulphide bond impairs transformation of mouse fibroblasts

We assessed transformation of NIH/3T3 fibroblasts expressing reduced *Akt1* mutants by the soft agar colony formation assay to test anchorage-independent oncogenic growth. It was previously shown that the somatic mutant E17K-Akt1, leads to oncogenic transformation of fibroblast cells (Carpten et al., 2007; Parikh et al., 2012). Colony measurements were based on previous reports of NIH/3T3 fibroblast (mouse), Rat1 fibroblast (rat) and CEF fibroblast (chicken) cell lines stably transfected with *Akt1*, capable of transforming cells *in vitro* and inducing tumour growth in *in vivo* models (Aoki et al., 1998; Carpten et al., 2007; Liu et al., 2004; Parikh et al., 2012). Measurements of <19 μm was an individual cell incapable of colony formation, 20-40 μm was considered a mid-range sized colony, and >41 μm was considered a high-range sized colony.

Unstimulated stably transfected NIH/3T3 fibroblasts were incubated in soft agar for 21 days and imaged (**Figure 5.3**). Measurements of 300 individual NIH/3T3 fibroblasts or colonies were analysed in each cell population (**Table 5.1**). As expected, NIH/3T3 fibroblasts expressing the *LeGO-iG2* vector control did not form colonies; indicating no transformation of cells (<19 μm). NIH/3T3 fibroblasts expressing constitutively inactive *T308AS473A-Akt1* mutant similarly formed very few mid-range (20-40 μm) or high-range sized colonies (>41 μm). Notably, NIH/3T3 fibroblasts expressing disulphide bond mutants *C60S-Akt1* (****p<0.0001; ****p<0.0001), *C77S-Akt1* (****p<0.0001; ****p<0.0001) and *C60SC77S-Akt1* (***p<0.001; ****p<0.0001) were found to be incapable of forming mid-range or high-range sized colonies when compared to *WTAkt1*. NIH/3T3 fibroblasts expressing *MyrAkt1* significantly formed high-range sized colonies not only compared to *WTAkt1*, but across the cohort (****p<0.0001); demonstrating its highly malignant transforming ability.

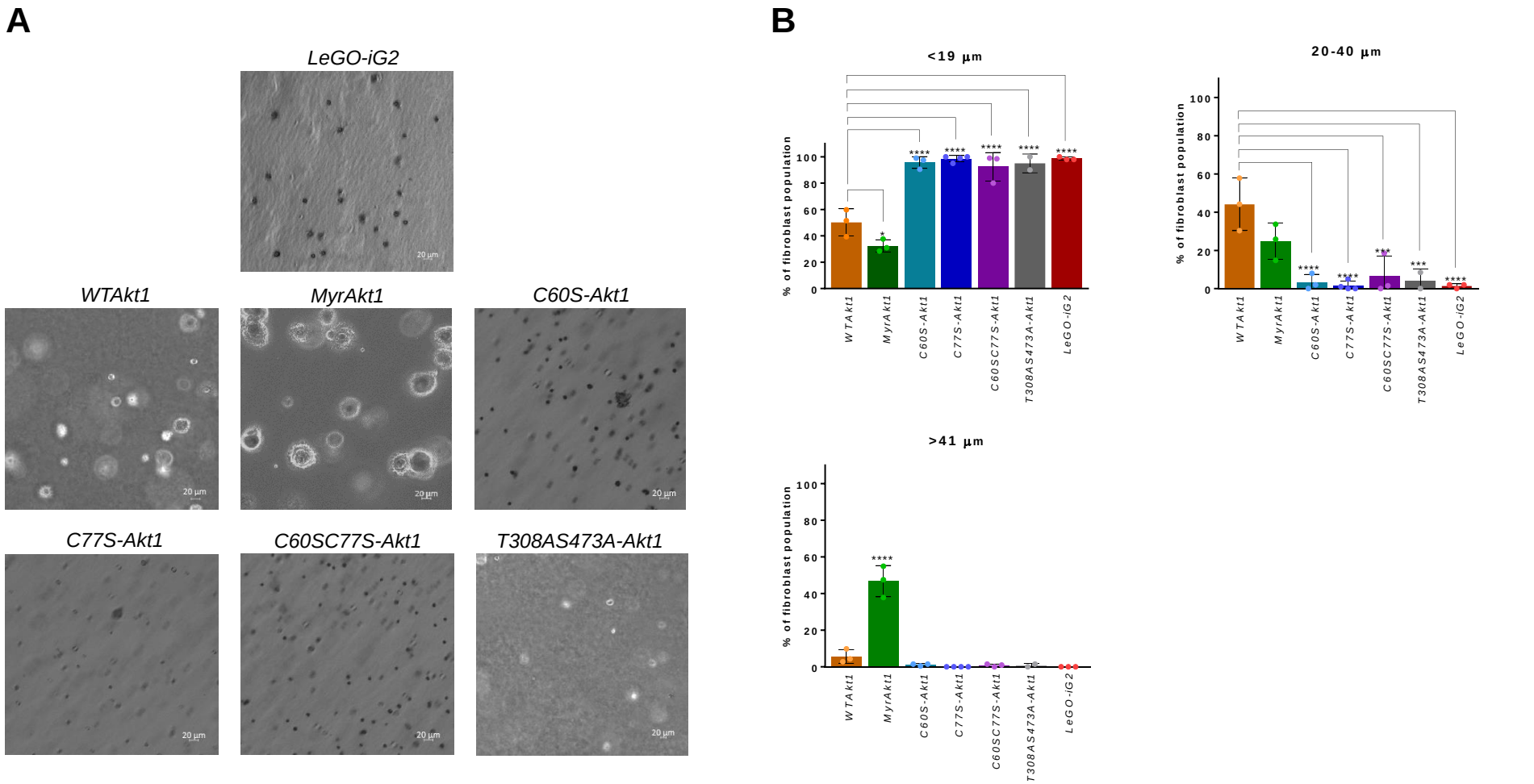

Figure 5.3 Expression of the Akt1 Cys^{60}–Cys^{77} disulphide bond impairs transformation of NIH/3T3 mouse fibroblasts.
NIH/3T3 fibroblasts were grown in 0.6% (w/v) soft agar and 2× DMEM (1:1) in a 6-well plate. Images were taken after 21 days of incubation at the 4× objective. **A.** Images displayed are representative of three independent experiments in duplicate. **B.** Column graph of colony measurements in each fibroblast population (%) expressing *Akt1* constructs. Data are expressed as the mean ± s.d (One-way ANOVA, *p<0.05; ***p<0.001; ****p<0.0001).

Table 5.1 Cell and colony measurements of NIH/3T3 mouse fibroblasts expressing *Akt1* mutants.

Mean percentage of each fibroblast population in 3 independent soft agar colony formation assays displayed in Figure 5.3. Data are expressed as the mean ± s.d.

NIH/3T3 fibroblasts	<19 μm (%)	20-40 μm (%)	>41 μm (%)
LeGO-iG2	99.2±1.1	0.8±1.1	0.0±0.0
WTAkt1	50.2±10.3	44.1±13.8	5.7±3.7
MyrAkt1	30.4±7.8	27.8±10.9	41.8±13.3
C60S-Akt1	95.5±4.4	3.3±4.2	1.2±0.6
C77S-Akt1	98.5±2.4	1.5±2.4	0.0±0.0
C60SC77S-Akt1	92.5±10.8	6.7±10.3	0.8±0.8
T308AS473A-Akt1	95.0±7.1	4.3±6.0	0.8±1.1

5.2.3 Ablation of the Akt1 Cys^{60}–Cys^{77} disulphide bond impairs Akt1 phosphorylation in mouse fibroblasts

Phosphorylation of Akt1 is the primary mechanism of regulating Akt1 activation and function (Chan et al., 2014). The transforming mutant E17K-Akt1 increased levels of Akt1 phosphorylation at both Thr^{308} and Ser^{473} residues when compared to WTAkt1, independent of growth factor stimulation (Carpten et al., 2007). Although no transformative capabilities were observed in NIH/3T3 fibroblasts expressing reduced *Akt1* mutants, we further examined phosphorylation and activation of Akt in response to insulin *in vitro.* NIH/3T3 fibroblasts were serum-starved for 2 h and activated with insulin for 30 min. Akt1 is catalytically inactive in serum-starved cells (Franke et al., 1995), growth factor stimulation, i.e. insulin, induces kinase activity of Akt1 in cells (Alessi et al., 1996a; Gonzalez & McGraw, 2009).

Protein expression levels of Akt and downstream substrates in whole cell lysates were determined by immunoblotting (IB) (**Figure 5.4A**). Expression levels of pan-Akt (total Akt) protein detected in NIH/3T3 fibroblasts expressing *LeGO-iG2* vector control represent the endogenous Akt protein expression in NIH/3T3 fibroblasts. In NIH/3T3 fibroblasts expressing *WTAkt1* or *C60S-Akt1,* total Akt protein levels were found to be higher due to heterologous Akt1 expression. Nonetheless, in fibroblasts expressing *MyrAkt1* or *C60SC77S-Akt1*, heterologous expression of Akt1 did not lead to an increase in total Akt protein. In NIH/3T3 fibroblasts expressing *C77S-Akt1* and *T308AS473A-Akt1*, total Akt protein levels were moderately increased when compared to NIH/3T3 fibroblasts expressing *LeGO-iG2*, but not to the same extent as NIH/3T3 fibroblasts expressing *WTAkt1* or *C60S-Akt1*.

In response to insulin stimulation, NIH/3T3 fibroblasts expressing *LeGO-iG2* and *WTAkt1* exhibited phosphorylation of Akt at Thr^{308} (****$p<0.0001$) and Ser^{473} (*$p=0.01$) (**Figure 5.4B**)

in response to insulin. In insulin-stimulated NIH/3T3 fibroblasts expressing *C60S-Akt1*, comparable levels of phosphorylation of Thr^{308} and Ser^{473} were detected, indicating that the mutation of Cys^{60} to Ser does not appreciably perturb phosphorylation of Akt. However, insulin-stimulated NIH/3T3 fibroblasts expressing *C77S-Akt1* and *C60SC77S-Akt1*, phosphorylation of Thr^{308} and Ser^{473} was only slightly increased to a level similar to that of NIH/3T3 fibroblasts expressing constitutively inactive *T308AS473A-Akt1*. This suggested the mutation of Cys^{77} to Ser in Akt1 impairs phosphorylation of Akt. Despite low levels of total Akt expression in NIH/3T3 fibroblasts transfected with *MyrAkt1*, Thr^{308} and Ser^{473} were highly phosphorylated independent of insulin stimulation, indicating MyrAkt1 protein is constitutively activated.

Phosphorylation of Akt downstream substrates of GSK3α/β at Ser^{21}/Ser^{9}, and FoxO1 at Ser^{256} corresponded with insulin-mediated Akt phosphorylation (**Figure 5.4**). Upon insulin stimulation, GSK3α/β and FoxO1 were phosphorylated in NIH/3T3 fibroblasts expressing *LeGO-iG2* vector control, *WTAkt1* and *C60S-Akt1*. In NIH/3T3 fibroblasts expressing constitutively active *MyrAkt1*, GSK3α/β and FoxO1 were phosphorylated independent of insulin stimulation. Low expression of phosphorylated GSK3α/β and FoxO1 were observed in insulin-stimulated NIH/3T3 fibroblasts expressing constitutively inactive *T308AS473A-Akt1*. Interestingly, phosphorylation of GSK3α/β and FoxO1 was not affected by the mutation of Cys^{77} to Ser. NIH/3T3 fibroblasts expressing *C77S-Akt1* and *C60SC77S-Akt1* showed comparable phosphorylation of GSK3α/β and FoxO1 to NIH/3T3 fibroblasts expressing *WTAkt1*.

.

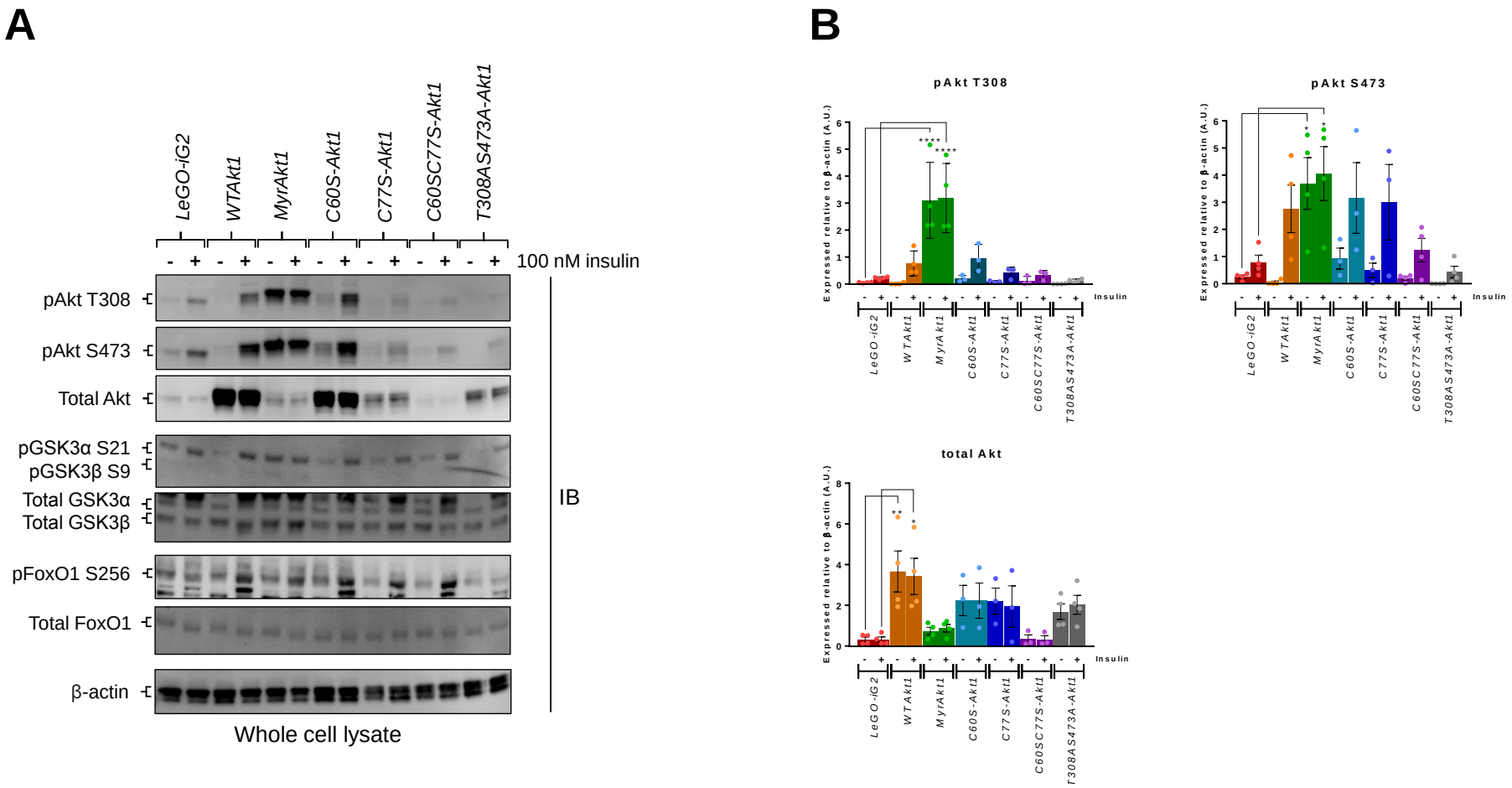

Figure 5.4 Ablation of the Akt1 Cys^{60}–Cys^{77} disulphide bond impairs Akt1 phosphorylation in whole cell lysates.
NIH/3T3 fibroblasts were untreated or stimulated with insulin (100 nM) for 30 min. NIH/3T3 fibroblasts were harvested in lysis buffer (5 mM EDTA, 1% (v/v) Triton X-100 in 1× PBS). Immunoblots (IB) are representative of three independent experiments. **A.** IB of whole cell lysates (50 µg) detecting total and phospho-GSK3α/β (S21/S9) (51/46 kDa), FoxO1 (S256) (82 kDa) and Akt (T308/S473) (60 kDa). β-actin is the loading control. **B.** Densitometry analyses in arbitrary units (A.U.) of blots displayed in A. Data are expressed as the mea ± s.d (One-way ANOVA, *p=0.01; **p<0. 01; ****p<0.0001).

5.2.4 Ablation of the Akt1 Cys^{60}–Cys^{77} disulphide bond impairs Akt1 downstream activity in mouse fibroblasts

To measure the activity of heterologous protein expression in stably transfected NIH/3T3 fibroblasts, wild-type and mutant Akt1 recombinant proteins were immunoprecipitated from whole cell lysate by the HA-epitope tag engineered in the N-terminus of all full-length *Akt1* DNA constructs (**Figure 5.1**). Subsequently, immunoprecipitated Akt1 activity was assessed by its ability to phosphorylate recombinant GSK3α substrate to confirm my previous observations of Akt phosphorylation in whole cell lysate (**Figure 5.4**). Immunoprecipitation analyses enabled the discrimination of exogenous Akt1 from endogenous Akt1 protein in NIH/3T3 fibroblasts and was a test of the veracity of the results in whole cell lysates.

As expected, there was no immunoprecipitation of Akt1 protein in *LeGO-iG2* vector control NIH/3T3 fibroblasts, which also indicates that the endogenous protein was not captured in the pull-down. Phosphorylation (**Figure 5.5A**) and activity (**Figure 5.6A**) of the immunoprecipitated Akt1 protein was measured. Activity was indicated by Akt1 phosphorylation of recombinant GSK3α substrate. Consistent with our whole cell lysate immunoblots, immunoprecipitated WTAkt1 protein was phosphorylated in an insulin-dependent manner and activated Akt phosphorylated recombinant GSK3α substrate.

NIH/3T3 fibroblasts expressed lower levels of constitutively active MyrAkt1 than WTAkt1 protein. Low amounts of MyrAkt1 protein were also immunoprecipitated from NIH/3T3 fibroblasts. Nonetheless, MyrAkt1 protein was significantly phosphorylated at Thr^{308} (p**<0.01; p***<0.001) and Ser^{473} (****p<0.0001) independent of insulin stimulation (**Figure 5.5B**), and exhibited activity towards recombinant GSK3α substrate similar to WTAkt1 protein, when protein level is taken into account (**Figure 5.6B**). The single mutation

of Cys^{60} to Ser in Akt1 slightly reduced phosphorylation of Akt1 at Thr^{308} and Ser^{473}, furthermore, impaired its ability to phosphorylate GSK3α when compared to WTAkt1 protein (*$p<0.05$). The mutation of Cys^{77} to Ser in Akt1 reduced phosphorylation of Akt1 at Thr^{308} and Ser^{473} to an almost undetectable level. Moreover, its ability to phosphorylate GSK3α was moderately decreased when compared to WTAkt1 protein (*$p<0.05$). Double Cys mutant (C60SC77S-Akt1) similarly reduced phosphorylation of Akt1 at Thr^{308} and Ser^{473} to an almost undetectable level, and displayed no downstream activity toward GSK3α (**$p<0.01$). As expected, immunoprecipitated constitutively inactive T308AS473A-Akt1 protein displayed no phosphorylation of Akt1 and little activity toward GSK3α s (**$p<0.01$).

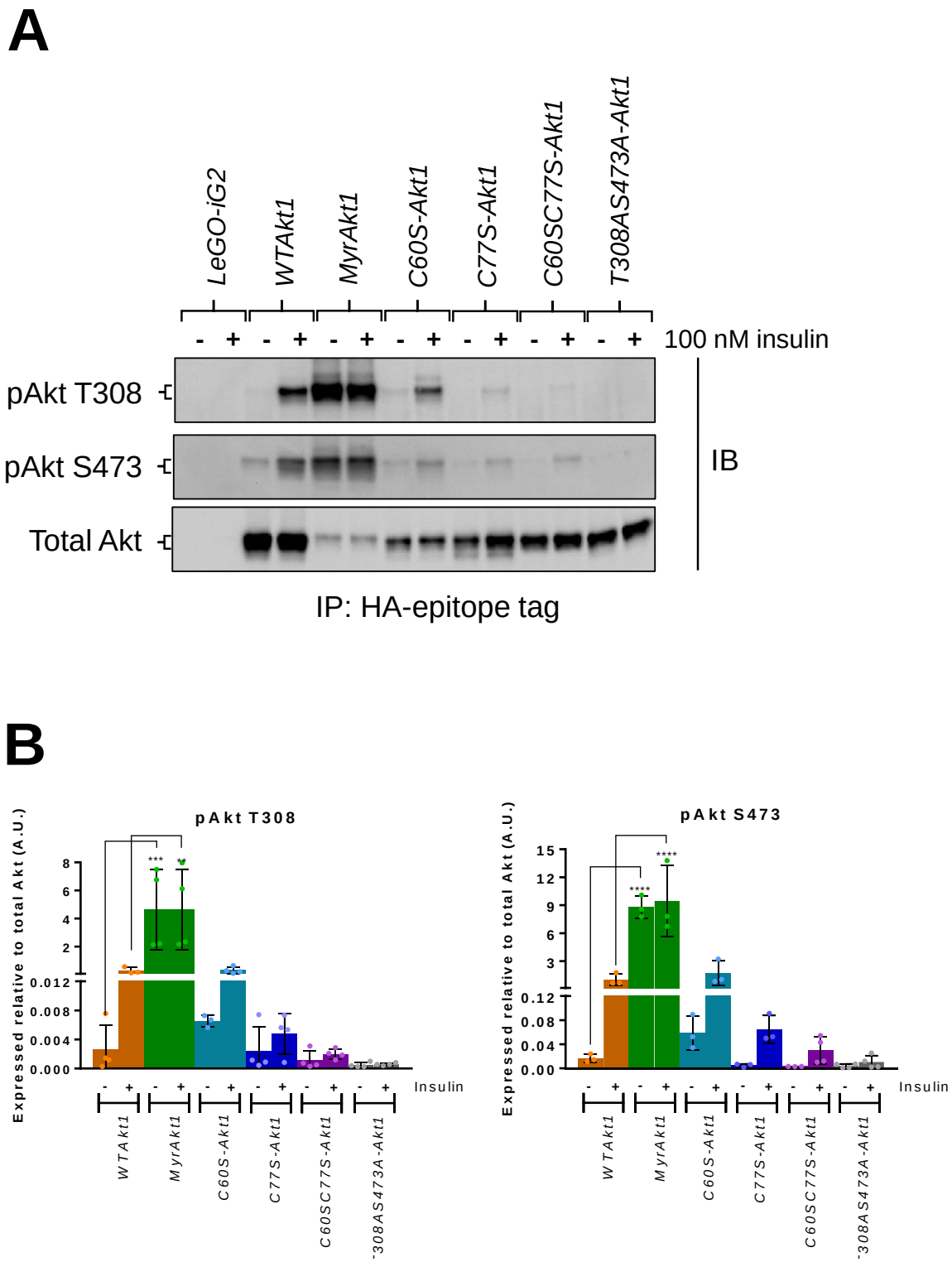

Figure 5.5 Ablation of the Akt1 Cys^{60}–Cys^{77} disulphide bond impairs Akt1 phosphorylation.

NIH/3T3 fibroblasts were untreated or stimulated with insulin (100 nM) for 30 min. NIH/3T3 fibroblasts were harvested in lysis buffer (5 mM EDTA, 1% (v/v) Triton X-100 in 1× PBS). Immunoprecipitation (IP) of Akt1 with a HA-epitope tag antibody. Immunoblots (IB) are representative of three independent experiments. **A.** IB detecting total and phospho-Akt (T308/S473) (60 kDa). **B.** Densitometry analyses of blots displayed in A. Data are expressed as the mean ± s.d (One-way ANOVA, p**<0.01, p***<0.001; ****p<0.0001).

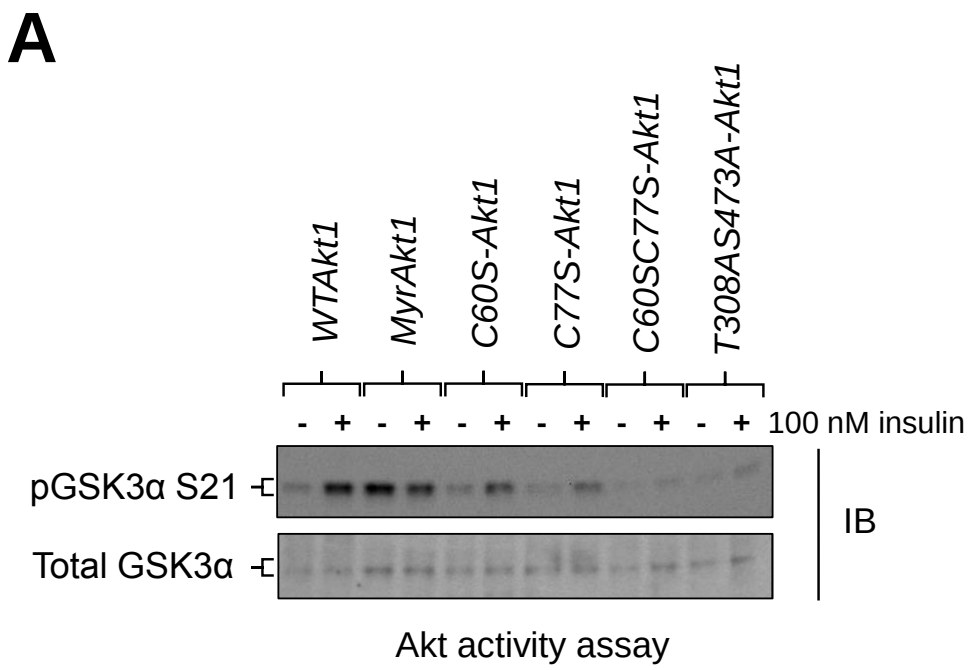

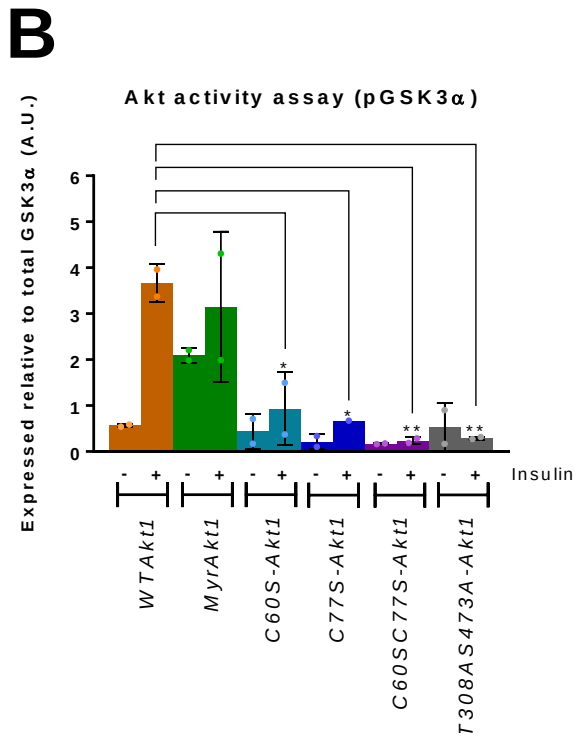

Figure 5.6 Ablation of the Akt1 Cys^{60}–Cys^{77} disulphide bond impairs Akt1 downstream activation.

Downstream activity of immunoprecipitated Akt1 protein was measured by the addition of recombinant GSK3α substrate. Immunoblots (IB) are representative of two independent experiments. **A.** IB detecting total and phospho-GSK3α (S21) (51 kDa). **B.** Densitometry analyses of blots displayed in A. Data are expressed as the mean ± s.d. (One-way ANOVA, p*<0.05, p**<0.01).

5.3 Discussion

The mechanism of Akt1 activation is heavily dependent on the role of its PH domain (Bellacosa et al., 1998). Perturbations of the PH–kinase domain interaction is associated with tumour progression. The most common transforming somatic mutation in Akt1 is located at the lipid binding site of the PH domain (Carpten et al., 2007; Parikh et al., 2012). E17K-Akt1 is an activating mutation identified in cancer patients that alters lipid binding specificity by relieving the PH domain-mediated autoinhibition of Akt1 (Askham et al., 2010; Boormans et al., 2010; Carpten et al., 2007; Cohen et al., 2010; Davies et al., 2008; De Marco et al., 2015; Ding et al., 2008; Kim et al., 2008; Parikh et al., 2012; Stephens et al., 2012). The somatic mutant C77F-Akt1, also located near the lipid binding pocket of the PH domain, was previously identified in a breast cancer patient (Cerami et al., 2012; Ellis et al., 2012; Gao et al., 2013; Yi et al., 2012). Crystal structures of truncated PH domain of Akt1 showed that the absence of the Cys^{60}–Cys^{77} disulphide bond enabled co-crystallisation with phospholipid IP_4, suggesting the reduced form of PH domain promotes PIP_3 lipid binding interaction (**Figure 3.5B**), however, my membrane binding data and *in vitro* studies of full-length Akt1 has shown otherwise.

In this chapter, I showed that the redox state of the Cys^{60}–Cys^{77} disulphide bond plays a vital role in Akt1 activity, in response to growth factor stimulation. Mutation of Cys^{60} or Cys^{77} to Ser in the PH domain of Akt1 led to differential effects on Akt1 function in NIH/3T3 fibroblasts. Mutation of Cys^{60} to Ser in Akt1 resulted in moderately reduced levels of Akt phosphorylation in NIH/3T3 fibroblasts when compared to WTAkt1. Interestingly, the mutation of Cys^{77} to Ser in Akt1 resulted in the near ablation of Akt phosphorylation.

Non-transformative capabilities of NIH/3T3 fibroblasts expressing disulphide bond mutants (*C60S-Akt1*, *C77S-Akt1* or *C60SC77S-Akt1*) suggest that oxidation to form the Cys^{60}–Cys^{77}

disulphide bond may be required to induce oncogenic transformative effects. Moreover, decreased levels of Akt phosphorylation in these NIH/3T3 fibroblasts may be explained by their altered ability to localise at the plasma membrane (**Figure 4.5**). The ability to recruit Akt to the membrane was somewhat decreased by the mutation of Cys^{60} to Ser compared to the wild-type. Moreover, a complete loss of recruitment was prompted by the mutation of Cys^{77} to Ser. This correlated with levels of Akt phosphorylation in NIH/3T3 fibroblasts expressing *C60S-Akt1* and *C77S-Akt1*, respectively.

My results suggest that the mutation of Cys^{77} to Ser heavily impairs full-length Akt1 membrane recruitment and subsequently cannot be activated by PIP_3. I postulate that the mutation of Cys^{77} to Ser induces the intramolecular interaction between the PH and kinase domains of Akt1 to promote its autoinhibition. To test this hypothesis, I aimed to assess the effect of the Cys^{60}–Cys^{77} disulphide bond on the binding interaction between the PH–kinase domains by co-immunoprecipitation *in vitro*. A previous study has shown co-transfected truncated E17K-PH/WT-KD weakens the PH–kinase domain interaction when compared to truncated WT-PH/WT-KD, increasing phosphorylation of the kinase (Parikh et al., 2012). I therefore transiently co-transfected truncated wild-type and reduced *Akt1* PH domain constructs (*WT-PH*, *C60S-PH*, *C77S-PH* and *C60SC77S-PH*) with the truncated wild-type kinase domain (*WT-KD*) construct in HEK293T cells, however, co-expression of both constructs was unsuccessful and after several attempts this experiment was not pursued further.

My investigations have shown the relevance of the Cys^{77} to Ser mutation in full-length Akt1 for Akt function *in vitro*. My data suggested the formation of the Cys^{60}–Cys^{77} disulphide bond is required in membrane recruitment and subsequent Akt1 activation. I propose that the Cys^{60}–Cys^{77} disulphide bond is an allosteric disulphide bond that controls the autoinhibition of Akt1

by controlling the conformation of the PH–kinase domain interface. To test my findings in an *in vivo* model, I next examined the role of the Akt1 Cys^{60}–Cys^{77} disulphide bond in zebrafish embryos.

6. The Cys^{60}–Cys^{77} disulphide bond is involved in physiological function of Akt1 *in vivo*

6.1 Introduction

New blood vessel formation, or angiogenesis, in tumours enables the supply of excess nutrients and oxygen to meet their increased demands of cell metabolism (Hanahan & Weinberg, 2011). The vasculature of an organism undergoes constant growth and remodelling during embryogenesis but enters quiescence and retains morphogenetic plasticity once it has reached adulthood. To form new sprouting vessels, signal transduction via VEGF receptors regulate angiogenesis (Ellertsdottir et al., 2010). Perturbation of the PI3K/Akt/mTOR signalling pathway is often implicated in the increase of VEGF-induced angiogenesis (Zhong et al., 2000). Akt upregulates the translation of HIF1α in response to increased glucose and oxygen availability in solid cancers (Harada et al., 2009). HIF1α subsequently activates VEGF, which plays a vital role in the branching, sprouting and remodelling of new blood vessels through the activation of endothelial cells (Hoeben et al., 2004; Kitamura et al., 2008). Endothelial cells predominantly express the *Akt1* isoform (Chen et al., 2005), which is a key mediator for survival and migration of endothelial cells; essential for vascular development (Lee et al., 2014; Yu et al., 2015).

The PI3K/Akt/mTOR signalling pathway is also known to interact with the Delta-Notch signalling pathway, which is essential for normal vascular remodelling through negative regulation of endothelial cell formation (Leslie et al., 2007; Thurston & Kitajewski, 2008). Perturbation of the Delta-Notch signalling pathway is not only implicated in tumour angiogenesis (Siekmann & Lawson, 2007; Thurston & Kitajewski, 2008) but is also linked to human neurodevelopmental diseases (Cornell & Eisen, 2002; Jeffery et al., 2015). Ablation of

Akt and *mTOR* in the brain results in the disruption of cell cycle progression of neural progenitor cells during development (Ka et al., 2014; Wang et al., 2016). Although *Akt3* is the predominant isoform found in the brain, *Akt1* and *Akt2* are also moderately expressed (Chan et al., 2014). Hemimegalencephaly – malformation of the brain characterised by an enlarged cerebral hemisphere, contains the somatic transforming mutation E17K in *Akt3* (Poduri et al., 2012). This activating mutation is homologous to the E17K mutation in *Akt1* and *Akt2* and is linked to somatic overgrowth disorders (Keppler-Noreuil et al., 2016). Decreased levels of Akt1 protein have also being associated with schizophrenia (Emamian, 2012). Akt1 has also been found to play a role in supporting cardiac development (Cohen, 2013).

To understand physiological functions of Akt1 in vertebrate systems, *Akt1* knockout organisms have previously been generated. *Akt1*-null mice (*Mus musculus*) displayed growth retardation and impaired vascular maturation; resulting in developmental and heart defects, significantly increasing perinatal mortality (Ackah et al., 2005; Chang et al., 2010; Chen et al., 2005). Abnormalities in neuronal morphology were also observed in *Akt1* deficient mice (Lai et al., 2006). In zebrafish (*Danio rerio*), loss of *Akt1* resulted in defective arterial development (Ren et al., 2010) and precocious neuronal differentiation (Cheng et al., 2013); indicating an evolutionary conserved role of Akt1 as a key regulator in zebrafish embryonic development.

Zebrafish embryos rapidly form a complete primary organ system within 48 hours post-fertilisation (hpf). Transparency of their embryos is advantageous for live imaging of early-stage vasculature development and cellular patterning in whole vertebrae without invasive methods (Chávez et al., 2016). The zebrafish model is a useful organism for studying the biological functions of the Cys^{60}–Cys^{77} disulphide bond in the PH domain of Akt1. The *Tg(fli1a:EGFP)* zebrafish line expressing fluorescence in blood vessels (Lawson & Weinstein,

2002) was chosen to assess phenotype of zebrafish embryos injected with wild-type and mutant *Akt1* constructs.

In previous chapters, I revealed the Cys^{60}–Cys^{77} disulphide bond in the PH domain of Akt1 as an important regulator of Akt1 function *in vitro*. Mutation of Cys^{60} to Ser slightly reduced Akt1 lipid binding and somewhat impacted Akt1 phosphorylation, whilst mutation of Cys^{77} to Ser heavily impaired all aspects of Akt1 function. In this chapter, we performed microinjections of nucleic acids into zebrafish embryos to report the function of the Cys^{60}–Cys^{77} disulphide bond in Akt1 on angiogenesis, growth and survival during zebrafish development. We further analysed the effect of the Cys^{60}–Cys^{77} disulphide bond on the activation of downstream *Akt1* genes responsible for neural differentiation in zebrafish (Chung et al., 2011; Cornell & Eisen, 2002; Park et al., 2000; Riley et al., 1999). Although additional studies of disulphide bond *Akt1* mutants in *in vivo* models are required, I postulate that the Cys^{60}–Cys^{77} disulphide bond in the PH domain of Akt1 is an allosteric disulphide bond required for normal physiological functions of Akt1.

6.2 Results

To examine the functional relevance of the Cys^{60}–Cys^{77} disulphide bond in the PH domain of Akt1 in the zebrafish *in vivo* model, I designed transgenic constructs encoding the sequence of full-length human *Akt1* inserted in the *pDESTTol2* transposon vector. Previously described in the *in vitro* studies, Cys^{60} and/or Cys^{77} residues in the PH domain of Akt1 were mutated to Ser (C60S, C77S and C60SC77S). Constitutively active Akt1 (Myr) contains an N-terminus Lck tag sequence (MGCGCSSHPEDD). The constitutively inactive Akt1 mutant cannot be phosphorylated as Thr^{308} and Ser^{473} residues are mutated to Ala (T308AS473A).

Transgenic *Akt1* clones were constructed by the Tol2kit cloning system as described by Kwan and colleagues; based on *att* site-specific Gateway™ BP and LR recombination cloning (Hartley et al., 2000; Kwan et al., 2007). Middle-entry clones of full-length wild-type (*pME/WTAkt1*), constitutively active mutant *(pME/MyrAkt1),* disulphide bond mutants *(pME/C60S-Akt1, pME/C77S-Akt1* and *pME/C60SC77S-Akt1*) and constitutively inactive mutant *(pME/T308AS473A-Akt1)* were constructed by Gateway™ BP recombination cloning (**Figure 6.1A**).

To facilitate fluorescence-based phenotypic visualisation, transgenic DNA of full-length wild-type (*pDestTol2/ubb:WTAkt1-p2a-tomato*), constitutively active mutant *(pDestTol2/ubb; MyrAkt1-p2a-tomato),* disulphide bond mutants (*pDestTol2/ubb:C60S-Akt1-p2a-tomato, pDestTol2/ubb:C77S-Akt1-p2a-tomato* and *pDestTol2/ubb:C60SC77S-Akt1-p2a-tomato*) and constitutively inactive mutant *(pDestTol2/ubb:T308AS473A-Akt1-p2a-tomato*) *Akt1* were constructed by Gateway™ LR recombination cloning (**Figure 6.1B**). The *pDestTol2* vector contains *Tol2* transposable elements flanked the DNA cassette at both ends to enable germline transgenesis (Kawakami, 2007). Zebrafish endogenous ubiquitin (*ubb*) promoter at the 5' end

drives transgenic expression of mutant *Akt1* constructs of interest and the polyadenylated tandem-tomato fluorescent cassette (*p2a-tdTomato*) at the 3' end as a single mRNA transcript. Picornavirus *p2a* sequence is a ribosome skipping site (Kim et al., 2011) that enables co-expression of mutant *Akt1* and red fluorescent protein *tdTomato* for tracking ectopic *Akt1* expression. Transgenic *Akt1* mutants were subsequently co-injected with Tol2 transposase mRNA in *Tg*(*fli1a:EGFP*) embryos at the one-cell stage.

In this chapter, uninjected embryos were the control with no injection of *Akt1* mutant constructs. Embryos injected with *WTAkt1* is the wild-type control. Embryos injected with constitutively active *MyrAkt1* and constitutively inactive *T308AS473A-Akt1* were positive oncogenic and negative kinase-dead controls, respectively. Disulphide bond *Akt1* mutants (single or double Cys mutations) were denoted as reduced *Akt1* mutants. All *Akt1* constructs were designed without the stop codon to allow translation of the *p2a-tdTomato* section of each construct. This fluorescent tandem Tomato tag facilitated the screening of embryos with ectopic *Akt1* expression by fluorescence microscopy prior to analyses. Injected embryos were raised to adults for breeding; however, expression of constructed *Akt1* mutants were not passed onto F1 progeny.

A

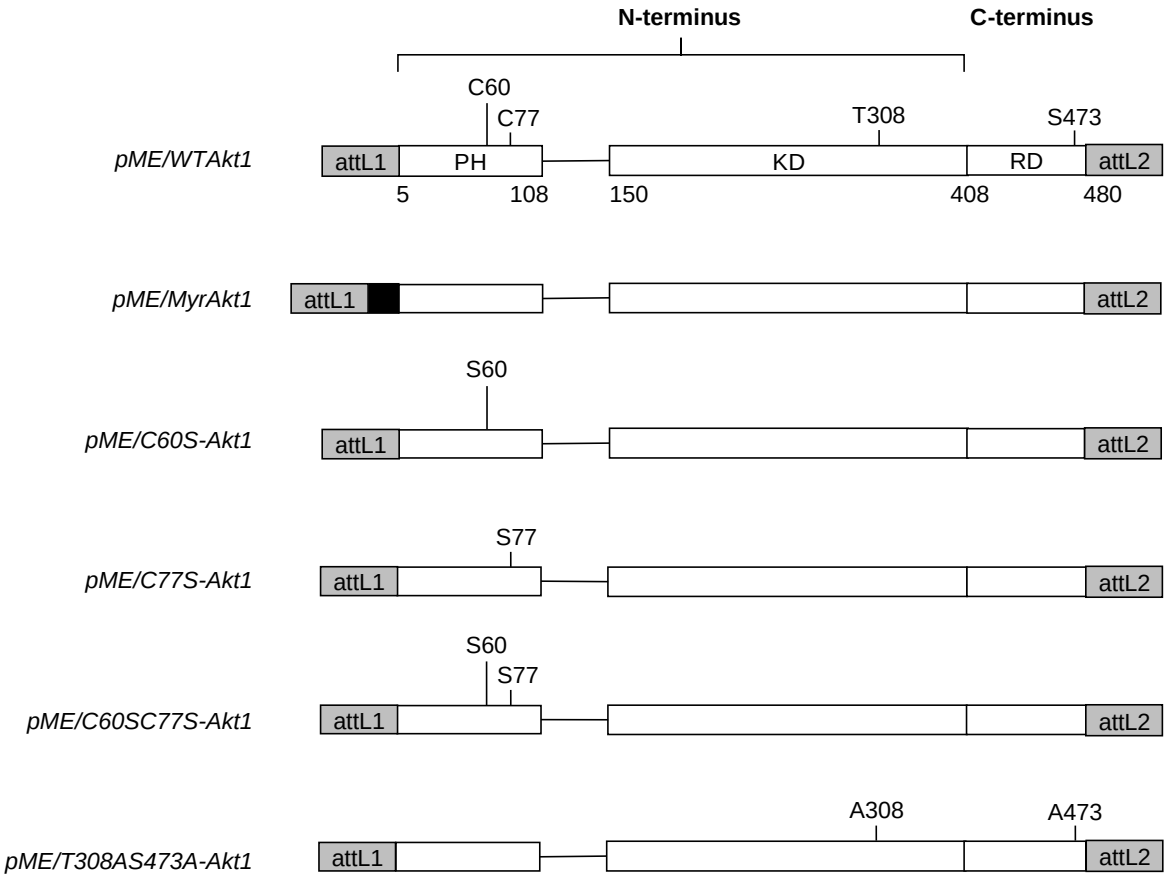
N-terminus
C-terminus
C60
C77
T308
S473
pME/WTAkt1
attL1
PH
KD
RD
attL2
5
108
150
408
480
pME/MyrAkt1
attL1
attL2
S60
pME/C60S-Akt1
attL1
attL2
S77
pME/C77S-Akt1
attL1
attL2
S60
S77
pME/C60SC77S-Akt1
attL1
attL2
A308
A473
pME/T308AS473A-Akt1
attL1
attL2

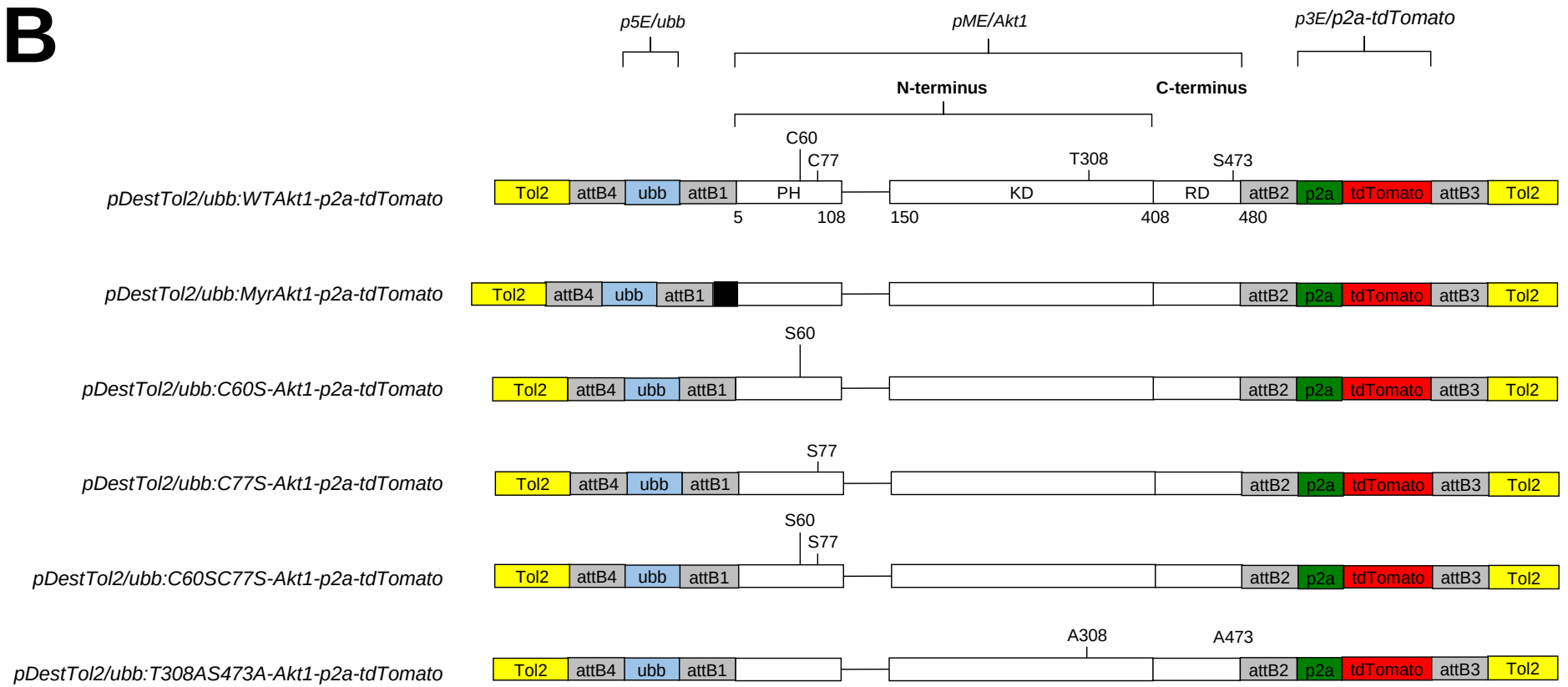

Figure 6.1 Schematic representation of designed *pME/Akt1* and *pDestTol2/ubb:Akt1-p2a-tdTomato* constructs.
The pleckstrin homology (PH), kinase (KD) and regulatory (RD) domains of Akt1 are indicated. Positions of functional or mutated amino acid residues in the domains are noted. Lck tag encoding the myristoylation signal is indicated as a black box. Mutant human *Akt1* constructs where cysteine (C) is replaced by serine (S); threonine (T) and S are replaced by alanine (A), are generated by the PCR-based, SLIM hybridisation method (Chiu et al., 2004; Chiu et al., 2008). **A.** Middle-entry *pME/Akt1* clones constructed by Gateway™ BP recombination cloning of *pDONR™221* donor vector and *Akt1* PCR product. **B.** Transgenic *pDestTol2/ubb:Akt1-p2a-tdTomato* clones constructed by Gateway™ LR recombination cloning of *pDestTol2* destination vector, middle-entry *pME*/*Akt1* as shown in A, *p5E*/*ubb* 5'-entry zebrafish ubiquitin promoter, and *p3E/p2a-tdTomato* 3'-entry polyadenylated tandem Tomato.

6.2.1 Ablation of the Akt1 Cys^{60}–Cys^{77} disulphide bond induces angiogenesis in zebrafish

In the trunk of the zebrafish, homologous mesodermal segments derived from somites give rise to skeletal muscles during embryogenesis (Stickney et al., 2000). Between pairs of somites are sprouting intersegmental vessels (ISV); the recognised paradigm used to study angiogenesis in the zebrafish model (Blum et al., 2008). The process of ISV formation via angiogenesis is accompanied by endothelial cell migration and differentiation (Blum et al., 2008). Endothelial cells sprout from the dorsal aorta and posterior cardinal vein to form to the intersegmental artery and vein (Ellertsdottir et al., 2010), together, they are termed as intersegmental vessels (ISV) that run along the vertical myotomal boundaries of the zebrafish trunk and into the dorsal longitudinal anastomotic vessel (Isogai et al., 2001). ISV growth in zebrafish embryo is also similar to that of mouse embryo (Ellertsdottir et al., 2010). Within 48 hours post-fertilisation (hpf), zebrafish embryos form a complete primary organ system. ISVs in the trunk and tail are lumenised and active in circulation (Childs et al., 2002; Isogai et al., 2001; Kimmel et al., 1995). We examined the redox state of the Cys^{60}–Cys^{77} disulphide bond in the PH domain of Akt1, on the process of angiogenesis during zebrafish development. We determined whether overexpression of *Akt1* mutants perturbed vasculature formation during zebrafish embryogenesis. Wild-type *Tg*(*fli1a:EGFP*) zebrafish embryos were injected at the one-cell stage with transgenic *Akt1* DNA constructs. ISV formation was termed 'complete' if they branched from the dorsal aorta or posterior cardinal vein, fully extending into the dorsal longitudinal anastomotic vessel.

Zebrafish embryos were imaged at 48 hpf to capture optimal Akt1 expression and ISV formation due to the transient expression of *Akt1* (**Figure 6.2A**). Akt1 was not ubiquitously expressed throughout the entire organism, and only observed in a few muscle striations in the trunk extending across somite. ISV in 200 individual embryos were analysed in each injected

population (**Table 6.1**). Complete ISVs formation in uninjected embryos was the reference point (**Figure 6.2B**). *Tg*(*fli1a:EGFP*) embryos injected with constitutively active *MyrAkt1* and double cysteine mutant *C60SC77S-Akt1* modestly increased complete formation of ISVs, but was not statistically significant compared to *Tg*(*fli1a:EGFP*) embryos injected with *WTAkt1*. *Tg*(*fli1a:EGFP*) embryos injected with single cysteine mutant *C60S-Akt1* (One-way ANOVA, **p<0.01) and *C77S-Akt1* (One-way ANOVA, *p<0.05) significantly increased complete formation of ISVs when compared to *Tg*(*fli1a:EGFP*) embryos injected with *WTAkt1*. *Tg*(*fli1a:EGFP*) embryos injected with constitutively inactive mutant *T308AS473A-Akt1* moderately decreased complete formation of ISVs, however, was not statistically significant when compared to *Tg*(*fli1a:EGFP*) embryos injected with *WTAkt1*.

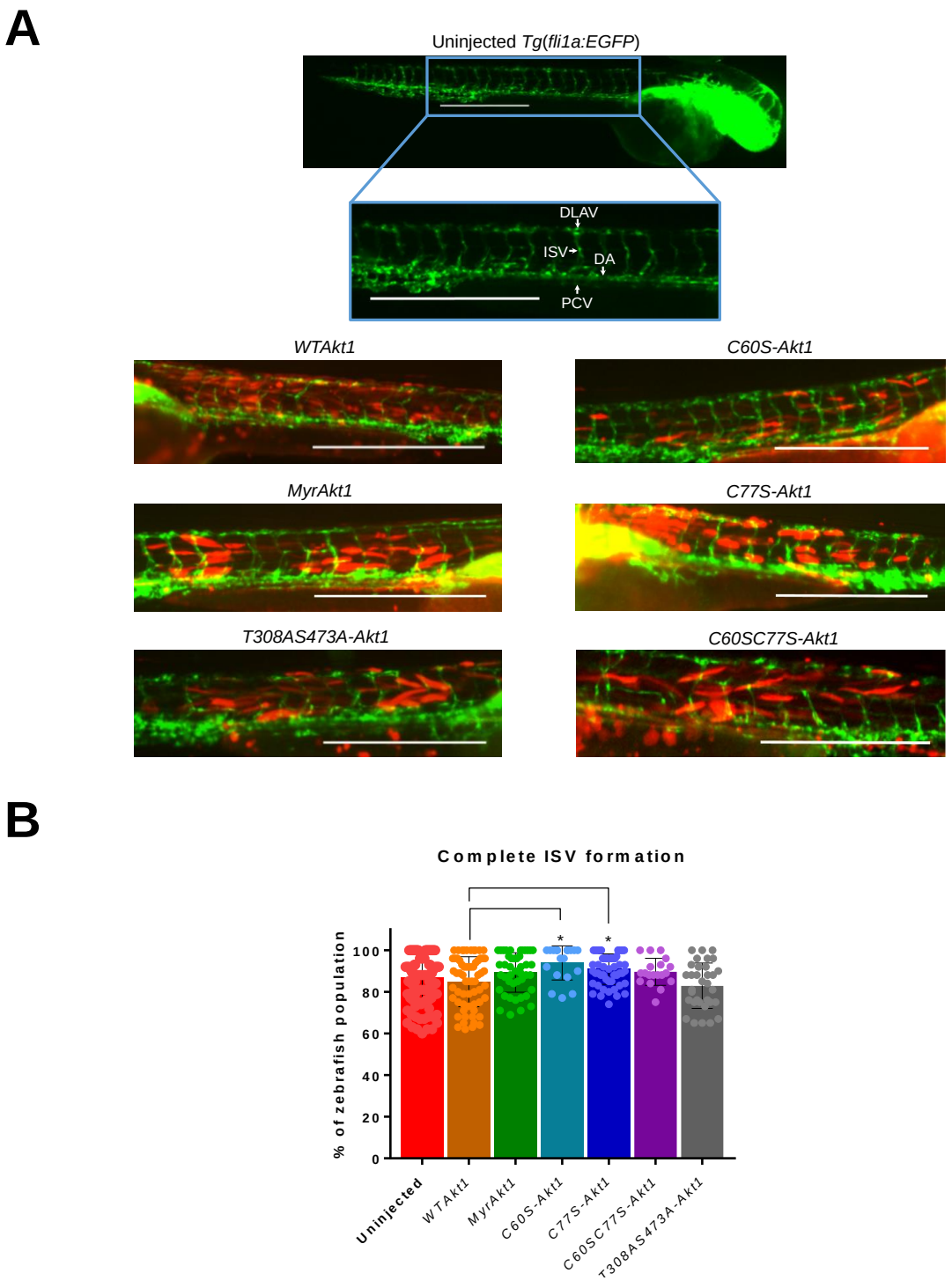

Figure 6.2 Ablation of the Akt1 Cys^{60}–Cys^{77} disulphide bond increases intersegmental vessel formation in the zebrafish model.
Tg(fli1a:EGFP) zebrafish embryos were injected with human *Akt1* constructs at the one-cell stage. **A.** Representative images of vascular growth in an individual embryo at 48 hpf are displayed under the 40× objective. Blue box indicates the trunk. Injected *Akt1* mutants are expressed in muscle striations labelled red (tdTomato). Intersegmental vessels (ISV) branching from the dorsal aorta (DA) or posterior cardinal vein (PCV) into the dorsal longitudinal anastomotic vessel (DLAV) are labelled green (EGFP). White scale bar indicates 500 µm. **B.** Complete formation of ISVs were analysed. Data are expressed as the mean ± s.d (One-way ANOVA, *p<0.05).

Table 6.1 Completeness of intersegmental vessel formation in *Tg(fli1a:EGFP)* zebrafish embryos injected with *Akt1* mutants.
Mean percentage of each injected *Tg(fli1a:EGFP)* embryo population in ten independent experiments displayed in Figure 6.2.

Tg(fli1a:EGFP) zebrafish embryos	Complete ISV formation (%)
Uninjected	86.7 ± 11.3
WTAkt1	84.9 ± 12.0
MyrAkt1	89.3 ± 9.3
C60S-Akt1	93.9 ± 7.4
C77S-Akt1	90.9 ± 7.2
C60SC77S-Akt1	89.6 ± 6.5
T308AS473A-Akt1	82.9 ± 10.9

6.2.2 Ablation of the Akt1 Cys^{60}–Cys^{77} disulphide bond perturbs development of zebrafish

A single clutch of zebrafish embryos will develop at variable rates, therefore the measurement of time post-fertilisation is not considered an adequate indicator for developmental progress (Kimmel et al., 1995). During the early stages of embryonic development, genetic changes can perturb zebrafish growth (Parichy et al., 2009). We therefore determined the effect of the Cys^{60}–Cys^{77} disulphide bond in *Tg*(*fli1a:EGFP*) embryos injected with reduced *Akt1* constructs on zebrafish development by measuring their growth (mm) (**Figure 6.3**). Standard length of the snout to the vent is the preferred indicator for developmental staging of zebrafish embryos due to the high correlation between fish size and physiological rates (Fuiman et al., 1998). Growth measurements of 200 individual *Tg*(*fli1a:EGFP*) embryos were examined in each injected population (**Table 6.2**). Uninjected *Tg*(*fli1a:EGFP*) embryo measurements were the normal reference point. As expected, *Tg*(*fli1a:EGFP*) embryos injected with constitutively active *MyrAkt1* were significantly larger in size when compared to *Tg*(*fli1a:EGFP*) embryos injected with *WTAkt1* (One-way ANOVA, ****p<0.0001); whereas *Tg*(*fli1a:EGFP*) embryos injected with constitutively inactive *T308AS473A-Akt1* were significantly stunted compared to *Tg*(*fli1a:EGFP*) embryos injected with *WTAkt1* (One-way ANOVA, ***p<0.001). Injection of single cysteine mutants *C60S-Akt1* and *C77S-Akt1* did not affect growth of *Tg*(*fli1a:EGFP*) embryos when compared to *Tg*(*fli1a:EGFP*) embryos injected with *WTAkt1*. Interestingly, *Tg*(*fli1a:EGFP*) embryos injected with double cysteine mutant *C60SC77S-Akt1* significantly increased growth when compared to *Tg*(*fli1a:EGFP*) embryos injected with *WTAkt1* (One-way ANOVA, ****p<0.0001).

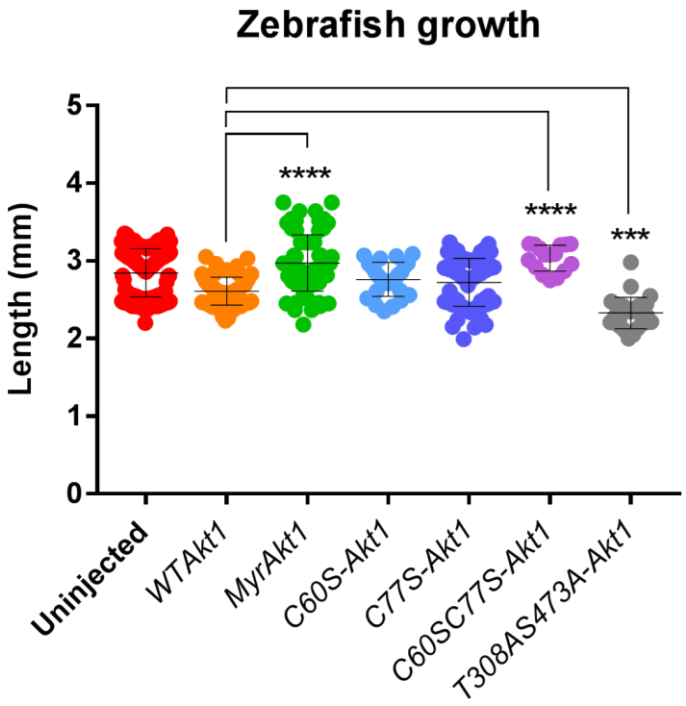

Figure 6.3 Ablation of the Akt1 Cys^{60}–Cys^{77} disulphide bond increases growth in the zebrafish model.
Developmental stage was measured by snout to vent length of individual *Tg(fli1a:EGFP)* zebrafish embryos at 48 hpf. Data are expressed as the mean ± s.d (One-way ANOVA, ***p<0.001; ****p<0.0001).

Table 6.2 Growth measurements of *Tg(fli1a:EGFP)* zebrafish embryos injected with *Akt1* mutants.
Mean measurements of each injected *Tg(fli1a:EGFP)* embryo displayed in Figure 6.3.

Tg(fli1a:EGFP) zebrafish embryos	Length from snout to vent (mm)
Uninjected	2.8 ± 0.3
WTAkt1	2.6 ± 0.2
MyrAkt1	3.0 ± 0.4
C60S-Akt1	2.8 ± 0.2
C77S-Akt1	2.7 ± 0.3
C60SC77S-Akt1	3.0 ± 0.2
T308AS473A-Akt1	2.3 ± 0.2

6.2.3 Ablation of the Akt1 Cys^{60}–Cys^{77} disulphide bond does not affect survival of zebrafish

It was previously observed that *Akt1* deletion in a mouse model hindered heart development, resulting in high rates of perinatal mortality (Chang et al., 2010), whereas *Akt2* deletion by *CRISPR/Cas9* technology in the zebrafish model exhibited only partial lethality (Zhang et al., 2017). We determined the role of the Cys^{60}–Cys^{77} disulphide bond in Akt1 on zebrafish embryo survival. Survival rates of zebrafish embryos injected with human *Akt1* mutant constructs were normalised to survival rates of uninjected embryos (**Figure 6.4**). Survival rates of *Tg*(*fli1a:EGFP*) embryos injected with *MyrAkt1*, reduced *Akt1* and *T308AS473A-Akt1* mutants were not statistically significant when compared to *Tg*(*fli1a:EGFP*) embryos injected with *WTAkt1*. Although *Akt1* injections proved to be slightly more lethal when comparing survival rates of uninjected embryos, however, this is possibly attributed to genetic changes induced by the expression of *Akt1* constructs or physical injury from the injector needle. Constitutively active *MyrAkt1* injections slightly rescued *Tg*(*fli1a:EGFP*) embryo survival when compared to *Tg*(*fli1a:EGFP*) embryos injected with *WTAkt1* at 24 hpf, but was somewhat lethal at 48 hpf. Embryos injected with reduced *Akt1* did not cause lethality when compared to *Tg*(*fli1a:EGFP*) embryos injected with *WTAkt1* at 24 hpf. However, *Tg*(*fli1a:EGFP*) embryos injected with single cysteine mutant *C60S-Akt1* slightly rescued zebrafish survival, whilst single and double Cys^{77} mutant injections were shown to be somewhat lethal when compared to *Tg*(*fli1a:EGFP*) embryos injected with *WTAkt1* at 48 hpf. *Tg*(*fli1a:EGFP*) embryos injected with constitutively inactive *T308AS473A-Akt1* slightly reduced survival rates when compared to *Tg*(*fli1a:EGFP*) embryos injected with *WTAkt1* at both time points.

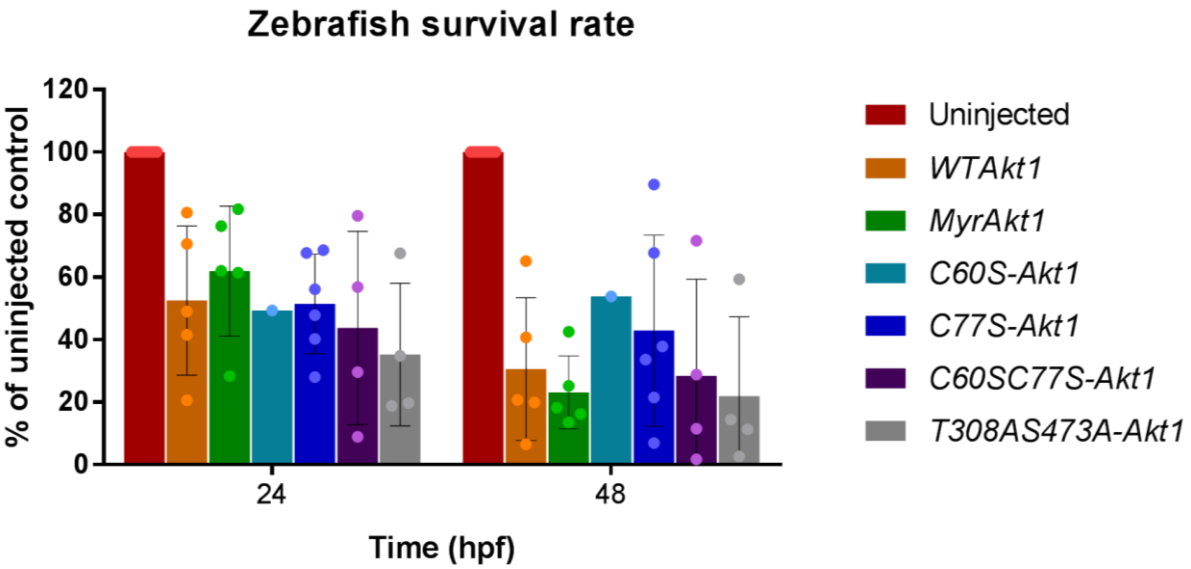

Figure 6.4 Ablation of the Akt1 Cys^{60}–Cys^{77} disulphide bond does not increase mortality in the zebrafish model.
Survival rates of *Tg(fli1a:EGFP)* embryos at 24 and 48 hpf. Embryos injected with human *Akt1* constructs were normalised to uninjected *Tg(fli1a:EGFP)* embryos. Data are expressed as the mean ± s.d.

6.2.4 Ablation of the Akt1 Cys^{60}–Cys^{77} disulphide bond does not affect Akt activity in zebrafish

Human Akt1 has a high degree of similarity compared to zebrafish Akt1; with 89% sequence identity and 94% conserved amino acids (Cheng et al., 2013). Moreover, Cys^{60} and Cys^{77} residues of interest are also evolutionarily conserved in zebrafish. *Akt1* is primarily transcribed during the early stages of development in the zebrafish model, and is essential in the regulation of angiogenesis (Liu et al., 2008) and proliferation of neural progenitor cells (Sinor & Lillien, 2004). Loss of *Akt1* causes precocious neuronal differentiation in the zebrafish model (Cheng et al., 2013; Jeffery et al., 2015); observed as an increase of the differentiated neuronal marker, ELAV like neuron-specific RNA binding protein 3 (*Elavl3/HuC*) (Park et al., 2000); and concurrent decrease of the neural progenitor markers from the Delta-Notch signalling pathway, also responsible for angiogenic endothelial cell formation (Siekmann & Lawson, 2007): *DeltaA* (Riley et al., 1999), hairy-related 8a (*Her8a*) (Chung et al., 2011) and neurogenin 1 (*Ngn1*) (Cheng et al., 2013; Cornell & Eisen, 2002). To investigate the redox state of the Cys^{60}–Cys^{77} disulphide bond in Akt1 on the expression of downstream *Akt1* genes in zebrafish embryos injected with reduced *Akt1* constructs were analysed by RT-qPCR (**Figure 6.5**).

Elavl3 expression in *Tg*(*fli1a:EGFP*) embryos injected with constitutively active *MyrAkt1* and reduced *Akt1* and was around half that of *Tg*(*fli1a:EGFP*) embryos injected with *WTAkt1*; connoting an increase in differentiated neurons. Unexpectedly, levels of *Elavl3* expression were also decreased in *Tg*(*fli1a:EGFP*) embryos injected with constitutively inactive *T308AS473A-Akt1* by 50% when compared to *Tg*(*fli1a:EGFP*) embryos injected with *WTAkt1*.

DeltaA expression in *Tg*(*fli1a:EGFP*) embryos injected with constitutively active *MyrAkt1* and *C77S-Akt1* were moderately increased by around 33% when compared to *Tg*(*fli1a:EGFP*)

embryos injected with *WTAkt1*. Levels of *DeltaA* expression in *Tg*(*fli1a:EGFP*) embryos injected with *C60S-Akt1* and *C60SC77S-Akt1* were 2.5-fold higher than *Tg*(*fli1a:EGFP*) embryos injected with *WTAkt1*. This implied that the Cys^{60} mutation decreased the number of neuronal progenitor cells. Interestingly, levels of *DeltaA* expression were also moderately increased in *Tg*(*fli1a:EGFP*) embryos injected with constitutively inactive *T308AS473A-Akt1* by 50% more than *Tg*(*fli1a:EGFP*) embryos injected with *WTAkt1*.

Her8a expression in *Tg*(*fli1a:EGFP*) embryos injected with constitutively active *MyrAkt1* were increased by 50%, whereas *Tg*(*fli1a:EGFP*) embryos injected with constitutively inactive *T308AS473A-Akt1* decreased by 50% when compared to *Tg*(*fli1a:EGFP*) embryos injected with *WTAkt1* as expected. Levels of *Her8a* expression in *Tg*(*fli1a:EGFP*) embryos injected with reduced *Akt1* were around half that of *Tg*(*fli1a:EGFP*) embryos injected with *WTAkt1*; implicating defects of neuronal differentiation during embryo development.

Ngn1 expression in *Tg*(*fli1a:EGFP*) embryos injected with constitutively active *MyrAkt1*, single cysteine mutant *C60S-Akt1* and constitutively inactive *T308AS473A-Akt1* were comparable to *Tg*(*fli1a:EGFP*) embryos injected with *WTAkt1*. Expression in *Tg*(*fli1a:EGFP*) embryos injected with double cysteine mutant *C60SC77S-Akt1* were increased by 2-fold when compared to *Tg*(*fli1a:EGFP*) embryos injected with *WTAkt1*; denoting an increase in differentiated neurons. Contrastingly, levels of *Ngn1* expression in *Tg*(*fli1a:EGFP*) embryos injected with single cysteine mutant *C77S-Akt1* were half that of *Tg*(*fli1a:EGFP*) embryos injected with *WTAkt1*; implying neuronal developmental defects.

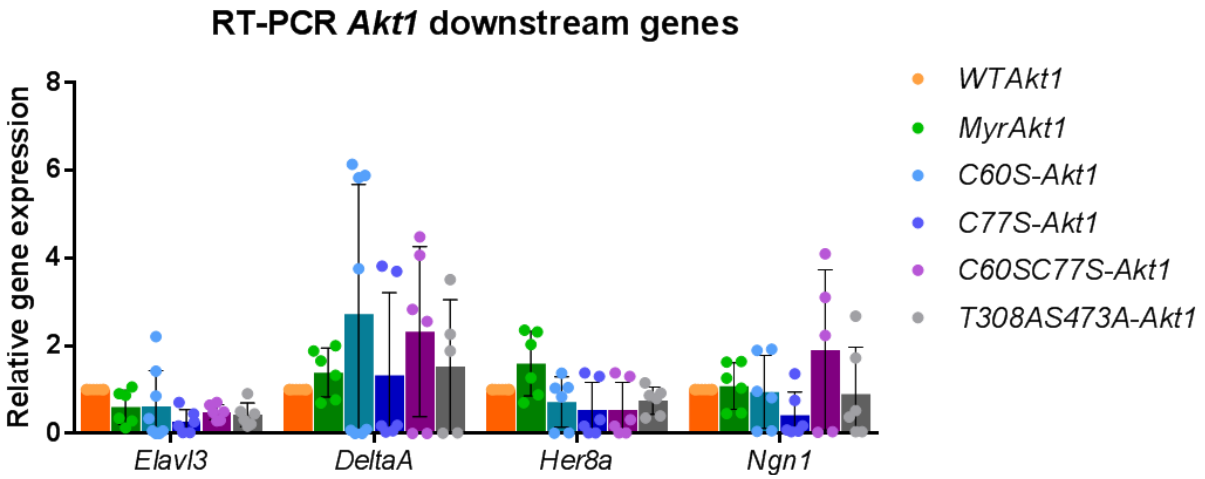

Figure 6.5 Ablation of the Akt1 Cys^{60}–Cys^{77} disulphide bond does not affect expression of selected *Akt1* downstream genes in the zebrafish model.
Tg(fli1a:EGFP) embryo cDNA was isolated by RT-qPCR. Gene transcripts of ELAV like neuron-specific RNA binding protein 3 (*Elavl3*), *DeltaA*, Hairy-related 8a (*Her8a*) and neurogenin 1 (*Ngn1*) were normalised to housekeeper TATA-binding protein (*Tbp*) expression. Gene expression of target genes were normalised relative to *Tg(fli1a:EGFP)* embryos injected with *WTAkt1*. Results are expressed in numbers of fold. Data are expressed as the mean ± s.d.

6.3 Discussion

A range of physiological processes are regulated by Akt; a highly conserved human serine/threonine protein kinase critically involved in the tight regulation of the PI3K/Akt/mTOR signalling pathway (Kitamura et al., 1998). Akt plays an essential role in the development of organisms. Akt phosphorylates to activate or inhibit various downstream substrates responsible for cell growth and survival, angiogenesis and neuronal differentiation (Vasudevan & Garraway, 2010).

The role of Akt in survival and phenotype were previously studied *in vivo*; in zebrafish injected with mRNA morpholinos against *Akt1* (Cheng et al., 2013) and zebrafish engineered to lack the *Akt2* gene via *CRISPR/Cas9* technology (Zhang et al., 2017). The *Akt1* morphants showed neuronal and developmental abnormalities during embryonic development, whilst *Akt2*-null zebrafish exhibited growth deficiencies and partial lethality. My *in vivo* data of *Tg(fli1a:EGFP)* zebrafish embryos injected with full-length human *Akt1* constructs were relatively comparable.

In this chapter, I showed that the redox state of the Cys^{60}–Cys^{77} disulphide bond in human full-length *Akt1* is involved in the induction of angiogenesis in *Tg(fli1a:EGFP)* zebrafish embryos. The completeness of ISV formation in the zebrafish organism is a recognised paradigm of studying angiogenesis (Blum et al., 2008); vascular malformations of the embryos were deemed as a developmental abnormality. Mutations of Cys^{60} to Ser and/or Cys^{77} to Ser were observed to affect the induction of angiogenesis during zebrafish embryonic development. *Tg*(*fli1a:EGFP*) embryos injected with single cysteine mutants *C60S-Akt1* and *C77S-Akt1* increased the rate of ISV completion when compared to *Tg*(*fli1a:EGFP*) embryos injected with *WTAkt1*. Moreover, *Tg*(*fli1a:EGFP*) embryos injected with double mutant *C60SC77S-Akt1*

moderately increased completeness of ISV formation but was not statistically significant when compared to *Tg*(*fli1a:EGFP*) embryos injected with *WTAkt1*.

Interestingly, *Tg*(*fli1a:EGFP*) embryos injected with single cysteine mutants *C60S-Akt1* and *C77S-Akt1*, did not stunt the growth of zebrafish embryos when compared to *Tg*(*fli1a:EGFP*) embryos injected with *WTAkt1*. Although, *Tg*(*fli1a:EGFP*) embryos injected with double cysteine mutant *C60SC77S-Akt1* significantly increased growth.

Akt1 also plays an essential role in neural differentiation in zebrafish by phosphorylating downstream targets of *Akt1* (Cheng et al., 2013; Jeffery et al., 2015). As determined by RT-qPCR, expression of disulphide bond *Akt1* mutants in zebrafish embryos did not significantly alter gene expression of neural progenitor and differentiated neuronal markers downstream of *Akt1*.

To further examine the phosphorylation state of Akt in zebrafish embryos injected with human disulphide bond *Akt1* mutants, expression levels of both human and zebrafish Akt proteins were discernable as different sized bands by immunoblotting. Protein expression levels of zebrafish and human pan-Akt (total Akt) were detected, however, phosphorylated Akt at Thr^{308} and Ser^{473} were not detected and this experiment was not pursued further.

Limitations of this study were that Akt1 was transiently expressed in *Tg(fli1a:EGFP)* zebrafish model. Despite the use of the *pDestTol2* gene transfer vector, new zebrafish lines expressing human *Akt1* constructs were unable to be generated. The ramifications were that human *Akt1* constructs were not ubiquitously expressed throughout the zebrafish organism; and thus, complete ISV formation, growth and development, and expression of downstream *Akt1* targets

may be attributed to endogenous zebrafish *Akt1*. To fully elucidate the function of disulphide bond *Akt1* mutants *in vivo*, a zebrafish line lacking the *Akt1* gene via *CRISPR/Cas9* technology is preferred; as seen in a previous study of *Akt2* function in a zebrafish model (Zhang et al., 2017).

I have so far shown the redox state of the Cys^{60}–Cys^{77} disulphide bond in the PH domain of Akt1 potentially plays a role in physiological functions of Akt1 in the zebrafish model. Reduced human *Akt1* was observed to increase the induction of angiogenesis and development of zebrafish embryos, however, was unable to activate downstream targets of *Akt1*. Additional *in vivo* studies investigating the role of the Cys^{60}–Cys^{77} disulphide bond in physiological function of Akt1 are required.

7. Conclusions & Future Directions

This thesis focuses on the role of a potential allosteric disulphide bond identified in the PH domain of Akt and its impact in Akt function. Cleavage of allosteric disulphide bonds has been shown to alter function of various proteins involved in various biological systems i.e. thrombosis and haemostasis (Butera et al., 2018; Passam et al., 2018); as well as a growing number found in cancer-related proteins (Hogg, 2013). From an analysis of labile disulphide bonds in all X-ray structures from the PDB, my colleagues and I identified a potential allosteric disulphide bond, Cys^{60}–Cys^{77}, in the PH domain of the serine/threonine protein kinase, Akt1. It was only recently discovered that Akt is allosterically activated by phospholipid PIP_3 at the plasma membrane via its N-terminal PH domain (Ebner et al., 2017). The mechanism by which Akt dissociates from the plasma membrane, and therefore its inactivation, is unknown. I hypothesised that the Cys^{60}–Cys^{77} disulphide bond, located near the lipid binding pocket in the PH domain of Akt, is an allosteric disulphide that regulates Akt autoinhibition. I explored the role of the Akt Cys^{60}–Cys^{77} disulphide bond in *in vitro* and *in vivo* systems. In the *in vitro* setting, I determined that the Cys^{60}–Cys^{77} disulphide bond is involved in Akt plasma membrane binding, and consequently, is essential for Akt activation and autoinhibition in mouse fibroblasts. In the *in vivo* model, the Cys^{60}–Cys^{77} disulphide bond was observed to play a role in the biological function of Akt in angiogenesis and growth development of zebrafish embryos. Together, my findings suggest that the Cys^{60}–Cys^{77} disulphide bond is an allosteric bond that is involved in PH domain-mediated autoinhibition of Akt. The Cys^{60}–Cys^{77} disulphide bond is therefore a potential cancer drug target.

7.1 Identification of the Cys^{60}–Cys^{77} disulphide bond in the PH domain of Akt1

Using a bioinformatic approach, my colleagues and I identified labile disulphide bonds in all protein structures from the PDB (**Chapter 3**). The labile nature of some of these disulphide bonds implied their cleavability; and visual inspection of some of these labile disulphides suggested an allosteric function. At the time of writing this thesis, five known allosteric disulphide bonds were among the 511 labile disulphide bonds identified in all PDB X-ray structures; validating this approach to uncover more potential allosteric disulphide bonds. By comparing the distribution of the 20 disulphide configurations between the entire PDB and labile disulphides, two differences were notable. Labile disulphide bonds were observed to be enriched with catalytic +/–RHhook disulphide bonds; and on the other hand, contained fewer structural –LHspiral disulphide bonds (Schmidt et al., 2006). Of the 67 proteins in the labile disulphide dataset that have a +/–RHhook configuration, 22 of them are oxidoreductases. Labile disulphide bonds are enriched in bonds linking α-helices and loops. Catalytic disulphide bonds of oxidoreductases link an α-helix to another or a loop structure, and undergo cycles of reduction and oxidation and there are several examples of oxidised and reduced structures in the PDB; hence their prevalence in the labile disulphide dataset.

Secondary structures of labile disulphide bonds were also investigated. Allosteric –RHstaple disulphide bonds often link adjacent strands in the same antiparallel β-sheet or constrain β-loops (Matthias et al., 2002; Wouters et al., 2004). In the labile disulphide bonds dataset, the Cys^{60}–Cys^{77} disulphide bond was identified in truncated Akt1-PH. Crystal structures show Akt1-PH has seven β-strands forming two orthogonal anti-parallel β-sheets, closed at one end by the C-terminal α-helix (Milburn et al., 2003). In all apo structures of Akt1-PH, the Cys^{60}–Cys^{77} disulphide bond is oxidised and has an archetypical –RHstaple allosteric disulphide

configuration. The Cys^{60}–Cys^{77} disulphide bond is cleaved in all structures of Akt1-PH bound to IP_4, the head group of phospholipid PIP_3; resulting in a significant conformational change. This discovery warranted further investigations on the potential functional role of the Cys^{60}–Cys^{77} disulphide bond in Akt1 plasma membrane binding.

7.2 The role of the Cys^{60}–Cys^{77} disulphide bond in Akt1 plasma membrane localisation

Crystal structures and membrane binding data of truncated reduced Akt-PH bound to phospholipid suggested that full-length reduced Akt was the membrane-bound, active form of the protein. My data of full-length Akt2 plasma membrane binding capabilities has shown otherwise. Truncated reduced Akt1-PH domain had slightly stronger binding affinity for PIP_3 than the wild-type, whereas ablation of the disulphide bond in full-length Akt2 profoundly impaired Akt plasma membrane binding (**Chapter 4**). The differing results in membrane binding between the truncated Akt1-PH domain and full-length Akt2 proteins is possibly due to the cysteine mutations affecting the configuration of PH domain binding to the kinase domain and thus autoinhibition of Akt.

A critical aspect that was not explored in the membrane binding study is the redox state of Cys^{60} and Cys^{77} in membrane-bound versus cytosolic Akt protein, in response to insulin stimulation in the cell. Cysteines residues are particularly susceptible to oxidative stress, inducing the formation of disulphide bonds (Goldstein et al., 2005; Paulsen & Carroll, 2013). As a product of growth factor stimulation, cellular ROS i.e. H_2O_2, a weak oxidant, increase the activation of Akt; implying that Akt is indeed redox-sensitive (Koundouros & Poulogiannis, 2018; Okoh et al., 2013; Ushio-Fukai et al., 1999). Bursts of H_2O_2 generated from growth factor stimulation last for 10 min in the cell (Lee et al., 1998). My mass spectrometry data has shown the Cys^{60}–Cys^{77} disulphide bond in total cellular WTAkt1 protein is >95% reduced in insulin-stimulated mouse fibroblasts. An aim for future studies is to capture and measure the redox state of the small fraction of total cellular Akt1 bound to the plasma membrane. My prediction is that this pool of membrane bound Akt1 will be oxidised, possibly induced by the burst of H_2O_2 as a product of insulin stimulation. The cysteine alkylators I have used are iodoacetamide-

based chemical probes that are poorly membrane permeable and cytotoxic at high concentrations (Abo & Weerapana, 2015). To capture the redox state of membrane-bound Akt1, the cysteine alkylators would require a longer timeframe for internalisation and equilibration in cells post-stimulation, which may not be technically feasible. Future work will instead utilise a caged electrophilic probe (Abo et al., 2017) to label cysteines in WTAkt1 protein subject to oxidation upon insulin stimulation of mouse fibroblasts. This approach has been used to quantify oxidative modifications of cysteines in live cells upon epidermal growth factor-stimulated ROS production (Abo & Weerapana, 2015). H_2O_2-induced oxidation of the other disulphide bond in Akt1 (Cys^{296}–Cys^{310}) was observed to dephosphorylate Akt1 through increased interaction with phosphatase PP2A, deactivating the kinase. However, mutations of Cys^{296} and Cys^{310} residues did not affect Akt1 phosphorylation or kinase activity (Ahmad et al., 2014).

7.3 The role of the Cys^{60}–Cys^{77} disulphide bond for Akt1 activity in mouse fibroblasts and zebrafish embryos

Akt1 activity is restricted to PIP_3-containing membranes (Ebner et al., 2017), signifying the importance of a functional PH domain. The PH domain of Akt1 binds to PIP_3 at the plasma membrane, exposing the activation loop and phosphorylation sites on the kinase and regulatory domains of Akt1 (Lučić et al., 2018). I explored the mechanism of PH domain-mediated Akt1 autoinhibition in this thesis. I have shown that the Cys^{60}–Cys^{77} disulphide bond impairs Akt1 phosphorylation and downstream substrate activation in mouse fibroblasts, suggesting it is involved in Akt1 autoinhibition (**Chapter 5**). Despite insulin stimulation, mutation of Cys^{60} to Ser in full-length Akt1 resulted in moderate impairment of Akt1 phosphorylation and activation in mouse fibroblasts, whereas mutation of Cys^{77} to Ser in full-length Akt1 led to the near ablation of phosphorylation of Akt1 and significant impairment of downstream activity. Studies in mouse fibroblasts suggested that oxidation of the Cys^{60}–Cys^{77} disulphide bond is required to induce oncogenic transformation of the cells. This result suggested that the Cys^{60}–Cys^{77} disulphide bond is critical for full-length Akt1 plasma membrane recruitment and subsequent activation by PIP_3.

Allosteric disulphide bonds are cleaved by oxidoreductases or thiol–disulphide exchange; altering the function of the protein in which they reside (Cook & Hogg, 2013). An important question that will be explored in a future study is how the Cys^{60}–Cys^{77} disulphide bond is cleaved in the cytosol. Thioredoxin is a small cytosolic oxidoreductase that maintains protein thiol homeostasis in the cell (Leveillard & Ait-Ali, 2017), and I postulate that it reduces the Cys^{60}–Cys^{77} disulphide bond of Akt1 to induce the PH domain-mediated autoinhibition. Future experiments will correlate thioredoxin activity in the cytosol with the redox state of the Akt1

Cys^{60}–Cys^{77} disulphide bond (Holmgren, 1995; Holmgren & Björnstedt, 1995; Montano et al., 2014).

I have shown the Cys^{60}–Cys^{77} disulphide bond affects the physiological function of Akt1 in a biological system (**Chapter 6**). Mutations of Cys^{60} and Cys^{77} to Ser in full-length Akt1 increased the induction of angiogenesis and growth of zebrafish embryos, suggesting the Cys^{60}–Cys^{77} disulphide bond in Akt1 is involved in zebrafish development. However, to better distinguish injected human Akt1 from endogenous zebrafish Akt1, this study will require further validation in a zebrafish model that ubiquitously expresses human Akt1. Multiple attempts were also made to examine the phosphorylation state of Akt1 in zebrafish embryos injected with human *Akt1* constructs. Protein expression levels of zebrafish and human pan-Akt (total Akt) were semi-quantitatively examined; however, phosphorylated Akt at Thr^{308} or Ser^{473} residues were not detected and this experiment was not pursued further.

7.4 The Cys^{60}–Cys^{77} disulphide bond in Akt1 is an allosteric disulphide involved in Akt1 function

A working model of the mechanistic role of the Cys^{60}–Cys^{77} disulphide bond in Akt1 function is presented in **Figure 7.1**. In the model, reduced Akt1 is the inactive form; it is unable to be phosphorylated and does not activate substrates due to the PH and kinase domains adopting an autoinhibitory conformation (**Figure 7.1A**). As a product of growth factor stimulation, bursts of ROS oxidise Akt1 to form the Cys^{60}–Cys^{77} disulphide bond. Oxidised Akt1 translocates to the plasma membrane and is allosterically activated by PIP_3 (Ebner et al., 2017), disrupting the autoinhibitory interaction between the PH–kinase domains of Akt1 (**Figure 7.1B**). Oxidised Akt1 is docked at the plasma membrane; PDK1 and mTORC2 have access to the activation loop in the kinase domain and phosphorylate Akt1 at Thr^{308} at Ser^{473} residues, respectively. Active Akt1 phosphorylates downstream substrates, namely FoxO1, GSK3 and TSC2 (**Figure 7.1C**). I propose that dissociation of active Akt1 from the plasma membrane; the rate-limiting step for Akt1 dephosphorylation and autoinhibition (Ebner et al., 2017; Lučić et al., 2018), is prompted by thioredoxin cleavage of the Cys^{60}–Cys^{77} disulphide bond, triggering PH domain-mediated autoinhibition. Reduced Akt1 is rapidly dephosphorylated by PP2A and PHLPP2 at Thr^{308} and Ser^{473} residues, respectively (**Figure 7.1D**).

Figure 7.1 Working model for the role of Cys^{60}–Cys^{77} disulphide bond in Akt1 activation and autoinhibition in the cell.
The pleckstrin homology (PH), kinase (KD) and regulatory (RD) domains of Akt1 are indicated. A. Reduced Akt1, defined by unpaired Cys^{60} and Cys^{77} thiols in the PH domain, is inactive and adopts an autoinhibitory conformation. B. Growth factor stimulation of receptor tyrosine kinase (RTK) phosphorylates phosphoinositide 3-kinase (PI3K) to further phosphorylate phosphatidylinositol-4,5-bisphosphate (PIP2) to phosphatidylinositol-3,4,5-trisphosphate (PIP_3). Growth factor stimulation also produce bursts of reactive oxygen species (ROS) that triggers formation of the Cys^{60}–Cys^{77} disulphide bond in the PH domain. Oxidised Akt1, defined by an intact Cys^{60}–Cys^{77} disulphide bond in the PH domain, translocates to the plasma membrane and is allosterically activated by PIP_3. Akt1 undergoes a conformational change; relieving PH domain-mediated autoinhibition of the kinase domain and allowing substrate access. **C.** Oxidised Akt1 at the plasma membrane is phosphorylated by phosphoinositide-dependent kinase 1 (PDK1) and mammalian target of rapamycin complex 2 (mTORC2) at Thr^{308} and Ser^{473}, respectively. Active Akt1 subsequently phosphorylates downstream substrates. **D.** Cytosolic oxidoreductase thioredoxin (Trx) is reduced by thioredoxin reductase (TrxR) by an NADPH-dependent mechanism, cleaving the Cys^{60}–Cys^{77} disulphide bond in the PH domain of Akt1. Reduced Akt1 dissociates from the plasma membrane and regains its autoinhibitory conformation. Reduced Akt1 is rapidly dephosphorylated by protein phosphatase 2 (PP2A) and PH domain and leucine rich repeat protein phosphatase (PHLPP2) at Thr^{308} and Ser^{473}, respectively.

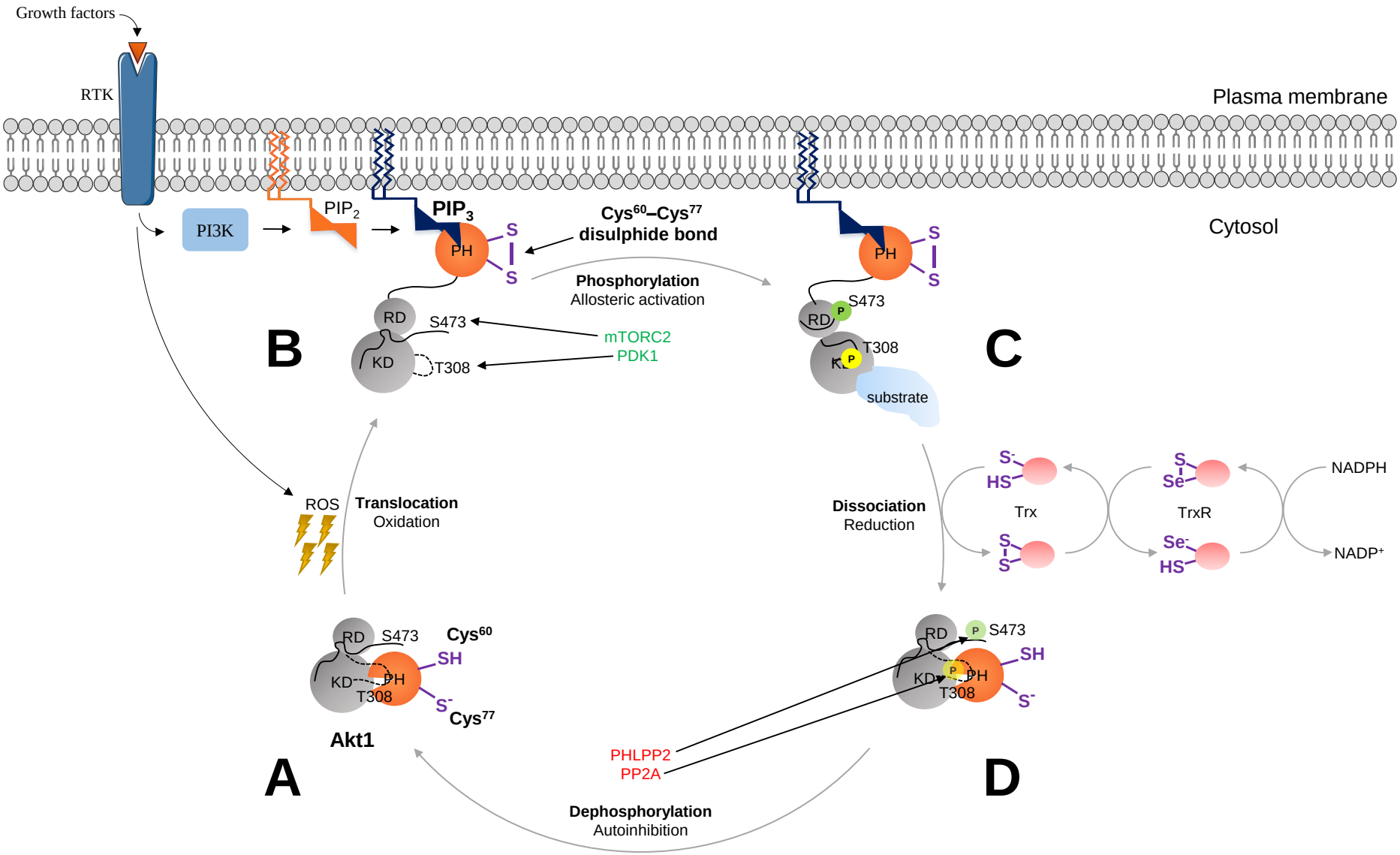
Growth factors
RTK
Plasma membrane
PI3K
PIP2
PIP3
Cys60–Cys77
disulphide bond
Cytosol
PH
S
S
Phosphorylation
Allosteric activation
RD
S473
KD
T308
mTORC2
PDK1
B
C
P
substrate
ROS
Translocation
Oxidation
Dissociation
Reduction
S-
HS
Trx
S
Se
TrxR
NADPH
NADP+
Se-
HS
Cys60
SH
S-
Cys77
Akt1
A
D
PHLPP2
PP2A
Dephosphorylation
Autoinhibition

7.5 Targeting the Akt1 Cys^{60}–Cys^{77} disulphide bond in cancer

Another interesting aspect of this study is the relevance of the Cys^{60}–Cys^{77} disulphide bond in other isoforms of Akt. Akt1 is ubiquitously expressed in all tissues. Akt2 is expressed in metabolically active tissue e.g. liver, adipose tissue and muscle. Akt3 is predominantly expressed in the brain and testes (Chan et al., 2014; Yang et al., 2004). When overexpressed, Akt1 is known to be involved in the progression of the breast (Carpten et al., 2007; Stephens et al., 2012; Yi et al., 2012), endometrial (Cohen et al., 2010), prostate (Boormans et al., 2010), bladder (Askham et al., 2010), NSCLC (De Marco et al., 2015; Ding et al., 2008), blood (Kim et al., 2008) and melanoma (Davies et al., 2008) cancers. Akt2 is often linked to diabetes mellitus type 2 (Cohen, 2013) and Akt3 is associated with neurological disorders (Poduri et al., 2012). The development of Akt isozyme-selective therapies has long been a challenge due to the high degree of amino acid sequence homology of the kinase domains but diverge in the PH and regulatory domains (Nitulescu et al., 2016). The amino acid sequence of the PH domain of Akt1 is more similar to Akt2 than Akt3; therefore the role of the Cys^{60}–Cys^{77} disulphide bond in Akt2 is presumably similar to Akt1. The amino acid sequence of the linker region that connects the PH and kinase domains of Akt is also poorly conserved between the isoforms. This sequence variation has led to the development of allosteric Akt inhibitors that have isozyme specificity and lower toxicity (Nitulescu et al., 2016).

For example, the isoform-specific Cys^{124} residue in the linker region of Akt2 is sensitive to endogenous H_2O_2 (Wani et al., 2014; Wani et al., 2011). Oxidation of Akt2 promotes cell migration and cell cycle distribution (G_1-S transition), a possible factor in the development of diabetes mellitus type 2 (Wani et al., 2014; Wani et al., 2011). Another study has shown the isoform-specific Cys^{119} residue in the linker region of Akt3 is sensitive to the electrophilic lipid

4-hydroxynonenal, inhibiting Akt3 activity in mammalian cells and the zebrafish model (Long & Aye, 2017; Long et al., 2017).

Targeting allosteric disulphide bonds in proteins is still a relatively new approach for the treatment of cancer. Future research will include the development of an inhibitor that impairs the function and formation of the Cys^{60}–Cys^{77} allosteric disulphide bond in the PH domain of Akt1 (**Figure 7.2**). Cysteine-directed electrophiles can be designed to target poorly reactive cysteines in an activity-based manner (Shannon & Weerapana, 2015). Thiol alkylators containing a weak electrophilic moiety will be designed to modify only the functionally relevant Cys^{60} and Cys^{77} residues in activated Akt1.

Current examples of anti-angiogenic and anti-cancer thiol alkylating drug compounds include 4-(*N*-(*S*-glutathionylacetyl)amino)phenylarsonous acid (GSAO) and its derivative 4-(*N*-(*S*-penicillaminylacetyl)amino)phenylarsonous acid (PENAO). GSAO and PENAO are trivalent arsenical compounds that cross-link Cys^{57} and Cys^{257} in human adenine nucleotide translocase (ANT) of the inner-mitochondrial membrane. Cys^{160} and Cys^{257} residues in ANT are usually disulphide bonded in quiescent cells and so these compounds selectively target proliferating tumour cells (Park et al., 2012). Inhibition of ANT leads to the partial uncoupling of oxidative phosphorylation, resulting in mitochondrial membrane permeability transition, superoxide production and tumour cell death (Decollogne et al., 2015; Dilda et al., 2009; Dilda & Hogg, 2007; Dilda et al., 2008; Don et al., 2003; Elliott et al., 2012; Park et al., 2012; Ramsay et al., 2011; Shen et al., 2015). GSAO and PENAO recently completed Phase I clinical trials and was well tolerated in patients with solid tumours refractory to standard treatment. No significant organ toxicity was observed (trial identifiers CTA-21106-0222-001 and ANCTRN12612000908831) (Elliott et al., 2012; Horsley et al., 2013). GSAO has a short t½

of 10.1 min (Horsley et al., 2013), but its efficacy is limited by the expression of multidrug resistance proteins 1 and 2 (MRP1/2). PENAO accumulates in tumour cells 85-fold faster than GSAO due to the decreased rate of export via MRP1/2 (Dilda et al., 2009) however, has an unexpectedly long t½ in human circulation of 5-9 days. These pharmacokinetic findings warrant further investigations of an appropriate dosage schedule and to identify combination therapies with other known metabolic inhibitors.

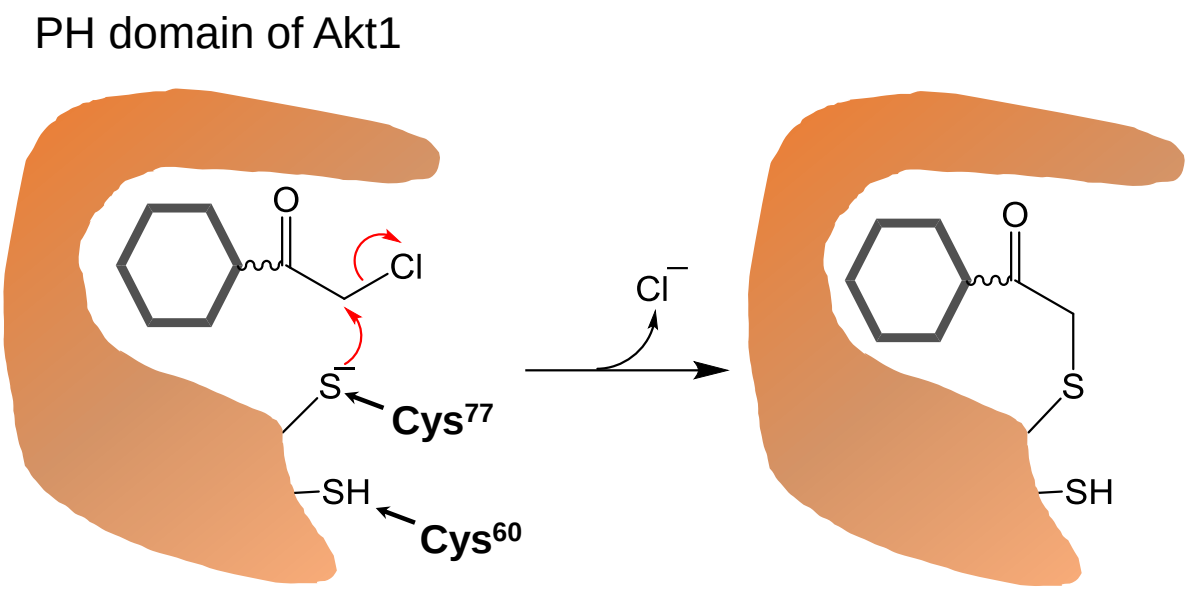

Figure 7.2 Blocking the formation of the Cys^{60}–Cys^{77} disulphide bond in the PH domain of Akt1 with a targeted thiol alkylator.
A targeted thiol alkylator can be designed to disrupt the formation of the Cys^{60}–Cys^{77} disulphide bond in the PH domain of Akt1. The reactive electrophilic group of the compound (chloroacetyl moiety is pictured) is brought into close proximity to an unpaired Cys^{77} residue in the PH domain of reduced Akt1, thereby blocking thiol–disulphide exchange and inactivating the kinase. The hexagon cartoon represents a non-defined structure that interacts with the binding pocket of the PH domain. The wavy line in the compound represents a non-defined structure.

8. References

Abo, M., Bak, D. W., & Weerapana, E. (2017). Optimization of Caged Electrophiles for Improved Monitoring of Cysteine Reactivity in Living Cells. *ChemBioChem, 18*(1), 81-84.

Abo, M., & Weerapana, E. (2015). A caged electrophilic probe for global analysis of cysteine reactivity in living cells. *J Am Chem Soc, 137*(22), 7087-7090.

Ackah, E., Yu, J., Zoellner, S., Iwakiri, Y., Skurk, C., Shibata, R., Ouchi, N., Easton, R. M., Galasso, G., Birnbaum, M. J., Walsh, K., & Sessa, W. C. (2005). Akt1/protein kinase Bα is critical for ischemic and VEGF-mediated angiogenesis. *J Clin Invest, 115*(8), 2119-2127.

Ahamed, J., Versteeg, H. H., Kerver, M., Chen, V. M., Mueller, B. M., Hogg, P. J., & Ruf, W. (2006). Disulfide isomerization switches tissue factor from coagulation to cell signaling. *Proc Natl Acad Sci USA, 103*(38), 13932-13937.

Ahmad, F., Nidadavolu, P., Durgadoss, L., & Ravindranath, V. (2014). Critical cysteines in Akt1 regulate its activity and proteasomal degradation: Implications for neurodegenerative diseases. *Free Radic Biol Med, 74*, 118-128.

Aicart-Ramos, C., Valero, R. A., & Rodriguez-Crespo, I. (2011). Protein palmitoylation and subcellular trafficking. *Biochim Biophys Acta, 1808*(12), 2981-2994.

Ainavarapu, S. R. K., Wiita, A. P., Dougan, L., Uggerud, E., & Fernandez, J. M. (2008). Single-molecule force spectroscopy measurements of bond elongation during a bimolecular reaction. *J Am Chem Soc, 130*(20), 6479-6487.

Akbar, M., Calderon, F., Wen, Z., & Kim, H. Y. (2005). Docosahexaenoic acid: A positive modulator of Akt signaling in neuronal survival. *Proc Natl Acad Sci USA, 102*(31), 10858-10863.

Alessi, D. R., Andjelkovic, M., Caudwell, B., Cron, P., Morrice, N., Cohen, P., & Hemmings, B. A. (1996a). Mechanism of activation of protein kinase B by insulin and IGF-1. *EMBO J, 15*(23), 6541-6551.

Alessi, D. R., Caudwell, B., Andjelkovic, M., Hemmings, B. A., & Cohen, P. (1996b). Molecular basis for the substrate specificity of protein kinase B; comparison with MAPKAP kinase-1 and p70 S6 kinase. *FEBS Lett, 399*(3), 333-338.

Andjelkovic, M., Alessi, D. R., Meier, R., Fernandez, A., Lamb, N. J. C., Frech, M., Cron, P., Cohen, P., Lucocq, J. M., & Hemmings, B. A. (1997). Role of translocation in the activation and function of protein kinase B. *J Biol Chem, 272*(50), 31515-31524.

Aoki, M., Batista, O., Bellacosa, A., Tsichlis, P., & Vogt, P. K. (1998). The Akt kinase: Molecular determinants of oncogenicity. *Proc Natl Acad Sci USA, 95*(25), 14950-14955.

Arauz, E., Aggarwal, V., Jain, A., Ha, T., & Chen, J. (2016). Single-molecule analysis of lipid-protein interactions in crude cell lysates. *Anal Chem, 88*(8), 4269-4276.

Arnér, E. S. J., & Holmgren, A. (2000). Physiological functions of thioredoxin and thioredoxin reductase. *Eur J Biochem, 267*(20), 6102-6109.

Askham, J. M., Platt, F., Chambers, P. A., Snowden, H., Taylor, C. F., & Knowles, M. A. (2010). AKT1 mutations in bladder cancer: Identification of a novel oncogenic mutation that can co-operate with E17K. *Oncogene, 29*(1), 150-155.

Auwerx, J., Isacsson, O., Soderlund, J., Balzarini, J., Johansson, M., & Lundberg, M. (2009). Human glutaredoxin-1 catalyzes the reduction of HIV-1 gp120 and CD4 disulfides and its inhibition reduces HIV-1 replication. *Int J Biochem Cell Biol, 41*(6), 1269-1275.

Azimi, I., Matthias, L. J., Center, R. J., Wong, J. W., & Hogg, P. J. (2010). Disulfide bond that constrains the HIV-1 gp120 V3 domain is cleaved by thioredoxin. *J Biol Chem, 285*(51), 40072-40080.

Baldus, I. B., & Gräter, F. (2012). Mechanical force can fine-tune redox potentials of disulfide bonds. *Biophys J, 102*(3), 622-629.

Banerji, S., Lawrance, W., Metcalfe, C., Briggs, D. C., Yamauchi, A., Dushek, O., van der Merwe, P. A., Day, A. J., & Jackson, D. G. (2016). Homodimerization of the lymph vessel endothelial receptor LYVE-1 through a redox-labile disulfide is critical for hyaluronan binding in lymphatic endothelium. *J Biol Chem, 291*(48), 25004-25018.

Barbouche, R., Miquelis, R., Jones, I. M., & Fenouillet, E. (2003). Protein-disulfide isomerase-mediated reduction of two disulfide bonds of HIV envelope glycoprotein 120 occurs post-CXCR4 binding and is required for fusion. *J Biol Chem, 278*(5), 3131-3136.

Barnett, S. F., Defeo-Jones, D., Fu, S., Hancock, P. J., Haskell, K. M., Jones, R. E., Kahana, J. A., Kral, A. M., Leander, K., Lee, L. L., Malinowski, J., McAvoy, E. M., Nahas, D. D., Robinson, R. G., & Huber, H. E. (2005). Identification and characterization of pleckstrin-homology-domain-dependent and isoenzyme-specific Akt inhibitors. *Biochem J, 385*(Pt 2), 399-408.

Barthel, A., Okino, S. T., Liao, J., Nakatani, K., Li, J., Whitlock, J., J. P. , & Roth, R. A. (1999). Regulation of GLUT1 gene transcription by the serine/threonine kinase Akt1. *J Biol Chem, 274*(29), 20281-20286.

Baxter, R. C. (2014). IGF binding proteins in cancer: mechanistic and clinical insights. *Nat Rev Cancer, 14*(5), 329-341.

Bekendam, R. H., Bendapudi, P. K., Lin, L., Nag, P. P., Pu, J., Kennedy, D. R., Feldenzer, A., Chiu, J., Cook, K. M., Furie, B., Huang, M., Hogg, P. J., & Flaumenhaft, R. (2016). A substrate-driven allosteric switch that enhances PDI catalytic activity. *Nat Commun, 7*(12579), 1-11.

Bellacosa, A., Chan, T. O., Ahmed, N. N., Datta, K., Malstrom, S., Stokoe, D., McCormick, F., Feng, J., & Tsichlis, P. (1998). Akt activation by growth factors is a multiple-step process: the role of the PH domain. *Oncogene, 17*(3), 313-325.

Bellacosa, A., Kumar, C. C., Cristofano, A. D., & Testa, J. R. (2005). Activation of AKT kinases in cancer: Implications for therapeutic targeting. *Adv Cancer Res, 94*, 29-86.

Berndt, N., Yang, H., Trinczek, B., Betzi, S., Zhang, Z., Wu, B., Lawrence, N. J., Pellecchia, M., Schonbrunn, E., Cheng, J. Q., & Sebti, S. M. (2010). The Akt activation inhibitor TCN-P inhibits Akt phosphorylation by binding to the PH domain of Akt and blocking its recruitment to the plasma membrane. *Cell Death Differ, 17*(11), 1795-1804.

Bessière, L., Todeschini, A. L., Auguste, A., Sarnacki, S., Flatters, D., Legois, B., Sultan, C., Kalfa, N., Galmiche, L., & Veitia, R. A. (2015). A hot-spot of in-frame duplications activates the oncoprotein AKT1 in juvenile granulosa cell tumors. *EBioMedicine, 2*(5), 421-431.

Beurel, E., Grieco, S. F., & Jope, R. S. (2015). Glycogen synthase kinase-3 (GSK3): regulation, actions, and diseases. *Pharmacol Ther, 148*, 114-131.

Blum, Y., Belting, H. G., Ellertsdottir, E., Herwig, L., Luders, F., & Affolter, M. (2008). Complex cell rearrangements during intersegmental vessel sprouting and vessel fusion in the zebrafish embryo. *Dev Biol, 316*(2), 312-322.

Boormans, J. L., Korsten, H., Ziel-van der Made, A. C., van Leenders, G. J., Verhagen, P. C., & Trapman, J. (2010). E17K substitution in AKT1 in prostate cancer. *Br J Cancer, 102*(10), 1491-1494.

Bowley, S. R., Fang, C., Merrill-Skoloff, G., Furie, B. C., & Furie, B. (2017). Protein disulfide isomerase secretion following vascular injury initiates a regulatory pathway for thrombus formation. *Nat Commun, 8*(14151), 1-13.

Buller, C. L., Loberg, R. D., Fan, M. H., Zhu, Q., Park, J. L., Vesely, E., Inoki, K., Guan, K. L., & Brosius, F. C., 3rd. (2008). A GSK-3/TSC2/mTOR pathway regulates glucose uptake and GLUT1 glucose transporter expression. *Am J Physiol Cell Physiol, 295*(3), C836-C843.

Butera, D., Cook, K. M., Chiu, J., Wong, J. W., & Hogg, P. J. (2014). Control of blood proteins by functional disulfide bonds. *Blood, 123*(13), 2000-2007.

Butera, D., Passam, F., Ju, L., Cook, K. M., Woon, H., Aponte-Santamaría, C., Gardiner, E., Davis, A. K., Murphy, D. A., Bronowska, A., Luken, B. M., Baldauf, C., Jackson, S., Andrews, R., Gräter, F., & Hogg, P. J. (2018). Autoregulation of von Willebrand factor function by a disulfide bond switch. *Sci Adv, 4*(2), 1-12.

Butera, D., Wind, T., Lay, A. J., Beck, J., Castellino, F. J., & Hogg, P. J. (2013). Characterization of a reduced form of plasma plasminogen as the precursor for angiostatin formation. *J Biol Chem, 289*(5), 2992-3000.

Buzzai, M., Bauer, D. E., Jones, R. G., Deberardinis, R. J., Hatzivassiliou, G., Elstrom, R. L., & Thompson, C. B. (2005). The glucose dependence of Akt-transformed cells can be reversed by pharmacologic activation of fatty acid *β*-oxidation. *Oncogene, 24*(26), 4165-4173.

Calleja, V., Alcor, D., Laguerre, M., Park, J., Vojnovic, B., Hemmings, B. A., Downward, J., Parker, P. J., & Larijani, B. (2007). Intramolecular and intermolecular interactions of protein kinase B define its activation in vivo. *PLoS Biol, 5*(4), e95.

Calleja, V., Laguerre, M., Parker, P. J., & Larijani, B. (2009). Role of a novel PH-kinase domain interface in PKB/Akt regulation: structural mechanism for allosteric inhibition. *PLoS Biol, 7*(1), e17.

Carpten, J. D., Faber, A. L., Horn, C., Donoho, G. P., Briggs, S. L., Robbins, C. M., Hostetter, G., Boguslawski, S., Moses, T. Y., Savage, S., Uhlik, M., Lin, A., Du, J., Qian, Y. W.,

Zeckner, D. J., Tucker-Kellogg, G., Touchman, J., Patel, K., Mousses, S., Bittner, M., Schevitz, R., Lai, M. H., Blanchard, K. L., & Thomas, J. E. (2007). A transforming mutation in the pleckstrin homology domain of AKT1 in cancer. *Nature, 448*(7152), 439-444.

Carracedo, A., & Pandolfi, P. P. (2008). The PTEN-PI3K pathway: of feedbacks and cross-talks. *Oncogene, 27*(41), 5527-5541.

Cerami, E., Gao, J., Dogrusoz, U., Gross, B. E., Sumer, S. O., Aksoy, B. A., Jacobsen, A., Byrne, C. J., Heuer, M. L., Larsson, E., Antipin, Y., Reva, B., Goldberg, A. P., Sander, C., & Schultz, N. (2012). The cBio cancer genomics portal: an open platform for exploring multidimensional cancer genomics data. *Cancer Discov, 2*(5), 401-404.

Chalhoub, N., & Baker, S. J. (2009). PTEN and the PI3-kinase pathway in cancer. *Annu Rev Pathol, 4*, 127-150.

Chan, C.-H., Jo, U., Kohrman, A., Rezaeian, A. H., Chou, P.-C., Logothetis, C., & Lin, H.-K. (2014). Posttranslational regulation of Akt in human cancer. *Cell Biosci, 4*(59), 1-9.

Chan, T. O., Zhang, J., Rodeck, U., Pascal, J. M., Armen, R. S., Spring, M., Dumitru, C. D., Myers, V., Li, X., Cheung, J. Y., & Feldman, A. M. (2011). Resistance of Akt kinases to dephosphorylation through ATP-dependent conformational plasticity. *Proc Natl Acad Sci USA, 108*(46), E1120-E1127.

Chang, Z., Zhang, Q., Feng, Q., Xu, J., Teng, T., Luan, Q., Shan, C., Hu, Y., Hemmings, B. A., Gao, X., & Yang, Z. (2010). Deletion of Akt1 causes heart defects and abnormal cardiomyocyte proliferation. *Dev Biol, 347*(2), 384-391.

Chávez, M. N., Aedo, G., Fierro, F. A., Allende, M. L., & Egana, J. T. (2016). Zebrafish as an emerging model organism to study angiogenesis in development and regeneration. *Front Physiol, 7*(56), 1-15.

Chen, J., Somanath, P. R., Razorenova, O., Chen, W. S., Hay, N., Bornstein, P., & Byzova, T. V. (2005). Akt1 regulates pathological angiogenesis, vascular maturation and permeability in vivo. *Nat Med, 11*(11), 1188-1196.

Chen, V. M., Ahamed, J., Versteeg, H. H., Berndt, M. C., Ruf, W., & Hogg, P. J. (2006). Evidence for activation of tissue factor by an allosteric disulfide bond. *Biochemistry, 45*(39), 12020-12028.

Cheng, Y.-C., Hsieh, F.-Y., Chiang, M.-C., Scotting, P. J., Shih, H.-Y., Lin, S.-J., Wu, H.-L., & Lee, H.-T. (2013). Akt1 mediates neuronal differentiation in zebrafish via a reciprocal interaction with notch signaling. *PLoS One, 8*(1), e54262.

Childs, S., Chen, J.-N., Garrity, D. M., & Fishman, M. C. (2002). Patterning of angiogenesis in the zebrafish embryo. *Development, 129*(4), 973-982.

Chiu, J., & Hogg, P. J. (2019). Allosteric disulfides: Sophisticated molecular structures enabling flexible protein regulation. *J Biol Chem, 294*(8), 2949-2960.

Chiu, J., March, P. E., Lee, R., & Tillett, D. (2004). Site-directed, Ligase-Independent Mutagenesis (SLIM): a single-tube methodology approaching 100% efficiency in 4 h. *Nucleic Acids Res, 32*(21), e174.

Chiu, J., Passam, F., Butera, D., & Hogg, P. J. (2015). Protein disulfide isomerase in thrombosis. *Semin Thromb Hemost, 41*(7), 765-773.

Chiu, J., Tillett, D., Dawes, I. W., & March, P. E. (2008). Site-directed, Ligase-Independent Mutagenesis (SLIM) for highly efficient mutagenesis of plasmids greater than 8kb. *J Microbiol Meth, 73*(2), 195-198.

Chiu, J., Wong, J. W. H., Gerometta, M., & Hogg, P. J. (2014a). Mechanism of dimerization of a recombinant mature vascular endothelial growth factor C. *Biochemistry, 53*(1), 7-9.

Chiu, J., Wong, J. W. H., & Hogg, P. J. (2014b). Redox regulation of methionine aminopeptidase 2 activity. *J Biol Chem, 289*(21), 15035-15043.

Cho, W., Hu, Y., Baek, K., & Kim, H. (2017). A high-throughput fluorometric assay for lipid-protein binding. *Method Enzymol, 583*, 1-18.

Chung, P.-C., Lin, W.-S., Scotting, P. J., Hsieh, F.-Y., Wu, H.-L., & Cheng, Y.-C. (2011). Zebrafish Her8a is activated by Su(H)-dependent notch signaling and is essential for the inhibition of neurogenesis. *PLoS One, 6*(4), e19394.

Cohen, M. M., Jr. (2013). The AKT genes and their roles in various disorders. *Am J Med Genet Part A, 161A*(12), 2931-2937.

Cohen, Y., Shalmon, B., Korach, J., Barshack, I., Fridman, E., & Rechavi, G. (2010). AKT1 pleckstrin homology domain E17K activating mutation in endometrial carcinoma. *Gynecol Oncol, 116*(1), 88-91.

Cook, K. M., & Hogg, P. J. (2013). Post-translational control of protein function by disulfide bond cleavage. *Antioxid Redox Signal, 18*(15), 1987-2015.

Cook, K. M., McNeil, H. P., & Hogg, P. J. (2013). Allosteric control of *β*II-tryptase by a redox active disulfide bond. *J Biol Chem, 288*(48), 34920-34929.

Cornell, R. A., & Eisen, J. S. (2002). Delta/notch signaling promotes formation of zebrafish neural crest by repressing neurogenin 1 function. *Development, 129*(11), 2639-2648.

Costa, C., Pereira, S., Lima, L., Peixoto, A., Fernandes, E., Neves, D., Neves, M., Gaiteiro, C., Tavares, A., Gil da Costa, R. M., Cruz, R., Amaro, T., Oliveira, P. A., Ferreira, J. A., & Santos, L. L. (2015). Abnormal protein glycosylation and activated PI3K/Akt/mTOR pathway: role in bladder cancer prognosis and targeted therapeutics. *PLoS One, 10*(11), e0141253.

Cremers, C. M., & Jakob, U. (2013). Oxidant sensing by reversible disulfide bond formation. *J Biol Chem, 288*(37), 26489-26496.

Cross, D. A., Alessi, D. R., Cohen, P., Andjelkovich, M., & Hemmings, B. A. (1995). Inhibition of glycogen synthase kinase-3 by insulin mediated by protein kinase B. *Nature, 378*(6559), 785-789.

Cuneo, M. J., & London, R. E. (2010). Oxidation state of the XRCC1 N-terminal domain regulates DNA polymerase β binding affinity. *Proc Natl Acad Sci U S A, 107*(15), 6805-6810.

Datta, S. R., Dudek, H., Tao, X., Masters, S., Fu, H., Gotoh, Y., & Greenberg, M. E. (1997). Akt phosphorylation of BAD couples survival signals to the cell-intrinsic death machinery. *Cell, 91*(2), 231-241.

Davies, M. A., Stemke-Hale, K., Tellez, C., Calderone, T. L., Deng, W., Prieto, V. G., Lazar, A. J., Gershenwald, J. E., & Mills, G. B. (2008). A novel AKT3 mutation in melanoma tumours and cell lines. *Br J Cancer, 99*(8), 1265-1268.

de la Cruz-Herrera, C. F., Campagna, M., Lang, V., del Carmen Gonzalez-Santamaria, J., Marcos-Villar, L., Rodriguez, M. S., Vidal, A., Collado, M., & Rivas, C. (2015). SUMOylation regulates AKT1 activity. *Oncogene, 34*(11), 1442-1450.

De Marco, C., Malanga, D., Rinaldo, N., De Vita, F., Scrima, M., Lovisa, S., Fabris, L., Carriero, M. V., Franco, R., Rizzuto, A., Baldassarre, G., & Viglietto, G. (2015). Mutant AKT1-E17K is oncogenic in lung epithelial cells. *Oncotarget, 6*(37), 39634-39650.

DeBerardinis, R. J., Lum, J. J., Hatzivassiliou, G., & Thompson, C. B. (2008). The biology of cancer: metabolic reprogramming fuels cell growth and proliferation. *Cell Metab, 7*(1), 11-20.

Decollogne, S., Joshi, S., Chung, S. A., Luk, P. P., Yeo, R. X., Nixdorf, S., Fedier, A., Heinzelmann-Schwarz, V., Hogg, P. J., & Dilda, P. J. (2015). Alterations in the

mitochondrial responses to PENAO as a mechanism of resistance in ovarian cancer cells. *Gynecol Oncol, 138*(2), 363-371.

Diehl, J. A., Cheng, M., Roussel, M. F., & Sherr, C. J. (1998). Glycogen synthase kinase-3β regulates cyclin D1 proteolysis and subcellular localization. *Genes Dev, 12*(22), 3499-3511.

Dieterich, W., Ehnis, T., Bauer, M., Donner, P., Volta, U., Riecken, E. O., & Schuppan, D. (1997). Identification of tissue transglutaminase as the autoantigen of celiac disease. *Nature Med, 3*(7), 797-801.

Dilda, P. J., Decollogne, S., Weerakoon, L., Norris, M. D., Haber, M., Allen, J. D., & Hogg, P. J. (2009). Optimization of the antitumor efficacy of a synthetic mitochondrial toxin by increasing the residence time in the cytosol. *J Med Chem, 52*(20), 6209-6216.

Dilda, P. J., & Hogg, P. J. (2007). Arsenical-based cancer drugs. *Cancer Treat Rev, 33*(6), 542-564.

Dilda, P. J., Ramsay, E. E., Corti, A., Pompella, A., & Hogg, P. J. (2008). Metabolism of the tumor angiogenesis inhibitor 4-(*N*-(*S*-glutathionylacetyl)amino)phenylarsonous acid. *J Biol Chem, 283*(51), 35428-35434.

Ding, L., Getz, G., Wheeler, D. A., Mardis, E. R., McLellan, M. D., Cibulskis, K., Sougnez, C., Greulich, H., Muzny, D. M., Morgan, M. B., Fulton, L., Fulton, R. S., Zhang, Q., Wendl, M. C., Lawrence, M. S., Larson, D. E., Chen, K., Dooling, D. J., Sabo, A., Hawes, A. C., Shen, H., Jhangiani, S. N., Lewis, L. R., Hall, O., Zhu, Y., Mathew, T., Ren, Y., Yao, J., Scherer, S. E., Clerc, K., Metcalf, G. A., Ng, B., Milosavljevic, A., Gonzalez-Garay, M. L., Osborne, J. R., Meyer, R., Shi, X., Tang, Y., Koboldt, D. C., Lin, L., Abbott, R., Miner, T. L., Pohl, C., Fewell, G., Haipek, C., Schmidt, H., Dunford-Shore, B. H., Kraja, A., Crosby, S. D., Sawyer, C. S., Vickery, T., Sander, S., Robinson, J., Winckler, W., Baldwin, J., Chirieac, L. R., Dutt, A., Fennell, T., Hanna,

M., Johnson, B. E., Onofrio, R. C., Thomas, R. K., Tonon, G., Weir, B. A., Zhao, X., Ziaugra, L., Zody, M. C., Giordano, T., Orringer, M. B., Roth, J. A., Spitz, M. R., Wistuba, II, Ozenberger, B., Good, P. J., Chang, A. C., Beer, D. G., Watson, M. A., Ladanyi, M., Broderick, S., Yoshizawa, A., Travis, W. D., Pao, W., Province, M. A., Weinstock, G. M., Varmus, H. E., Gabriel, S. B., Lander, E. S., Gibbs, R. A., Meyerson, M., & Wilson, R. K. (2008). Somatic mutations affect key pathways in lung adenocarcinoma. *Nature, 455*(7216), 1069-1075.

Don, A. S., Kisker, O., Dilda, P., Donoghue, N., Zhao, X., Decollogne, S., Creighton, B., Flynn, E., Folkman, J., & Hogg, P. J. (2003). A peptide trivalent arsenical inhibits tumor angiogenesis by perturbing mitochondrial function in angiogenic endothelial cells. *Cancer Cell, 3*(5), 497-509.

Ebner, M., Lucic, I., Leonard, T. A., & Yudushkin, I. (2017). PI(3,4,5)P3 engagement restricts Akt activity to cellular membranes. *Mol Cell, 65*(3), 416-431.

Ellertsdottir, E., Lenard, A., Blum, Y., Krudewig, A., Herwig, L., Affolter, M., & Belting, H. G. (2010). Vascular morphogenesis in the zebrafish embryo. *Dev Biol, 341*(1), 56-65.

Elliott, M. A., Ford, S. J., Prasad, E., Dick, L. J., Farmer, H., Hogg, P. J., & Halbert, G. W. (2012). Pharmaceutical development of the novel arsenical based cancer therapeutic GSAO for phase I clinical trial. *Int J Pharmaceut, 426*(1-2), 67-75.

Ellis, M. J., Ding, L., Shen, D., Luo, J., Suman, V. J., Wallis, J. W., Van Tine, B. A., Hoog, J., Goiffon, R. J., Goldstein, T. C., Ng, S., Lin, L., Crowder, R., Snider, J., Ballman, K., Weber, J., Chen, K., Koboldt, D. C., Kandoth, C., Schierding, W. S., McMichael, J. F., Miller, C. A., Lu, C., Harris, C. C., McLellan, M. D., Wendl, M. C., DeSchryver, K., Allred, D. C., Esserman, L., Unzeitig, G., Margenthaler, J., Babiera, G. V., Marcom, P. K., Guenther, J. M., Leitch, M., Hunt, K., Olson, J., Tao, Y., Maher, C. A., Fulton, L. L., Fulton, R. S., Harrison, M., Oberkfell, B., Du, F., Demeter, R., Vickery, T. L.,

Elhammali, A., Piwnica-Worms, H., McDonald, S., Watson, M., Dooling, D. J., Ota, D., Chang, L. W., Bose, R., Ley, T. J., Piwnica-Worms, D., Stuart, J. M., Wilson, R. K., & Mardis, E. R. (2012). Whole-genome analysis informs breast cancer response to aromatase inhibition. *Nature, 486*(7403), 353-360.

Elstrom, R. L., Bauer, D. E., Buzzai, M., Karnauskas, R., Harris, M. H., Plas, D. R., Zhuang, H., Cinalli, R. M., Alavi, A., Rudin, C. M., & Thompson, C. B. (2004). Akt Stimulates Aerobic Glycolysis in Cancer Cells. *Cancer Res, 64*(11), 3892-3899.

Emamian, E. S. (2012). AKT/GSK3 signaling pathway and schizophrenia. *Front Mol Neurosci, 5*, 33.

Franke, T. F., Yang, S. I., Chan, T. O., Datta, K., Kazlauskas, A., Morrison, D. K., Kaplan, D. R., & Tsichlis, P. N. (1995). The protein kinase encoded by the Akt proto-oncogene is a target of the PDGF-activated phosphatidylinositol 3-kinase. *Cell, 81*, 727-736.

Frech, M., Andjelkovic, M., Ingley, E., Reddy, K. K., Falck, J. R., & Hemmings, B. A. (1997). High affinity binding of inositol phosphates and phosphoinositides to the pleckstrin homology domain of RAC/protein kinase B and their influence on kinase activity. *J Biol Chem, 272*(13), 8474-8481.

Fuiman, L. A., Poling, K. R., & Higgs, D. M. (1998). Quantifying developmental progress for comparative studies of larval fishes. *Copeia, 1998*(3), 602-611.

Fujita, N., Sato, S., Katayama, K., & Tsuruo, T. (2002). Akt-dependent phosphorylation of p27Kip1 promotes binding to 14-3-3 and cytoplasmic localization. *J Biol Chem, 277*(32), 28706-28713.

Gallina, A., Hanley, T. M., Mandel, R., Trahey, M., Broder, C. C., Viglianti, G. A., & Ryser, H. J. (2002). Inhibitors of protein-disulfide isomerase prevent cleavage of disulfide bonds in receptor-bound glycoprotein 120 and prevent HIV-1 entry. *J Biol Chem, 277*(52), 50579-50588.

Ganapathy-Kanniappan, S., & Geschwind, J. F. H. (2013). Tumor glycolysis as a target for cancer therapy: progress and prospects. *Mol Cancer, 12*(152), 1-11.

Gandy, J. C., Rountree, A. E., & Bijur, G. N. (2006). Akt1 is dynamically modified with O-GlcNAc following treatments with PUGNAc and insulin-like growth factor-1. *FEBS Lett, 580*(13), 3051-3058.

Gao, J., Aksoy, B. A., Dogrusoz, U., Dresdner, G., Gross, B., Sumer, S. O., Sun, Y., Jacobsen, A., Sinha, R., Larsson, E., Cerami, E., Sander, C., & Schultz, N. (2013). Integrative analysis of complex cancer genomics and clinical profiles using the cBioPortal. *Sci Sig, 6*(269), 1-19.

Garcia-Echeverria, C., & Sellers, W. R. (2008). Drug discovery approaches targeting the PI3K/Akt pathway in cancer. *Oncogene, 27*(41), 5511-5526.

Garcia-Manyes, S., Liang, J., Szoszkiewicz, R., Kuo, T. L., & Fernandez, J. M. (2009). Force-activated reactivity switch in a bimolecular chemical reaction. *Nat Chem, 1*(3), 236-242.

Giannakopoulos, B., Gao, L., Qi, M., Wong, J. W., Yu, D. M., Vlachoyiannopoulos, P. G., Moutsopoulos, H. M., Atsumi, T., Koike, T., Hogg, P., Qi, J. C., & Krilis, S. A. (2012). Factor XI is a substrate for oxidoreductases: enhanced activation of reduced FXI and its role in antiphospholipid syndrome thrombosis. *J Autoimmun, 39*(3), 121-129.

Gingras, A.-C., Kennedy, S. G., O'Leary, M. A., Sonenberg, N., & Hay, N. (1998). 4E-BP1, a repressor of mRNA translation, is phosphorylated and inactivated by the Akt(PKB) signaling pathway. *Genes Dev, 12*, 502-513.

Goldstein, B. J., Mahadev, K., Wu, X., Zhu, L., & Motoshima, H. (2005). Role of insulin-induced reactive oxygen species in the insulin signaling pathway. *Antioxid Redox Signal, 7*(7-8), 1021-1031.

Gonzalez, E., & McGraw, T. E. (2009). Insulin-modulated Akt subcellular localization determines Akt isoform-specific signaling. *Proc Natl Acad Sci USA, 106*(17), 7004-7009.

Gopalan, G., He, Z., Balmer, Y., Romano, P., Gupta, R., Heroux, A., Buchanan, B. B., Swaminathan, K., & Luan, S. (2004). Structural analysis uncovers a role for redox in regulating FKBP13, an immunophilin of the chloroplast thylakoid lumen. *Proc Natl Acad Sci USA, 101*(38), 13945-13950.

Hanahan, D., & Weinberg, R. A. (2000). The hallmarks of cancer. *Cell, 100*(1), 57-70.

Hanahan, D., & Weinberg, R. A. (2011). Hallmarks of cancer: the next generation. *Cell, 144*(5), 646-674.

Harada, H., Itasaka, S., Kizaka-Kondoh, S., Shibuya, K., Morinibu, A., Shinomiya, K., & Hiraoka, M. (2009). The Akt/mTOR pathway assures the synthesis of HIF-1α protein in a glucose- and reoxygenation-dependent manner in irradiated tumors. *J Biol Chem, 284*(8), 5332-5342.

Hartley, J. L., Temple, G. F., & Brasch, M. A. (2000). DNA cloning using *in vitro* site-specific recombination. *Genome Res, 10*(11), 1788-1795.

Heng, J., Guo, X., Wu, W., Wang, Y., Li, G., Chen, M., Peng, L., Wang, S., Dai, L., Tang, L., & Wang, J. (2017). Integrated analysis of promoter mutation, methylation and expression of AKT1 gene in Chinese breast cancer patients. *PLoS One, 12*(3), e0174022.

Hers, I., Vincent, E. E., & Tavare, J. M. (2011). Akt signalling in health and disease. *Cell Signal, 23*(10), 1515-1527.

Hoeben, A., Landuyt, B., Highley, M. S., Wildiers, H., Van Oosterom, A. T., & De Bruijn, E. A. (2004). Vascular endothelial growth factor and angiogenesis. *Pharmacol Rev, 56*(4), 549-580.

Hogg, P. J. (2003). Disulfide bonds as switches for protein function. *Trends Biochem Sci, 28*(4), 210-214.

Hogg, P. J. (2013). Targeting allosteric disulphide bonds in cancer. *Nature Rev Cancer, 13*, 425-431.

Holland, E. C. (2000). Glioblastoma multiforme: The terminator. *Proc Natl Acad Sci USA, 97*(12), 6242-6244.

Holmgren, A. (1995). Thioredoxin structure and mechanism: conformational changes on oxidation of the active-site sulfhydryls to a disulfide. *Structure, 3*(3), 239-243.

Holmgren, A., & Björnstedt, M. (1995). Thioredoxin and thioredoxin reductase. *Method Enzymol, 252*(21), 199-208.

Horsley, L., Cummings, J., Middleton, M., Ward, T., Backen, A., Clamp, A., Dawson, M., Farmer, H., Fisher, N., Halbert, G., Halford, S., Harris, A., Hasan, J., Hogg, P., Gireesh Kumaran, G., Little, R., Parker, G. J. M., Potter, P., Saunders, M., Roberts, C., Shaw, D., Smith, N., Smythe, J., Taylor, A., Turner, H., Watson, Y., Dive, C., & Jayson, G. C. (2013). A phase 1 trial of intravenous 4-(*N*-(*S*-glutathionylacetyl)amino)phenylarsenoxide (GSAO) in patients with advanced solid tumours. *Cancer Chemother Pharmacol, 72*(6), 1343-1352.

Huang, B. X., Akbar, M., Kevala, K., & Kim, H. Y. (2011). Phosphatidylserine is a critical modulator for Akt activation. *J Cell Biol, 192*(6), 979-992.

Huang, B. X., Lee, R., Akbar, M., & Kim, H. Y. (2015). Threonine 34 phosphorylation by phosphoinositide-dependent protein kinase 1 facilitates dissociation of Akt from the plasma membrane. *Int J Biochem Cell Biol, 64*, 195-201.

Huang, D. W., Sherman, B. T., & Lempicki, R. A. (2009a). Bioinformatics enrichment tools: paths toward the comprehensive functional analysis of large gene lists. *Nucleic Acids Res, 37*(1), 1-13.

Huang, D. W., Sherman, B. T., & Lempicki, R. A. (2009b). Systematic and integrative analysis of large gene lists using DAVID bioinformatics resources. *Nat Protoc, 4*(1), 44-57.

Huang, J., & Manning, B. D. (2008). The TSC1-TSC2 complex: a molecular switchboard controlling cell growth. *Biochem J, 412*(2), 179-190.

Huang, J., & Manning, B. D. (2009). A complex interplay between Akt, TSC2 and the two mTOR complexes. *Biochem Soc Trans, 37*(Pt 1), 217-222.

Ioannou, Y., Zhang, J. Y., Passam, F. H., Rahgozar, S., Qi, J. C., Giannakopoulos, B., Qi, M., Yu, P., Yu, D. M., Hogg, P. J., & Krilis, S. A. (2010). Naturally occurring free thiols within 2-glycoprotein I in vivo: nitrosylation, redox modification by endothelial cells, and regulation of oxidative stress-induced cell injury. *Blood, 116*(11), 1961-1970.

Isogai, S., Horiguchi, M., & Weinstein, B. M. (2001). The vascular anatomy of the developing zebrafish: an atlas of embryonic and early larval development. *Dev Biol, 230*(2), 278-301.

James, S. R., Downes, C. P., Gigg, R., Grove, S. J. A., Holmes, A. B., & Alessi, D. R. (1996). Specific binding of the Akt-1 protein kinase to phosphatidylinositol 3,4,5-trisphosphate without subsequent activation. *Biochem J, 315*(Pt 3), 709-713.

Jeffery, J., Neyt, C., Moore, W., Paterson, S., Bower, N. I., Chenevix-Trench, G., Verkade, H., Hogan, B. M., & Khanna, K. K. (2015). Cep55 regulates embryonic growth and development by promoting Akt stability in zebrafish. *FASEB J, 29*(5), 1999-2009.

Jiang, Z. Y., Zhou, Q. L., Coleman, K. A., Chouinard, M., Boese, Q., & Czech, M. P. (2003). Insulin signaling through Akt/protein kinase B analyzed by small interfering RNA-mediated gene silencing. *Proc Natl Acad Sci USA, 100*(13), 7569-7574.

Jin, X., Stamnaes, J., Klock, C., DiRaimondo, T. R., Sollid, L. M., & Khosla, C. (2011). Activation of extracellular transglutaminase 2 by thioredoxin. *J Biol Chem, 286*(43), 37866-37873.

Jo, H., Lo, P.-K., Li, Y., Loison, F., Green, S., Wang, J., Silberstein, L. E., Ye, K., Chen, H., & Luo, H. R. (2011). Deactivation of Akt by a small molecule inhibitor targeting pleckstrin homology domain and facilitating Akt ubiquitination. *Proc Natl Acad Sci USA, 108*(16), 6486-6491.

Joh, E. H., Hollenbaugh, J. A., Kim, B., & Kim, D. H. (2012). Pleckstrin homology domain of Akt kinase: a proof of principle for highly specific and effective non-enzymatic anti-cancer target. *PLoS One, 7*(11), e50424.

Ka, M., Condorelli, G., Woodgett, J. R., & Kim, W. Y. (2014). mTOR regulates brain morphogenesis by mediating GSK3 signaling. *Development, 141*(21), 4076-4086.

Kaiser, B. K., Yim, D., Chow, I. T., Gonzalez, S., Dai, Z., Mann, H. H., Strong, R. K., Groh, V., & Spies, T. (2007). Disulphide-isomerase-enabled shedding of tumour-associated NKG2D ligands. *Nature, 447*(7143), 482-486.

Katz, B. A., & Kossiakoff, A. (1986). The crystallographically determined structures of atypical strained disulfides engineered into subtilisin. *J Biol Chem, 261*(33), 15480-15485.

Kawakami, K. (2007). Tol2: a versatile gene transfer vector in vertebrates. *Genome Biol, 8(Suppl 1)*(S7), 1-10.

Kellett-Clarke, H., Stegmann, M., Barclay, A. N., & Metcalfe, C. (2015). CD44 binding to hyaluronic acid Is redox regulated by a labile disulfide bond in the hyaluronic acid binding site. *PLoS One, 10*(9), e0138137.

Keppler-Noreuil, K. M., Parker, V. E., Darling, T. N., & Martinez-Agosto, J. A. (2016). Somatic overgrowth disorders of the PI3K/AKT/mTOR pathway & therapeutic strategies. *Am J Med Genet C Semin Med Genet, 172*(4), 402-421.

Keten, S., Chou, C. C., van Duin, A. C., & Buehler, M. J. (2012). Tunable nanomechanics of protein disulfide bonds in redox microenvironments. *J Mech Behav Biomed Mater, 5*(1), 32-40.

Kim, J. H., Lee, S. R., Li, L. H., Park, H. J., Park, J. H., Lee, K. Y., Kim, M. K., Shin, B. A., & Choi, S. Y. (2011). High cleavage efficiency of a 2A peptide derived from porcine teschovirus-1 in human cell lines, zebrafish and mice. *PLoS One, 6*(4), e18556.

Kim, M. S., Jeong, E. G., Yoo, N. J., & Lee, S. H. (2008). Mutational analysis of oncogenic AKT E17K mutation in common solid cancers and acute leukaemias. *Br J Cancer, 98*(9), 1533-1535.

Kim, S., Jang, Y.-S., Ha, S.-C., Ahn, J.-W., Kim, E.-J., Lim, J. H., Cho, C., Ryu, Y. S., Lee, S. K., Lee, S. Y., & Kim, K.-J. (2015). Redox-switch regulatory mechanism of thiolase from *Clostridium acetobutylicum*. *Nat Commun, 6*(1), 1-11.

Kimmel, C. B., Ballard, W. W., Kimmel, S. R., Ullmann, B., & Schilling, T. F. (1995). Stages of embryonic development of the zebrafish. *Dev Dynam, 203*, 253-310.

Kitamura, T., Asai, N., Enomoto, A., Maeda, K., Kato, T., Ishida, M., Jiang, P., Watanabe, T., Usukura, J., Kondo, T., Costantini, F., Murohara, T., & Takahashi, M. (2008). Regulation of VEGF-mediated angiogenesis by the Akt/PKB substrate girdin. *Nat Cell Biol, 10*(3), 329-337.

Kitamura, T., Ogawa, W., Sakaue, H., Hino, Y., Kuroda, S., Takata, M., Matsumoto, M., Maeda, T., Konishi, H., Kikkawa, U., & Kasuga, M. (1998). Requirement for activation of the serine-threonine kinase Akt (protein kinase B) in insulin stimulation of protein synthesis but not of glucose transport. *Mol Cell Biol, 18*(7), 3708-3717.

Kohn, A. D., Summers, S. A., Birnbaum, M. J., & Roth, R. A. (1996). Expression of a constitutively active Akt Ser/Thr kinase in 3T3-L1 adipocytes stimulates glucose uptake and glucose transporter 4 translocation. *J Biol Chem, 271*(49), 31372-31378.

Kotani, K., Ogawa, W., Hino, Y., Kitamura, T., Ueno, H., Sano, W., Sutherland, C., Granner, D. K., & Kasuga, M. (1999). Dominant negative forms of Akt (protein kinase B) and atypical protein kinase Cλ do not prevent insulin inhibition of phosphoenolpyruvate carboxykinase gene transcription. *J Biol Chem, 274*(30), 21305-21312.

Koundouros, N., & Poulogiannis, G. (2018). Phosphoinositide 3-kinase/Akt signaling and redox metabolism in cancer. *Front Oncol, 8*(160), 1-9.

Krock, B. L., Skuli, N., & Simon, M. C. (2011). Hypoxia-induced angiogenesis: good and evil. *Genes Cancer, 2*(12), 1117-1133.

Krycer, J. R., Sharpe, L. J., Luu, W., & Brown, A. J. (2010). The Akt-SREBP nexus: cell signaling meets lipid metabolism. *Trends Endocrinol Metab, 21*(5), 268-276.

Kubota, H., Noguchi, R., Toyoshima, Y., Ozaki, Y.-i., Uda, S., Watanabe, K., Ogawa, W., & Kuroda, S. (2012). Temporal coding of insulin action through multiplexing of the AKT pathway. *Mol Cell, 46*(6), 820-832.

Kumar, C. C., & Madison, V. (2005). AKT crystal structure and AKT-specific inhibitors. *Oncogene, 24*(50), 7493-7501.

Kunkel, M. T., Ni, Q., Tsien, R. Y., Zhang, J., & Newton, A. C. (2005). Spatio-temporal dynamics of protein kinase B/Akt signaling revealed by a genetically encoded fluorescent reporter. *J Biol Chem, 280*(7), 5581-5587.

Kuwajima, K., Ikeguchi, M., Sugawara, T., Hiraoka, Y., & Sugai, S. (1990). Kinetics of disulfide bond reduction in α-lactalbumin by dithiothreitol and molecular basis of superreactivity of the Cys6-Cys120 disulfide bond. *Biochemistry, 29*(36), 8240-8249.

Kwan, K. M., Fujimoto, E., Grabher, C., Mangum, B. D., Hardy, M. E., Campbell, D. S., Parant, J. M., Yost, H. J., Kanki, J. P., & Chien, C. (2007). The Tol2kit: A multisite gateway-based construction kit for *Tol2* transposon transgenesis constructs. *Dev Dynam, 236*(11), 3088-3099.

Lai, W. S., Xu, B., Westphal, K. G. C., Paterlini, M., Olivier, B., Pavlidis, P., Karayiorgou, M., & Gogos, J. A. (2006). Akt1 deficiency affects neuronal morphology and predisposes to abnormalities in prefrontal cortex functioning. *Proc Natl Acad Sci USA, 103*(45), 16906-16911.

Laine, J., Kunstle, G., Obata, T., & Noguchi, M. (2002). Differential regulation of Akt kinase isoforms by the members of the TCL1 oncogene family. *J Biol Chem, 277*(5), 3743-3751.

Laplante, M., & Sabatini, D. M. (2009). An emerging role of mTOR in lipid biosynthesis. *Curr Biol, 19*(22), R1046-R1052.

Lawson, N. D., & Weinstein, B. M. (2002). *In vivo* imaging of embryonic vascular development using transgenic zebrafish. *Dev Biol, 248*(2), 307-318.

Lazaris-Karatzas, A., Montine, K. S., & Sonenberg, N. (1990). Malignant transformation by a eukaryotic initiation factor subunit that binds to mRNA 5' cap. *Nature, 345*(6275), 544-547.

Lee, M. Y., Luciano, A. K., Ackah, E., Rodriguez-Vita, J., Bancroft, T. A., Eichmann, A., Simons, M., Kyriakides, T. R., Morales-Ruiz, M., & Sessa, W. C. (2014). Endothelial Akt1 mediates angiogenesis by phosphorylating multiple angiogenic substrates. *Proc Natl Acad Sci USA, 111*(35), 12865-12870.

Lee, S. R., Kwon, K. S., Kim, S. R., & Rhee, S. G. (1998). Reversible inactivation of protein-tyrosine phosphatase 1B in A431 cells stimulated with epidermal growth factor. *J Biol Chem, 273*(25), 15366-15372.

Lee, Y. H., Bae, H. C., Noh, K. H., Song, K. H., Ye, S. K., Mao, C. P., Lee, K. M., Wu, T. C., & Kim, T. W. (2015). Gain of HIF-1α under normoxia in cancer mediates immune adaptation through the AKT/ERK and VEGFA axes. *Clin Cancer Res, 21*(6), 1438-1446.

Leslie, J. D., Ariza-McNaughton, L., Bermange, A. L., McAdow, R., Johnson, S. L., & Lewis, J. (2007). Endothelial signalling by the notch ligand delta-like 4 restricts angiogenesis. *Development, 134*(5), 839-844.

Leslie, N. R., & Downes, C. P. (2004). PTEN function: how normal cells control it and tumour cells lose it. *Biochem J, 382*(Pt 1), 1-11.

Leveillard, T., & Ait-Ali, N. (2017). Cell signaling with extracellular thioredoxin and thioredoxin-like proteins: Insight into their mechanisms of action. *Oxid Med Cell Longev, 2017*, 8475125.

Li, J., Kim, K., Jeong, S.-Y., Chiu, J., Xiong, B., Petukhov, P. A., Dai, X., Li , X., Andrews, R. K., Du, X., Hogg, P. J., & Cho, J. (2018). Platelet protein disulfide isomerase promotes glycoprotein Ibα-mediated platelet-neutrophil interactions under thromboinflammatory conditions. *Circulation, 139*(10), 1300-1319.

Li, R., Wei, J., Jiang, C., Liu, D., Deng, L., Zhang, K., & Wang, P. (2013). Akt SUMOylation regulates cell proliferation and tumorigenesis. *Cancer Res, 73*(18), 5742-5753.

Li, W., & Gräter, F. (2010). Atomistic evidence of how force dynamically regulates thiol/disulfide exchange. *J Am Chem Soc, 132*(47), 16790-16795.

Liang, J., & Fernandez, J. M. (2009). Mechanochemistry: one bond at a time. *ACS Nano, 3*(7), 1628-1645.

Lin, C. H., Liu, S. Y., & Lee, E. H. (2016). SUMO modification of Akt regulates global SUMOylation and substrate SUMOylation specificity through Akt phosphorylation of Ubc9 and SUMO1. *Oncogene, 35*(5), 595-607.

Liu, L., Zhu, S., Gong, Z., & Low, B. C. (2008). K-ras/PI3K-Akt signaling is essential for zebrafish hematopoiesis and angiogenesis. *PLoS One, 3*(8), e2850.

Liu, X., Powlas, J., Shi, Y., Oleksijew, A. X., Shoemaker, A. R., De Jong, R., Oltersdorf, T., Giranda, V. L., & Luo, Y. (2004). Rapamycin inhibits Akt-mediated oncogenic transformation and tumor growth. *Anticancer Res, 24*(5A), 2697-2704.

Long, M. J. C., & Aye, Y. (2017). Privileged electrophile sensors: A resource for covalent drug development. *Cell Chem Biol, 24*(7), 787-800.

Long, M. J. C., Parvez, S., Zhao, Y., Surya, S. L., Wang, Y., Zhang, S., & Aye, Y. (2017). Akt3 is a privileged first responder in isozyme-specific electrophile response. *Nat Chem Biol, 13*(3), 333-338.

Lučić, I., Rathinaswamy, M. K., Truebestein, L., Hamelin, D. J., Burke, J. E., & Leonard, T. A. (2018). Conformational sampling of membranes by Akt controls its activation and inactivation. *Proc Natl Acad Sci USA, 115*(17), E3940-E3949.

Maccario, H., Perera, N. M., Davidson, L., Downes, C. P., & Leslie, N. R. (2007). PTEN is destabilized by phosphorylation on Thr366. *Biochem J, 405*(3), 439-444.

MacDonald, B. T., Tamai, K., & He, X. (2009). Wnt/β-catenin signaling: components, mechanisms, and diseases. *Dev Cell, 17*(1), 9-26.

Malojcić, G., & Glockshuber, R. (2010). The PAPS-independent aryl sulfotransferase and the alternative disulfide bond formation system in pathogenic bacteria. *Antioxid Redox Signal, 13*(8), 1247-1259.

Manning, B. D., & Cantley, L. C. (2007). AKT/PKB signaling: navigating downstream. *Cell, 129*(7), 1261-1274.

Manning, B. D., & Toker, A. (2017). AKT/PKB signaling: navigating the network. *Cell, 169*(3), 381-405.

Martin, A. C. (2005). Mapping PDB chains to UniProtKB entries. *Bioinformatics, 21*(23), 4297-4301.

Masure, S., Haefner, B., Wesselink, J.-J., Hoefnagel, E., Mortier, E., Verhasselt, P., Tuytelaars, A., Gordon, R., & Richardson, A. (1999). Molecular cloning, expression and characterization of the human serine/threonine kinase Akt-3. *Eur J Biochem, 265*(1), 353-360.

Matthias, L. J., Yam, P. T., Jiang, X. M., Vandegraaff, N., Li, P., Poumbourios, P., Donoghue, N., & Hogg, P. J. (2002). Disulfide exchange in domain 2 of CD4 is required for entry of HIV-1. *Nat Immunol, 3*(8), 727-732.

Mauney, C. H., Rogers, L. C., Harris, R. S., Daniel, L. W., Devarie-Baez, N. O., Wu, H., Furdui, C. M., Poole, L. B., Perrino, F. W., & Hollis, T. (2017). The SAMHD1 dNTP triphosphohydrolase is controlled by a redox switch. *Antioxid Redox Signal, 27*(16), 1317-1331.

Metcalfe, C., Cresswell, P., & Barclay, A. N. (2012). Interleukin-2 signalling is modulated by a labile disulfide bond in the CD132 chain of its receptor. *Open Biol, 2*(1), 110036.

Milburn, C. C., Deak, M., Kelly, S. M., Price, N. C., Alessi, D. R., & van Aalten, D. M. F. (2003). Binding of phosphatidylinositol 3,4,5-trisphosphate to the pleckstrin homology domain of protein kinase B induces a conformational change. *Biochem J, 375*, 531-538.

Moeller, B. J., Cao, Y., Li, C. Y., & Dewhirst, M. W. (2004). Radiation activates HIF-1 to regulate vascular radiosensitivity in tumors: Role of reoxygenation, free radicals, and stress granules. *Cancer Cell, 5*(5), 429-441.

Mohammad, A., Bon Ramos, A., Lee, B. W., Cohen, S. W., Kiani, M. K., Iwata-Reuyl, D., Stec, B., & Swairjo, M. A. (2017). Protection of the queuosine biosynthesis enzyme QueF from irreversible oxidation by a conserved intramolecular disulfide. *Biomolecules, 7*(1), 1-13.

Montano, S. J., Lu, J., Gustafsson, T. N., & Holmgren, A. (2014). Activity assays of mammalian thioredoxin and thioredoxin reductase: fluorescent disulfide substrates, mechanisms, and use with tissue samples. *Anal Biochem, 449*, 139-146.

Neary, C. L., & Pastorino, J. G. (2013). Akt inhibition promotes hexokinase 2 redistribution and glucose uptake in cancer cells. *J Cell Physiol, 228*(9), 1943-1948.

Niecknig, H., Tug, S., Reyes, B. D., Kirsch, M., Fandrey, J., & Berchner-Pfannschmidt, U. (2012). Role of reactive oxygen species in the regulation of HIF-1 by prolyl hydroxylase 2 under mild hypoxia. *Free Radic Res, 46*(6), 705-717.

Nishii, W., Kukimoto-Niino, M., Terada, T., Shirouzu, M., Muramatsu, T., Kojima, M., Kihara, H., & Yokoyama, S. (2015). A redox switch shapes the Lon protease exit pore to facultatively regulate proteolysis. *Nat Chem Biol, 11*(1), 46-51.

Nitulescu, G. M., Margina, D., Juzenas, P., Peng, Q., Olaru, O. T., Saloustros, E., Fenga, C., Spandidos, D., Libra, M., & Tsatsakis, A. M. (2016). Akt inhibitors in cancer treatment: The long journey from drug discovery to clinical use (Review). *Int J Oncol, 48*(3), 869-885.

Norris, D. M., Yang, P., Krycer, J. R., Fazakerley, D. J., James, D. E., & Burchfield, J. G. (2017). Improved Akt reporter reveals intra- and inter-cellular heterogeneity and oscillations in signal transduction. *J Cell Sci, 130*(16), 2757-2766.

O'Brien, J., Wilson, I., Terry Orton, T., & Pognan, F. (2000). Investigation of the Alamar Blue (resazurin) fluorescent dye for the assessment of mammalian cell cytotoxicity. *Eur J Biochem, 267*(17), 5421-5426.

Okoh, V. O., Felty, Q., Parkash, J., Poppiti, R., & Roy, D. (2013). Reactive oxygen species via redox signaling to PI3K/AKT pathway contribute to the malignant growth of 4-hydroxy estradiol-transformed mammary epithelial cells. *PLoS One, 8*(2), e54206.

Okuzumi, T., Fiedler, D., Zhang, C., Gray, D. C., Aizenstein, B., Hoffman, R., & Shokat, K. M. (2009). Inhibitor hijacking of Akt activation. *Nat Chem Biol, 5*(7), 484-493.

Ou, W., & Silver, J. (2006). Role of protein disulfide isomerase and other thiol-reactive proteins in HIV-1 envelope protein-mediated fusion. *Virology, 350*(2), 406-417.

Pap, M., & Cooper, G. M. (1998). Role of glycogen synthase kinase-3 in the phosphatidylinositol 3-kinase/Akt Cell Survival pathway. *J Biol Chem, 273*(32), 19929-19932.

Parichy, D. M., Elizondo, M. R., Mills, M. G., Gordon, T. N., & Engeszer, R. E. (2009). Normal table of postembryonic zebrafish development: staging by externally visible anatomy of the living fish. *Dev Dynam, 238*(12), 2975-3015.

Parikh, C., Janakiraman, V., Wu, W.-I., Foo, C. K., Kljavin, N. M., Chaudhuri, S., Stawiski, E., Lee, B., Lin, J., Li, H., Lorenzo, M. N., Yuan, W., Guillory, J., Jackson, M., Rondon, J., Franke, Y., Bowman, K. K., Sagolla, M., Stinson, J., Wu, T. D., Wu, J., Stokoe, D., Stern, H. M., Brandhuber, B. J., Lin, K., Skelton, N. J., & Seshagiri, S. (2012). Disruption of PH-kinase domain interactions leads to oncogenic activation of AKT in human cancers. *Proc Natl Acad Sci USA, 109*(47), 19368-19373.

Park, D., Chiu, J., Perrone, G. G., Dilda, P. J., & Hogg, P. J. (2012). The tumour metabolism inhibitors GSAO and PENAO react with cysteines 57 and 257 of mitochondrial adenine nucleotide translocase. *Cancer Cell Int, 12*(1), 11.

Park, H. C., Kim, C. H., Bae, Y. K., Yeo, S. Y., Kim, S. H., Hong, S. K., Shin, J., Yoo, K. W., Hibi, M., Hirano, T., Miki, N., Chitnis, A. B., & Huh, T. L. (2000). Analysis of upstream elements in the HuC promoter leads to the establishment of transgenic zebrafish with fluorescent neurons. *Dev Biol, 227*(2), 279-293.

Pasquarello, C., Sanchez, J. C., Hochstrasser, D. F., & Corthals, G. L. (2004). *N-t*-butyliodoacetamide and iodoacetanilide: two new cysteine alkylating reagents for relative quantitation of proteins. *Rapid Commun Mass Sp, 18*(1), 117-127.

Passam, F., Chiu, J., Ju, L., Pijning, A., Jahan, Z., Mor-Cohen, R., Yeheskel, A., Kolsek, K., Tharichen, L., Aponte-Santamaria, C., Grater, F., & Hogg, P. J. (2018). Mechano-redox control of integrin de-adhesion. *Elife, 7*, e34843.

Patwardhan, P., & Resh, M. D. (2010). Myristoylation and membrane binding regulate c-Src stability and kinase activity. *Mol Cell Biol, 30*(17), 4094-4107.

Paulsen, C. E., & Carroll, K. S. (2013). Cysteine-mediated redox signaling: chemistry, biology, and tools for discovery. *Chem Rev, 113*(7), 4633-4679.

Pijning, A. E., Chiu, J., Yeo, R. X., Wong, J. W. H., & Hogg, P. J. (2018). Identification of allosteric disulfides from labile bonds in X-ray structures. *Roy Soc Open Sci, 5*(2), 171058.

Pinkas, D. M., Strop, P., Brunger, A. T., & Khosla, C. (2007). Transglutaminase 2 undergoes a large conformational change upon activation. *PLoS Biol, 5*(12), e327.

Pjura, P. E., Matsumura, M., Wozniak, J. A., & Matthews, B. W. (1990). Structure of a thermostable disulfide-bridge mutant of phage T4 lysozyme shows that an engineered cross-link in a flexible region does not increase the rigidity of the folded protein. *Biochemistry, 29*(10), 2592-2698.

Plugis, N. M., Palanski, B. A., Weng, C.-H., Albertelli, M., & Khosla, C. (2017). Thioredoxin-1 selectively activates transglutaminase 2 in the extracellular matrix of the small intestine. *J Biol Chem, 292*(5), 2000-2008.

Plugis, N. M., Weng, N., Zhao, Q., Palanski, B. A., Maecker, H. T., Habtezion, A., & Khosla, C. (2018). Interleukin 4 is inactivated via selective disulfide-bond reduction by extracellular thioredoxin. *Proc Natl Acad Sci USA, 115*(35), 8781-8786.

Poduri, A., Evrony, G. D., Cai, X., Elhosary, P. C., Beroukhim, R., Lehtinen, M. K., Hills, L. B., Heinzen, E. L., Hill, A., Hill, R. S., Barry, B. J., Bourgeois, B. F., Riviello, J. J., Barkovich, A. J., Black, P. M., Ligon, K. L., & Walsh, C. A. (2012). Somatic activation of AKT3 causes hemispheric developmental brain malformations. *Neuron, 74*(1), 41-48.

Pore, N., Jiang, Z., Shu, H. K., Bernhard, E., Kao, G. D., & Maity, A. (2006). Akt1 activation can augment hypoxia-inducible factor-1α expression by increasing protein translation through a mammalian target of rapamycin-independent pathway. *Mol Cancer Res, 4*(7), 471-479.

Porstmann, T., Santos, C. R., Griffiths, B., Cully, M., Wu, M., Leevers, S., Griffiths, J. R., Chung, Y. L., & Schulze, A. (2008). SREBP activity is regulated by mTORC1 and contributes to Akt-dependent cell growth. *Cell Metab, 8*(3), 224-236.

Powell, D. J., Hajduch, E., Kular, G., & Hundal, H. S. (2003). Ceramide disables 3-phosphoinositide binding to the pleckstrin homology domain of protein kinase B (PKB)/Akt by a PKCζ-dependent mechanism. *Mol Cell Biol, 23*(21), 7794-7808.

Rampersad, S. N. (2012). Multiple applications of Alamar Blue as an indicator of metabolic function and cellular health in cell viability bioassays. *Sensors, 12*(9), 12347-12360.

Ramsay, E. E., Hogg, P. J., & Dilda, P. J. (2011). Mitochondrial metabolism inhibitors for cancer therapy. *Pharm Res, 28*(11), 2731-2744.

Ravilious, G. E., Nguyen, A., Francois, J. A., & Jez, J. M. (2012). Structural basis and evolution of redox regulation in plant adenosine-5′-phosphosulfate kinase. *Proc Natl Acad Sci USA, 109*(1), 309-314.

Reiser, K., Francois, K. O., Schols, D., Bergman, T., Jornvall, H., Balzarini, J., Karlsson, A., & Lundberg, M. (2012). Thioredoxin-1 and protein disulfide isomerase catalyze the reduction of similar disulfides in HIV gp120. *Int J Biochem Cell Biol, 44*(3), 556-562.

Ren, B., Deng, Y., Mukhopadhyay, A., Lanahan, A. A., Zhuang, Z. W., Moodie, K. L., Mulligan-Kehoe, M. J., Byzova, T. V., Peterson, R. T., & Simons, M. (2010). ERK1/2-Akt1 crosstalk regulates arteriogenesis in mice and zebrafish. *J Clin Invest, 120*(4), 1217-1228.

Ribas-Arino, J., & Marx, D. (2012). Covalent mechanochemistry: theoretical concepts and computational tools with applications to molecular nanomechanics. *Chem Rev, 112*(10), 5412-5487.

Riley, B. B., Chiang, M., Farmer, L., & Heck, R. (1999). The deltaA gene of zebrafish mediates lateral inhibition of hair cells in the inner ear and is regulated by pax2.1. *Development, 126*, 5669-5678.

Risso, G., Pelisch, F., Pozzi, B., Mammi, P., Blaustein, M., Colman-Lerner, A., & Srebrow, A. (2013). Modification of Akt by SUMO conjugation regulates alternative splicing and cell cycle. *Cell Cycle, 12*(19), 3165-3174.

Rowland, M. M., Gong, D., Bostic, H. E., Lucas, N., Cho, W., & Best, M. D. (2012). Microarray analysis of Akt PH domain binding employing synthetic biotinylated analogs of all seven phosphoinositide headgroup isomers. *Chem Phys Lipids, 165*(2), 207-215.

Sagong, H.-Y., & Kim, K.-J. (2017). Structural basis for redox sensitivity in *Corynebacterium glutamicum* diaminopimelate epimerase: an enzyme involved in l-lysine biosynthesis. *Sci Rep, 7*, 42318.

Santos, C. R., & Schulze, A. (2012). Lipid metabolism in cancer. *FEBS J, 279*(15), 2610-2623.

Schindelin, J., Arganda-Carreras, I., Frise, E., Kaynig, V., Longair, M., Pietzsch, T., Preibisch, S., Rueden, C., Saalfeld, S., Schmid, B., Tinevez, J. Y., White, D. J., Hartenstein, V., Eliceiri, K., Tomancak, P., & Cardona, A. (2012). Fiji: an open-source platform for biological-image analysis. *Nat Methods, 9*(7), 676-682.

Schmidt, B., Ho, L., & Hogg, P. J. (2006). Allosteric disulfide bonds. *Biochemistry, 45*, 7429-7433.

Seibel, N. M., Eljouni, J., Nalaskowski, M. M., & Hampe, W. (2007). Nuclear localization of enhanced green fluorescent protein homomultimers. *Anal Biochem, 368*(1), 95-99.

Seidman, C. E., Struhl, K., Sheen, J., & Jessen, T. (2001). *Introduction of plasmid DNA into cells* (Vol. 37:II:1.8:1.8.1-1.8.10).

Shannon, D. A., & Weerapana, E. (2015). Covalent protein modification: the current landscape of residue-specific electrophiles. *Curr Opin Chem Biol, 24*, 18-26.

Shen, H., Decollogne, S., Dilda, P. J., Hau, E., Chung, S. A., Luk, P. P., Hogg, P. J., & McDonald, K. L. (2015). Dual-targeting of aberrant glucose metabolism in glioblastoma. *J Exp Clin Cancer Res, 34*, 14.

Siddiqui, N., & Sonenberg, N. (2015). Signalling to eIF4E in cancer. *Biochem Soc Trans, 43*(5), 763-772.

Siekmann, A. F., & Lawson, N. D. (2007). Notch signalling limits angiogenic cell behaviour in developing zebrafish arteries. *Nature, 445*(7129), 781-784.

Sinor, A. D., & Lillien, L. (2004). Akt-1 expression level regulates CNS precursors. *J Neurosci, 24*(39), 8531-8541.

Song, G., Ouyang, G., & Bao, S. (2005). The activation of Akt/PKB signaling pathway and cell survival. *J Cell Mol Med, 9*(1), 59-71.

Staal, S. P. (1987). Molecular cloning of the akt oncogene and its human homologues *AKT1* and *AKT2*: Amplication of *AKT1* in a primary human gastric adenocarcinoma. *Proc Natl Acad Sci USA, 84*(14), 5034-5037.

Staal, S. P., Hartley, J. H., & Rowe, W. P. (1977). Isolation of transforming murine leukemia viruses from mice with a high incidence of spontaneous lymphoma. *Proc Natl Acad Sci USA, 74*(7), 3065-3067.

Stephens, P. J., Tarpey, P. S., Davies, H., Van Loo, P., Greenman, C., Wedge, D. C., Nik-Zainal, S., Martin, S., Varela, I., Bignell, G. R., Yates, L. R., Papaemmanuil, E., Beare, D., Butler, A., Cheverton, A., Gamble, J., Hinton, J., Jia, M., Jayakumar, A., Jones, D., Latimer, C., Lau, K. W., McLaren, S., McBride, D. J., Menzies, A., Mudie, L., Raine, K., Rad, R., Chapman, M. S., Teague, J., Easton, D., Langerod, A., Oslo Breast Cancer, C., Lee, M. T., Shen, C. Y., Tee, B. T., Huimin, B. W., Broeks, A., Vargas, A. C., Turashvili, G., Martens, J., Fatima, A., Miron, P., Chin, S. F., Thomas, G., Boyault, S., Mariani, O., Lakhani, S. R., van de Vijver, M., van 't Veer, L., Foekens, J., Desmedt, C., Sotiriou, C., Tutt, A., Caldas, C., Reis-Filho, J. S., Aparicio, S. A., Salomon, A. V., Borresen-Dale, A. L., Richardson, A. L., Campbell, P. J., Futreal, P. A., & Stratton, M. R. (2012). The landscape of cancer genes and mutational processes in breast cancer. *Nature, 486*(7403), 400-404.

Stickney, H. L., Barresi, M. J. F., & Devoto, S. H. (2000). Somite development in zebrafish. *Dev Dynam, 219*(3), 287-303.

Stopa, J. D., Neuberg, D., Puligandla, M., Furie, B., Flaumenhaft, R., & Zwicker, J. I. (2017). Protein disulfide isomerase inhibition blocks thrombin generation in humans by interfering with platelet factor V activation. *JCI Insight, 2*(1), e89373.

Sun, M., Wang, G., Paciga, J. E., Feldman, R. I., Yuan, Z.-Q., Ma, X.-L., Shelley, S. A., Jove, R., Tsichlis, P. N., Nicosia, S. V., & Cheng, J. Q. (2001). AKT1/PKBα kinase is frequently elevated in human cancers and its constitutive activation is required for oncogenic transformation in NIH3T3 cells. *Am J Pathol, 159*(2), 431-437.

Sun, X. F., Sun, Z. Y., Pan, B., Li, L., & Shen, W. (2012). Alteration in methylation pattern of oncogene Akt1 promoter region in bladder cancer. *Mol Biol Rep, 39*(5), 5631-5636.

Sundaresan, N. R., Pillai, V. B., Wolfgeher, D., Samant, S., Vasudevan, P., Parekh, V., Raghuraman, H., Cunningham, J. M., Gupta, M., & Gupta, M. P. (2011). The

deacetylase SIRT1 promotes membrane localization and activation of Akt and PDK1 during tumorigenesis and cardiac hypertrophy. *Sci Signal, 4*(182), ra46.

Sutton, K. A., Black, P. J., Mercer, K. R., Garman, E. F., Owen, R. L., Snell, E. H., & Bernhard, W. A. (2013). Insights into the mechanism of X-ray-induced disulfide-bond cleavage in lysozyme crystals based on EPR, optical absorption and X-ray diffraction studies. *Acta Crystallogr D Biol Crystallogr, 69*(Pt 12), 2381-2394.

Swaminathan, S., & Eswaramoorthy, S. (2000). Structural analysis of the catalytic and binding sites of *Clostridium botulinum* neurotoxin B. *Nature Struct Biol, 7*, 693-699.

Tan, S.-X., Ng, Y., Meoli, C. C., Kumar, A., Khoo, P. S., Fazakerley, D. J., Junutula, J. R., Vali, S., James, D. E., & Stöckli, J. (2012). Amplification and demultiplexing in insulin-regulated Akt protein kinase pathway in adipocytes. *J Biol Chem, 287*(9), 6128-6138.

Testa, J. R., & Bellacosa, A. (2001). AKT plays a central role in tumorigenesis. *Proc Natl Acad Sci USA, 98*(20), 10983-10985.

Testa, J. R., & Tsichlis, P. N. (2005). AKT signaling in normal and malignant cells. *Oncogene, 24*(50), 7391-7393.

Thurston, G., & Kitajewski, J. (2008). VEGF and delta-notch: interacting signalling pathways in tumour angiogenesis. *Br J Cancer, 99*(8), 1204-1209.

Tzivion, G., Dobson, M., & Ramakrishnan, G. (2011). FoxO transcription factors; Regulation by AKT and 14-3-3 proteins. *Biochim Biophys Acta, 1813*(11), 1938-1945.

Ushio-Fukai, M., Alexander, R. W., Akers, M., Yin, Q., Fujio, Y., Walsh, K., & Griendling, K. K. (1999). Reactive oxygen species mediate the activation of Akt/protein kinase B by angiotensin II in vascular smooth muscle cells. *J Biol Chem, 274*(32), 22699-22704.

Várnai, P., Bondeva, T., Tamás, P., Tóth, B., Buday, L., Hunyady, L., & Balla, T. (2005). Selective cellular effects of overexpressed pleckstrin-homology domains that recognize

PtdIns(3,4,5) suggest their interaction with protein binding partners. *J Cell Sci, 118*(Pt 20), 4879-4888.

Vasudevan, K. M., & Garraway, L. A. (2010). AKT signaling in physiology and disease. *Curr Top Microbiol Immunol, 347*, 105-133.

Vivanco, I., & Sawyers, C. L. (2002). The phosphatidylinositol 3-kinase–AKT pathway in human cancer. *Nat Rev Cancer, 2*(7), 489-501.

Wang, L., Zhou, K., Fu, Z., Yu, D., Huang, H., Zang, X., & Mo, X. (2016). Brain development and Akt signaling: the crossroads of signaling pathway and neurodevelopmental diseases. *J Mol Neurosci, 61*(3), 379-384.

Wang, S., Huang, X., Sun, D., Xin, X., Pan, Q., Peng, S., Liang, Z., Luo, C., Yang, Y., Jiang, H., Huang, M., Chai, W., Ding, J., & Geng, M. (2012). Extensive crosstalk between *O*-GlcNAcylation and phosphorylation regulates Akt signaling. *PLoS One, 7*(5), e37427.

Wang, X., McCullough, K. D., Franke, T. F., & Holbrook, N. J. (2000). Epidermal growth factor receptor-dependent Akt activation by oxidative stress enhances cell survival. *J Biol Chem, 275*(19), 14624-14631.

Wani, R., Bharathi, N. S., Field, J., Tsang, A. W., & Furdui, C. M. (2014). Oxidation of Akt2 kinase promotes cell migration and regulates G1-S transition in the cell cycle. *Cell Cycle, 10*(19), 3263-3268.

Wani, R., Qian, J., Yina, L., Bechtold, E., King, S. B., Poole, L. B., Paek, E., Tsang, A. W., & Furdui, C. M. (2011). Isoform-specific regulation of Akt by PDGF-induced reactive oxygen species. *Proc Natl Acad Sci USA, 108*(26), 10550-10555.

Warburg, O. (1956a). On respiratory impairment in cancer cells. *Science, 124*(3125), 269-270.

Warburg, O. (1956b). On the origin of cancer cells. *Science, 123*(3191), 309-314.

Warburg, O., Wind, F., & Negelein, E. (1927). The metabolism of tumors in the body. *J Gen Physiol, 8*(6), 519-530.

Ward, P. S., & Thompson, C. B. (2012). Metabolic reprogramming: A cancer hallmark even warburg did not anticipate. *Cancer Cell, 21*(3), 297-308.

Webb, A. E., & Brunet, A. (2014). FOXO transcription factors: key regulators of cellular quality control. *Trends Biochem Sci, 39*(4), 159-169.

Webb, A. E., Kundaje, A., & Brunet, A. (2016). Characterization of the direct targets of FOXO transcription factors throughout evolution. *Aging Cell, 15*, 673-685.

Weber, K., Bartsch, U., Stocking, C., & Fehse, B. (2008). A multicolor panel of novel lentiviral "gene ontology" (LeGO) vectors for functional gene analysis. *Mol Ther, 16*(4), 698-706.

Weber, K., Thomaschewski, M., Benten, D., & Fehse, B. (2012). RGB marking with lentiviral vectors for multicolor clonal cell tracking. *Nat Protoc, 7*(5), 839-849.

Weinberg, S. E., & Chandel, N. S. (2015). Targeting mitochondria metabolism for cancer therapy. *Nat Chem Biol, 11*(1), 9-15.

Weiner, S. J., Kollman, P. A., Case, D. A., Singh, U. C., Ghio, C., Alagona, G., Profeta, S., & Weiner, P. (1984). A new force field for molecular mechanical simulation of nucleic acids and proteins. *J Am Chem Soc, 106*(3), 765-784.

Wells, J. A., & Powers, D. B. (1986). *In vivo* formation and stability of engineered disulfide bonds in subtilisin. *J Biol Chem, 261*(14), 6564-6570.

Wendel, H. G., Silva, R. L., Malina, A., Mills, J. R., Zhu, H., Ueda, T., Watanabe-Fukunaga, R., Fukunaga, R., Teruya-Feldstein, J., Pelletier, J., & Lowe, S. W. (2007). Dissecting eIF4E action in tumorigenesis. *Genes Dev, 21*(24), 3232-3237.

Wetzel, R. R., Perry, L. J., Baase, W. A., & Becktel, W. J. (1988). Disulfide bonds and thermal stability in T4 lysozyme. *Proc Natl Acad Sci USA, 85*(2), 401-405.

Wiita, A. P., Ainavarapu, S. R., Huang, H. H., & Fernandez, J. M. (2006). Force-dependent chemical kinetics of disulfide bond reduction observed with single-molecule techniques. *Proc Natl Acad Sci USA, 103*(19), 7222-7227.

Wiita, A. P., Perez-Jimenez, R., Walther, K. A., Grater, F., Berne, B. J., Holmgren, A., Sanchez-Ruiz, J. M., & Fernandez, J. M. (2007). Probing the chemistry of thioredoxin catalysis with force. *Nature, 450*(7166), 124-127.

Wolf, A., Agnihotri, S., Micallef, J., Mukherjee, J., Sabha, N., Cairns, R., Hawkins, C., & Guha, A. (2011). Hexokinase 2 is a key mediator of aerobic glycolysis and promotes tumor growth in human glioblastoma multiforme. *J Exp Med, 208*(2), 313-326.

Wong, J. W., & Hogg, P. J. (2010). Analysis of disulfide bonds in protein structures. *J Thromb Haemost, 8*(10), 2345-2345.

Wouters, M. A., Lau, K. K., & Hogg, P. J. (2004). Cross-strand disulphides in cell entry proteins: Poised to act. *Bioessays, 26*(1), 73-79.

Wu, D., & Pan, W. (2010). GSK3: a multifaceted kinase in Wnt signaling. *Trends Biochem Sci, 35*(3), 161-168.

Wu, W. I., Voegtli, W. C., Sturgis, H. L., Dizon, F. P., Vigers, G. P., & Brandhuber, B. J. (2010). Crystal structure of human AKT1 with an allosteric inhibitor reveals a new mode of kinase inhibition. *PLoS One, 5*(9), e12913.

Yamaguchi, H., & Wang, H.-G. (2001). The protein kinase PKB/Akt regulates cell survival and apoptosis by inhibiting Bax conformational change. *Oncogene, 20*, 7779-7786.

Yang, J., Cron, P., Good, V. M., Thompson, V., Hemmings, B. A., & Barford, D. (2002). Crystal structure of an activated Akt/protein kinase B ternary complex with GSK3-peptide and AMP-PNP. *Nat Struct Biol, 9*(12), 940-944.

Yang, W. L., Wang, J., Chan, C. H., Lee, S. W., Campos, A. D., Lamothe, B., Hur, L., Grabiner, B. C., Lin, X., Darnay, B. G., & Lin, H. K. (2009). The E3 ligase TRAF6 regulates Akt ubiquitination and activation. *Science, 325*(5944), 1134-1138.

Yang, W. L., Wu, C. Y., Wu, J., & Lin, H. K. (2010). Regulation of Akt signaling activation by ubiquitination. *Cell Cycle, 9*(3), 487-497.

Yang, Z.-Z., Tschopp, O., Baudry, A., Dummler, B., Hynx, D., & Hemmings, B. A. (2004). Physiological functions of protein kinase B/Akt. *Biochem Soc Trans, 32*(Pt 2), 350-354.

Yi, K. H., Axtmayer, J., Gustin, J. P., Rajpurohit, A., & Lauring, J. (2012). Functional analysis of non-hotspot AKT1 mutants found in human breast cancers identifies novel driver mutations: implications for personalized medicine. *Oncotarget, 4*(1), 29-34.

Yi, K. H., & Lauring, J. (2015). Recurrent AKT mutations in human cancers: functional consequences and effects on drug sensitivity. *Oncotarget, 7*(4), 4241-4251.

Yi, M. C., Melkonian, A. V., Ousey, J. A., & Khosla, C. (2018). Endoplasmic reticulum–resident protein 57 (ERp57) oxidatively inactivates human transglutaminase 2. *J Biol Chem, 293*(8), 2640-2649.

Yost, C., Torres, M., Miller, J. R., Huang, E., Kimelman, D., & Moon, R. T. (1996). The axis-inducing activity, stability, and subcellular distribution of β-catenin is regulated in Xenopus embryos by glycogen synthase kinase 3. *Genes Dev, 10*(12), 1443-1454.

Yu, H., Littlewood, T., & Bennett, M. (2015). Akt isoforms in vascular disease. *Vascul Pharmacol, 71*, 57-64.

Yu, J. S., & Cui, W. (2016). Proliferation, survival and metabolism: the role of PI3K/AKT/mTOR signalling in pluripotency and cell fate determination. *Development, 143*(17), 3050-3060.

Zehir, A., Benayed, R., Shah, R. H., Syed, A., Middha, S., Kim, H. R., Srinivasan, P., Gao, J., Chakravarty, D., Devlin, S. M., Hellmann, M. D., Barron, D. A., Schram, A. M.,

Hameed, M., Dogan, S., Ross, D. S., Hechtman, J. F., DeLair, D. F., Yao, J., Mandelker, D. L., Cheng, D. T., Chandramohan, R., Mohanty, A. S., Ptashkin, R. N., Jayakumaran, G., Prasad, M., Syed, M. H., Rema, A. B., Liu, Z. Y., Nafa, K., Borsu, L., Sadowska, J., Casanova, J., Bacares, R., Kiecka, I. J., Razumova, A., Son, J. B., Stewart, L., Baldi, T., Mullaney, K. A., Al-Ahmadie, H., Vakiani, E., Abeshouse, A. A., Penson, A. V., Jonsson, P., Camacho, N., Chang, M. T., Won, H. H., Gross, B. E., Kundra, R., Heins, Z. J., Chen, H. W., Phillips, S., Zhang, H., Wang, J., Ochoa, A., Wills, J., Eubank, M., Thomas, S. B., Gardos, S. M., Reales, D. N., Galle, J., Durany, R., Cambria, R., Abida, W., Cercek, A., Feldman, D. R., Gounder, M. M., Hakimi, A. A., Harding, J. J., Iyer, G., Janjigian, Y. Y., Jordan, E. J., Kelly, C. M., Lowery, M. A., Morris, L. G. T., Omuro, A. M., Raj, N., Razavi, P., Shoushtari, A. N., Shukla, N., Soumerai, T. E., Varghese, A. M., Yaeger, R., Coleman, J., Bochner, B., Riely, G. J., Saltz, L. B., Scher, H. I., Sabbatini, P. J., Robson, M. E., Klimstra, D. S., Taylor, B. S., Baselga, J., Schultz, N., Hyman, D. M., Arcila, M. E., Solit, D. B., Ladanyi, M., & Berger, M. F. (2017). Mutational landscape of metastatic cancer revealed from prospective clinical sequencing of 10,000 patients. *Nat Med*, *23*(6), 703-713.

Zhang, D., Wang, J., Zhou, C., & Xiao, W. (2017). Zebrafish *akt2* is essential for survival, growth, bone development, and glucose homeostasis. *Mech Develop*, *143*, 42-52.

Zhang, J., Wang, X., Vikash, V., Ye, Q., Wu, D., Liu, Y., & Dong, W. (2016). ROS and ROS-mediated cellular signaling. *Oxid Med Cell Longev*, *2016*, 4350965.

Zhang, X., Gan, L., Pan, H., Guo, S., He, X., Olson, S. T., Mesecar, A., Adam, S., & Unterman, T. G. (2002). Phosphorylation of serine 256 suppresses transactivation by FKHR (FOXO1) by multiple mechanisms. Direct and indirect effects on nuclear/cytoplasmic shuttling and DNA binding. *J Biol Chem*, *277*(47), 45276-45284.

Zhang, X., Tang, N., Hadden, T. J., & Rishi, A. K. (2011). Akt, FoxO and regulation of apoptosis. *Biochim Biophys Acta, 1813*(11), 1978-1986.

Zhao, Y., Butler, E. B., & Tan, M. (2013). Targeting cellular metabolism to improve cancer therapeutics. *Cell Death Dis, 4*, e532.

Zhong, H., Chiles, K., Feldser, D., Laughner, E., Hanrahan, C., Georgescu, M. M., Simons, J. W., & Semenza, G. L. (2000). Modulation of hypoxia-inducible factor 1 expression by the epidermal growth factor/phosphatidylinositol 3-kinase/PTEN/AKT/FRAP pathway in human prostate cancer cells: Implications for tumor angiogenesis and therapeutics. *Cancer Res, 60*(6), 1541-1545.

Zhou, A., Carrell, R. W., Murphy, M. P., Wei, Z., Yan, Y., Stanley, P. L., Stein, P. E., Broughton Pipkin, F., & Read, R. J. (2010). A redox switch in angiotensinogen modulates angiotensin release. *Nature, 468*(7320), 108-111.

Zhou, B., Baldus, I. B., Li, W., Edwards, S. A., & Grater, F. (2014). Identification of allosteric disulfides from prestress analysis. *Biophys J, 107*(3), 672-681.

Zhou, H., Li, X.-M., Meinkoth, J., & Pittman, R. N. (2000). Akt regulates cell survival and apoptosis at a postmitochondrial level. *J Cell Biol, 151*(3), 483-494.